NASA CR-132636

DEVELOPMENT, FABRICATION AND CALIBRATION OF A POROUS SURFACE MICROPHONE IN AN AEROFOIL

By D.U. Noiseux
N.B. Noiseux
Y. Kadman

Prepared under Contract No. NAS1-12672 by

BOLT BERANEK AND NEWMAN INC.
50 Moulton Street
Cambridge, Massachusetts 02138

for

NATIONAL AERONAUTICS AND SPACE ADMINISTRATION

TABLE OF CONTENTS

TABLE OF CONTENTS (Cont.)

1. INTRODUCTION

This report describes the development of a porous surface microphone in an airfoil. This sensor is intended to measure acoustic signals in a turbulent airflow and to minimize the so-called flow noise. This sensor, because of its airfoil, can operate over a wide range of yaw angles, 0° to 90°, without excessive flow noise and over a wide range of flow velocities.

An earlier attempt at designing this type of sensor[1] had established that it can significantly reject flow noise. However, this earlier design revealed two major limitations: its frequency response decreases rapidly with increasing frequency; the mechanism of this effect was not quite understood; the frequency spectrum of flow noise showed regions of excessive noise which were attributed to flow separation on the airfoil when the yaw angle was increased from zero degrees. This earlier design had been evaluated only in a low flow velocity of approximately 22 m/sec (74 ft/sec).

There are three main objectives in the present work; these objectives have been realized.

First, the acoustic properties of the type of porous materials used in the Airfoil Sensor, and their effects on the frequency response of the sensor have been analyzed and tested. As a consequence of this study, the frequency response of the sensor has been considerably extended. It is now possible to predict with fair accuracy, the frequency response of a sensor for a given porous material or to prescribe a porous material for a given frequency response.

---

[1] Noiseux, D.U., "Study of Porous Surface Microphones for Acoustic Measurements in Wind Tunnels," NASA CR-114593; April 1973, BBN Report No. 2539.

Secondly, an accurate airfoil was selected, having a smaller thickness-to-chord ratio and a new Airfoil Sensor designed. The flow separation experienced with the earlier design has now been avoided at any yaw angle of the sensor in the air flow.

Finally, this new sensor was calibrated acoustically, and its flow noise evaluated, in the new and quiet BBN wind tunnel at flow velocities up to 70 m/sec.

The results of these three objectives are given in detail in the present report. Other aspects of this new sensor have been examined in a parallel effort, and the results described in a separate report[2]. These aspects are: the vibration sensitivity of the new sensor in airflow and the relative importance of the vibration induced noise compared with the flow noise; the effect of airflow on the acoustic response, (frequency response and directivity) of the new sensor.

The analytical and experimental results given in the present report, appeared in the course of this work as technical memos; each memo described a certain topic, drew conclusions and outlined the next effort. The group of eleven memos represent the complete results. These memos are appended to the present report as eleven appendices.

The results of this work is reviewed in the following sections which are introductions to the appendices. Section 2 deals with the analytical and experimental investigation of porous materials in thin sheets. Section 3 shows the dependence of the

---

[2] Noiseux, D.U., "Study of a Porous Microphone Sensor in an Airfoil," March 1975, NASA CR-137652, BBN Report No. 3022.

frequency response of the Airfoil Sensor on the specific acoustic admittances of the porous strips. Section 4 introduces the fabrication of the sensor including its base and stand. Section 5 indicates the acoustic characteristics of the sensor. Section 6 introduces the results of flow noise. Finally, Section 7 presents some conclusions.

2. POROUS STRIPS

2.1 Introduction

The porous strips used in the Airfoil Porous Surface Sensor must satisfy many requirements, besides having the correct specific acoustic resistance at low frequencies. The requirements are: (1) the specific acoustic impedance of a porous strip must be uniform along its length and width; (2) the porous strips must be rigid, and (3) the specific acoustic impedance must be real and independent of frequency.

(a) The first requirement has been examined previously[3]. It is shown, for a given mean specific acoustic resistance r_o, and its rms variations Δr along the length of the strips, and for a spatial scale x_o of these variations, that the directivity function of a porous surface sensor of length L is affected; in particular, the envelope of the minor lobes of the directivity function w(k), instead of decreasing inversely with wavenumber k as in the ideal line sensor, becomes limited to a certain low level given by

$$w(k) \cong \frac{\Delta r}{r_o} \sqrt{\frac{2x_o}{L}} \quad ; \qquad k \to \text{very large} \qquad (1)$$

For example, if we let

$$\frac{\Delta r}{r_o} = 0.1$$

$$\frac{x_o}{L} = 0.1$$

[3] See Reference 1, Appendix I: "Tolerances of the Porous Pipe Microphone."

we find that the envelope of the minor lobes of the directivity function is limited to 0.5×10^{-1} or -26 dB.

Since the minor lobes of the directivity function do most of the filtering of flow noise, especially at high wavenumbers, it follows that the non-uniformity of the acoustic impedance of the porous surface restricts the reduction of flow noise which could be achieved with a very uniform porous surface.

(b) The porous strip must obviously be rigid if the specific acoustic impedance of the strips is to depend exclusively on the porosity of the material. In practice, this requirement means that the first bending mode of the porous strip, as set on the sensor, should have a resonance frequency which is higher than the highest frequency of interest.

(c) The specific acoustic impedance of the porous strip was assumed in the original[4] analysis of the porous surface sensors to be real and independent of frequency. Under this assumption, the frequency response $s(\omega)$ of the sensor becomes constant. If residual effects are introduced in the analysis, like the viscous shear layer inside the cavity of the sensor, or a specific acoustic impedance of the porous strips which depends on frequency, we can readily show that the response of the sensor will not remain constant.

A complete analysis of the response of the sensor including these residual effects have so far proven to be intractable. However, under a special condition, we can relate directly the frequency response of the sensor to the impedance of the porous strips. This result will be discussed in Sec. III.

---

[4] Noiseux, D.U. and Horwath, T., "Design of a Porous Surface Microphone for the Rejection of Flow Noise," Submitted to Journal of Acoustical Society of America.

The impedance of thin porous strip as a function of frequency becomes an essential part of the specification of the porous strips if the sensor is prescribed to have a desired frequency response.

The impedance of thin porous strips of practical porous materials is examined in two approaches. In the first approach, we derive the driving point and transfer admittances y_{11} and y_{12} of thin porous strips; this is done in Sec. 2.2. In the second approach, the complex transfer admittances of thin porous strips are measured directly; the results are presented in Sec. 2.3.

2.2 Waves in Porous Material

The propagation of pressure fluctuations in porous materials is analyzed in Appendix I. The wavenumber q of propagation is given by

$$q^2 = \left[ik_o \frac{\sigma'}{\rho_0 c_0} - k_o^2 \frac{\rho_0'}{\rho_0} \right] \Omega\alpha \qquad (2)$$

where Ω is the porosity of the material, σ' is its flow resistivity, $\rho_0 c_0$ is the characteristic impedance of the gas inside the pores, ρ_0' is the effective density of the gas inside the pores, α is the ratio of specific heats of the gas and k_o is the wavenumber of the gas:

$$k = \omega/c_o \qquad (3)$$

ω being the circular frequency in radians per second. The second term inside the bracket of Eq. (2) represents the mass reactance of the gas inside the pores; this term is negligible in the frequency range of application of the sensor, leaving

$$q \cong \left[ik_o \frac{\sigma'}{\rho_0 c_0} \Omega\alpha \right]^{1/2} \tag{4}$$

which is the wavenumber of a purely resistive porous material. The value of $|q|$ is much larger than k_o in the frequency range of interest, indicating a relatively low phase velocity; the real and imaginary part of q are equal; the real part causes a large attenuation as a function of distance x into the porous material.

For thin strips of porous material, of thickness h, it is convenient to consider the specific driving point and transfer admittances y_{11} and y_{12} defined in Fig. 1, by

$$y_{11} = \frac{u_1}{P_1} \Bigg|_{P_2 = 0} \tag{5a}$$

$$y_{12} = \frac{u_2}{P_1} \Bigg|_{P_2 = 0} \tag{5b}$$

When a pressure wave is applied to a thin, rigid, porous surface, and this wave has a wavenumber component k_1 along the porous surface, the wavenumber of propagation in the porous surface becomes

$$\gamma = \pm \left[q^2 + k_1^2 \right]^{1/2} \tag{6a}$$

$$= \pm \left[\frac{ik_o \sigma' \Omega\alpha}{\rho_0 c_0} + k_1^2 \right]^{1/2} \tag{6b}$$

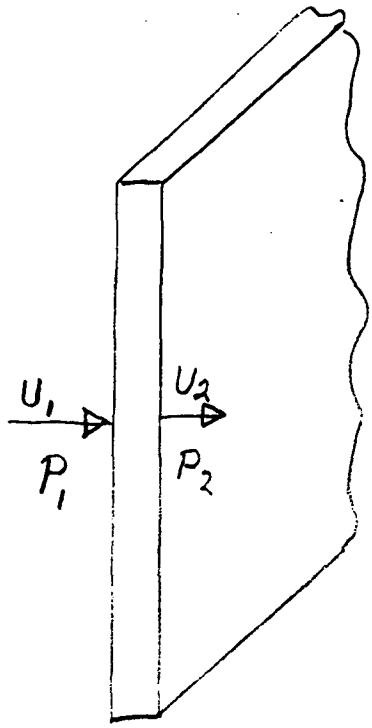

$$y_{11} = \left.\frac{U_1}{P_1}\right|_{P_2 = 0}$$

$$y_{12} = \left.\frac{U_2}{P_1}\right|_{P_2 = 0}$$

FIG. 1. DEFINITIONS OF THE ADMITTANCES y_{11} AND y_{12}.

and the admittances y_{11} and y_{12} are found to be

$$y_{11}r = \frac{\gamma h}{\tanh(\gamma h)} \tag{7a}$$

$$y_{12}r = \frac{\gamma h}{\sinh(\gamma h)} \tag{7b}$$

where

$$r = \sigma' h \tag{7c}$$

is the low frequency value of the specific acoustic resistance of the thin rigid porous sheet of thickness h.

The results of Eq. (5) through (7) are presented in Appendix II.

When the pressure wave is an acoustic wave propagating at grazing incidence along the length of the strip then

$$k_1 = k_0$$

in Eq. (6); we can show again that k_0^2 is negligible compared with q^2 in the frequency region of interest. However, when the pressure wave is subsonic, as in the case of turbulent flow over the porous surface, then k_1 can be much larger than k_0, with the result that the real part of γ will be larger and that these pressure fluctuations will be attenuated by the porous strip. Although this attenuation occurs mostly at higher frequencies it is useful in reducing the high frequency part of the flow noise. This attenuation occurs in addition to the reduction of flow noise provided by the directivity of the sensor.

For acoustic waves at grazing incidence, or any incidence, the argument γh becomes

$$\gamma h \cong (1+i)\ \beta \tag{8a}$$

$$\beta = \left[k_o h \frac{r}{\rho_0 c_0}\ \Omega\alpha \right]^{1/2} \tag{8b}$$

Since γh is complex, the admittances y_{11} and y_{12} are complex; y_{11} increases with increasing frequency; y_{12} decreases with increasing frequency. The values of $y_{11}r$ and $y_{12}r$ are calculated in Appendix III, showing their modulus and phase.

The results of Eqs. (7) and (8) show that even for a purely resistive porous material, the admittances of thin, rigid, sheets of this porous material become complex at, sufficiently high frequencies. The phase velocity inside the porous material is much lower than the sound velocity in the gas; $|\gamma| >> k_o$; the condition for the admittances to remain real and constant is found to be

$$\beta^2 \leq 1 \tag{9}$$

where β is given by Eq. (8b).

The implication of Eqs. (7) through (9) to the response of the sensor is presented in Sec. 3.

2.3 Measurements of the Transfer Admittance y_{12} of Thin, Porous Samples

The transfer admittance y_{12} of a thin, porous material is much easier to measure than the driving point admittance y_{11}. If the experimental values of y_{12} agree with the values calculated in Eqs. (7) and (8) from $r/\rho_0 c_0$, Ω, α, and h, then we will infer that the thin porous material behaves like the ideal, thin, and purely resistive, porous material. The experimental results turn out to be very close to the ideal porous material.

The measurement technique is described in Appendix IV, together with the calculation routine which yield the modulus $|y_{12}|$ and its phase. The measurements were made up to 13 kHz. A more elaborate setup would be required to extend the measurements beyond 13 kHz.

The experimental results of $|y_{12}|$ and its phase are given in Appendix V, for six different samples of porous metals.

The linearity of the porous samples is also tested, and its results are shown in Appendix VI. Two special samples of thin porous materials were ordered under specifications; these results are given in Appendix VIII. In addition, the uniformity of the specific acoustic resistance of these two samples is examined and discussed.

A number of conclusions appear from the experimental results. They are listed and discussed briefly as follows:

i - All the porous metal samples behaved like purely resistive porous materials. This is established by calculating the values of γh in Eq. (8), and computing y_{12}, modulus and phase, from Eq. (7b). The calculated and measured values agreed very well. The calculated and measured phases of y_{12} are more important than

the modulus because, as usual, phase changes appear earlier in the frequency spectrum and are more readily recognized than changes in the modulus.

ii - All porous metal samples are very linear (at least up to acoustic pressures of 156 dB re 0.0002 μbar) except the samples of sintered metal screens. This type of material should be avoided because the local pressure fluctuations, expecially those caused by a turbulent flow, could be large; the small acoustic pressure would be distorted by the presence of the large pressure fluctuations and its spectrum modified.

iii - All samples show gross variations of their specific acoustic resistance measured at low frequencies, contrary to the claims of the manufacturers. It follows that acceptable porous strips must be selected from many samples, each sample being measured for its local specific resistance.

(d) The porous material finally selected is a stainless steel made of sintered particles. This material has a rather high rigidity compared with felt metals and is less expensive to produce.

3. FREQUENCY RESPONSE OF A POROUS SURFACE SENSOR

An earlier attempt[5] at determining the relation between the complex impedance of the porous surface and the frequency response of a porous surface sensor was not successful. A different and better approach is developed in Appendix VII. The results are readily summarized by

$$s(\omega) \cong \frac{y_{12}(\omega)}{y_{11}(\omega)} \tag{10}$$

where $s(\omega)$ is the frequency response of a porous surface sensor, normalized to unity at low frequencies and y_{11}, y_{12} are the specific admittances of the porous surface.

Using Eqs. (7) and (8) for the ideal porous strips of finite thickness h, we get

$$s(\omega) = [\cosh\gamma h]^{-1} \tag{11}$$

where γh is given by Eq. (8). If Eq. (11) is plotted as a function of β^2, then $s(\omega)$ is given as a function of a normalized frequency

$$s(\omega) = [\cosh(1+i)\beta]^{-1} \tag{12}$$

This result is compared with earlier experimental results of the frequency response of a Porous Pipe Sensor and the first design of a Porous Strip Sensor. The values of β are calculated

---

[5] See Reference 1, Appendix III.

for the porous materials of these two sensors and the measured values of $s(\omega)$ replotted as a function of β^2. The agreement between calculated values using Eq. (12) and the measured values is remarkably good; it is within 2 dB. Since the response of actual sensors are influenced by other effects, like the shear boundary layers inside their cavities, which have not been included in the calculations, it is concluded that the result, Eq. (12), is a good approximation of the influence of the complex value of the admittances of the porous surfaces on the frequency response of the sensors.

In designing a Porous Surface Sensor, the result of Eq. (12) is used to determine the allowed thickness of the porous strip. The procedure is applied to a Porous Strip Sensor designed for uniform sensitivity along its porous surface, as follows.

(a) The length L of the porous strips determine the directivity of the sensor. Having chosen the value of L for the desired directivity, the specific acoustic resistance r follows,

$$\frac{r}{\rho_0 c_0} = L/d$$

where d is the maximum depth of the wedge shape cavity and $\rho_0 c_0$ is the characteristic impedance of the gas in the porous material.

(b) The allowed variation $\Delta r/r$ of the specific acoustic resistance r should be kept less than 0.1 (or 1 dB) and its scale of variation along the strip should be small (less than 1 inch) to insure that the envelope of the minor lobes of the directivity will reach a value of less than -25 dB.

(c) The thickness h of the porous strips is selected to give a value of β^2 near unity at the highest frequency of interest. Smaller values of β^2 are not desirable because attenuation of the flow noise by the transfer admittance y_{12} of the porous strip at large values of k_1, see Eq. (6b), would not be achieved.

(d) Finally, the width of the porous strip and of the acoustic cavity is decided by the rigidity of the porous strip, such that the resonance frequency of the first bending mode of the clamped-clamped strip is above the frequency range of interest for the sensor. The frequency of the first lateral mode of the acoustic cavity should also fall beyond the frequency range of interest.

4. FABRICATION OF POROUS SURFACE AIRFOIL SENSOR MODEL 342

The mechanical design of Porous Surface Airfoil Sensor, Model 342, is given in Appendix XI. The cross-section of the airfoil chosen is NACA-64-012 which has a much smaller thickness-to-chord ratio than the airfoil used in the earlier design[6].

The material of the porous strips is specified.

A base for the sensor has also been designed and fabricated. This base is a continuation of the airfoil; it allows the electrical leads of the preamplifier to be channeled *inside* the base and through a pipe. The pipe is inserted inside another but larger aerofoil which is the stand for the complete assembly.

---

[6] See Reference 1.

5. ACOUSTIC RESPONSE OF THE SENSOR

The acoustic response of the Airfoil Sensor is the ratio of its output voltage e to the pressure of a plane harmonic of direction and wavenumber $\underset{\sim}{k}_o$:

$$\frac{e}{p} = s(\omega)\ w(\underset{\sim}{k}_o) \tag{13}$$

where $w(\underset{\sim}{k}_o)$ is the directivity function normalized to unity when the direction of $\underset{\sim}{k}_o$ is along the axis of the sensor and head-on, $s(\omega)$ is the frequency response measured at the maximum of the directivity function.

The frequency response and directivity functions of the airfoil sensor have been measured in an anechoic room; the results are given in Appendix V.

The frequency response $s(\omega)$, normalized to unity at low frequencies follows closely the prediction of Eq. (12) for the type and thickness of porous material in the sensor. The resonances in the frequency region between 15 kHz and 20 kHz are attributed to the first bending mode of the porous strips and to the first lateral mode of the acoustic cavity. Both resonances could be shifted to higher frequencies by using narrower strips and a narrower acoustic cavity.

The directivity function $w(\underset{\sim}{k}_o)$ at least for its main lobe follows closely the directivity function a line sensor, end-fired, of the same length L as the porous strips:

$$w(\underset{\sim}{k}_o) = \frac{\sin[k_o(1-\cos\theta)L/2]}{k_o(1-\cos\theta)L/2} \tag{14}$$

where θ is the angle of $\underset{\sim}{k}_o$ with respect to the main axis of the porous strips. The envelope of the minor lobes measured do not decrease continuously with increasing k_o, but become limited to a level of roughly -25 dB. This value agrees roughly with the value given by Eq. (1) for the variations of the specific resistance of the porous surface also shown in Appendix V.

6. FLOW NOISE

The Airfoil Porous Surface Sensor is inserted in the free jet of the quiet BBN wind tunnel and its output analyzed in third octave bands for a wide range of flow velocities, 26 to 70 m/sec, (84 to 234 ft/sec) and for yaw angles 0° to 90° in increments of 15°. The output of the sensor in these conditions has been called flow noise.

The flow noise of the Airfoil Sensor is compared at the same flow velocities with the flow noise of a Bruel and Kjaer half-inch condenser microphone with a nose cone always pointing in the direction of airflow. The ratio of the flow noise of the B&K sensor to the flow noise of the Airfoil Sensor is called the flow noise reduction of the Airfoil Sensor.

As a reference for the *acoustic* component of noise in the wind tunnel, the B&K sensor is set out of the flow in a location where the noise radiated by the Airfoil Sensor and its stand is minimum. This location is identified as "location 2" in Fig. 8 of Appendix X. At "location 2" the noise measured is called the "out-of-flow noise".

All the flow noises measured are converted to equivalent sound pressure of a plane acoustic wave incident along the axis of the Sensors, by dividing the noise voltages by the sensitivity and frequency response $s(\omega)$ of each Sensor.

The details of the test set-ups and all the experimental results appear in Appendix X. These results are reviewed in the following paragraphs.

A typical result of flow noise levels for the Airfoil Sensor and the B&K Sensor, is shown in Fig. 2, at flow velocity of 62 m/sec. The corresponding flow noise reduction of the Airfoil Sensor is shown in Fig. 3. These results represent the particular

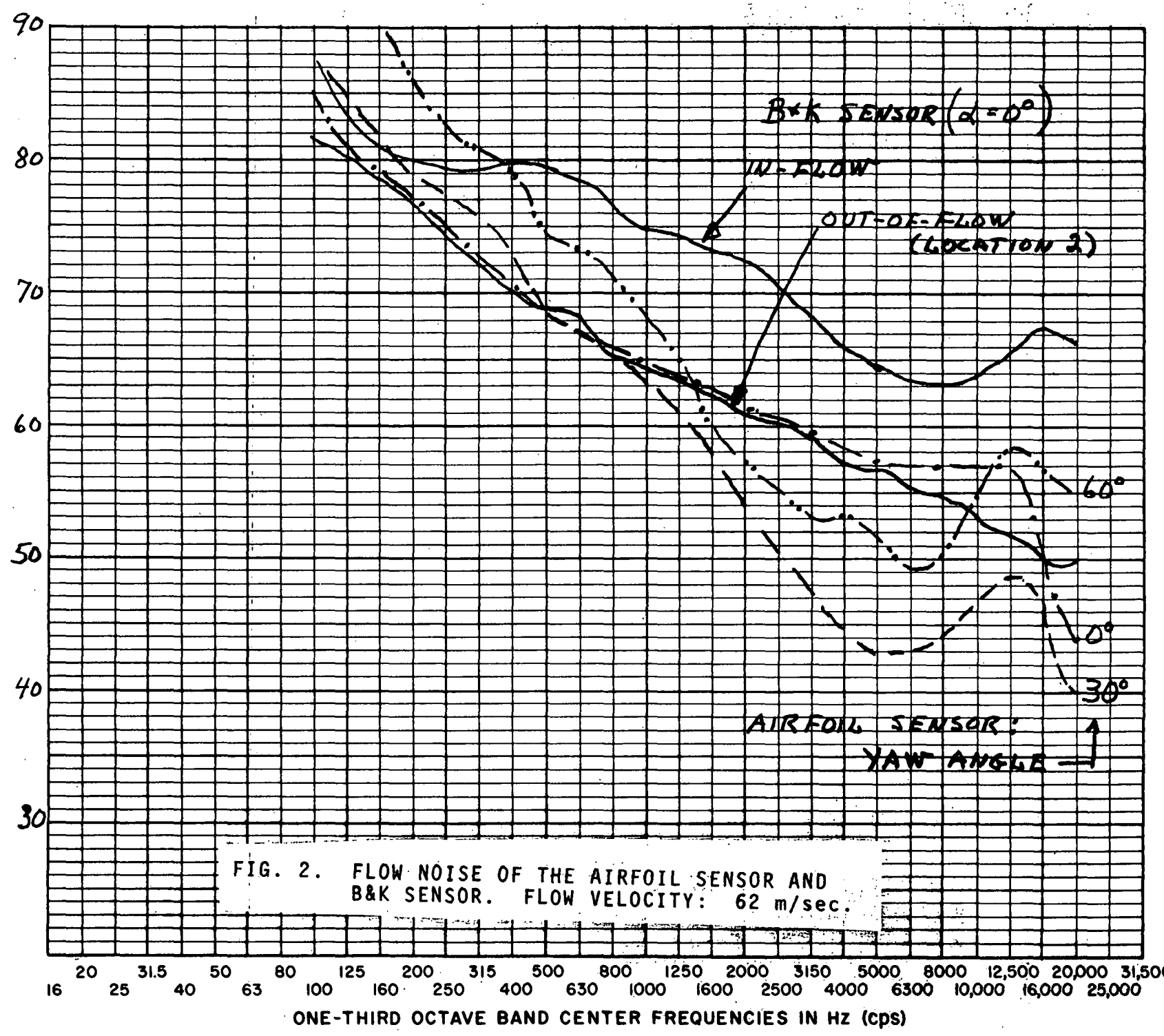

FIG. 2. FLOW NOISE OF THE AIRFOIL SENSOR AND B&K SENSOR. FLOW VELOCITY: 62 m/sec.

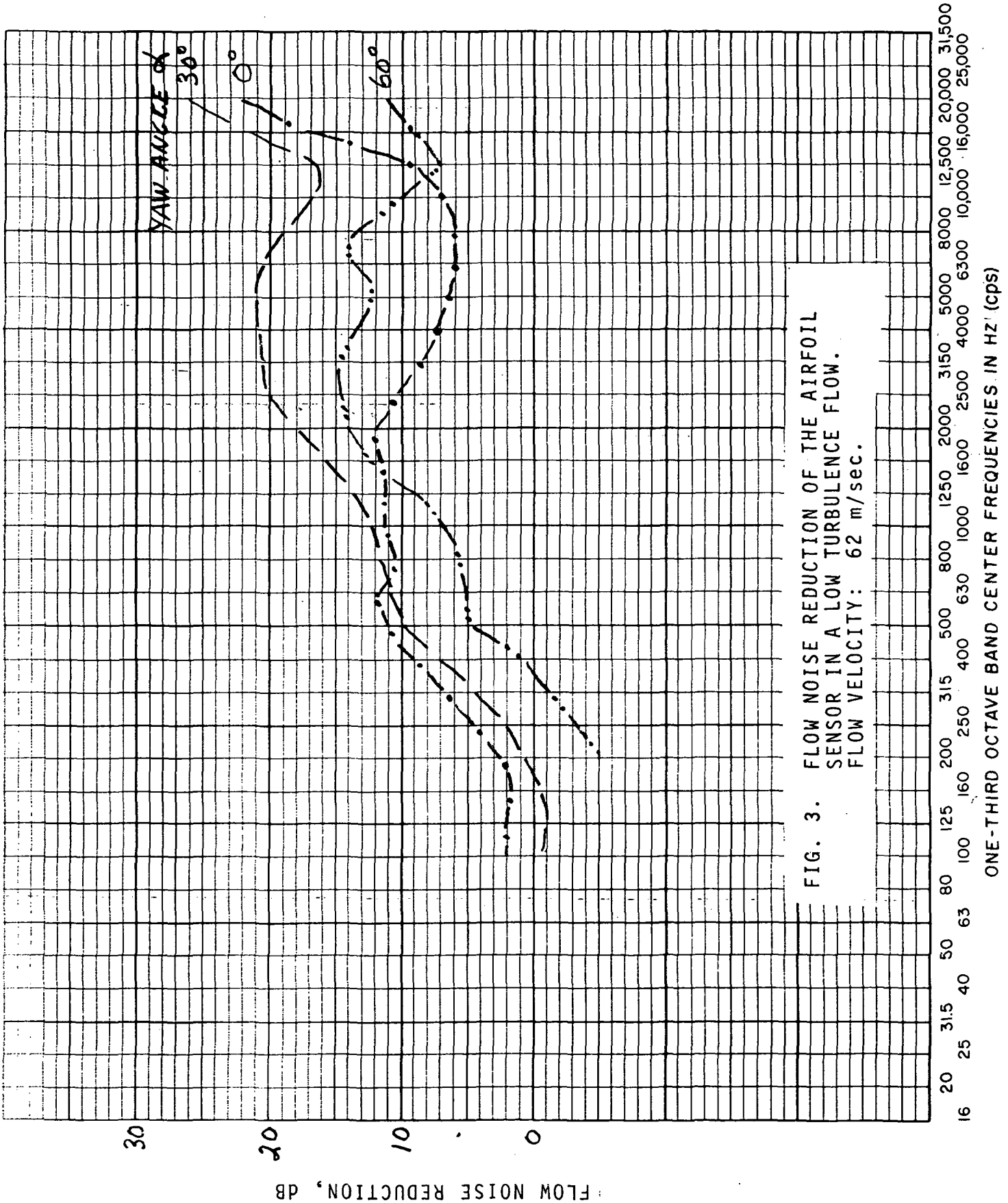

FIG. 3. FLOW NOISE REDUCTION OF THE AIRFOIL SENSOR IN A LOW TURBULENCE FLOW. FLOW VELOCITY: 62 m/sec.

conditions of the BBN wind tunnel and of the stand supporting the sensors in the flow. If these conditions are changed, for example by decreasing some way the turbulence of the free flow (which is already very low; see Fig. 2 of Appendix X), the levels of flow noise of the sensors, and the flow noise reduction of the Airfoil Sensor, would be somewhat changed.

The same type of results at a lower flow velocity of 31 m/sec, (100 ft/sec), is shown in Fig. 4. The out-of-flow noise relative to the in-flow noise is larger in Fig. 4 than in Fig. 2 and consequently, the flow noise reduction of the Airfoil Sensor is smaller.

The flow noise reduction achieved by the Airfoil Sensor is due, in part, to its acoustic directivity and in part to its ability of rejecting pressure fluctuations having wavelengths smaller than the acoustic wavelength, like the pressure fluctuations associated with turbulence. When the so-called flow noise contains mostly acoustic components, the flow noise reduction of the Airfoil Sensor is due mostly to its acoustic directivity and may be rather small, as in Fig. 4. When the flow noise includes a relative larger contribution due to turbulence in the free flow, the flow noise reduction of the Airfoil Sensor increases. As an example of higher turbulence in another experiment[6] (not reported here), Fig. 5 shows the larger flow noise reduction obtained by the Aerofoil Sensor. The conditions of Fig. 5, where a test object is in the flow and the Airfoil Sensor measures the acoustic signals emitted downstream by the object, are possibly closer to many practical measurements in wind tunnels than the conditions of a free jet.

The results of flow noise of the Airfoil Sensor at all yaw angles, 0° to 90°, suggests that no significant flow separation

---

[6] See Reference 2, Appendix V.

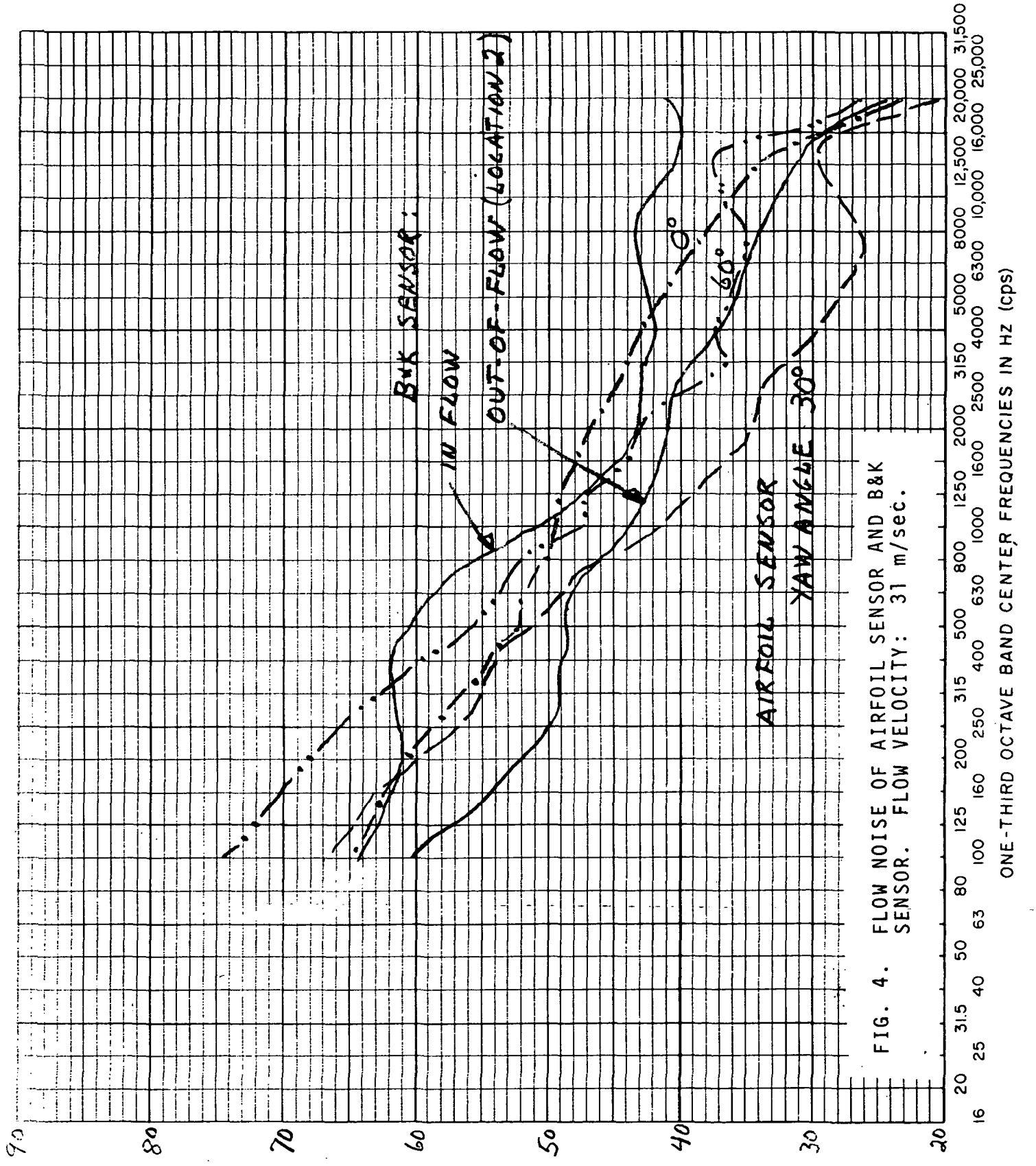

FIG. 4. FLOW NOISE OF AIRFOIL SENSOR AND B&K SENSOR. FLOW VELOCITY: 31 m/sec.

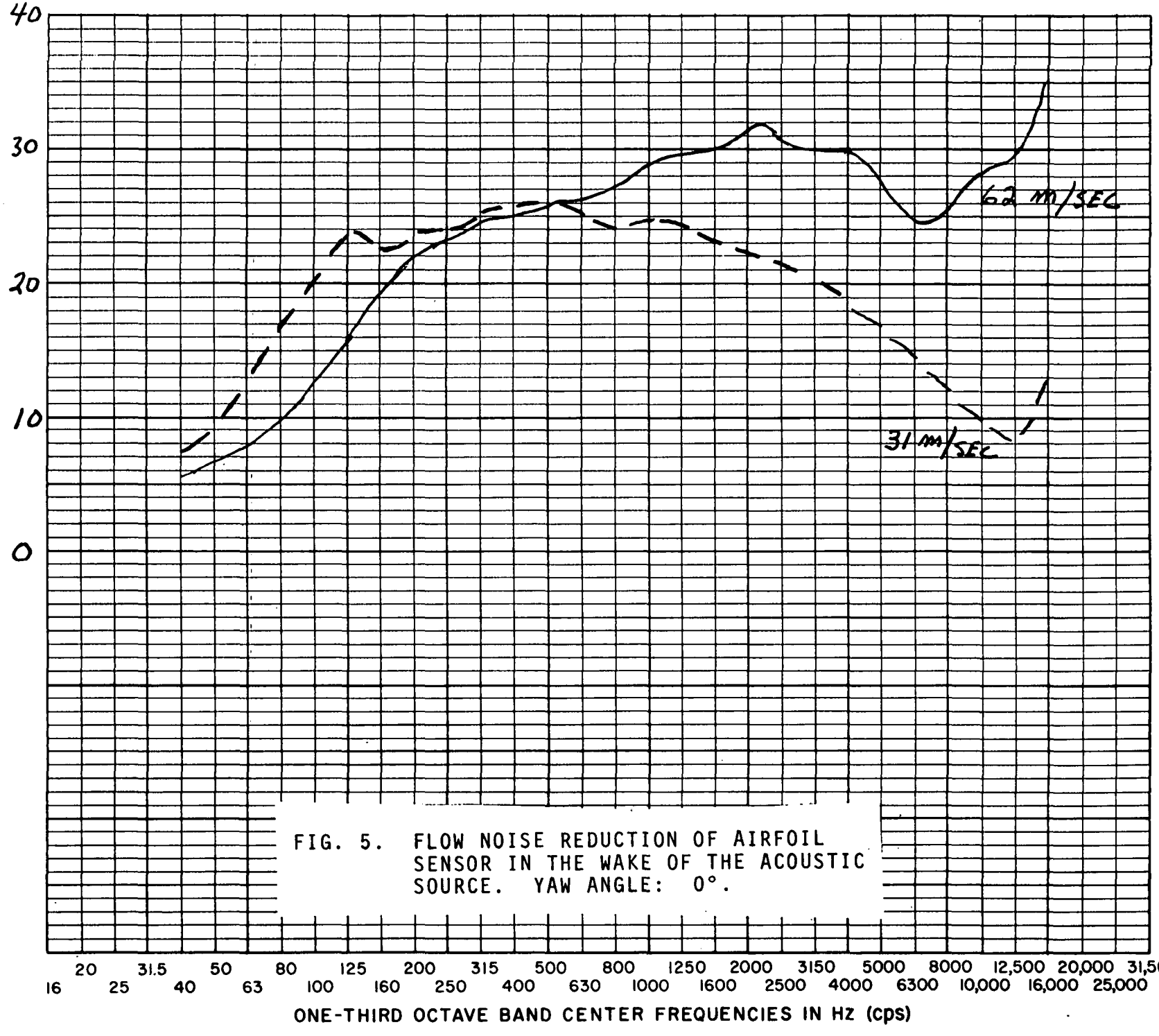

FIG. 5. FLOW NOISE REDUCTION OF AIRFOIL SENSOR IN THE WAKE OF THE ACOUSTIC SOURCE. YAW ANGLE: 0°.

occurred. This is a market improvement over the earlier design[7]. This is due to the new aerofoil chosen for the present design.

The interesting result that the flow noise is minimum at a yaw angle of 30° is not well understood.

The flow noise of the Airfoil Sensor, Fig. 2, shows a peak in the vicinity of 12.5 kHz for any yaw angle. The frequency of this peak does not change with flow velocity; hence, we conclude that it is not of aerodynamic origin, like flow separation, or trailing edge noise. The frequency of this peak is lower than the resonance frequencies observed in the frequency response, which occur above 15 kHz. We cannot yet explain this peak in flow noise. We have considered the possibility that the porous strip is more strongly excited by a turbulent flow at the first resonance frequency of the strip, than by an acoustic plane wave because the bending wave velocity of the strip is lower than the sound velocity in air at the first resonance. However, the maximum response should still occur at the resonance frequency of the first mode; this is not quite the situation found in Fig. 2.

We notice, also, that the flow noise of the B&K sensor increases with frequency above 6.3 kHz in Fig. 2. The peak of this flow noise is around 16 kHz. It may be that the acoustic sensitivity of the B&K sensor is modified by the presence of flow and, in fact, drops at high flow velocity. This hypothesis could explain the peak of flow noise of the B&K sensor shown in Fig. 2, because these results include the acoustic sensitivity of the

---

[7] See Reference 1.

sensors: the output noise voltages have been divided by the frequency response of the sensors.

The experimental results of flow noise have not yet been analyzed in detail. A first step in this analysis would be to identify the different causes of flow noises and assess their relative contribution. For example, we could organize the causes of flow noise in three groups: (1) acoustic noises like the acoustic noise created by the fan, the ambient noise, the lip noise radiated by the nozzle; this latter noise may explain why the noise reduction of the airfoil sensor is greatest at a yaw angle of 30°; (2) the noises associated with the turbulence in the free jet[8] causing, for example, leading edge noise at the tip of the sensors; (3) the noises created by the sensor itself[9] and its stand like the trailing edge noise, the turbulent boundary layer (if any) over the sensitive surface of the sensors, etc.

Without a detailed analysis of the different causes of flow noise, it is difficult to assess quantitatively the performance of the Airfoil Sensor. Its flow noise reduction like those of Figs. 3 and 5, show that the Airfoil Sensor performs as anticipated but without showing the limits of its performance.

---

[8] Fuchs, H.V., "Measurement of Pressure Fluctuations Within Subsonic Turbulent Jets," Journal of Sound and Vibration, (1972), 22(3), 361-378.

[9] Hayden, R.E., "Noise from Interaction of flow with Rigid Surfaces: A Review of Current Status in Prediction Techniques," NASA CR-2126, October 1972.

7. CONCLUSIONS

The investigation of the admittances of thin porous materials, and the analysis of the relation between these admittances and the frequency response of the Porous Surface Microphone in an Airfoil, have led to a much improved frequency response of this sensor. Based on these results, it appears now that Porous Surface Sensors with predictable frequency response and even with higher frequency response than the present model can be designed with confidence.

The use of an accurate aerofoil with small thickness-to-chord ratio has almost completely eliminated the noise component due to flow separation which was evident in the earlier design. It follows that the Airfoil Sensor can be used over the full range of yaw angles without severe penalty in flow noise.

The measurements of flow noise have been extended to higher flow velocities, up to 70 m/sec, than in the earlier tests. Hence, the present results of flow noise are applicable to measurements in many wind tunnels.

The flow noise reduction of the Airfoil Sensor is not inconsistent which is what was anticipated. It is larger when the turbulence in the flow is larger because this sensor is most effective in reducing subsonic pressure fluctuations which have wavelengths smaller than the sonic wavelengths.

Some improvements in the present design are desirable. The most obvious ones are (1) to eliminate the resonances in its frequency response in the frequency region between 15 kHz and 20 kHz; (2) to decrease the peak in flow noise found in the region of 12.5 kHz; and (3) to use more uniform porous materials which could enhance the acoustic directivity by reducing the levels of its minor lobes; at the same time the flow noise would also be reduced.

APPENDIX I

ACOUSTIC WAVES IN A RIGID POROUS MATERIAL

This memo and the next one examine the transmission through porous materials as a wave phenomenon in the gas inside the porous material. The porous material itself is assumed to be infinitely rigid.

The purpose of this analysis is to develop more rigorous expressions for the self and transfer admittances of a porous sheet.

In the present Memo, the wave equation in an isotropic porous material is derived. The derivation is similar to the derivation given by Morse and Ingard[1]; however, the present derivation is given in more details and with reference to the high values of resistivity which are found in the applications to Porous Surface sensors.

I. WAVE EQUATION

Consider an elementary volume of an isotropic porous material which has dimensions very small compared to a wavelength but very large compared with the size of the pores. The gas density ρ_e averaged over the elementary volume is

$$\rho_e = \Omega\rho_0 \qquad (1)$$

where ρ_0 is the density of the free gas and Ω is the porosity: it is the fraction of the elementary volume occupied by the gas.

Let $\underset{\sim}{u}$ be the average velocity of the gas, averaged over the surface of the elementary volume; $\underset{\sim}{u}$ is much smaller than the local velocity $\underset{\sim}{u}'$ of the gas in a pore, when the porosity Ω is very small.

---

[1] P.M. Morse and K.U. Ingard, "Theoretical Acoustics", McGraw Hill Book Co., 1968, pp. 252-

For these definitions of $\underset{\sim}{u}$ and ρ_e, the equation of continuity is

$$\frac{\partial \rho_e}{\partial t} + \rho_0 \operatorname{div} \underset{\sim}{u} = 0 \qquad (2a)$$

This is proven by examining the equation of continuity in its integral form,

$$\frac{\partial}{\partial t} \int_{\text{elementary volume}} \rho_e \, dv = \rho_0 \int_{A'=\text{surface of pores}} \underset{\sim}{u}' \cdot d\underset{\sim}{A}' = \rho_0 \int_{\text{surface of volume}} \underset{\sim}{u} \cdot d\underset{\sim}{A}$$

and applying the divergence theorem; Eq. (2) and (1) become

$$\Omega \frac{\partial \rho_0}{\partial t} + \rho_0 \operatorname{div} \underset{\sim}{u} = 0 \qquad (2b)$$

The equation of state of the gas inside a pore is very likely to be isothermal over the frequency range of interest, for porous materials having a very low porosity:

$$\partial p = \frac{P_a}{\rho_0} \partial \rho_0 \qquad (3)$$

where P_a is the ambient pressure of the gas inside the pores.

The momentum equation is modified to include the viscous friction of the gas. This is derived first for the one dimensional case where the elementary volume is thought of consisting of a bundle of fine tubes; it is then generalized to the three dimensional case.

Consider a small tube inside cross section A' and length Δx (which is the length of the elementary volume). For each tube we have

$$(\rho_0' A' \Delta \times \frac{\partial}{\partial t} + \sigma' A' \Delta x) u_x' = -\Delta F = -\Delta p A' \tag{4a}$$

where u_x' is the average velocity over the cross section A' in the x direction of the tube, ΔF is the force difference applied between the two ends of the tube, σ' is the resistivity of the tube; ρ_0' is the effective density of the gas inside the tube; the value of ρ_0' is larger than the actual density ρ_0 because the velocity distribution in a cross section of the tube is not uniform. Rewriting (4a), we get:

$$(\rho_0' \frac{\partial}{\partial t} + \sigma') u_x' = - \frac{\Delta p}{\Delta x} \tag{4b}$$

For a bundle of tubes having a net cross section A, Eq. (4b) is integrated over the cross-section A:

$$(\rho_0' \frac{\partial}{\partial t} + \sigma') \int u_x' \, dA = - \frac{\Delta p}{\Delta x} \int dA \tag{4c}$$

However, from the definition of the component u_x of $\underset{\sim}{u}$, which is the average velocity on a *face of the elementary volume*, we find

$$\int u_x' \, dA = u_x A \tag{4d}$$

and (4c) reduces to

$$(\rho_0' \frac{\partial}{\partial t} + \sigma') u_x = - \frac{\partial p}{\partial x} \tag{4e}$$

This last result is generalized to the three-dimensional case:

$$(\rho_0' \frac{\partial}{\partial t} + \sigma') \underset{\sim}{u} = - \text{grad } p \tag{5}$$

It is, at first, surprising that the average velocity $\tilde{u}$ over a surface of the elementary volume and the pressure gradient are related to the effective density ρ_0' and the resistivity σ' *of a pore* and not to the average density ρ_e and average resistivity of the porous material. This is readily explained by again considering a bundle of tubes set in a solid; the solid is considered as having an infinite density and an infinite resistivity; when the impedances of the tubes and of the solid are combined *in parallel*, the results (5) follow.

Equation (5) could be used to define the specific acoustic impedance of a very thin porous sheet, when the wavelength inside the porous material is very small compared with the thickness h of porous sheet; the gradient of p times h becomes the net pressure difference P across the porous sheet:

$$z = \frac{P}{u_x} = (i\omega\rho_0' + \sigma')\, h \qquad (6a)$$

indicating that the specific acoustic resistance of the porous sheet is $\sigma' h$ and the specific acoustic reactance of the porous sheet is $\omega\rho_0' h$.

For a circular tube of very small radius "a" we find[2]

$$\rho_0' = \frac{4}{3}\,\rho_0 \qquad (6b)$$

$$\sigma' = \frac{8\eta}{a^2} \qquad (6c)$$

where η is the coefficient of viscosity of the gas.

---

[2]L.L. Beranek, "Acoustics", p 135.

Eq. 5.48

These equations apply for

$$a < 0.2/\sqrt{f}\ , \text{ cm.}$$

The ratio of the reactance X to the resistance r of the specific acoustic impedance,

$$\frac{X}{r} = \frac{\omega \rho_0'}{\sigma'} \tag{6d}$$

does not depend on the porosity Ω but on the size of the pores; for a pore having a circular cross section (see Eqs. 6b and 6c) the ratio depends on the effective radius "a", to the second power:

$$\frac{X}{r} = \frac{\omega (4/3) \rho_0 a^2}{8\eta} \tag{6e}$$

Returning to the wave equation, Eqs. (2b), (3) and (5) are combined to yield

$$\left[\rho_0' \frac{\partial}{\partial t} + \sigma'\right] \frac{\Omega}{P_a} \frac{\partial p}{\partial t} = \nabla^2 p \tag{7}$$

which is the wave equation in an isotropic porous material of very low porosity (isothermal gas). For a harmonic wave of frequency ω, (7) becomes the modified Hemholtz equation:

$$(-\omega^2 \rho_0' + i\omega\sigma') \frac{\Omega}{P_a} p = \nabla^2 p \tag{8}$$

For our purpose, it is convenient to introduce the acoustic wavenumber k_0 of the free gas:

$$k_0 = \omega / c_0 \tag{9}$$

where c_0 is the sound velocity in the free gas; the sound velocity c_0 is related to the average gas pressure P_a through an adiabatic process:

$$\alpha P_a = \rho_0 c_0^2 \tag{10}$$

where α is the ratio of specific heats: $\alpha = 1.4$ for air. Equations (9) and (10) yield

$$\left[-k_0^2 \frac{\rho_0'}{\rho_0} + ik_0 \frac{\sigma'}{\rho_0 c_0}\right] \Omega\alpha p = \nabla^2 p \tag{11}$$

Finally, a harmonic plane progressive wave inside the porous material,

$$p = e^{qx} \tag{12}$$

introduced in (11) yields the wavenumber q of the porous material:

$$q^2 = \left[-k_0^2 \frac{\rho_0'}{\rho_0} + ik_0 \frac{\sigma'}{\rho_0 c_0}\right] \Omega\alpha \tag{13}$$

$$q_{1,2} = \pm \left(q_r + iq_i\right) \tag{14}$$

where q_r is the real part of q and q_i is the imaginary part; q_i contributes to wave propagation and q_r to the attenuation; we can also write

$$q_{1,2} = q_0 e^{i\psi_{1,2}} \tag{15a}$$

$$q_0 = \left[\left(k_0^2 \frac{\rho_0'}{\rho_0}\right)^2 + \left(\frac{k_0\sigma'}{\rho_0 c_0}\right)^2\right]^{1/4} (\Omega\alpha)^{1/2} \tag{15b}$$

$$\psi_1 = \frac{1}{2}\left[\pi - \tan^{-1} \frac{\sigma'}{\omega\rho_0'}\right] \tag{15c}$$

$$= \pi/2 - \tan^{-1} \frac{\sigma'}{\omega\rho_0'}$$

$$\psi_2 = \psi_1 - \pi = \frac{\pi}{2} - \frac{1}{2}\tan^{-1}\frac{\sigma'}{\omega\rho_0 r} \qquad (15d)$$

giving

$$q_r = q_0 \cos\psi \qquad (15e)$$

$$q_i = q_0 \sin\psi \qquad (15f)$$

The two wavenumbers q_1 and q_2 are shown in Fig. 1, one wavenumber being associated with plane waves propagating in one direction, the other wavenumber being associated with the opposite direction.

II. SOME NUMERICAL VALUES

A. Critical Frequency

Before solving the wave equation inside the porous material for different boundary conditions, we should examine the values of q_i and q_r for an isotropic porous material, similar to the material used in the porous surface sensors. This material is specified by its specific acoustic resistance r only, the reactance being yet unknown. For the previous designs of the porous strip sensors we had

$$r = \sigma' h$$
$$\cong 50\ \rho_0 c_0$$

where h is the thickness of the porous strip, which is approximately 3 mm. Hence, in cgs units

$$\frac{\sigma'}{\rho_0 c_0} = \frac{50}{0.3} = 166 \ ; \quad \text{cgs units}$$

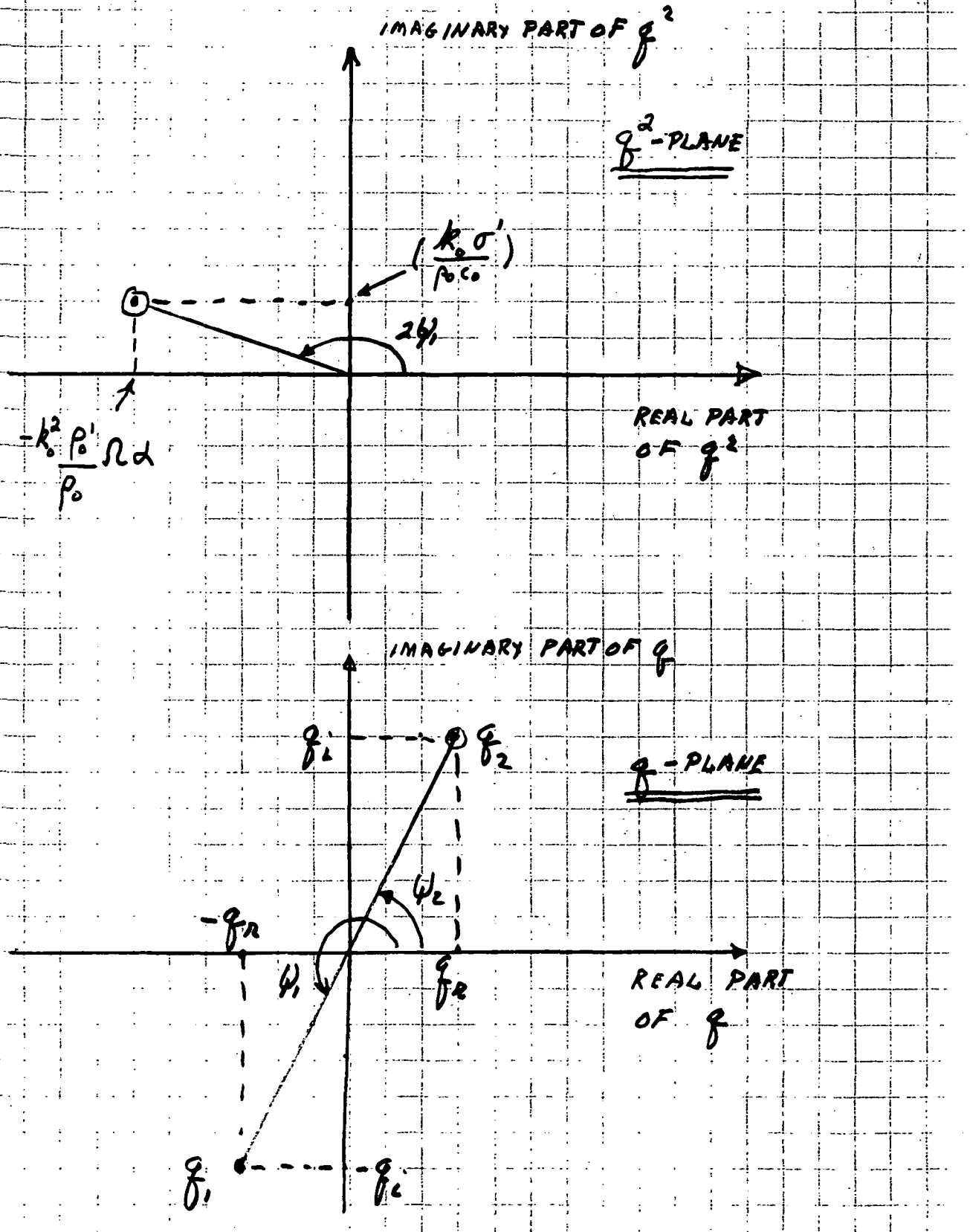

FIG 1: WAVENUMBER $q = q_R + i q_2$

OF AN ISOTROPIC POROUS MATRIAL

This material will behave as purely resistive material if in Eq. (11) the term $-k_0^2 \rho_0'/\rho_0$ associated with the mass of the gas inside the porous material is negligible compared with the term $ik_0 \sigma'/\rho_0 c_0$ associated with the viscosity of the gas:

$$k_0^2 \frac{\rho_0'}{\rho_0} << \frac{k_0 \sigma'}{\rho_0 c_0} \tag{16a}$$

or

$$k_0 << \frac{\sigma'}{c_0 \rho_0'} \tag{16b}$$

$$\omega << \frac{\sigma'}{\rho_0'} \tag{16c}$$

If we further assume that the pores are round, (using Eq. 6b to relate ρ_0' to ρ_0) we get

$$\omega << \frac{3\sigma'}{4\rho_0} \tag{16d}$$

With the numerical values

$$\sigma' = 166\ \rho_0 c_0$$

$$c_0 = 3.4 \times 10^4 \text{ cm/sec}$$

we get

$$f << \frac{3\sigma'}{8\pi\rho_0} = \frac{3 \times 166 c_0}{8\pi}$$

$$<< 5.9 \times 10^5 \text{ Hz}$$

If the frequency f is much less than 600 kHz, the porous material should behave like a purely resistive material under the assumptions that: (1) the porous material is isotropic, (2) the pores are very fine, uniform, circular of extremely small radius a:

$$a < 0.2/\sqrt{f} \text{ cm} \qquad (17)$$

For frequencies up to 10 kHz this criterion gives

$$a < 0.2 \times 10^{-2} \text{ cm}$$

$$< 2 \times 10^{-5} \text{ meter}$$

$$< 20 \text{ microns; } f \leq 10 \text{ kHz}$$

In order to reach the upper limit of 600 kHz the radius a of a pore would have to be less than 2.6 microns.

Whether a real porous material is purely resistive depends on how valid the two assumptions above are. The requirement of the size of a pore in terms of circular pores is only a convenient measure; the actual pores do not have to be circular. Nevertheless, the critical frequency beyond which the reactive part of acoustic impedance becomes important depends very strongly on the "radius" or equivalent radius of the pore; it depends on the inverse square of this "radius". A small increase of radius of the pores or a distribution of pore sizes having a wide range of "radii" would very much lower the value of this critical frequency. This critical frequency can only be obtained by actual measurements of the acoustic impedances of samples of porous materials.

B. Wavenumber q of Purely Resistive Porous Material

In the following Memo No 2 we will examine the effects of the finite thickness of a porous material on its specific acoustic impedance. It is well known that a material, like the ideal fluid which has a purely real characteristic impedance, presents a complex specific acoustic impedance when finite boundaries are imposed. Thus, even if the porous material satisfies the assumptions of negligible reactive component in its bulk properties,

$$\omega << \frac{\sigma'}{\rho'} ,$$

a finite thickness of this porous material can yield a complex specific acoustic impedance.

This analysis will assume that the bulk properties of the porous material has no reactive component, and a finite thickness of this material is analyzed for a specific boundary condition.

As a help for the analysis presented in Memo No 2 we assume a purely resistive porous material and compare its wavenumber q with the wavenumber k_0 of the free gas. Returning to Eq. (13) we get by neglecting the first term

$$q = \pm (1+i) \left[\frac{k_0 \sigma'}{2\rho_0 c_0} \Omega\alpha \right]^{1/2} \qquad (18a)$$

$$= \pm (q_r + iq_i) \qquad (18b)$$

$$\frac{q_i}{k_0} = \frac{q_r}{k_0} = \left[\frac{\sigma' \Omega\alpha}{2k_0 \rho_0 c_0} \right]^{1/2} \qquad (18c)$$

The real or imaginary part of q increases as the square root of frequency.

Numerical values of q_i are shown in Fig. 2 and compared with k_0, for the porous material used in the porous strip sensors:

$$\frac{\sigma'}{\rho_0 c_0} = \frac{50}{h}$$

$$h = 1.5 \text{ mm}$$

$$\Omega = 0.2$$

$$\alpha = 1.4$$

The porosity Ω has been estimated from the density of the porous material, which is about 80% of the density of the solid.

$$q_i = \left[\frac{\sigma'}{\rho_0 c_0} \frac{\Omega \alpha k_0}{2}\right]^{1/2}$$

$$= 9.3 \times 10^{-2} \sqrt{f} \text{ , cm}^{-1}$$

$$k_0 = 1.85 \times 10^{-4} f \text{ ; cm}^{-1}$$

Figure 2 shows that the wavenumber q_i, of the ideal porous material is larger than the wavenumber k_0 of the free gas, in the frequency range up to 200 kHz; at 10 kHz the ratio is almost 5. It follows that the phase velocity in the porous material is not greater than approximately one fifth the phase velocity in air, at frequencies less than 10 kHz. The condition that a porous plate be "thin" compared to a wavelength, requires that its thickness be no more than approximately one fifth of what would be required for a sheet of "air". The criterion for the thickness of the porous

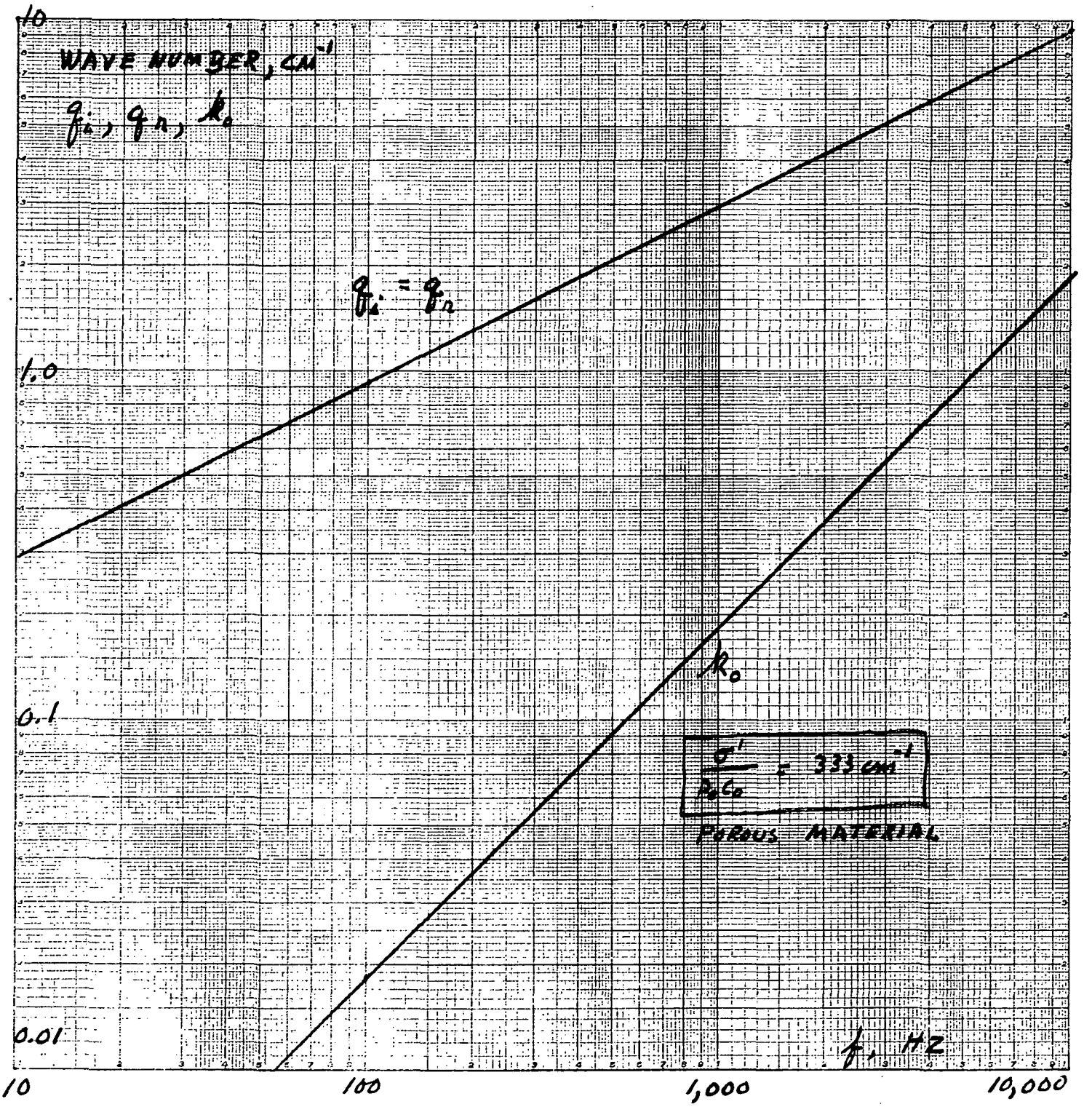

FIG. 2: WAVENUMER COMPONENTS, q_i, q_n OF AN IDEAL POROUS MATERIAL, AND k_o OF AIR.

material, whatever that criterion will be, will have to be satisfied only at the highest frequency of interest, because the wavelength in the porous material is inversely proportional to the square root of frequency.

APPENDIX II

SPECIFIC ACOUSTIC ADMITTANCE OF A PURELY RESISTIVE POROUS MATERIAL IN A THIN, RIGID SHEET

This memo describes the properties of a purely resistive porous material in thin sheets. It will be shown that the specific acoustic admittances of these sheets become complex at sufficiently high frequencies.

The results are useful for the evaluation of the specific acoustic admittances of samples of real porous sheets; they will also be used later to explain the drop in frequency response of a porous surface sensor, due to the porous material itself.

We assume that the porous material is purely resistive, in the sense that the mass reaction associated with the effective density ρ_o' of the gas in a pore is negligible compared with the viscous force. The porous material is a flat sheet of thickness h; a plane acoustic wave is applied to its outer face as shown in Fig. 1. The porous sheet will be characterized by the specific admittances y_{11} and y_{12} defined:

$$y_{11} = \left.\frac{u_1}{P_1}\right|_{P_2=0} \tag{1}$$

$$y_{12} = \left.\frac{u_2}{P_1}\right|_{P_2=0} \tag{2}$$

These admittances will be a function of the angle of incidence of the applied plane wave.

The direction of incidence of the plane wave, given by the angle θ, is kept general. Later the results will specialized to two cases: grazing incidence, $\theta=0$, corresponding to situation specified for the frequency response of the Porous Strip sensor; normal incidence, $\theta = \pi/2$, corresponding tc the test set up which will measure the admittances of samples of different porous materials.

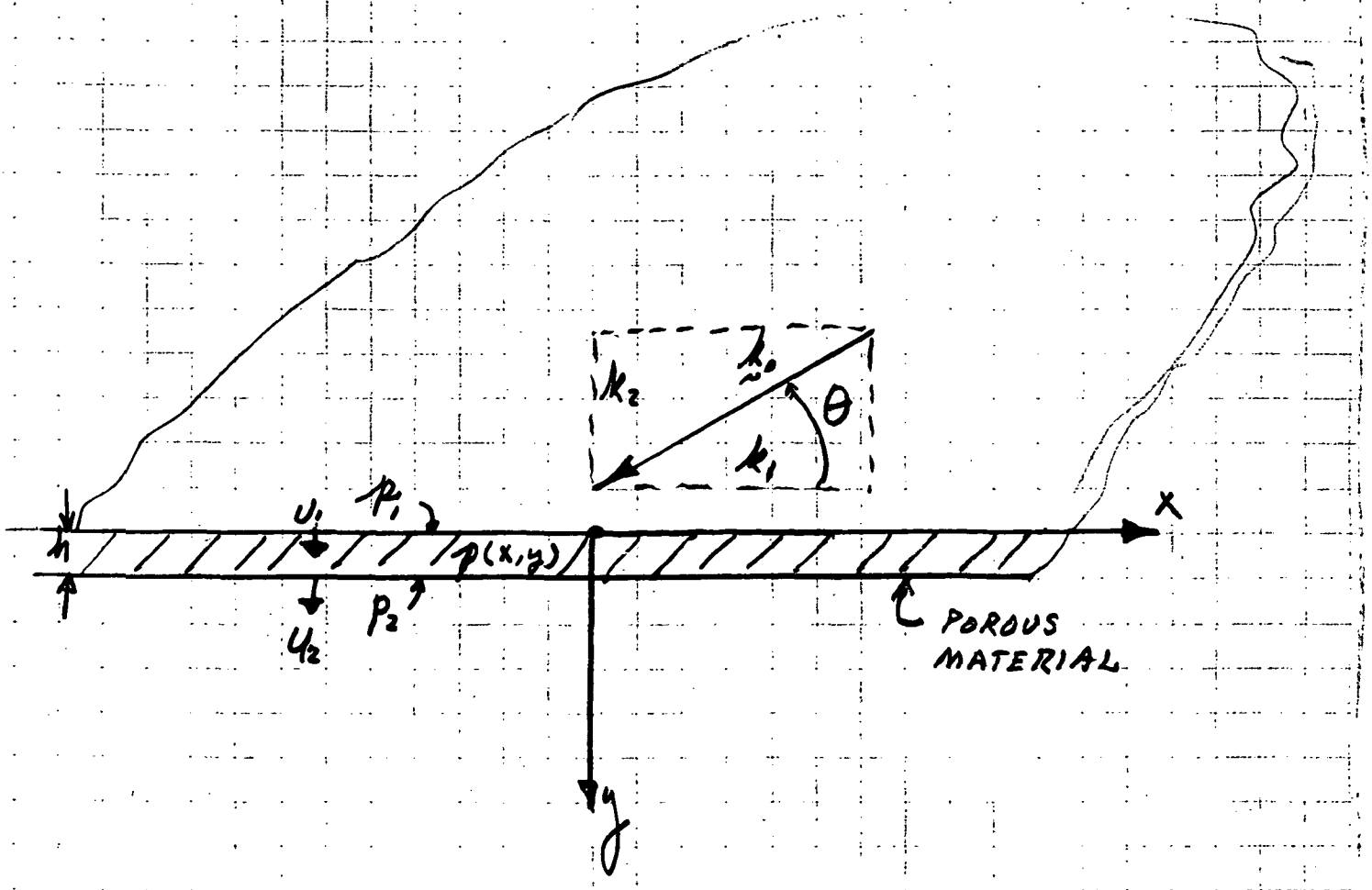

FIG-1- PLANE WAVE APPLIED TO A SHEET OF POROUS MATERIAL

When the mass reaction caused by the effective density ρ_o' of the gas inside a pore is neglected, the wave equation in the porous material reduces to the equation of diffusion. For the harmonic case, Eq. (11) of Appendix I reduces to

$$q_o^2 \, p = \nabla^2 p \tag{3}$$

where

$$q_o^2 = \frac{ik_o \sigma' \Omega \alpha}{\rho_o c_o} \tag{4}$$

is the square of the wavenumber q_o in a purely resistive porous material. The momentum equation (5) of Memo No. 1 reduces to

$$\sigma' \, \underset{\wedge}{u} = -\text{grad } p \tag{5}$$

We assume that a plane progressive wave is incident upon the porous surface, with free field pressure

$$P_o \, e^{i(k_1 x - k_2 y)} \quad ;$$

upon reflection on the porous surface, the pressure p_1 on the surface has the form

$$p_1(x,o) = P_1 \, e^{ik_1 x} \tag{6a}$$

where

$$k_1 = k_o \cos \theta \tag{6b}$$

and θ is the angle of incidence measure with respect to the plane of the porous surface.

The pressure $p(x,y)$ inside the porous material will have the form

$$p(x,y) = P(y)\, e^{ik_1 x} \tag{7}$$

where P(y) is a function of the distance y from the porous surface; the x dependence is the same as the applied pressure p_1: this is imposed by the continuity of normal velocity u_1 at the surface y = 0.

Introducing (7) in (3)

$$(q_o^2 + k_1^2)\, P(y) = \frac{\partial^2 P(y)}{\partial y^2} \tag{8}$$

and letting

$$P(y) = A\, e^{\gamma y} \tag{9}$$

in (8) we find the wavenumber γ in the y direction:

$$\gamma^2 = (q_o^2 + k_1^2) \tag{10a}$$

$$\gamma = \pm \left[i\, \frac{k_o \sigma' \Omega \alpha}{\rho_o c_o} + k_1^2 \right]^{\frac{1}{2}} . \tag{10b}$$

The general form of p(x,y) becomes

$$p(x,y) = (A_1 e^{\gamma y} + A_2 e^{-\gamma y})\, e^{ik_1 x} \tag{11}$$

Eq. (11) together with (5) will now be solved for the pressures at the boundaries, y = 0, y = h, specified for y_{11} and y_{12} in Eqs. (1) and (2).

From the boundary conditions

$$p(x,o) = P_1 \tag{12a}$$

$$p(x,h) = 0 \tag{12b}$$

we obtain

$$P_1 = A_1 + A_2 \tag{13a}$$

$$0 = A_1 e^{\gamma h} + A_2 e^{-\gamma h} \tag{13b}$$

yielding

$$A_1 = P_1/[1 - e^{2\gamma h}] \tag{14a}$$

$$A_2 = -P_1 e^{2\gamma h}/[1-e^{2\gamma h}] \tag{14b}$$

and

$$p(x,y) = P_1 \left[\frac{e^{\gamma y} - e^{-\gamma(y-2h)}}{1 - e^{2\gamma h}} \right] e^{ik_1 x} \quad . \tag{15}$$

The velocity u_y is obtained from (5) and (15)

$$u_y = \frac{-P_1 \gamma}{\sigma'} \frac{[e^{\gamma y} + e^{-\gamma(y-2h)}]}{1 - e^{2\gamma h}} e^{ik_1 x} \quad . \tag{16}$$

Using the notation

$$u_1 = u_y(o) \tag{17a}$$

$$u_2 = u_y(h) \tag{17b}$$

we find y_{11} and y_{12} of Eqs. (1) and (2) using (16) and (17):

$$y_{11} = \frac{-\gamma}{\sigma'} \frac{1 + e^{+2\gamma h}}{1 - e^{2\gamma h}}$$

$$= \frac{\gamma}{\sigma'} \coth(\gamma h) \tag{18}$$

$$y_{12} = \frac{-\gamma}{\sigma'} \frac{e^{\gamma h} + e^{+\gamma h}}{1-e^{2\gamma h}}$$

$$= \frac{\gamma}{\sigma'} \frac{1}{\sinh(\gamma h)} \tag{19}$$

where γ is given by (10b).

The basic results (18) and (19) will be examined in details. However we already have the anticipated result that y_{11} and y_{12} are in general complex because γ is complex; again, these results apply to a purely resistive porous material.

1. Low frequencies: $|\gamma h| << 1$

For small values of the arguments of the sinh and tanh the following approximations are used:

$$\sinh(\gamma h) \cong \gamma h + \frac{(\gamma h)^3}{3!} \ldots\ldots \tag{20a}$$

$$\tanh(\gamma h) \cong \gamma h \frac{\left[1 + \frac{(\gamma h)^2}{3!} \ldots\right]}{\left[1 + \frac{(\gamma h)^2}{2!} \ldots\ldots\right]}$$

$$\cong \gamma h \left(1 + \frac{(\gamma h)^2}{3} \ldots.\right)^{-1} \qquad (20b)$$

Keeping only the leading term of the series expansions we get

$$y_{11} = \frac{\gamma}{\sigma'} \frac{1}{\gamma h} \qquad (21a)$$

$$= \frac{1}{r} \qquad (21b)$$

where r is the specific acoustic resistance of the porous sheet at low frequencies:

$$r = \sigma' h \quad . \qquad (21c)$$

Similarly

$$y_{12} = y_{11} = \frac{1}{r} \qquad (22)$$

Eqs. (21b) and (22) are the low frequency approximations of the specific acoustic admittances of a thin porous sheet. The admittances are real and the time delay in transmission through the sheet is negligible.

2. Intermediate Frequencies: $|\gamma h| < 1$

At intermediate frequencies where the argument $|\gamma h|$ of sinh and tanh is still small, but not very small, we introduce the second term of the series expansions (20a) and (20b); we obtain

$$y_{11} = \frac{1}{r}\left[1 + \frac{(k_1 h)^2}{3} + i\,\frac{k_o h}{3}\left(\frac{r}{\rho_o c_o}\right)\Omega\alpha \ldots\right]^{-1}, \qquad (23a)$$

$$y_{12} = \frac{1}{r}\left[1 + \frac{(k_1 h)^2}{6} + i\,\frac{k_o h}{6}\left(\frac{r}{\rho_o c_o}\right)\Omega\alpha \ldots\right]^{-1}, \qquad (23b)$$

Both y_{11} and y_{12} become complex.

In the frequency range of interest, $f \leq 10$ kHz, and for the thin porous sheets used in the Porous Strip Sensors ($h = 0.3$ cm) the second term in each bracket is almost negligible:

$$\frac{(k_1 h)^2}{6} < \frac{(k_o h)^2}{6} = 0.5 \quad \text{at} \quad 10 \text{ kHz, for } y_{12}\,.$$

The third term, which makes the admittances complex become significant if

$$k_o h \geq \frac{3}{\frac{r}{\rho_o c_o}\Omega\alpha}\,; \qquad \text{for } y_{11} \qquad (24a)$$

$$k_o h \geq \frac{6}{\rho_o c_o \Omega\alpha}\,; \qquad \text{for } y_{12} \qquad (24b)$$

when the equality is met, the phase in y_{11} and y_{12} is $\pi/4$. The following example illustrates this mid-frequency range:

Consider a porous sheet similar to those used in the Porous Strip Sensors:

$$\frac{r}{\rho_o c_o} = 50$$

$$\Omega = 0.2$$

$$\alpha = 1.4$$

$$h = 1.5 \text{ mm}$$

then the critical frequency f_c for a phase shift of $\pi/4$ is

$$f_c = 8.3 \text{ kHz} \quad \text{for} \quad y_{11}$$

$$f_c = 16.6 \text{ kHz} \quad \text{for} \quad y_{12} \quad .$$

The phase shift in y_{11} is not significant because it affects only the pressure reflection coefficient at the surface of the porous material; for $r/\rho_o c_o >> 1$, this reflection coefficient remains very close to unity.

The phase shift in y_{12} is more important because y_{12} inters directly in the design equations of a porous surface sensor. We note that the admittance y_{12} has a reactive component simulating a mass reactance, although the porous material itself has been assumed to be purely resistive. For the example given above the phase shift of y_{12} is approximately 30^o at 10 kHz; the reactive part, in this example, is not negligible and it will affect the frequency response of a porous surface sensor.

The angle of incidence θ of the plane wave appears only in the x component k_1 of the acoustic wavenumber vector $\underset{\sim}{k}_o$. At intermediate frequencies, we have shown in the example that the term involving k_1 can be neglected for frequencies up to at least

10 kHz. It follows that y_{11} and y_{12} of porous examples could be measured at normal incidence, $\theta = \pi/2$, in a test jig and the results applied to all angles of incidence, provided $h \leq 0.3$ cm.

A thinner sheet (smaller value of h) for the same value of r would give a smaller value of the reactive parts of y_{11} and y_{12}. This is shown by examining the product Ωh in (23a) and (23b) where Ω as well as h would decrease: Ω decreases because the porous material will have to be slightly less porous to achieve the same value of r in a thinner sheet.

The range of intermediate frequencies is obviously the most interesting range for application to a porous surface sensor.

The high frequency range, which is examined next, is included only for compleness.

3. High Frequencies: $|\gamma h| >> 1$

At high frequencies the assumption of a purely resistive porous material may not be valid. Accepting nevertheless this assumption and using the results of (18) and (19) for y_{11} and y_{12}, and further realizing that the wavenumber γ has a large real part, it follows that

$$\tanh(\gamma d) \rightarrow 1 \quad ; \quad [\text{real part of } \gamma d] >> 1 \qquad (25a)$$

$$\sinh(\gamma d) \rightarrow e^{\gamma d}/2 ; \quad [\text{real part of } \gamma d] >> 1 \qquad (25b)$$

and we obtain

$$y_{11} = \frac{\gamma}{\sigma'} \quad ; \quad |\gamma d| >> 1 \qquad (26a)$$

$$y_{12} = 2y_{11}e^{-\gamma d} \quad ; \quad |\gamma d| >> 1 \qquad (26b)$$

where γ is still given by Eq. (10b). This expression for γ could vary drastically depending on the angle of incidence θ which is included in k_1. At normal incidence, $k_1 = 0$, we get

$$\gamma = (1 + i)\left[\frac{k_o \sigma' \Omega \alpha}{2\rho_o c_o}\right]^{\frac{1}{2}}$$

with equal real and imaginary parts to y_{11}; y_{12} has the factor $e^{-\gamma d}$ which represents a strong attenuation as well as a large delay in transmission; thus the transfer admittance y_{12} is indeed a complex quantity.

At grazing incidence, $k_1 = k_o$, the acoustic wavenumber k_o will dominate the wavenumber γ. Refering to the curve of q_o and k_o given in Fig. 2 of Appendix I, we see for the example of material and for this calculation, that this effect starts at a frequency above 20 kHz. From Eq. (10b), at grazing incidence, $k_1 = k_o$, we get, at high frequencies,

$$\gamma = \pm k_o$$

a real wavenumber. Hence at grazing incidence and high frequencies y_{11} and y_{12} become real again.

It follows that a test of y_{11} and y_{12}, at normal incidence at high frequencies, would not be applicable to y_{11} and y_{12} at grazing incidence. This conclusion is irrelevant because we do not intend at this time to investigate porous materials at frequencies very much higher than 10 kHz. If we were to use higher frequencies, it is very clear that the thickness be of the porous material would have to be much smaller than the value, $h = 0.3$ cm, used in the present designs of Porous Surface sensors.

CONCLUSIONS

The conclusions of this analysis have already been made at each step.

We emphasize again that all the preceeding results apply to a purely resistive porous material. Hence these results of y_{11} and y_{12} represent limiting values in the sense that real porous materials with the same value $r/\rho_o c_o$ will have higher impedances and higher reactive parts due to the contribution of the mass reactance of the gas in the pores.

APPENDIX III

SPECIFIC ACOUSTIC ADMITTANCE OF A PURELY RESISTIVE POROUS MATERIAL IN A THIN, RIGID SHEET (Continued)

This memo is a continuation of Appendix 2. The normalized admittances $y_{11}\ r$ and $y_{12}\ r$ of an ideal porous material in thin sheets are calculated for normal incidence as a function of a generalized frequency parameter β. These curves of $y_{11}\ r$ and $y_{12}\ r$ will be compared in Appendix 5 with the values measured for real porous materials.

I. Normalized Admittances

The admittances of an ideal porous material have been formulated in Appendix 2. The ideal porous material has been defined as a porous material where the mass reactance of the gas is negligible compared with the resistance. The specific admittances y_{11}, y_{12} are given by Eqs. (18 and 19) of Appendix 2:

$$y_{11}\ r = \frac{\gamma h}{\tanh(\gamma h)} \tag{1a}$$

$$y_{12}\ r = \frac{\gamma h}{\sinh(\gamma h)} \tag{1b}$$

where r is the specific acoustic resistance of the ideal material obtained at low frequencies and h is its thickness; γ is the complex wavenumber of the ideal porous material given by Eq. (10b) of Memo No. 2:

$$\gamma = \pm\left[\frac{ik_0\sigma'\Omega\alpha}{\rho_0 c_0} + k_1^2\right]^{\frac{1}{2}} \tag{2}$$

k_1 being the wavenumber component along the surface of the porous material for a plane wave excitation. In this memo we are considering a plane wave incident normally on the surface of the sample; hence $k_1 \equiv 0$. Under this condition the product γh becomes

$$\gamma h = (1+i)\beta \tag{3a}$$

$$\beta = \left[\frac{k_0 \sigma' \Omega \alpha}{2\rho_0 c_0} h^2\right]^{\frac{1}{2}}$$

$$= \left[\frac{k_0 h}{2} \left(\frac{r}{\rho_0 c_0}\right) \Omega\alpha\right]^{\frac{1}{2}} \tag{3b}$$

Therefore y_{11} and y_{12} can be written:

$$y_{12}\, r = \frac{(1+i)\beta}{\sinh[(1+i)\beta]} \tag{4a}$$

$$= \frac{(1+i)\beta}{\cos\beta \sinh\beta + i \sin\beta \cosh\beta}$$

$$y_{11}\, r = (1+i)\beta \frac{\cos\beta \cosh\beta + i \sin\beta \sinh\beta}{\cos\beta \sinh\beta + i \sin\beta \cosh\beta} \tag{4b}$$

Both $y_{11}\, r$ and $y_{12}\, r$ become real and equal to unity when $\beta << 1$ corresponding to low frequencies.

The asymptotic values of $y_{12}\, r$ and $y_{11}\, r$, for $k_1^2 = 0$, (see Eq. (26) of Appendix 1) become

$$y_{12}\, r = 2(1+i)\beta\, e^{-\beta}\, e^{-i\beta} \tag{5a}$$

$$y_{11}\, r = (1+i)\beta \tag{5b}$$

The modulus and phase of $y_{11}\, r$ and $y_{12}\, r$ have been calculated as a function of β and are shown in Figs. 1a, 1b and 2 as a function of β^2. The transformation to β^2 makes the abscissa proportional to frequency. The curves are used to plot $y_{11}\, r$ or $y_{12}\, r$ as a function

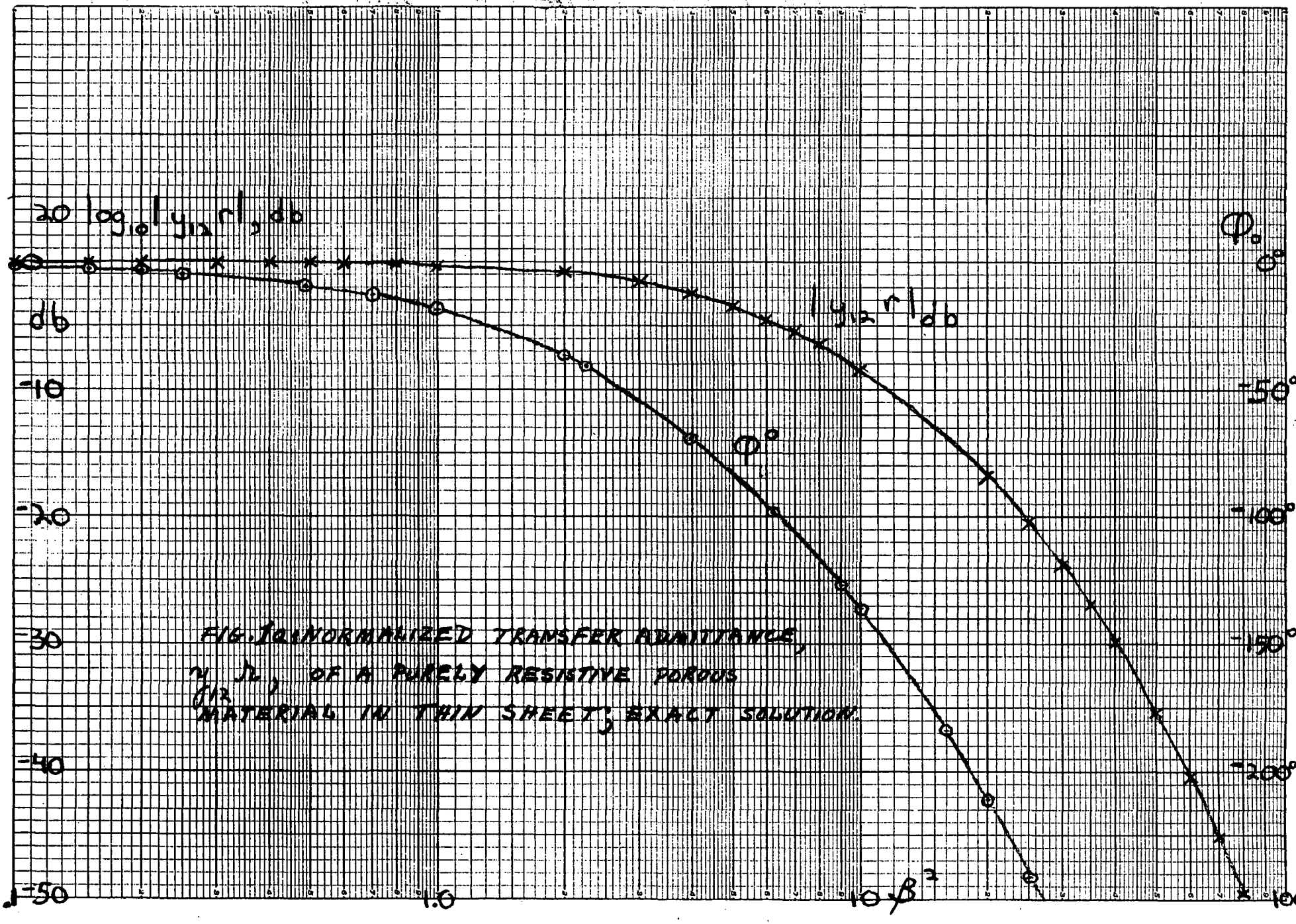

FIG. 1a NORMALIZED TRANSFER ADMITTANCE, y_{12} (β), OF A PURELY RESISTIVE POROUS MATERIAL IN THIN SHEET, EXACT SOLUTION.

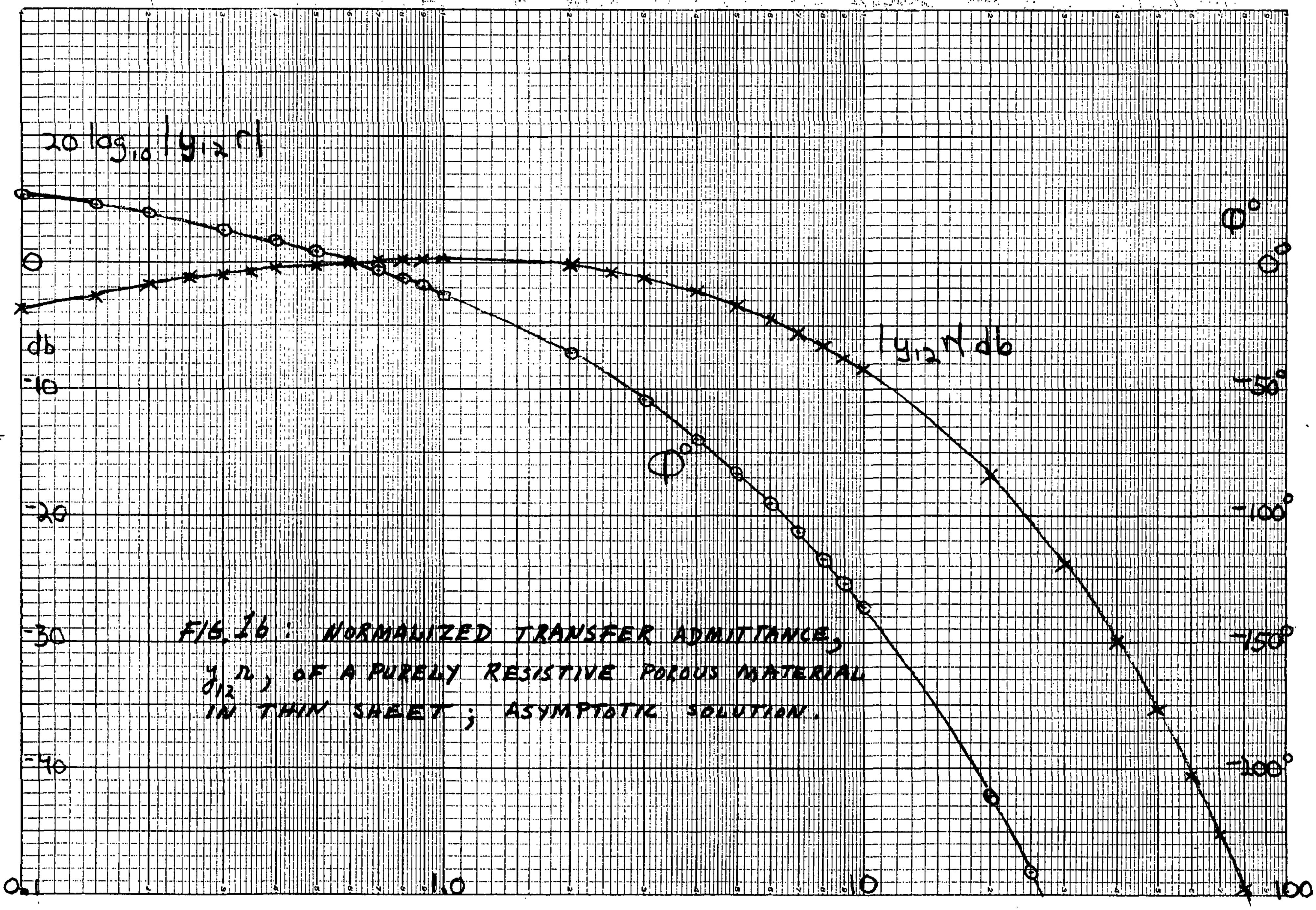

FIG. 1b: NORMALIZED TRANSFER ADMITTANCE, $y_{12}r$, OF A PURELY RESISTIVE POROUS MATERIAL IN THIN SHEET; ASYMPTOTIC SOLUTION.

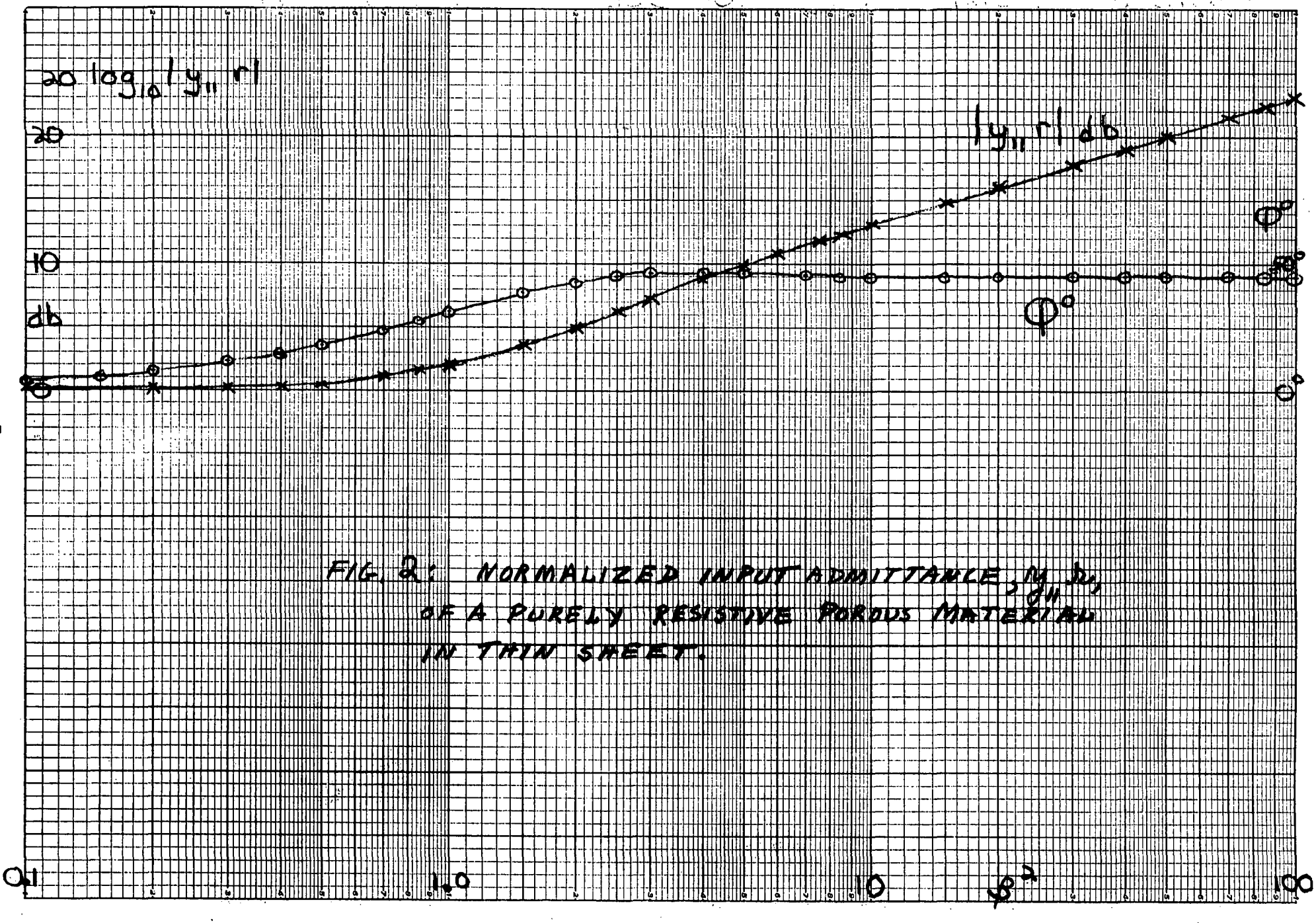

FIG. 2: NORMALIZED INPUT ADMITTANCE, y_{11}, OF A PURELY RESISTIVE POROUS MATERIAL IN THIN SHEET.

of frequency for a material specified by h, $r/\rho_0 c_0$, and the porosity Ω. Comparing the exact values and the asymptotic values of y_{12} r we find that they are very nearly equal for $\beta \geq 1$.

II. Isothermal Process

The calculations given in the first part assume an isothermal process inside the porous material: this is represented by the factor α in γ, where $\alpha = 1.4$ for air. This assumption is valid at low frequencies; the process will gradually change to an idiabatic one at sufficiently high frequencies. The center frequency f_c below which the process is isothermal, and the correction to be applied in the transition region of frequency, has been investigated by Daniels[1], as reported by Beranek[2]; the frequency f_c, for a closed cavity, is given by

$$f_c = \left(\frac{S}{KV}\right)^2 \qquad (6)$$

where S is the surface of the cavity, V is its volume, in cgs units; for air K = 3.89.

This result is applied to a porous material by assuming that it is made of a bundle of small tubes, of radius "a". For each tube, of length much larger than the radius, we get from (6)

$$f_c = \left(\frac{2}{Ka}\right)^2 \qquad (7)$$

---

[1] F.B. Daniels, "Acoustic Impedance of Enclosures", JASA, 19, pp 569-571, (1947).

[2] L.L. Beranek, "Acoustic Measurements", John Wiley & Sons, 1949, pp 143-147.

A capillary tube of radius a = 10 microns, gives

$$f_c \cong 250 \text{ kHz}$$

For the types of porous materials considered in the design of a porous strip sensor, the effective radius of the pores is of the order of 10 microns. Hence, the process of wave propagation inside the porous material will remain isothermal for frequencies beyond 10 kHz.

III. Flow Noise

The analysis of Appendix 2, is directly applicable to the case where the excitation is a plane wave and has *any* wavenumber component k_1 along the surface of the porous material. By not restricting k_1 to correspond to a sonic excitation,

$$k_1 \neq k_0 \cos\theta$$

the results of y_{11} and y_{12} remain general, provided the wavenumber component γ includes k_1, as already indicated in Eq. 10b of Appendix 2.

For subsonic noise, like flow noise, the wavenumber spectrum of the noise, is maximum in the region:

$$k_1\Big|_{max} \cong \omega/U = k_0/M$$

where M is the Mach number of the flow; hence k_1 can be much larger than k_0 and could easily be larger than $|q_0|$; (see Eq. 4 of Appendix 2).

When $k_1 \geq |q_0|$ the value of γ, will have a larger real part, and the transfer admittance y_{12} will decrease faster as a function of γ, than for the sonic case (where k_1 can be neglected). It follows that the finite thickness of the porous material is beneficial in providing an extra attenuation of the flow noise in a Porous Surface Sensor, beyond the attenuation provided by the line sensor itself, when $k_1 \geq q_0$. This extra attenuation of flow noise is realized only at high frequencies and/or at very low Mach numbers. An examination of the chart of Fig. 2 of Appendix 1, indicates that, at M = 0.1, the equality of $k_1|_{max}$ and k_0 occurs at 2.8 kHz; it follows that at M = 0.1 and at frequencies near 2.8 kHz and higher, the flow noise rejection of a porous strip sensor should be greater than the flow noise rejection predicted by a uniform line sensor.

APPENDIX IV

TEST SETUP FOR MEASURING THE TRANSFER ADMITTANCE OF POROUS MATERIALS IN THIN, RIGID SHEETS

This appendix describes the experimental setup and presents the calculation format for obtaining the transfer admittance y_{12} of a porous material in thin sheets.

I. Formulation of the Experiment

The test setup consists basically of an acoustic source which applies a pressure P_1 at the surface of a porous disc and measures the pressure transmitted through the porous disc and into a closed cavity. The pressure P_1 is monitored and the pressure P_3 at the back of the cavity is measured; see Fig. 1. The diameter of the porous sample and of the cavity are the same; therefore only the specific admittances of the sample and of the cavity enter in the formulation.

The calculation format assumes that only plane waves propagating along the axial direction of the setup are present. Radial wave components are possible at high frequencies; however it will be shown later in this appendix, that radial wave components are not excited to a significant degree, for frequencies up to approximately 10 kHz.

The test setup is characterized by the following equations. The porous sample is specified by the general equations:

$$u_1 = y_{11} P_1 - y_{12} P_2 \tag{1}$$

$$-u_2 = -y_{12} P_1 + y_{11} P_2 \tag{2}$$

where u_1, u_2 are the acoustic velocities at the faces 1 and 2 of the porous disc, P_1, P_2 are the acoustic pressures; the test sample is assumed to be symmetrical:

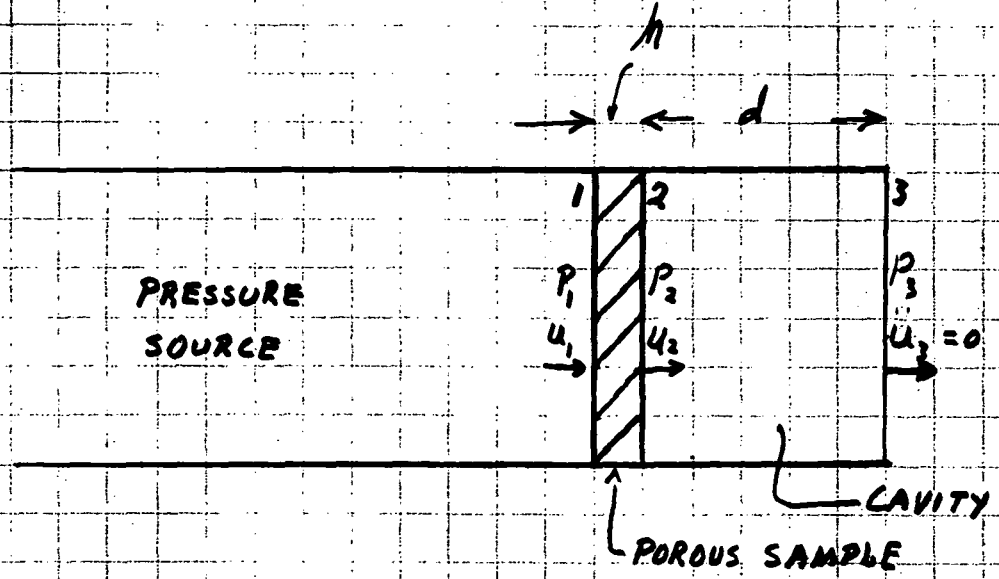

FIG. 1 : ACOUSTIC SYSTEM

$$y_{11} = y_{22} \tag{3a}$$

$$y_{21} = y_{12}$$

The specific admittances y_{11} and y_{12} of an isotropic porous material, have been examined in Appendix 2.

The acoustic cavity is characterized by

$$u_2 = y_c P_2 \tag{4}$$

$$P_3 = T P_2$$

where

$$y_c = \frac{i}{\rho_0 c_0} \tan (k_0 d) \tag{6}$$

$$T = [\cos(k_0 d)]^{-1} \tag{7}$$

and k_0 is the acoustic wave number of air, and d is the depth of the cavity.

We solve for the ratio P_3/P_1 by introducing (4) and (5) in (2), giving:

$$\frac{P_3}{P_1} = T \frac{y_{12}}{y_{11} + y_c} \tag{8}$$

At low frequencies, (see Appendix 2),

$$y_{11} = y_{12} = \frac{1}{r} \quad ; \quad \text{low frequencies} \tag{9a}$$

$$y_c = \frac{ik_0 d}{\rho_0 c_0} \quad ; \quad \text{low frequencies} \tag{9b}$$

$$T = 1 \quad ; \quad \text{low frequencies} \tag{9c}$$

where r is the specific resistance of the porous sample; therefore (8) becomes

$$\frac{P_3}{P_1} = \left[1 + ik_0 d \frac{r}{\rho_0 c_0}\right]^{-1} \quad ; \text{ low frequencies} \qquad (10a)$$

$$= \left[1 + i\omega \frac{d}{c_0}\left(\frac{r}{\rho_0 c_0}\right)\right]^{-1} \quad ; \text{low frequencies} \qquad (10b)$$

The ratio P_3/P_1 drops as sketched in Fig. 2, the break frequency, ω_{low}, being

$$\omega_\ell = \frac{c_0}{d}\left(\frac{\rho_0 c_0}{r}\right) \qquad (10c)$$

At high frequencies, $\omega >> \omega_\ell$ the admittance y_c of the cavity will become much larger than the self admittance y_{11} of the porous sample:

$$|y_{11}| << |y_c| \quad ; \quad \text{high frequencies;} \quad k_0 d < \pi/2 \qquad (11)$$

and the ratio P_3/P_1 becomes

$$P_3/P_1 = T \frac{y_{12}}{y_c} \quad ; \quad \text{high frequencies;} \quad k_0 d < \pi/2 \qquad (12a)$$

$$P_3/P_1 = \frac{y_{12}\rho_0 c_0}{i\, k_0 d} \times \left[\frac{k_0 d}{\sin k_0 d}\right] ; \text{ high frequency} \qquad (12b)$$

The pressure ratio, for y_{12} real and constant decreases inversely with frequency. The factor $[k_0 d/\sin k_0 d]$ is a correction for the depth d of the cavity; this correction affects only the modulus and not the phase of P_3/P_1 provided that the depth of the cavity is less than a half wavelength: $k_0 d < \pi$. When y_{12} is not real the response P_3/P_1 deviates from the ideal response shown in Fig. 2.

The normalized value $y_{12}\rho_0 c_0$ of a porous example is calculated from the measured value of P_3/P_1.

At low frequencies, we obtain the low frequency value of $y_{12}\rho_0 c_0$ from Eq. 10b:

$$\left[y_{12}\rho_0 c_0\right]^{-1} = \frac{r}{\rho_0 c_0} = \frac{\left(P_1/P_3\right) - 1}{ik_0 d} \quad ; \tag{13a}$$

a frequency ω is chosen above the break frequency ω_ℓ, $\omega > \omega_\ell$, where $P_3/P_1 << 1$; ω must not be too high in order that the low frequency approximation remains valid; for these conditions we get

$$\left[y_{12}\rho_0 c_0\right]^{-1} = \frac{r}{\rho_0 c_0} \cong \frac{\left|P_1/P_3\right|}{k_0 d} \tag{13b}$$

This value is used also to calculate the break frequency ω_ℓ, from (10c). The value of ω_ℓ will be needed in calculating the phase of $y_{12}\rho_0 c_0$.

At high frequencies, the value of $y_{12}\rho_0 c_0$ is calculated from (12b); the modulus is

$$\left|y_{12}\rho_0 c_0\right| = k_0 d \left|\frac{P_3}{P_1}\right| \frac{\sin k_0 d}{k_0 d} \quad ; \tag{14}$$

The calculation is simplified by noting that

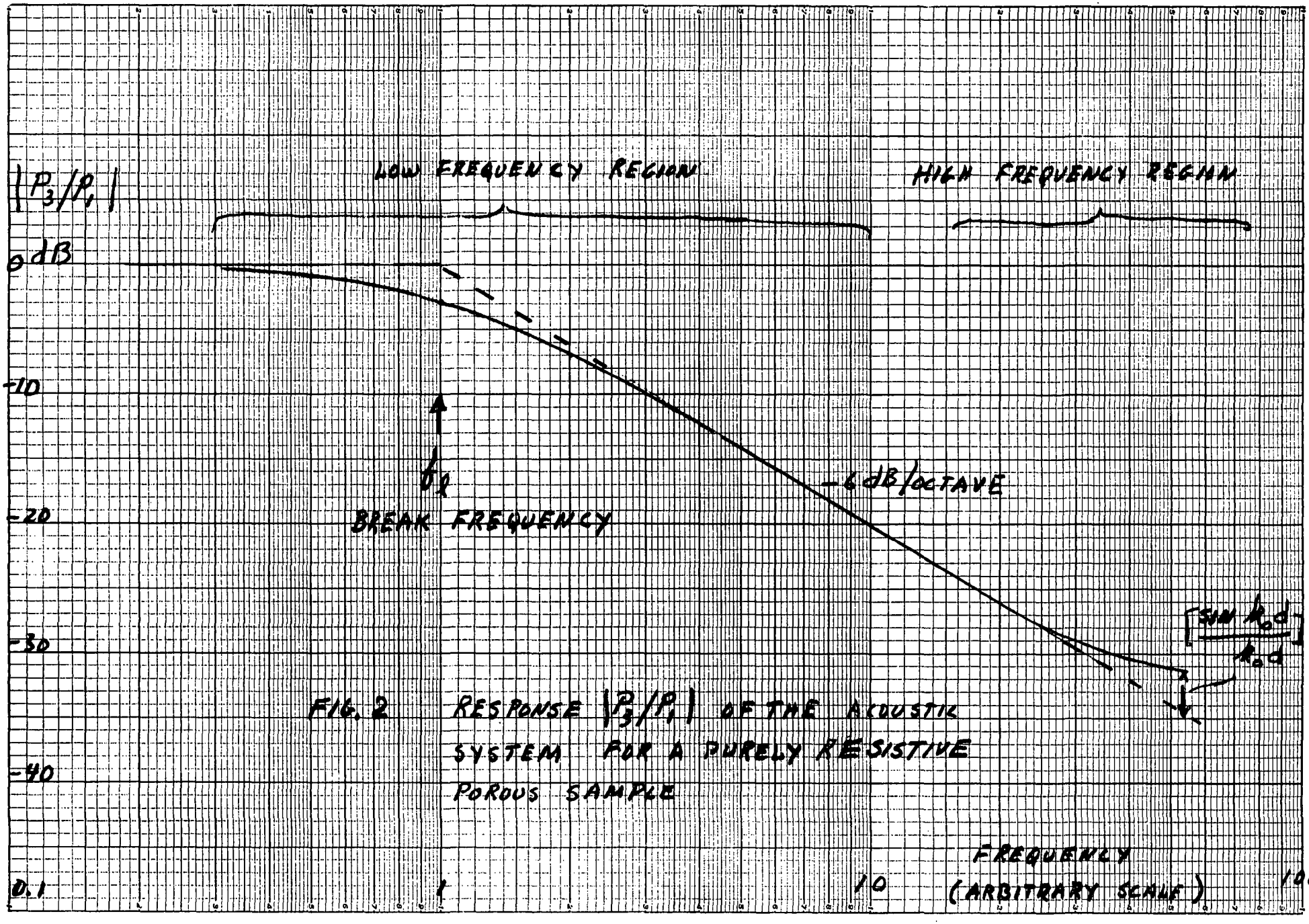

FIG. 2 RESPONSE $|P_3/P_1|$ OF THE ACOUSTIC SYSTEM FOR A PURELY RESISTIVE POROUS SAMPLE

$$[k_0 d|P_3/P_1|]^{-1}$$

corresponds to the low frequency value of $y_{12}\rho_0 c_0$; see Eq. (13b); it follows that the value of $y_{12}\rho_0 c_0$, is the difference, in dB, between the low frequency response $|P_3/P_1|$ *extended* to high frequencies, and the values P_3/P_1 measured at high frequencies. This procedure is illustrated in Fig. 3, where the correction $[\sin(k_0 d)]/k_0 d$, dictated by (14), has also been made.

During a test the pressure P_1 is maintained constant. The microphones measuring P_1 and P_3 need not have a known sensitivity, provided the ratio of their sensitivities is constant or is corrected for changes in sensitivities as a function of frequency. Since P_3 always appears in the ratio P_3/P_1, and P_3/P_1 tends to unity at $\omega << \omega\ell$, P_3 can be arbitrarily set to unity at low frequencies. This is done systematically in Fig. 3.

The phase angle ϕ of y_{12} is calculated from the measured phase of P_3/P_1, as follows:

First, the phase of P_3/P_1 is corrected for phase differences in the microphones and their electronics; the result is then compared with the phase associated with a purely real y_{12}, as shown in Fig. 4; this latter phase is calculated for the known value of the break frequency, f_ℓ, of the particular sample and test setup.

The final results for $y_{12}\rho_0 c_0$ of a given porous sample consist of

$r/\rho_0 c_0$,

$|y_{12} r|$ as a function of frequency,

ϕ as a function of frequency.

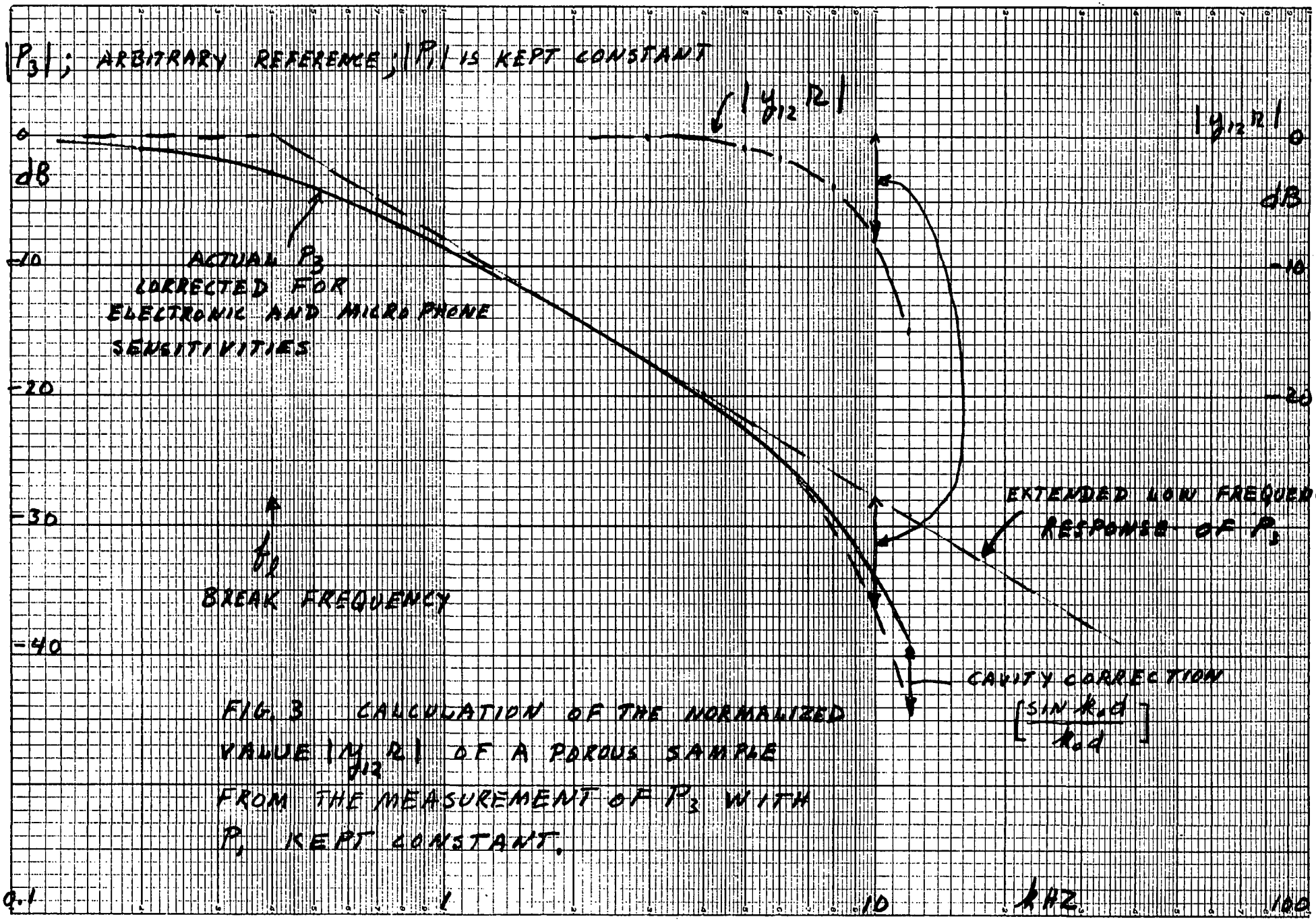

FIG. 3 CALCULATION OF THE NORMALIZED VALUE $|y_{12}R|$ OF A POROUS SAMPLE FROM THE MEASUREMENT OF P_3 WITH P_1 KEPT CONSTANT.

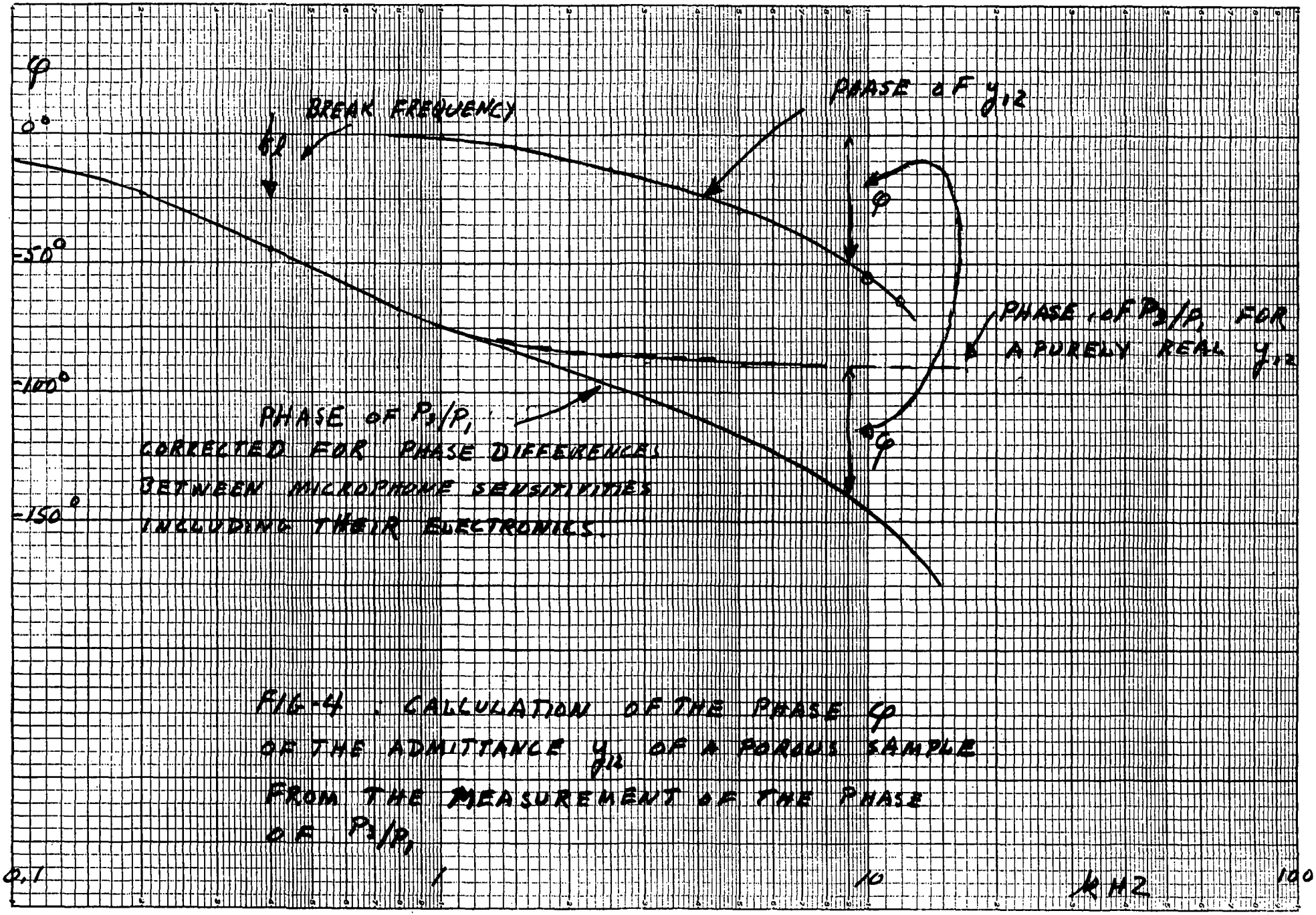

FIG-4 . CALCULATION OF THE PHASE φ OF THE ADMITTANCE y_{12} OF A POROUS SAMPLE FROM THE MEASUREMENT OF THE PHASE OF P_2/P_1

II. Test Setup

The test setup consists of a horn driver, a small monitor microphone to measure P_1 and a half inch condenser microphone to measure P_3. The details of the setup are shown in Fig. 5.

1. The monitor microphone has a frequency response which is flat to beyond 100 kHz; its diameter is 0.1 inch. The B&K type 4143 has a pressure response which is flat to 10 kHz with a slight rise of 1 dB at 20 kHz.

When the Microphone Plate and the Monitor Plate are assembled without the Sample Plate, the relative response of the microphones can be compared: this is shown in Fig. 6 where P_1 is held constant. The slight rise of P_3 at 10 kHz is caused by the off-set of the monitor microphone with respect to the reference surface of the P_3 microphone. This off-set is h_0 and is equal approximately to half of the diameter of the monitor microphone: it introduces a correction

$$\cos(k_0 h_0)$$

which is approximately 0.5 dB at 10 kHz. The rise in low frequency part of Fig. 6 is caused by the low frequency roll-off of the monitor microphone, which has a -3 dB point at approximately 50 Hz. In contrast the B&K microphone has a -3 dB point at 10 Hz.

2. The phase difference between the two microphones and their electronics is also measured without the sample plate. The phase difference of P_3 with respect to P_1 is shown in Fig. 7.

3. The distortion of the Horn driver is also measured with the two microphones without a sample plate. The distortion at the 1 kHz is shown in Fig. 8 as a function of the pressure. This distortion is slightly higher than the distortion caused by the P_3 microphone and therefore is attributed to the driver.

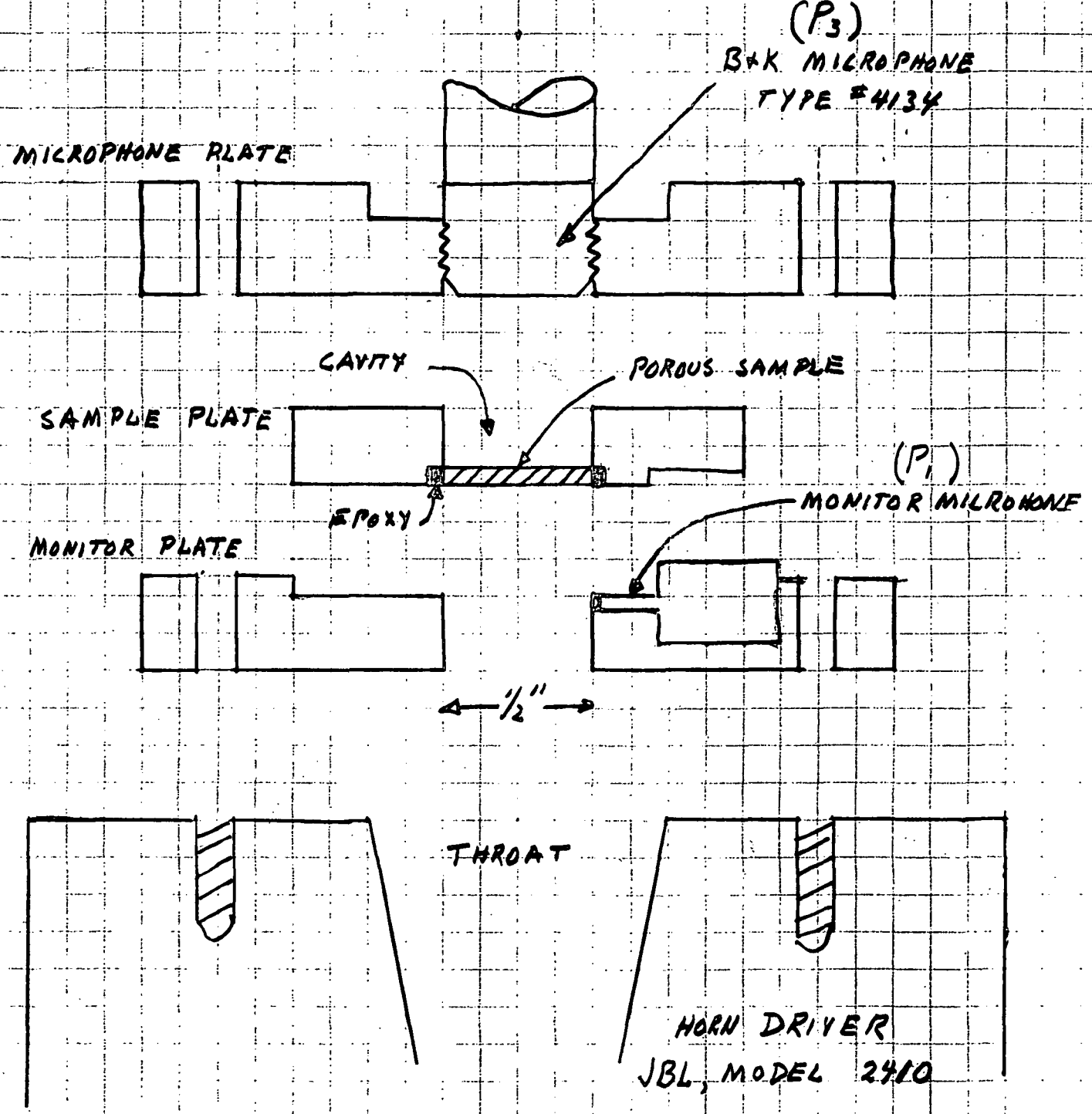

FIG. 5 : TEST SET-UP TO MEASURE THE TRANSFER ADMITTANCE y_{12} OF A POROUS SAMPLE

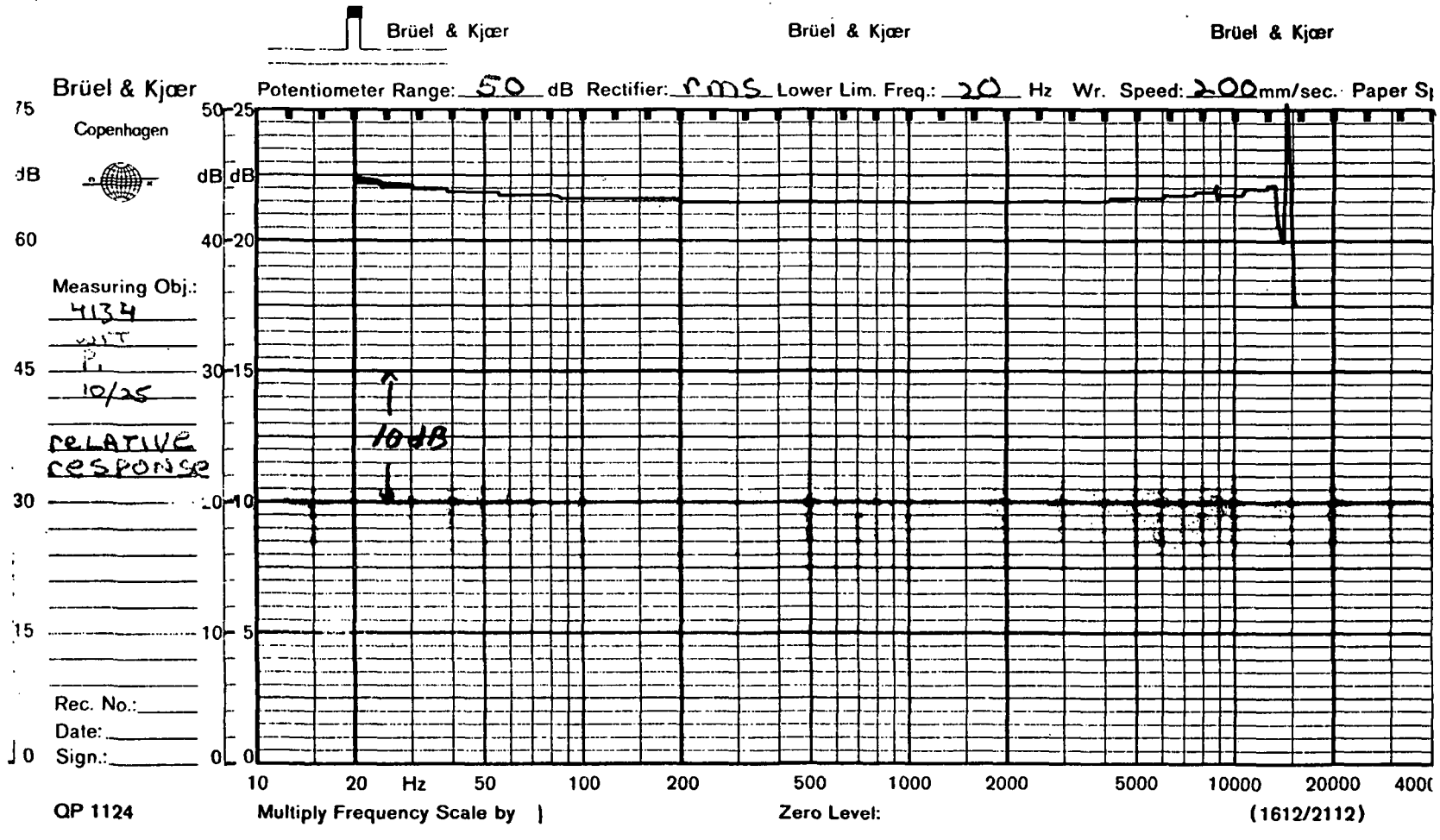

FIG. 6 RELATIVE FREQUENCY RESPONSE OF THE B&K CONDENSER MICROPHONE (P_2), WITH RESPECT TO THE MONITOR MICROPHONE (P_1).

PHASE [illegible] P_1

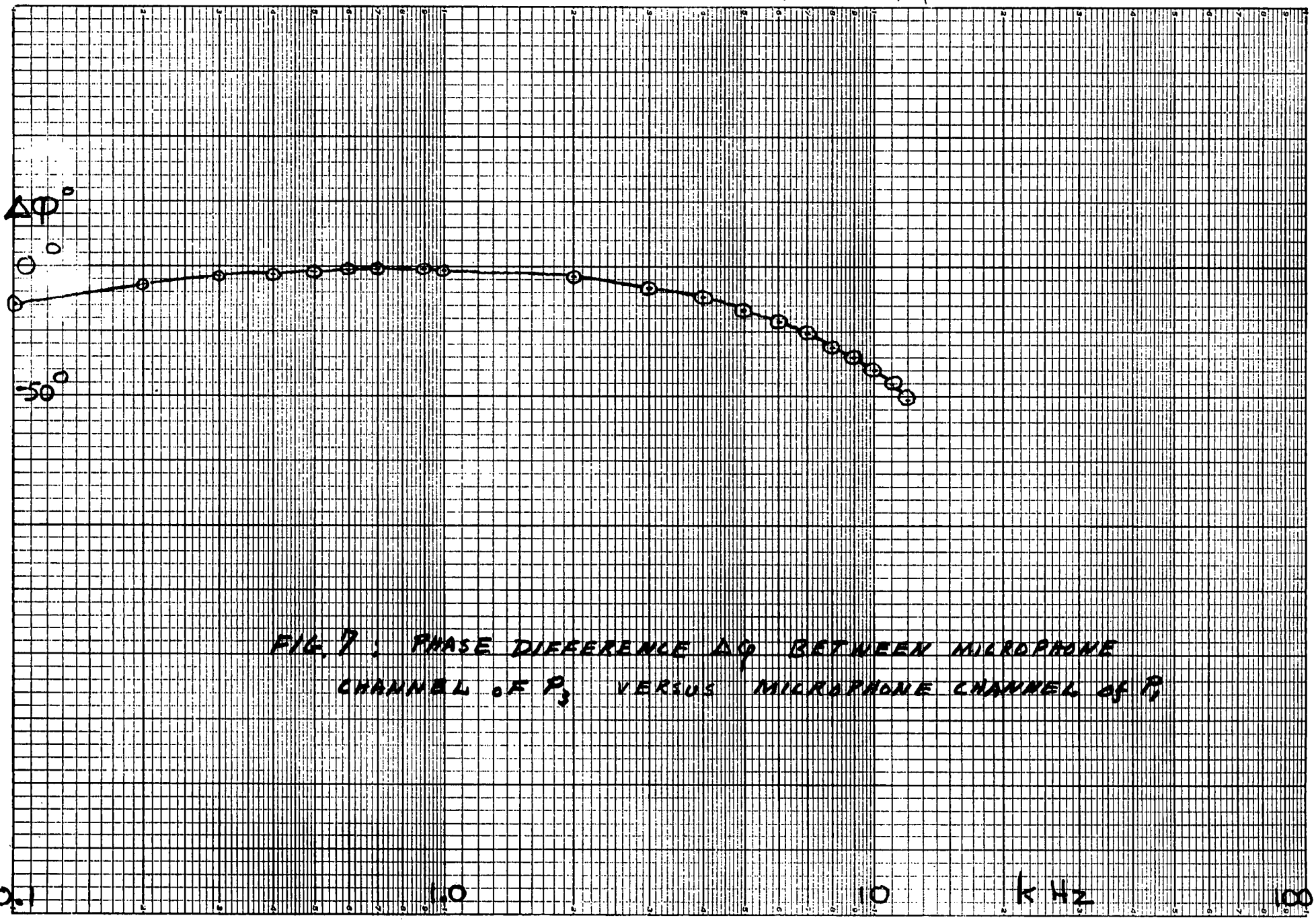

FIG. 7 ; PHASE DIFFERENCE $\Delta\varphi$ BETWEEN MICROPHONE CHANNEL OF P_3 VERSUS MICROPHONE CHANNEL OF P_1

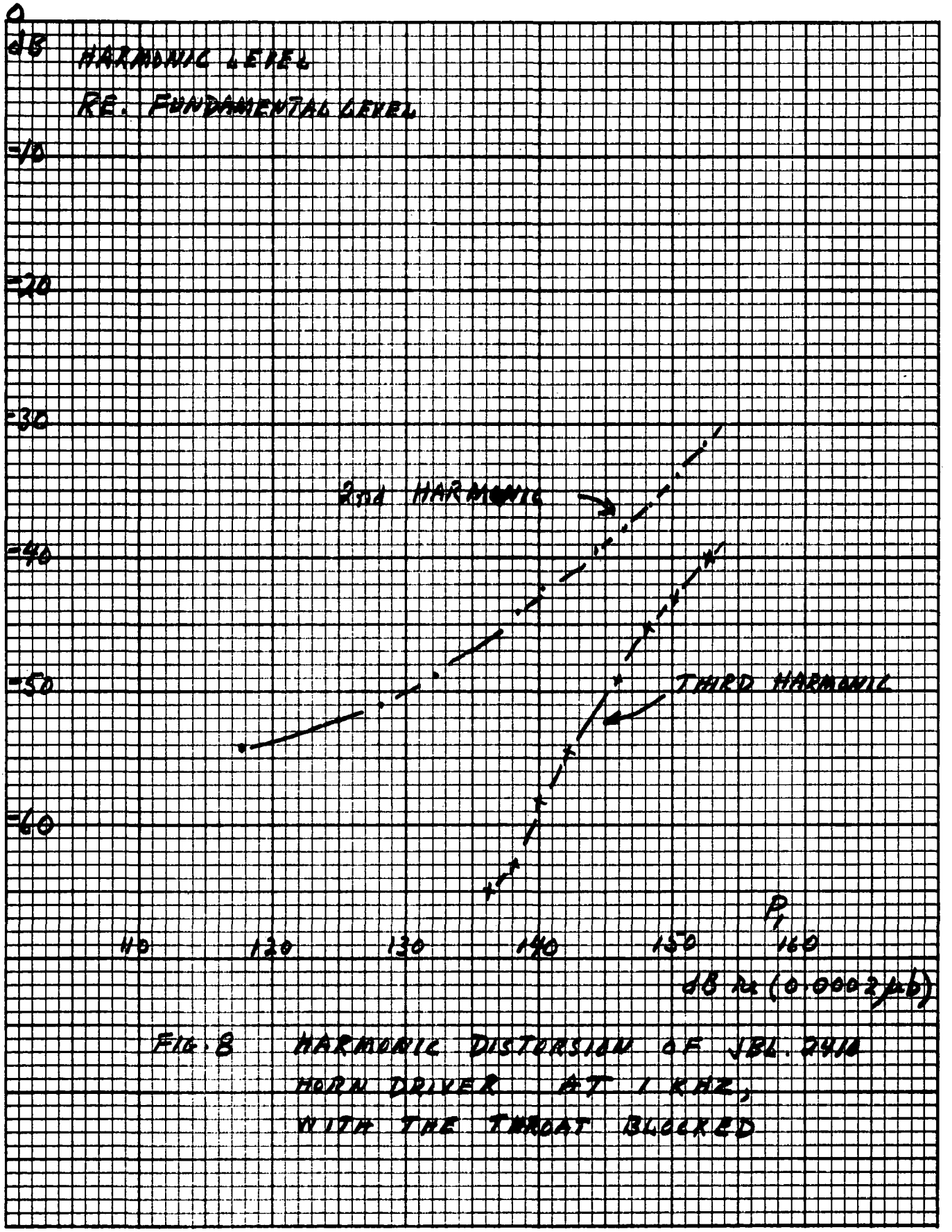

FIG. 8 HARMONIC DISTORTION OF JBL 2440 HORN DRIVER AT 1 KHZ, WITH THE THROAT BLOCKED

The distortion of Fig. 8 at 1 kHz will also apply to the distortion measured at P_1 with a porous sample, because the values of $r/\rho_0 c_0$ for all the samples to be tested are much larger than unity and simulate very nearly the same blocked condition of the results of Fig. 8.

The non-linearity of a porous sample will introduce its own distortion, in addition to the distortion shown in Fig. 8. Hence, the distortion measured at P_3, in excess of the distortion of the horn driver will be a measure of the non-linearity of a porous sample.

The horn driver can apply a very large acoustic pressure to a porous sample, as shown in Fig. 8. This is an important advantage of this setup; the non-linearity of a porous sample can be examined with the same setup, for pressures up to at least 153 dBSPL (re 0.0002 microbar).

4. A disadvantage of the setup is the high acceleration level which is generated at high frequencies. Figure 9 shows the acceleration level (in dB re 1G) of the P_3 microphone plate during a typical test, where the input pressure P_1 is 134 dB re 0.0002 microbar. Both the P_1 microphone and the B&K microphone are sensitive to acceleration. The P_1 microphone, being a small piezoelectric microphone is particularly sensitive to acceleration; in fact, the acceleration sensitivity of this small microphone and the high acceleration levels of the test setup are the main reason why the frequency range of the tests is limited to frequencies below 12 kHz.

The acceleration sensitivity of the B&K microphone is much smaller than the acceleration sensitivity of the monitor microphone P_1. However, the pressure level measured by the B&K microphone during a test of a porous sample decreases with

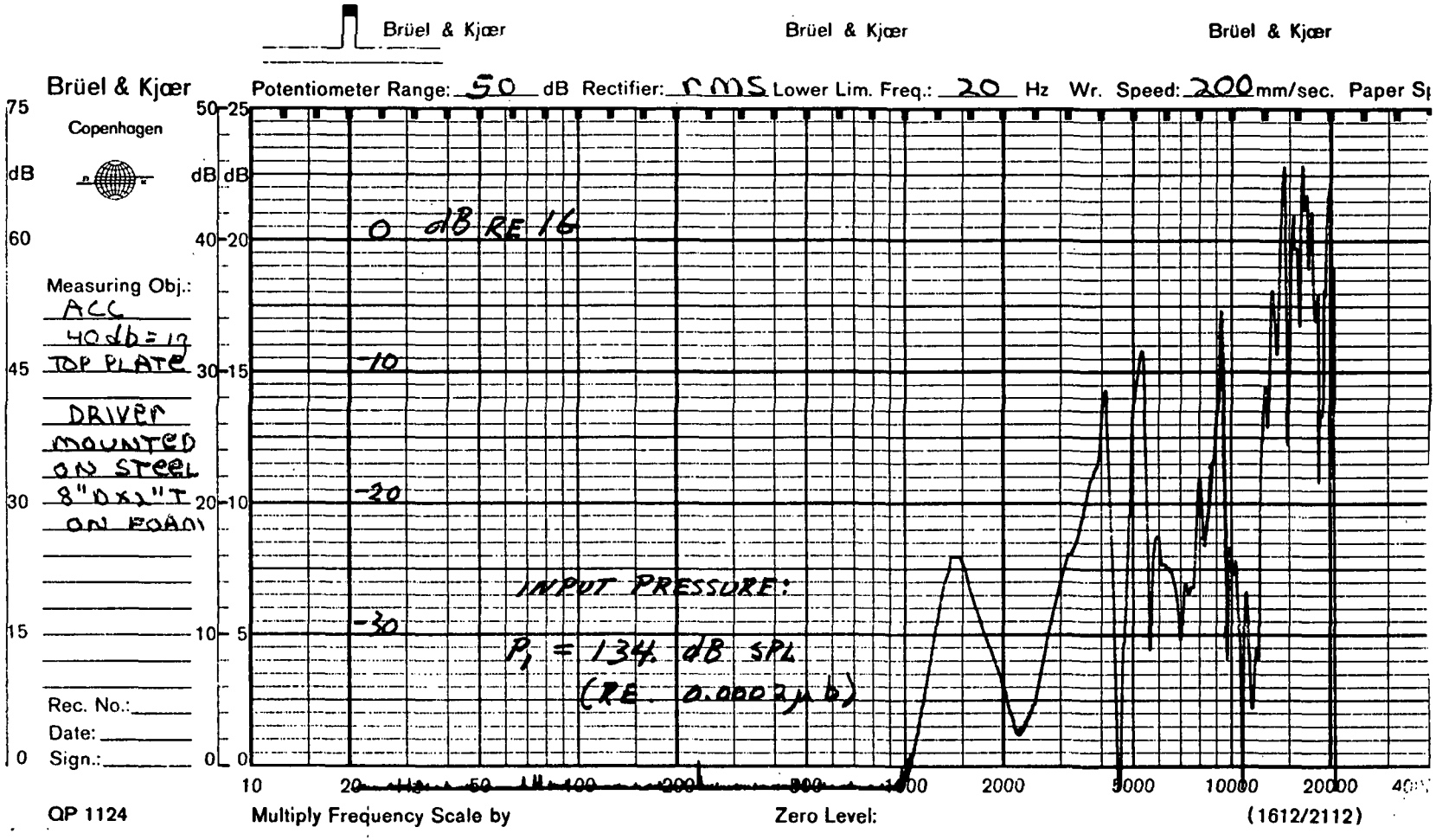

FIG. 9: ACCELERATION LEVEL OF MICROPHONE PLATE DURING A TEST OF A POROUS SAMPLE.

frequency. (See Fig. 2.) Hence, if the acceleration level of the test setup remains high at high frequencies, as shown in Fig. 9, the acceleration level will eventually contaminate the pressure signals at P_3. The acceleration sensitivity of a half inch B&K microphone in free air is approximately 80 dB SPL per G, where SPL is referenced to 0.0002 microbar. The acceleration sensitivity of the same microphone is a closed cavity is examined in Note I; it is shown for the size of acoustic cavity used in the test setup, that the acceleration sensitivity of the B&K microphone will not exceed its acceleration sensitivity in free air. It follows that the pressure level measured by the B&K microphone should be much larger than

80 dB + (acceleration level in dB re 1G)

This condition will be satisfied in all the tests.

5. Radial Modes

The formulation of Part I assumes a plane wave propagating along the axis of the test setup. We now examine the possibility of other than a plane wave propagating in the setup. We will show that, although other modes are possible, that they are inherently very much attenuated because the wavenumbers associated with these other modes is imaginary in the frequency region of interest and for the geometry of the test setup.

For simplicity, consider only symmetrical modes, those which do not depend on the polar angle. The pressure inside a cylinder with rigid walls has the form:

$$p(r,x) = \sum_{n=0,1,2\ \cdots} A_n J_o(k_{nr} r)\, e^{-ik_{nx}X}$$

where

$$k_0^2 = k_{nr}^2 + k_{nx}^2$$

and k_0 is the free wavenumber of the gas. The allowed radial components k_{nr} of wavenumber are

$$k_{or} = 0$$
$$k_{1r} = 3.85/a$$
$$k_{2r} = 7.0/a \qquad \text{etc.} \quad ....$$

where a is the radius of the cylinder; k_{or} corresponds to the plane wave, since $k_{ox} = k_0$. For the first radial mode to be present in an infinitely long cylinder k_{1x} must remain real: hence

$$k_{1x} = (k_0^2 - k_{1n}^2)^{\frac{1}{2}} \qquad \text{, real}$$

which requires

$$k_0 \geq k_{1r}$$

or that the frequency be

$$\omega \geq c_0 k_{1r} = \frac{c_0\ 3.85}{a}$$

$$f \geq \frac{c_0\ 3.85}{2\pi a} \quad , \quad \text{Hz}$$

For a half inch diameter cylinder, $f \geq 33$ kHz; for a one inch diameter we get $f \geq 16$ kHz.

These radial modes can exist in a long tube *if they are excited* and the frequency f is above the cut off frequency f of the mode; however, if the excitation is radially uniform, they will not be excited. For this reason we have chosen the best quality horn driver that we could find, so that radial modes in the horn would not be strongly excited.

Considering now a finite tube, like the short horn of the horn driver, or the acoustic cavity behind the porous sample, although the peak response of a radial mode response occurs at the frequencies set by

$$k_{nr} = k_0$$

the presence of this mode is felt at frequencies below this frequency. Hence, for finite tubes the frequency region unaffected by radial modes will be below that set by k_{nr}; unless, again, that mode is not significantly excited.

In the present test setup, the acceleration sensitivity of the monitor microphone P_1 appears to be more important than the likelyhood of a radial mode.

NOTE I: ACCELERATION SENSITIVITY OF THE P_3 MICROPHONE

When a rigid cylindrical cavity of height d, is vibrated with an axial velocity U_0, the pressure p(x) generated inside the cavity is

$$p(x) = -iU_0\rho_0 c_0 \frac{\sin[k_0(x-d/2)]}{\cos(k_0 d/2)}$$

where x is measured from one end of the cavity. At one end of the cavity, x=0 we get

$$p(0) = iU_0\rho_0 c_0 \quad \tan(k_0 d/2)$$

which can be approximated

$$p(0) \cong i\omega U_0 \rho_0 \frac{d}{2} \quad ; \quad k_0 d/2 < 1$$

Since $i\omega U_0$ is the acceleration we get the acceleration sensitivity

$$\frac{p(0)}{i\omega U_0} = \rho_0 d/2$$

which is equivalent to a surface density of fluid over the microphone surface. This surface density is less than the equivalent surface density of the fluid appearing on the surface of the microphone in free air,

$$\frac{2}{3}\rho_0 a$$

where a is the outer radius of the microphone, for the size of cavity used in the test setup:

$$\frac{2}{3} a > d/2$$

Hence, it follows that the acceleration sensitivity of the B&K microphone caused by the air in the cavity will not exceed the acceleration sensitivity of the same microphone in free air.

APPENDIX V

TEST RESULTS: TRANSFER ADMITTANCES y_{12} OF DIFFERENT POROUS MATERIALS

This appendix presents and discusses the test results of the measurements of the transfer admittances y_{12} of six different porous materials.

I. Transfer Admittance y_{12}

Samples of different porous materials have been tested by the apparatus described in Appendix 4. All the samples investigated are made of metal: the design of Porous Surface Sensors requires a rigid porous surface, which is more easily satisfied with porous metals. The porous materials selected are all commercially available as standard items. They are fabricated by three different processes:

Process A: sintered small metal particles
Process B: sintered metal fibers
Process C: sincered metal screens

The samples tested are listed in Table I. All are made with stainless steel; other non-corroding materials like bronze will be evaluated later.

The density ρ_s of each sample is measured; from the known density ρ_m of the metal the porosity Ω of the sample is calculated:

$$\Omega = 1 - \rho_s/\rho_m$$

This calculation assumes that the material is isotropic; the samples are likely to be not quite isotropic; the deviation from isotropicity of each sample will be discussed later in this memo.

The specific acoustic resistance r of each sample is normalized to the characteristic impedance $\rho_0 c_0$ of air, and listed in Table I for each sample. The values of r are obtained with the apparatus of Appendix 4.

TABLE I

CHARACTERISTICS OF POROUS SAMPLES

Sample No.	1	2	3	4	5	6
Process	A	B	C	B	A	A
Supplier	MOTT	Brunswick	Michigan Dynamics	Brunswick	MOTT	MOTT
Grade	5 micron.	FM:1104	Dynapore 401440	FM:1103	10 micron.	2 micron.
Material	Stain-less S. 316L	Stain-less S. 347	Stain-less S.	Stain-less S. 347	Stain-less S. 316L	Stain-less S. 316L
Thickness	1.64 mm	1.56 mm	1.27 mm	1.56 mm	1.48 mm	1.57 mm
ρ_s: density of sample	4.99 g/cc	3.46	6.96	2.70	4.96	5.16
ρ_m: density of material	7.9 g/cc	8.0	7.9	8.0	7.9	7.9
Ω: porosity	0.37	0.57	0.12	0.66	0.37	0.30
$r/\rho_0 c_0$: specific resistance	73	110	54	39	23	140
Frequency characteristics	Fig. S-1a	Fig. S-2a	Fig. S-3a	Fig. S-4a	Fig. S-5a	Fig. S-6a

The modulus and phase of y_{12} r as a function of frequency, for each sample, is given by a separate figure which is listed in Table I. These values are obtained with the apparatus of Appendix 4, and the calculations are carried out according to the format illustrated in that appendix.

II. Discussion

1. The frequency responses of the samples tested, modulus and phase, are in general agreement with the responses of ideal porous materials having the same thickness h, specific resistance r, and effective porosity Ω'. The agreement is not perfect, leaving us to suspect that, either the mass reactance of the gas inside the porous material may not be completely negligible, or the precision of the measurements are not sufficient to resolve the differences. The differences are rather small, either approximately 1 dB in the modulus of y_{12} r or approximately 10° to 20° in the phases of y_{12} r.

2. Another possible cause for the differences in the responses between a real porous material and the ideal porous material is that the latter one assumes that the porosity is isotropic. In fact, the porosity of real porous materials is likely to be non-isotropic.

An indirect way to obtain the effective porosity of a sample is to match the frequency responses of the sample with those of the ideal porous sample (see Fig. 1a of Appendix 3) and to note the value of β^2 at, say, 10 kHz for which the best match is obtained; from this value of β^2 and the values of h, $r/\rho_0 c_0$, the effective porosity Ω' is calculated. This result is shown in Table II. The effective porosity Ω' is nearly equal to the "isotropic" porosity Ω for samples #1, 2, 4 and 6.

TABLE II

Sample No.	Matching Responses to Ideal Porous Material: β^2 at 10 kHz	Matching Responses to Ideal Porous Material: Effective Porosity Ω'	From Table I: Isotropic Porosity Ω	Comparison
1	5.4	.35	.37	$\Omega' \cong \Omega$
2	11	.50	.57	$\Omega' \cong 0.88\ \Omega$
3	2.2	.25	0.12	$\Omega' \cong 2\ \Omega$
4	5.3	.67	.66	$\Omega' \cong \Omega$
5	2.3	.59	.37	$\Omega' \cong 1.4\ \Omega$
6	9.0	.34	.30	$\Omega' \cong 1.05\ \Omega$

The effective porosity Ω' of samples #3 and #5 are significantly larger than the isotropic porosity, indicating that these two materials are strongly non-isotropic. Since, for this sample, $\Omega' > \Omega$, it follows that the porosity in a direction normal to the surfaces of the sample is greater than the porosity in directions parallel to the surfaces of the sample.

h = 1.64 mm

SAMPLE 1 MOTT 5μ 73.2 PSI f_0 = 152 cps

$20 \log_{10} |y_{12}| f|$

$|y_{12}| f|$ db

φ°

0

db

-10

-20

0°

-50°

-100°

-150°

0.1 1.0 10 kHz 100

FIG. S-1-a : TRANSFER ADMITTANCE OF POROUS SAMPLE #1.

$h = 1.56$ mm

SAMPLE 2. BRUNSWICK 1104 $110 \rho_0 c_0$ $f_0 = 98$

$20 \log_{10} |y_{12} r|$

$|y_{12} r|$ db

$\varphi°$

0 db

-10

-20

0°

-50°

-100°

-150°

0.1 1.0 10 kHz 100

FIG. 5-2-a TRANSFER ADMITTANCE OF POROUS SAMPLE #2

h = 1.27 mm

Sample 3 Dynapore 54 poise f_o = 187 cps

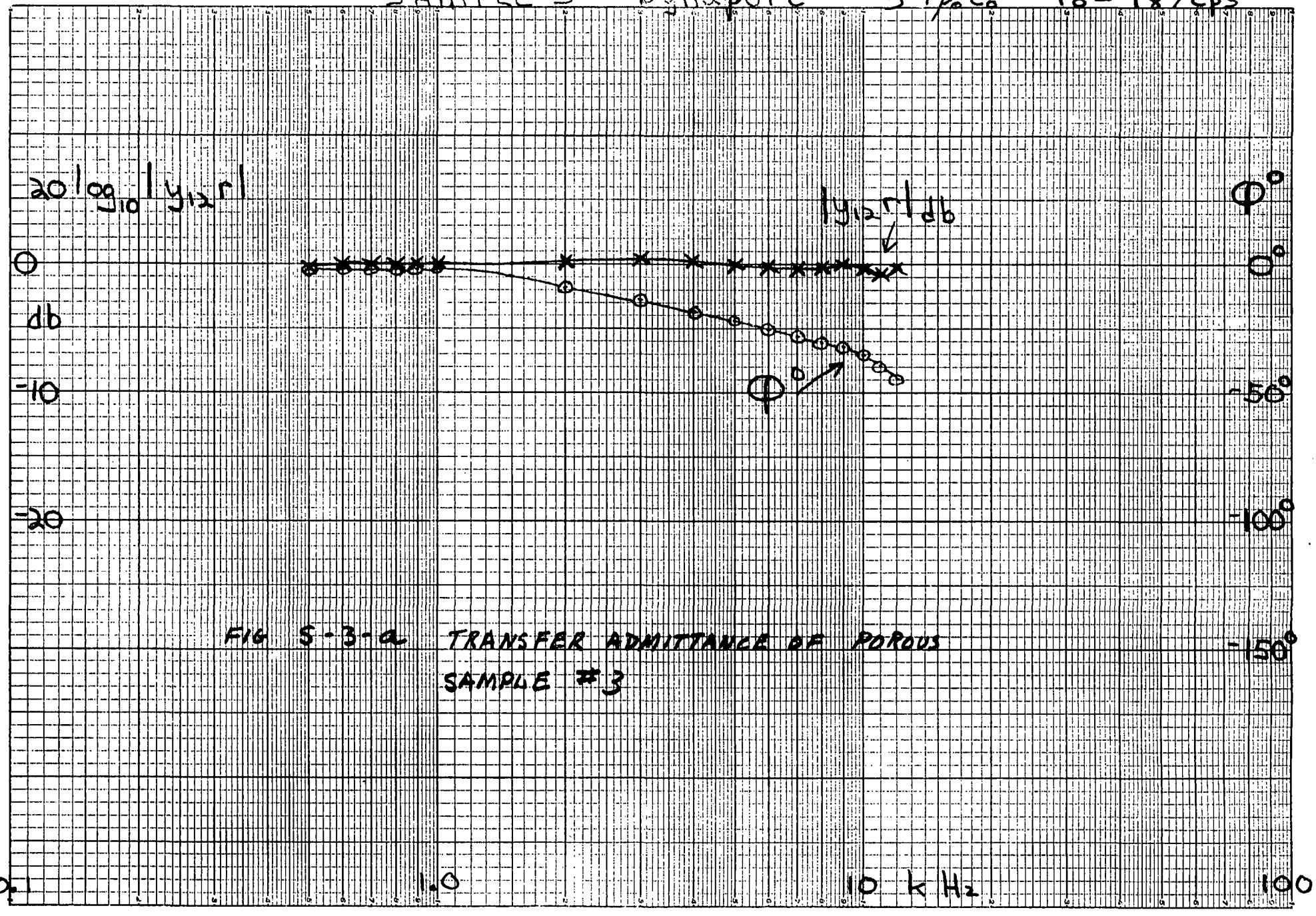

FIG 5-3-a TRANSFER ADMITTANCE OF POROUS SAMPLE #3

$h = 1.56$ mm

Sample 4 Brunswick 1103 $39\rho_0 c_0$ $f_0 = 272$

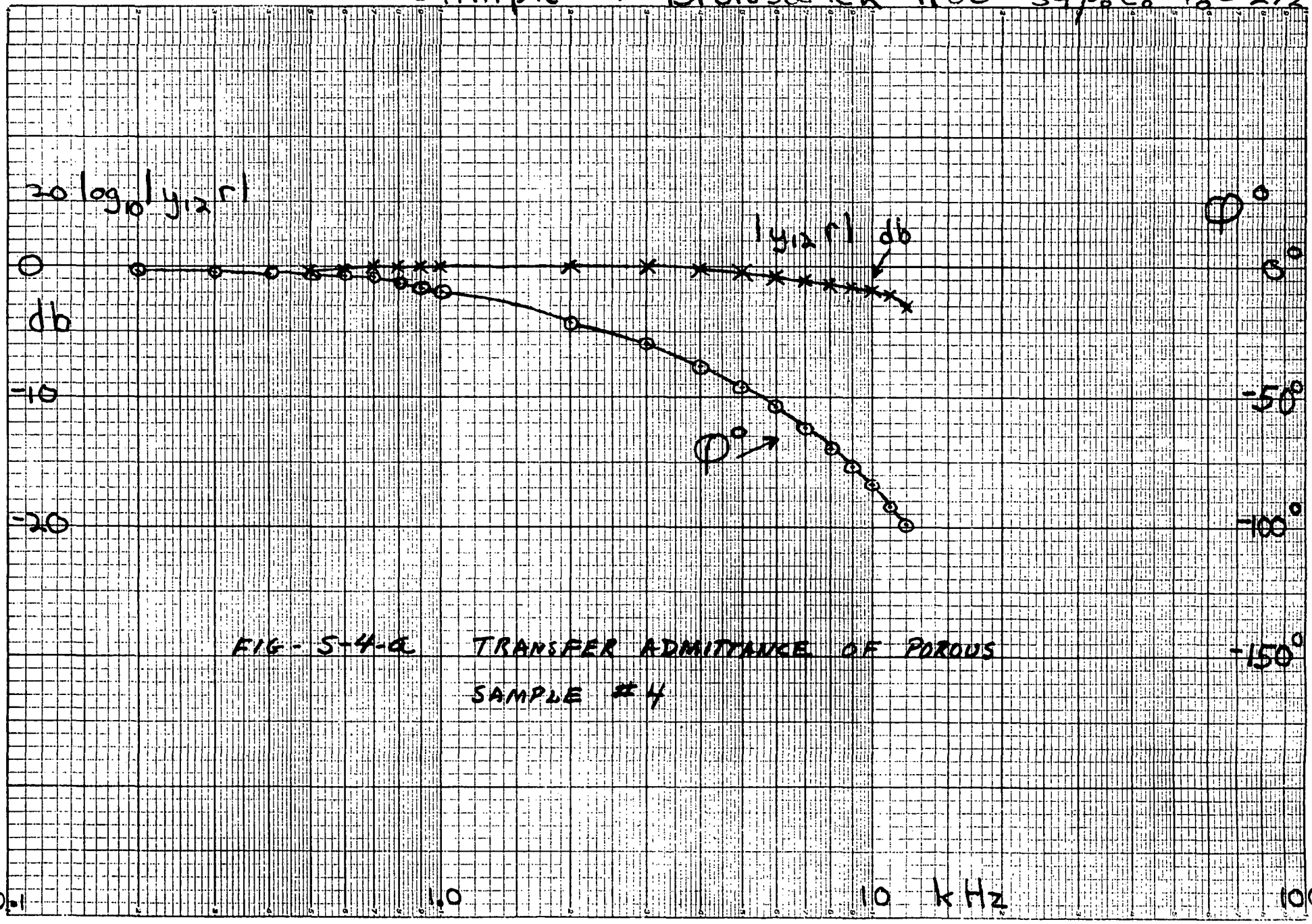

FIG - 5-4-a TRANSFER ADMITTANCE OF POROUS SAMPLE #4

$h = 1.48$ mm

Sample 5 Mott 10 μ 22.7% C_0 $f_0 = 452$ cps

$20 \log_{10} |y_{12} r|$

$|y_{12} r|$ db

$\Phi°$

db

0

-10

-20

0°

-50°

-100°

-150°

0.1 1.0 10 KHz 100

10

FIG. 5-5-a TRANSFER ADMITTANCE OF POROUS SAMPLE #5

h = 1.57 mm

Sample 6 Mott 2.μ 139pc f_o = 77 cps

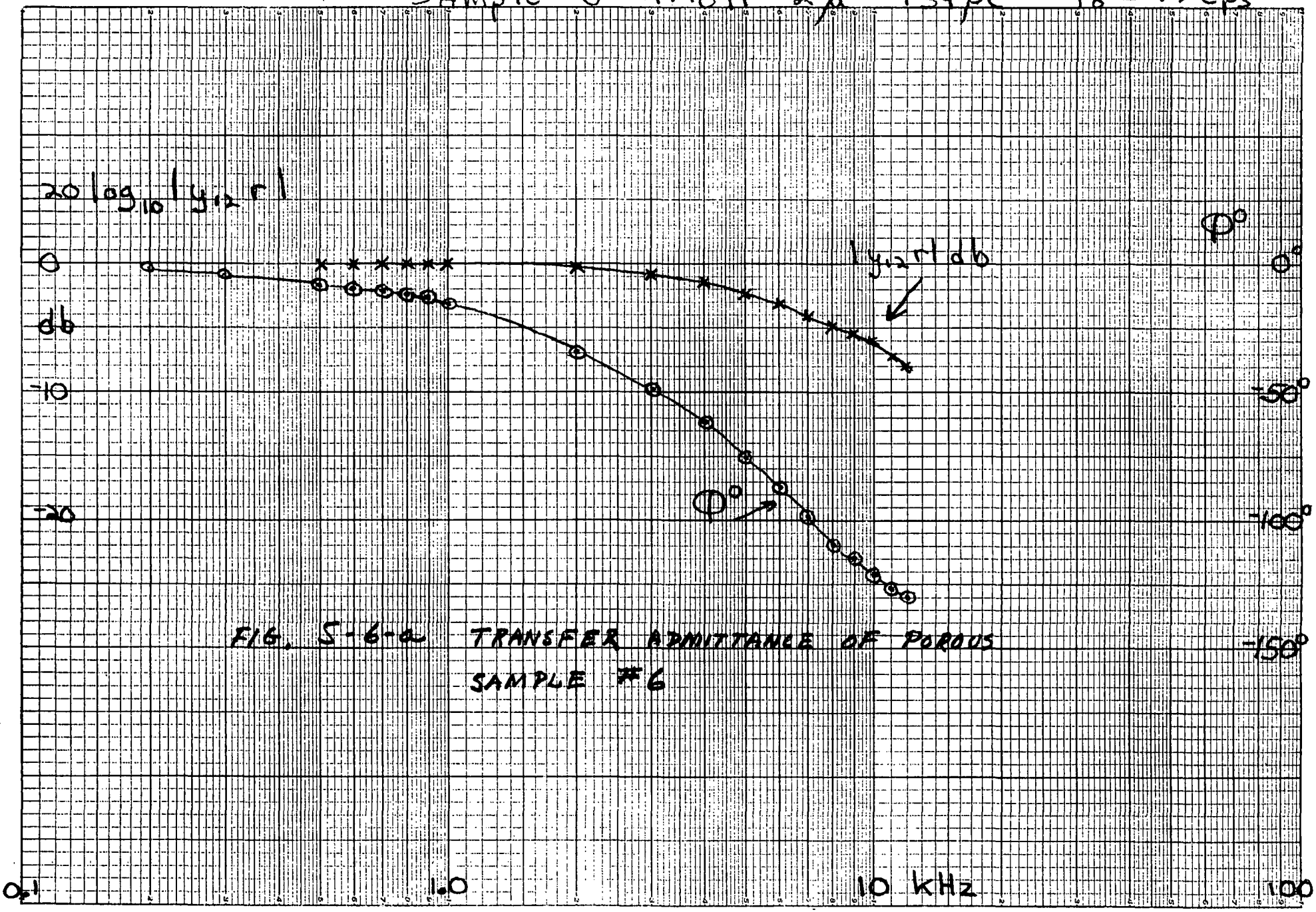

FIG. 5-6-a TRANSFER ADMITTANCE OF POROUS SAMPLE #6

APPENDIX VI

NON-LINEARITY OF THE SAMPLES OF POROUS MATERIALS

I. INTRODUCTION

For a constant gas flow through a porous surface, the pressure drop p is related to the velocity u by the approximate relation[1]

$$p = ru + su^2 \quad ; \quad \text{constant flow} \qquad (1)$$

where r is the flow resistance at low flow velocity, u is the average velocity at a surface; we have assumed a unit area of porous surface such that r is the specific resistance. The second order term represents the non-linearity of the porous material; it is called the inertial effect, arising at each surface where the low velocity u *at* the surface is transformed to a high local velocity u' inside the pores of the material; the transformation causes a significant pressure drop which is not related to the viscosity of the gas in the pores. The first order term represents the viscous loss *inside* the porous surface.

The resistance, at constant flow, is the ratio

$$p/u = r(1 + s/r\, u) \quad ; \quad \text{constant flow} \qquad (2)$$

which is non-linear. From the interpretation of the non-linear term as an "inertial effect" it follows that the ratio s/r becomes smaller, for larger resistances r; the inertial effect becomes relatively less important than the viscous effect.

When the flow u is due to acoustic pressures, the non-linear term in (2) is likely to be modified by the presence of an independent

---

[1]F.W. Cole, "Graphic Models for Acoustic Flow Resistance," paper given at the "American Society for Metals," 1969 Southern Metals Conference, Materials for Jet Engine Noise Abatement. Also appears as Technical Note MDD503, April 1969, from Michigan Dynamics.

tangential flow u_o of an air stream in the surface. This is the situation of a porous surface sensor in an airflow. Fortunately, only the non-linear term will be affected and this term should be very small for the type of porous material used in porous surface sensors. (The radiation impedance of the surface will be affected by a tangential flow; this effect will be investigated later.)

In these notes we examine the non-linearity of porous materials by measuring the harmonic distortion caused by the non-linearity of the material. We will find the maximum value of a harmonic pressure level which will cause a specified harmonic distortion. The same results will also yield the ratio s/r which represents the non-linearity.

The dynamic technique of harmonic distortion was chosen in preference to steady-state technique of measuring the constant pressure drop p for a steady flow u, because the first technique is more reliable for the small samples of high flow resistance which are investigated. The dynamic technique has also the convenience of showing directly the pressure level which can be applied to the porous surface, within an acceptable distortion level.

II. HARMONIC DISTORTION

A harmonic pressure at the frequency ω_1 is applied to a porous surface. The frequency ω_1 is low enough so that the porous material is purely resistive. The pressure p across the faces of the porous material oscillates about the ambient pressure, and the velocity u oscillates about zero. For this situation Eq. (1) is modified to account for the proper sign of p and u: when u is positive, then p is also positive:

$$p_+ = ru_+ + su_+^2 \tag{3a}$$

when u and p are negative, the nonlinear term changes its sign:

$$p_- = ru_- - su_-^2 \tag{3b}$$

This relation is sketched in Fig. 1.

Since p is now an odd function of u, only odd harmonics are generated by the non-linearity. The technique will consist of measuring the third harmonic at a frequency $3\omega_1$, the higher harmonics being negligible.

The test setup applies a pure tone pressure p,

$$p = P_i \sin\omega_1 t \tag{4}$$

and measures the velocity u which will be non-linear. However, u will be periodic; it can be expanded into a Fourier series:

$$u = \sum_n U_n \sin n\omega_1 t \quad ; \quad n=1,3,--- \tag{5a}$$

$$U_n = \frac{2}{T} \int_{-T/2}^{+T/2} u\sin(n\,\omega_1 t)\, dt \tag{5b}$$

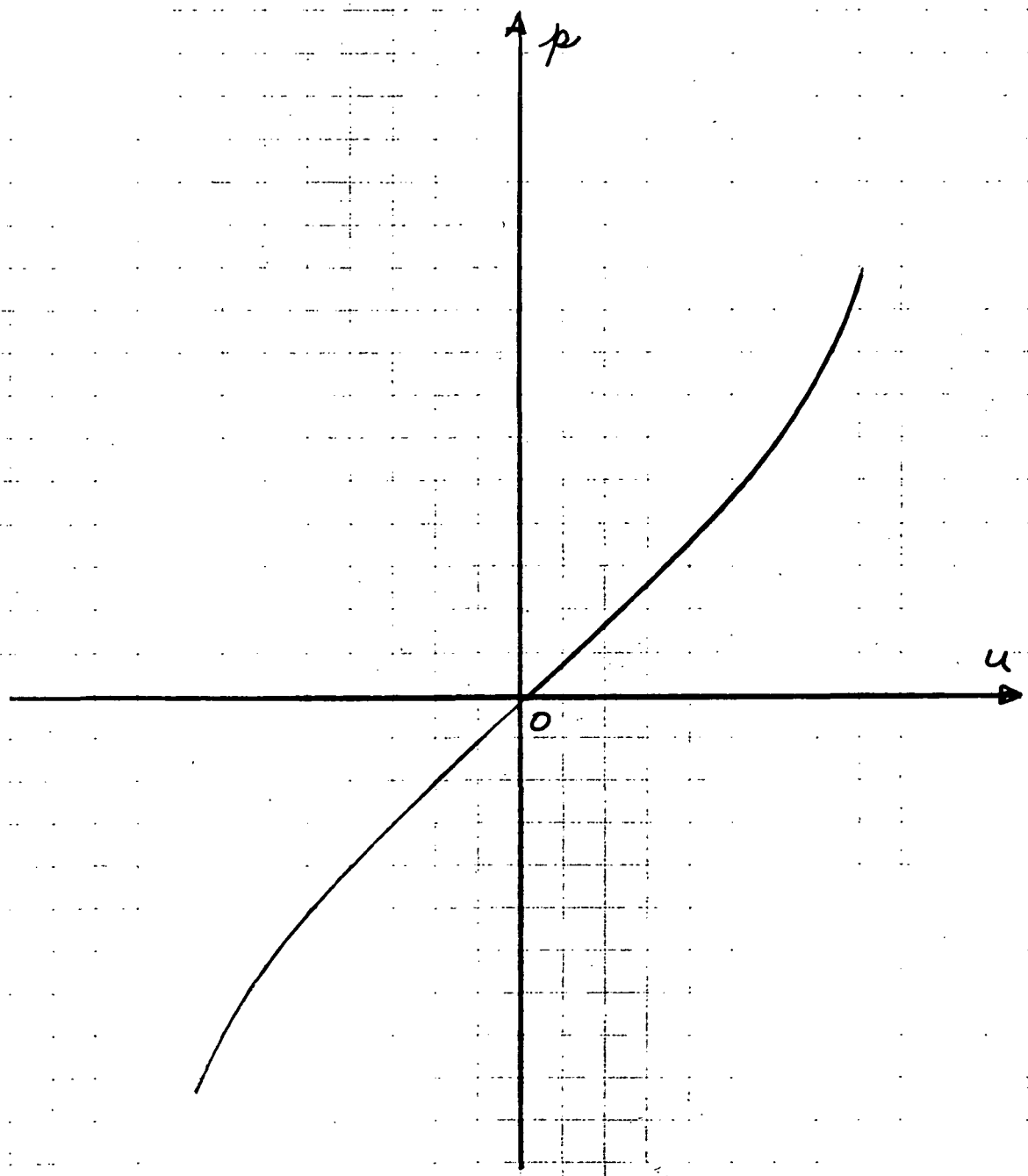

FIG 1 : NON-LINEARITY OF POROUS SURFACES

from which we will evaluate the ratio U_3/U_1 of the third harmonic to the fundamental; T is the period of the frequency ω_1.

We proceed first by expressing u as a function of p in (3a) and (3b); solving the two quadratic equations we get:

$$u_+ = p_+/r - p_+^2 \frac{s}{r^2} \quad \text{---} \tag{6a}$$

$$u_- = p_-/r + p_-^2 \frac{s}{r^2} \quad \text{---} \tag{6b}$$

leaving out the higher order terms; this approximation is acceptable provided that, during the test we satisfy

$$P_1 \frac{s}{r} << 1 \quad ; \tag{6c}$$

Introducing (4) and (6) in (5b) we have:

$$U_n = \frac{2P_1}{Tr}\left[\int_{-T/2}^{o} (\sin\omega_1 t + P_1\, s/r \sin^2\omega_1 t) \sin n\omega_1 t \, dt + \int_{o}^{T/2} (\sin u_1 t - P_1\, s/r \sin^2\omega_1 t) \sin n\omega_1 t \, dt\right] \tag{7}$$

Evaluating U_1 and U_3 we get

$$U_1 = P_1/r + \text{---} \tag{8a}$$

$$U_3 = \frac{-P_1{}^2 s}{r^2} \quad \frac{41}{30\pi} \tag{8b}$$

$$\left| \frac{U_3}{U_1} \right| = \frac{P_1 s}{r} \quad \frac{41}{30\pi} \tag{9a}$$

The test of harmonic distortion will yield the ratio $|U_3/U_1|$ at a known value of P_1, from which we can solve for s/r:

$$s/r = \left(\frac{U_3}{U_1}\right) \times \frac{1}{P_1} \quad \frac{30\pi}{41} \tag{10}$$

III. TESTS

The test for harmonic distortion caused by a porous sample requires a pressure source which has itself a very low distortion level. The horn driver and test set-up (see Appendix 4) used for measuring the admittances of a porous surface is used for the test of harmonic distortion. This application is mentioned in Appendix 4, pg. 10, and Fig. 8. Further investigation of the non-linearity caused by the horn driver revealed that a significantly lower distortion occurs at a frequency lower than 1 kHz; because, at 1kHz, the driver with its short horn closed at the surface of the porous sample experiences a first resonance (almost a quarter wave resonance of the short horn) which demands a relatively large displacement of the diaphragm of the driver. At frequencies below this first resonance the short horn, closed at the surface of the porous sample, becomes a stiffness impedance which limits the displacement of the diaphragm to a nearly constant and small value.

At 500 Hz the harmonic distortion of the P_1 monitor microphone is shown in Fig. 2, when the porous surface is blocked. The second and third harmonic distortion in Fig. 2 are smaller than those reported in Fig. 8 of Appendix 4.

The maximum sound pressure level applied is 156 dB SPL (re 0.0002 microbar); higher levels could have been achieved by using another power amplifier but at the cost of relatively higher levels of electronic distortion. The main harmonic distortion of the test set-up is the second harmonic; the third harmonic distortion is fortunately very low. Since the porous sample will introduce primarily third harmonic distortion, this distortion can be measured with the present test-set-up provided the overall distortion level measured by P_3 in the cavity above the porous sample is greater than the level shown in Fig. 2.

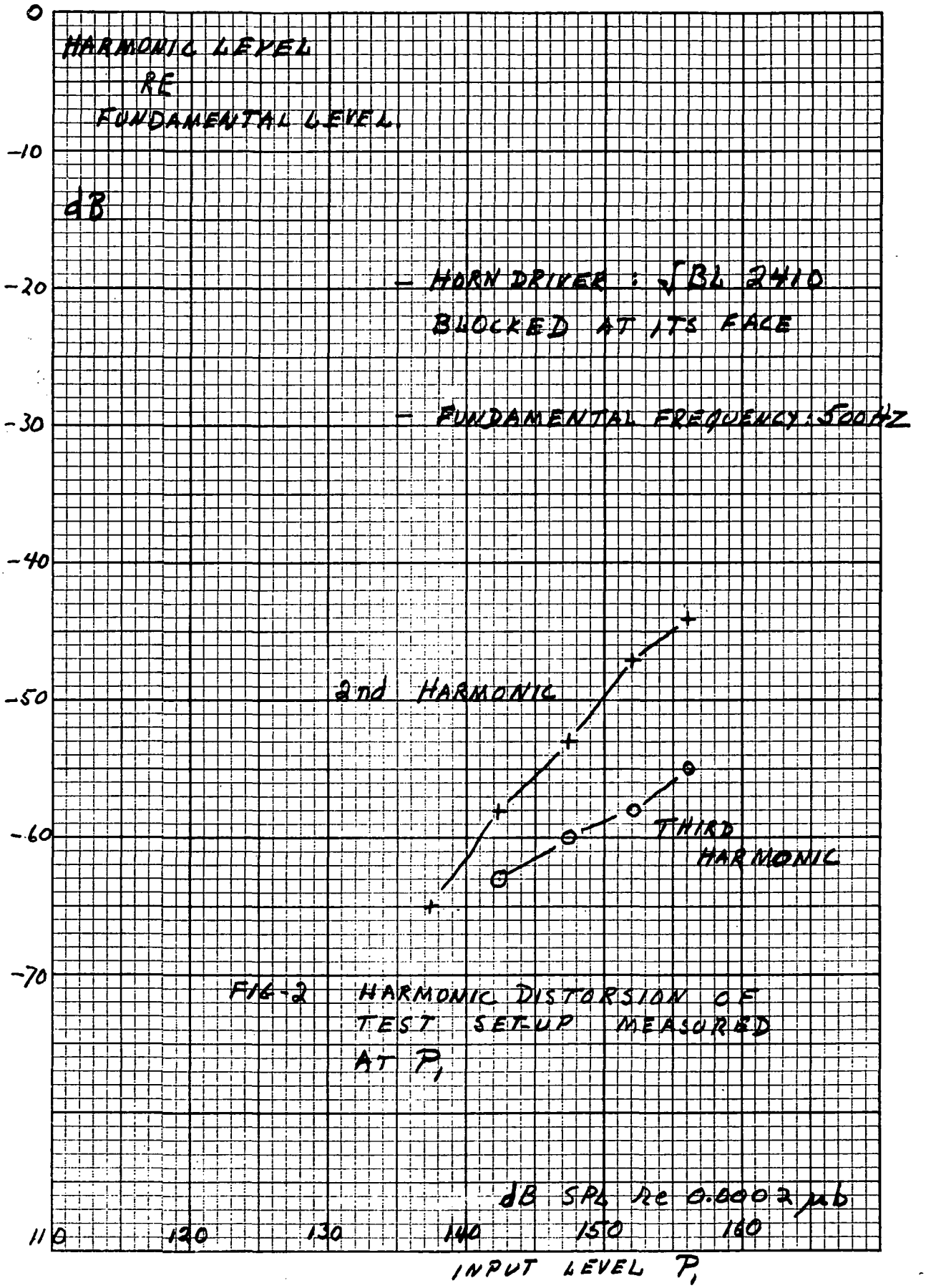

FIG-2 HARMONIC DISTORSION OF TEST SET-UP MEASURED AT P_1

The acoustic velocity u through the sample of resistance r in the test set-up is given by

$$P_1 = u\left(r + \frac{\alpha P_o}{i\omega h}\right) \tag{11}$$

$$= ur + P_3 \tag{12}$$

Since P_3 is in quadrature with ur we have

$$|P_1|^2 - |P_3|^2 = |ur|^2 \tag{13}$$

If P_3 is small compared with P_1 the acoustic velocity u becomes

$$|u| \simeq \frac{|P_1|}{r} \tag{14}$$

For 1 dB error in (14) compared with (13) we must satisfy

$$\left|\frac{P_3}{P_1}\right|^2 \leq 0.1$$

$$\left|\frac{P_3}{P_1}\right| \leq 0.31 \tag{15}$$

or, the level of P_3 should be at least 10 dB below the level of P_1. This is satisfied during the test by increasing, if necessary, the height h of the acoustic cavity.

Finally the relation

$$|P_3| = \left|\frac{\alpha P_o}{\omega h}\right| \; |u| \tag{16}$$

which relates $|P_3|$ to $|u|$ is measured experimentally at three frequencies, 500, 1000 and 1500 Hz, for each sample, after the unequality (15) has been established.

The experimental results of harmonic distortion for the six samples listed in Table I of Appendix 4 are presented in Figs. S-1b to S-6b. These results give the harmonic distortion of the velocity u through each sample, as a function of the pressure P_1 applied at 500 Hz.

The second harmonic is seen, for each sample to have a level roughly equal to the level shown in Fig. 2 for the applied pressure P_1: the porous samples do not create significant second harmonic distortion.

The levels of the third harmonic distortion of the samples exceed the levels of the third harmonic distortion of the horn driver only for sample No. 3; hence this material may cause undesirable non-linearities when used in a porous surface sensor when the pressure level being measured exceeds 145 dB SPL . All the other samples exhibit negligible distortion for pressure levels P_1 in excess of 156 dB SPL.

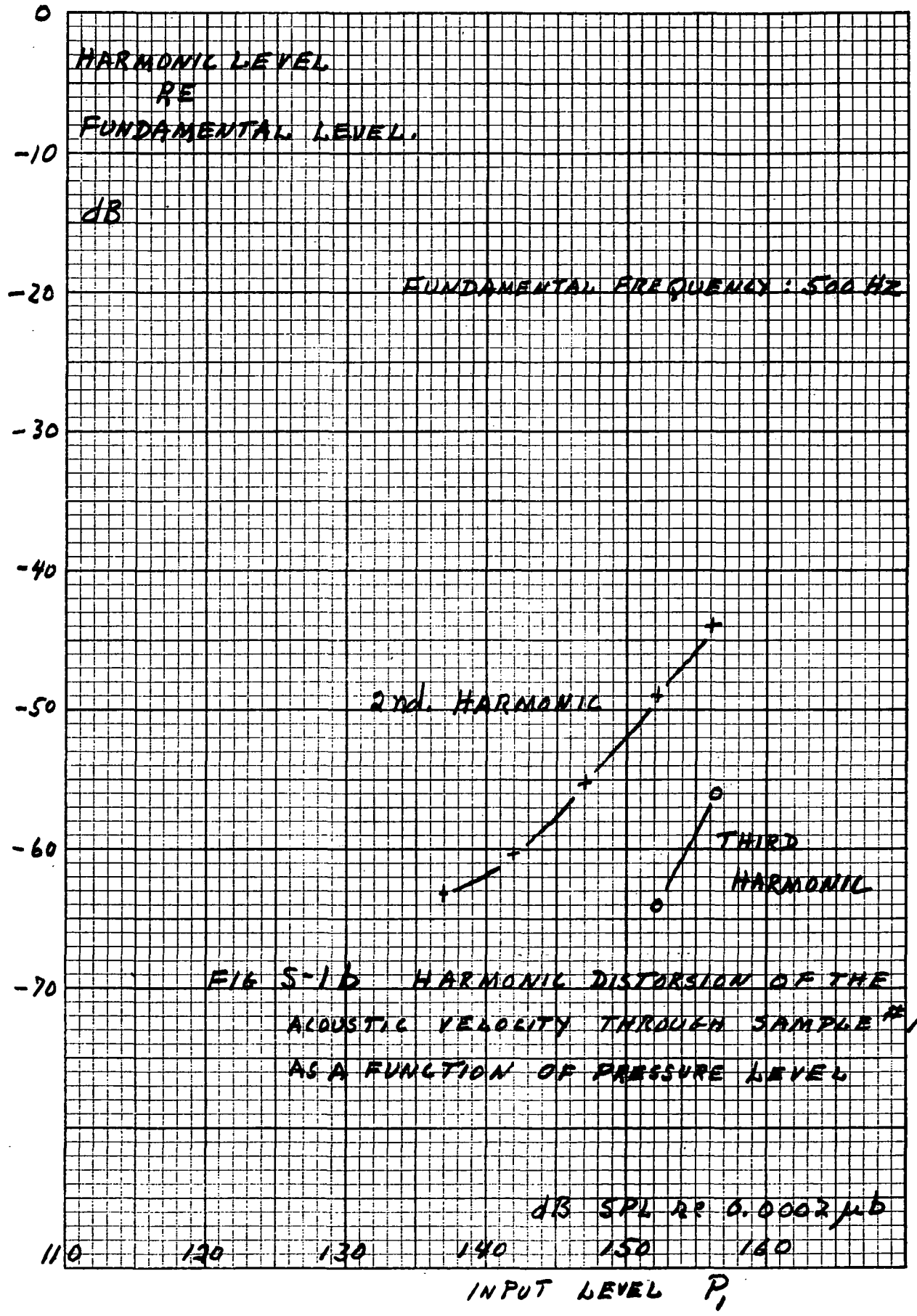

FIG 5-1b HARMONIC DISTORSION OF THE ACOUSTIC VELOCITY THROUGH SAMPLE #1 AS A FUNCTION OF PRESSURE LEVEL

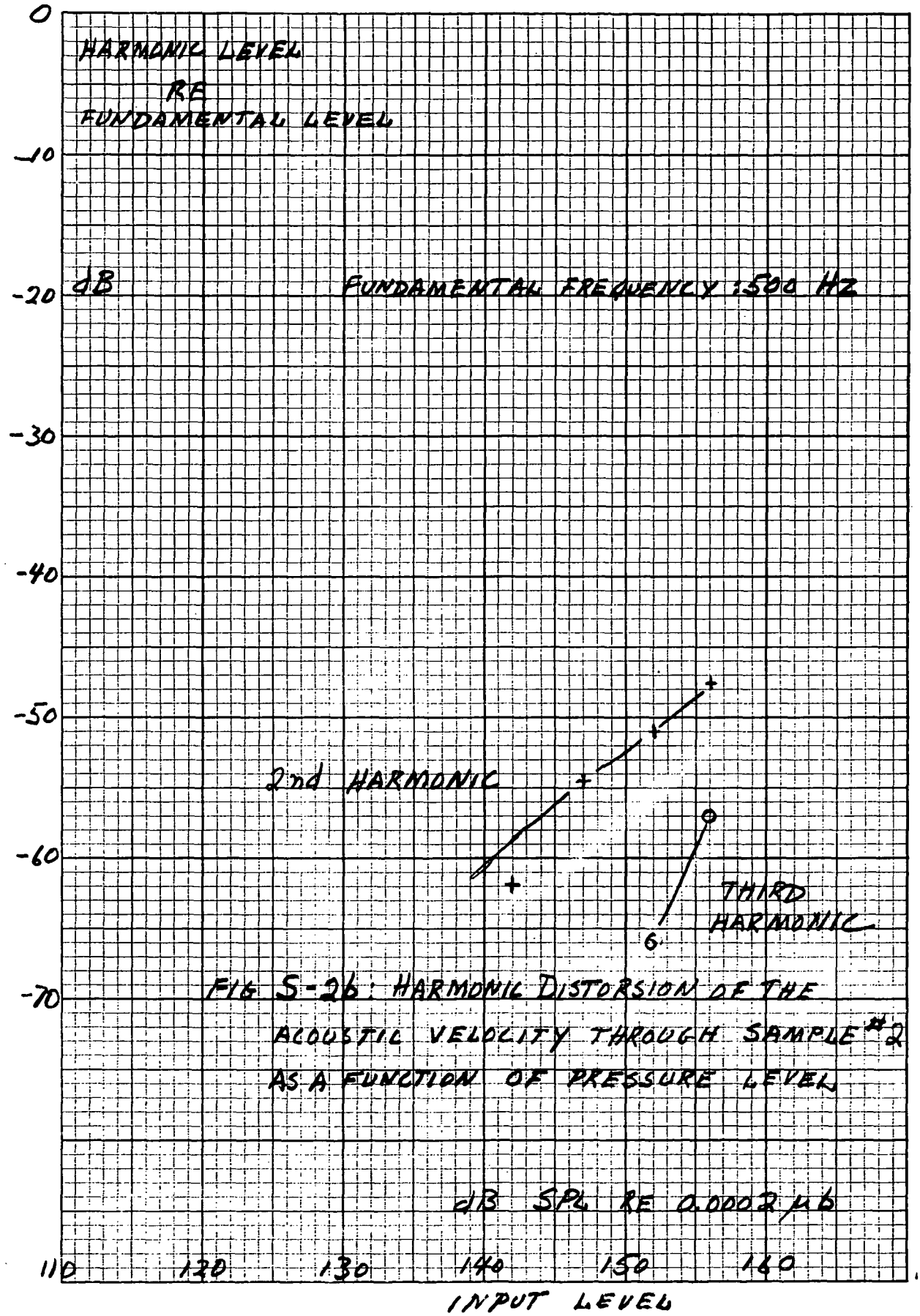

FIG 5-26: HARMONIC DISTORSION OF THE ACOUSTIC VELOCITY THROUGH SAMPLE #2 AS A FUNCTION OF PRESSURE LEVEL

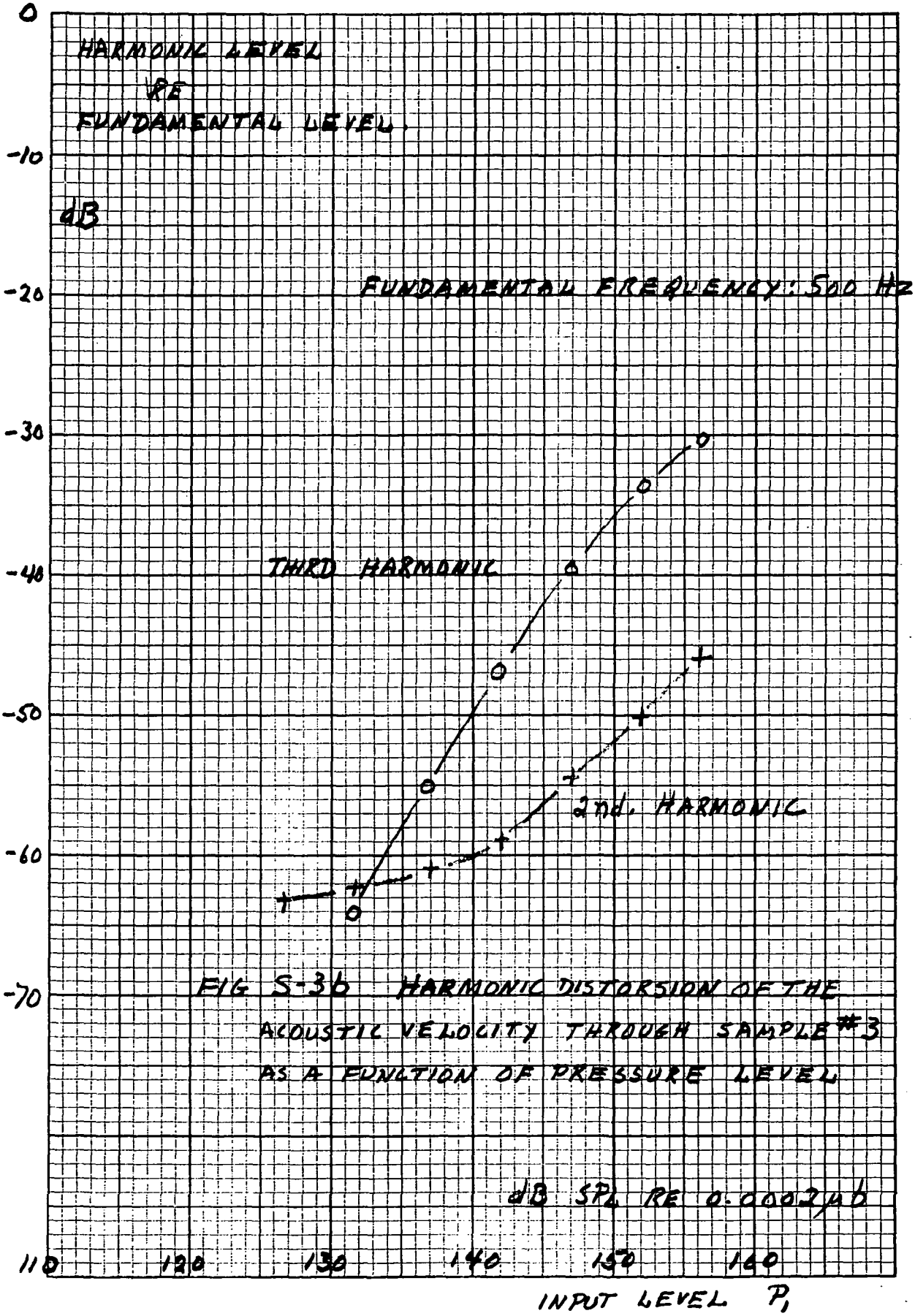

FIG S-3b HARMONIC DISTORSION OF THE ACOUSTIC VELOCITY THROUGH SAMPLE #3 AS A FUNCTION OF PRESSURE LEVEL

dB SPL RE 0.0002 μb

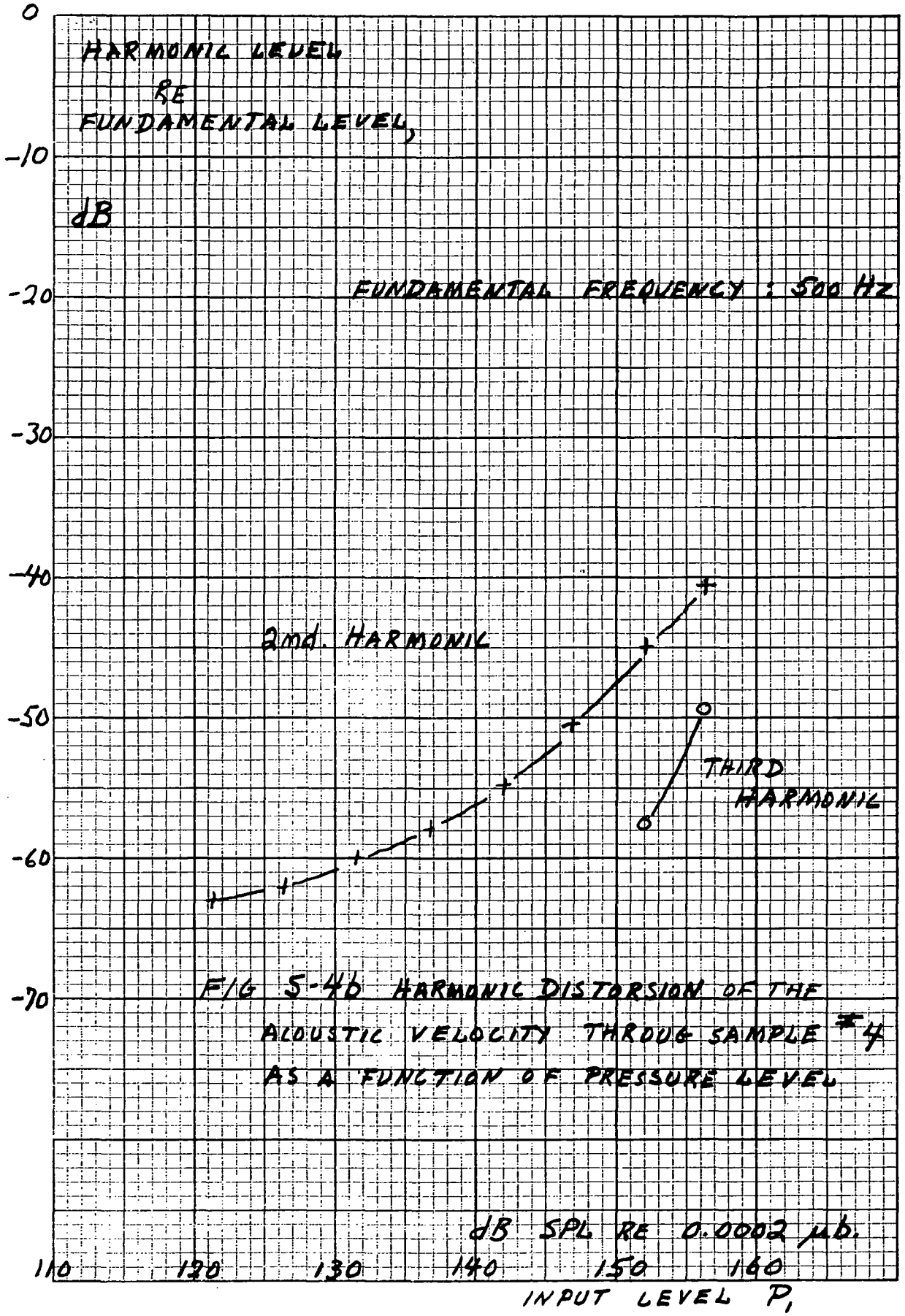

FIG 5-46 HARMONIC DISTORSION OF THE ACOUSTIC VELOCITY THROUG SAMPLE #4 AS A FUNCTION OF PRESSURE LEVEL

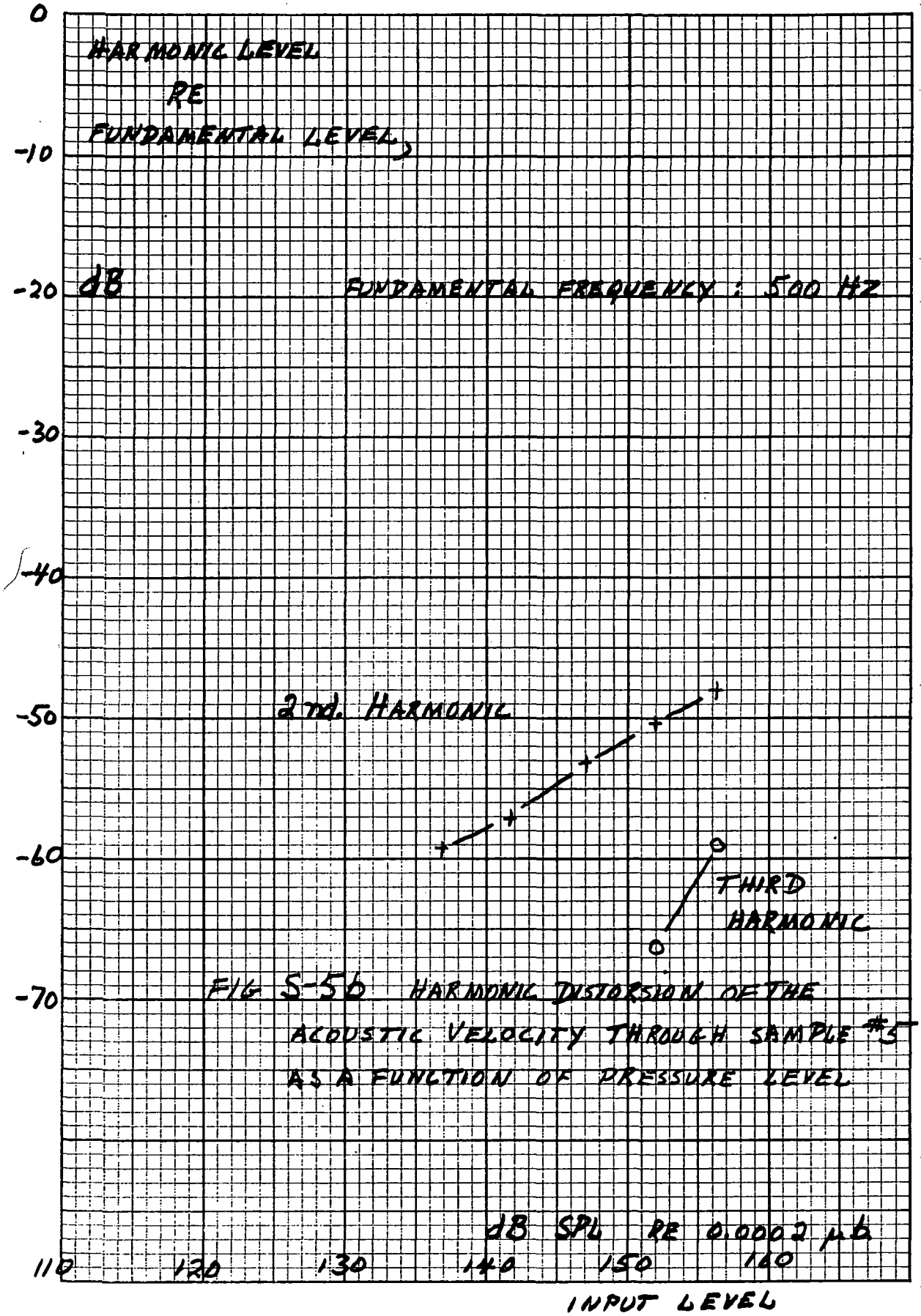

FIG 5-5b HARMONIC DISTORSION OF THE ACOUSTIC VELOCITY THROUGH SAMPLE #5 AS A FUNCTION OF PRESSURE LEVEL

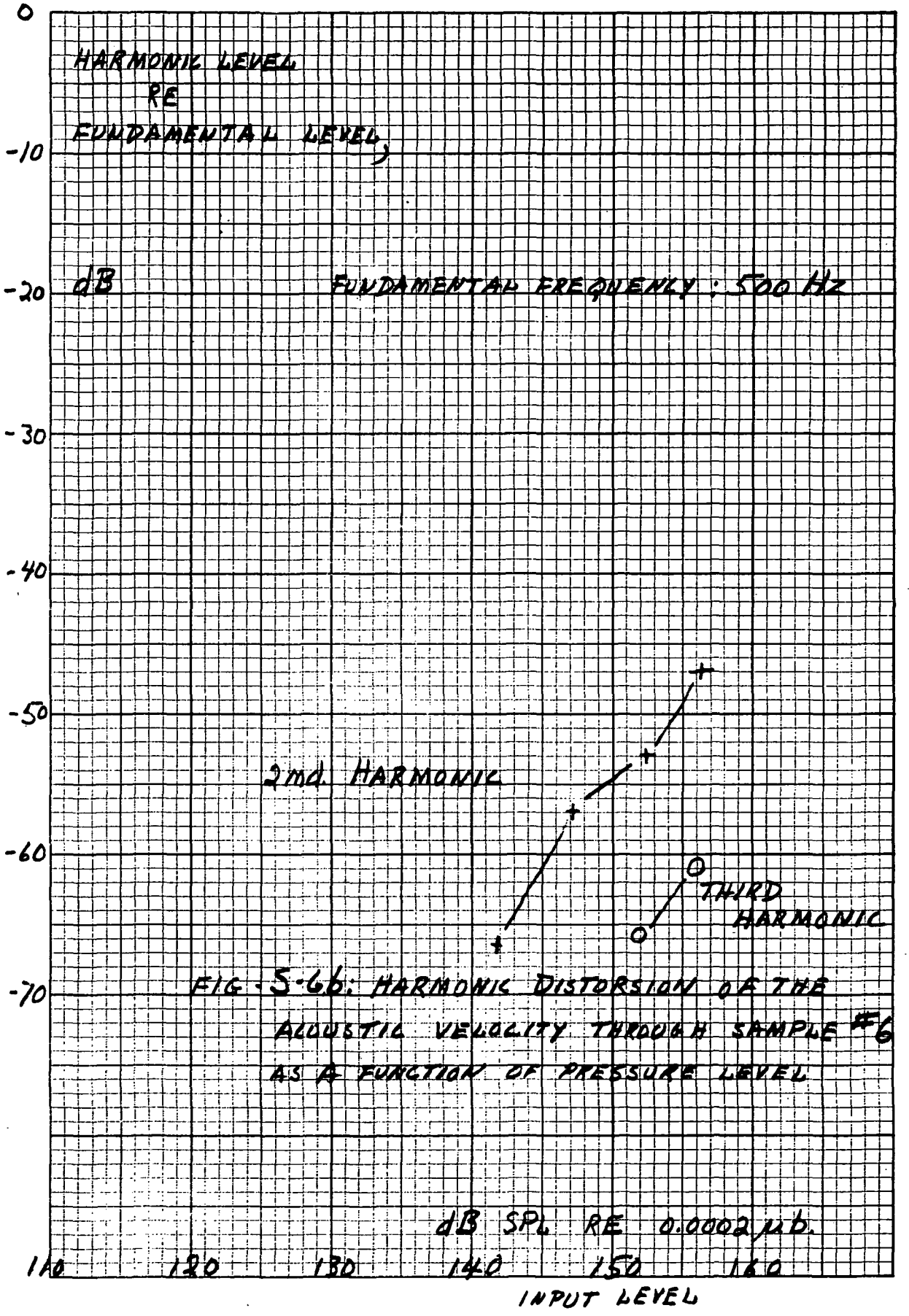

FIG. 5.66: HARMONIC DISTORTION OF THE ACOUSTIC VELOCITY THROUGH SAMPLE #6 AS A FUNCTION OF PRESSURE LEVEL

APPENDIX VII

FIRST ORDER PERTURBATION OF THE FREQUENCY RESPONSE OF AN IDEAL POROUS SURFACE SENSOR, INCLUDING THE COMPLEX ADMITTANCES OF THE POROUS SURFACE

The original analysis of a porous surface sensor, established first the condition of anechoicity in the forward direction inside the sensor and then proceeded to apply a reciprocity theorem in order to obtain the frequency response $s(\omega)$ and the directivity function $w(\underset{\sim}{k})$; this last approach allowed the directivity function to be obtained in closed form, showing, for a uniform porous surface sensor, that the directivity function is that of a uniformly delayed line sensor.

The only property of the porous surface used in the original analysis was its specific acoustic resistance r being real. The same resistance r is used for the self and the transfer impedance of the porous surface, thereby implying that the thickness of the porous surface has a negligible effect.

In the present memo, we reset the analysis of the frequency response $s(\omega)$ and directivity function $w(\underset{\sim}{k})$ of a porous surface sensor without using a reciprocity argument. The purpose of this different approach is not to obtain again the same results achieved by reciprocity, but rather to uncover a more convenient format which could explicitly show the effects of a complex impedance and a finite thickness of the porous surface on the frequency response of the sensor.

The analysis is first cast in rather general terms, but is still retaining the one-dimensional approach originally taken. The porous surface is now specified by its self admittance y_{11} and transfer admittance y_{12}.

The frequency response $s(\omega)$ can be pulled-out of this new analysis and the effect of y_{11}, y_{12} on $s(\omega)$ obtained. The present memo concentrates on this aspect.

I. DIFFERENTIAL EQUATION OF THE COUPLING BETWEEN OUTSIDE AND INSIDE PRESSURE FIELDS

Consider a section of a porous surface sensor, shown in Fig. 1. The section shown belongs to a porous strip sensor, for simplicity; however the analysis is applicable to the other designs, like a porous pipe sensor. A harmonic pressure $p_o(x)$, uniform in the y direction, at a frequency ω, is applied to the surface. (The harmonic time dependence $\exp(i\omega t)$ is suppressed in all the following notations). A pressure $p(x)$ inside the sensor is caused by $p_o(x)$. Both $p_o(x)$ and $p(x)$ can be complex.

The porous sensor surface is specified by its specific admittances y_{11} and y_{12}.

$$u(x) = p_o(x)y_{12} - p(x)y_{11} \tag{1}$$

where y_{11} and y_{12} are functions of frequency but not of x: the porous surface is assumed to be uniform. The acoustic velocity $u(x)$ is specified at the inside surface of the porous material. The porous material is assumed to be symmetrical at its two faces.

The inside cross section of the sensor is characterized at the location x by a specific admittance $y_+(x)$ for waves traveling in the +x direction and specific admittance $y_-(x)$ for waves traveling in the -x direction. Both $y_+(x)$ and $y_-(x)$ are functions of the location x of the cross section, and may be complex.

The increment ΔU of volume velocity at the inside porous surface is also related to an increment $\Delta p(x)$ of the inside pressure

$$\Delta U = ua\Delta x = [\Delta p(x)] \left(y_+(x) + y_-(x)\right) ah(x) \tag{2}$$

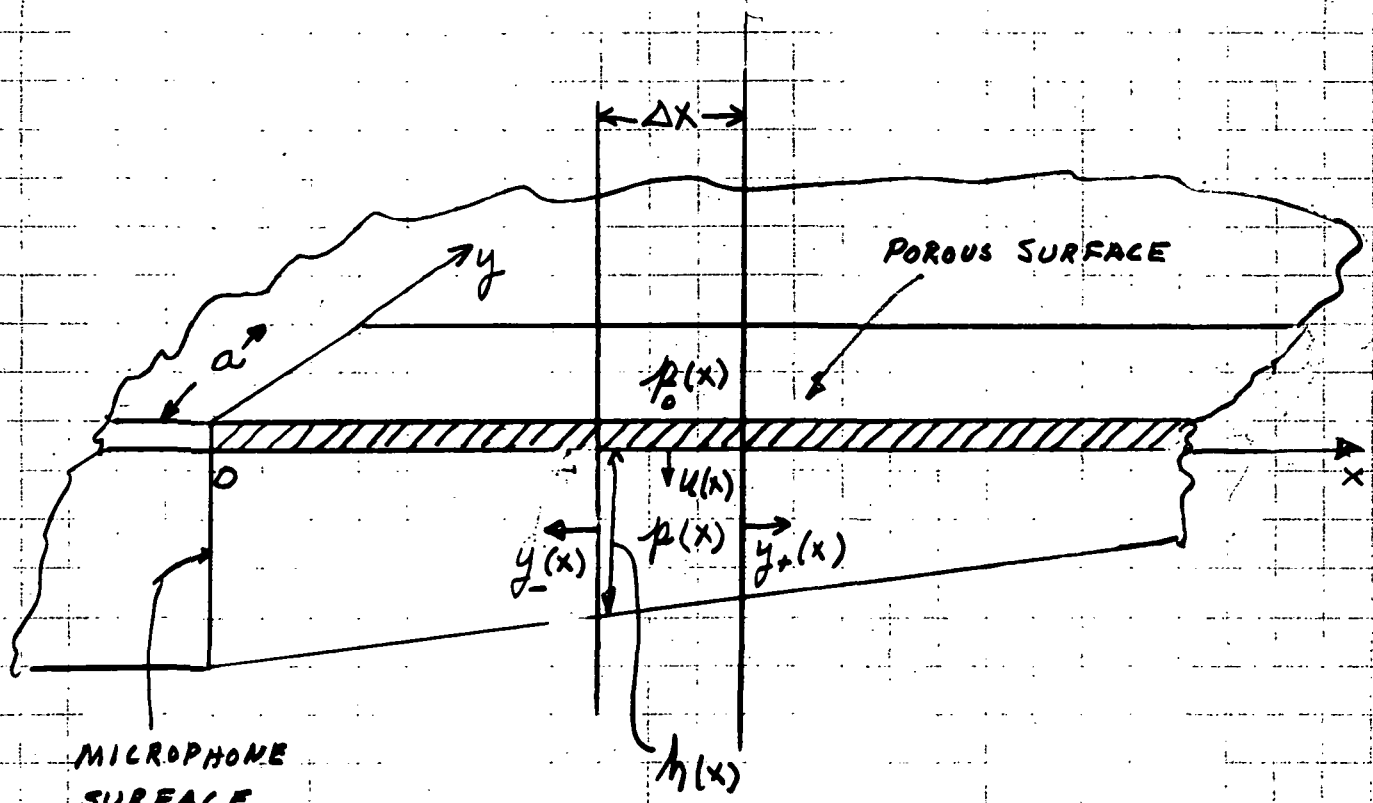

FIG-1 : CROSS-SECTION OF A POROUS SURFACE SENSOR

Introducing (2) in (1) we obtain

$$\frac{\partial p(x)}{\partial x}\,[y_+(x) + y_-(x)]h(x) = p_o(x)y_{12} - p(x)y_{11} \qquad (3)$$

where the limit $\Delta x \to \partial x$ has been taken.

Equation (3) is a perturbation of the ideal porous surface sensor in that the specific acoustic admittance of the porous surface is specified by the self admittance y_{11} and the transfer admittance y_{12}; we have kept the same geometry of the original sensor, represented by height h(x) of the air cavity. The admittances $y_+(x)$ and $y_-(x)$ will depend on the admittances y_{11} and y_{12}.

For the ideal sensor we had originally [1] assumed that

$$y_{11} = y_{12} = 1/r \qquad (4)$$

where r is the specific acoustic resistance of the porous surface, implying also that the transmission through the porous surface is instantaneous.

In Section II we develop a first order perturbation of the frequency response of a real sensor by introducing into (3) a particular condition satisfied by the ideal sensor.

---

[1] D. U. Noiseux, T. G. Horwath, "Design of a Porous Surface Sensor for the Rejection of Flow Noise," Submitted to JASA.

II. FREQUENCY RESPONSE $s(\omega)$

The frequency response $s(\omega)$ is the response of the sensor to an acoustic plane wave propagating along the axis of the sensor in the -x direction:

$$p_o(x) = P_o e^{ik_o x} \tag{5}$$

where k_o is the wavenumber of the outside gas.

The pressure wave $p(x)$ inside the sensor can be decomposed into two waves, propagating in the +x and -x directions:

$$p(x) = P_+(x)e^{-ik_i x} + P_-(x)e^{+ik_i x} \tag{6}$$

where we allow $P_+(x)$ and $P_-(x)$ to vary along x; k_i is the wavenumber of propagation of the waves inside the sensor; k_i is assumed to be real and equal to the free wavenumber of the inside gas. This last assumption applies to the ideal sensor; in a real sensor where y_{11} and y_{12} do not quite satisfy the ideal conditions, the wavenumber of propagation is likely to be complex; however, the real part of that wavenumber should be very nearly equal to k_i and the imaginary part (leading to attenuation of the waves) will be included in the fact that $P_-(x)$, $P_+(x)$ are allowed to be functions of x.

Introducing (5) and (6) in (3) we get

$$\left[e^{-ik_i x}\left(-ik_i P_+(x) + \frac{\partial P_+(x)}{\partial x}\right) + e^{ik_i x}\left(ik_i P_-(x) + \frac{\partial P_-(x)}{\partial x}\right)\right]\left[y_+(x) + y_-(x)\right]h(x)$$

$$= y_{12} P_o e^{ik_o x} - y_{11}\left[P_+(x)e^{-ik_i x} + P_-(x)e^{ik_i x}\right] \tag{7}$$

When the inside gas and the outside gas are identical and, further, when the direction of propagation of the outside plane wave is parallel to the axis of the sensor, then:

$$k_o = k_i \tag{8}$$

This is the condition leading to the frequency response $s(\omega)$, which can be defined by

$$s(\omega) = p(o)/P_o \quad ; \; k_o = k_i \tag{9}$$

$$= [P_+(o) + P_-(o)]/P_o \quad ; \quad k_o = k_i$$

$p(o)$ being the inside pressure at $x = 0$, which is the pressure at the surface of the microphone.

For the ideal porous surface sensor, with a high impedance microphone,

$$y_-(o) \cong 0 \tag{10}$$

and the conditions (4) and (8), we already know the sensitivity[1]:

$$s(\omega) = 1 \tag{11}$$

If we introduce the ideal conditions (4) and (8) into (7) we find that the right hand side of (7) becomes zero at $x = 0$

$$P_o - [P_+(o) + P_-(o)] = 0 \tag{12}$$

in order to satisfy (11). The left hand side of (7) must also be equal to zero for an ideal sensor. Reorganizing the left hand side of (7) we have, at $x = 0$,

$$ik_i[P_-(o) - P_+(o)] + \left\{\frac{\partial}{\partial x}[P_+(x) + P_-(x)\right\}_{x=0} = 0 \qquad (13)$$

We recognize that (13) is also satisfied by a plane wave inside a solid tube and incident on a hard boundary at the end of the tube, x=0: the incident and reflected pressures are equal

$$P_+(o) = P_-(o) \qquad (14a)$$

and their slopes are equal and of opposite signs:

$$\frac{\partial P_+(x)}{\partial x}\bigg|_{x=0} = -\frac{\partial P_-(x)}{\partial x}\bigg|_{x=0} \qquad (14b)$$

Hence, the ideal sensor with a high impedance microphone, during a test of its frequency response, has the same pressure field near the microphone surface as found in a tube with solid wall at a hard termination. The implication is that, near x=0, the acoustic volume velocity leaking through the porous wall is very small compared with the acoustic volume velocity of the waves propagating axially. Indeed, this is shown by (12) which states that, at x=0, the inside and outside pressures are equal such that the radial component of acoustic velocity is zero.

The statements (14) are satisfied only 1) when the incident pressure field is along the axis the porous surface, 2) and its wavenumber k_o is equal to the wavenumber k_i of the gas inside the sensor, 3) the microphone impedance is effectively infinite, and finally, 4) the admittances y_{11} and y_{12} are equal and equal to $1/r$, the specific resistance r of the porous surface satisfying the design equations.

When the four conditions listed above are not satisfied then Eqs. (14a) and (14b) do not follow.

We consider now a perturbation of the ideal porous surface sensor where y_{11} and y_{12} of the porous surface do not quite satisfy the ideal condition; we have

$$y_{11} \neq 1/r \tag{15a}$$

$$y_{12} \neq 1/r$$

As a result $y_+(x)$, which is the admittance of the cavity in the +x direction, is different from the value found in the ideal sensor; the admittance $y_-(o)$, which is the admittance of the microphone is still constrained to be zero, as in Eq. (10). The incident pressure field is axial and its wavenumber k_o is equal to k_i. If the inequalities (15a and 15b) are such that y_{11} and y_{12} are nearly equal to $1/r$, then the left hand side of Eq. (7) is nearly equal to zero at x=0. Letting the left hand side of (7) be a small quantity $\varepsilon(\omega)$ at x=0, Eq. (7) becomes, at x=0,

$$y_{12}P_o - y_{11}[P_+(o) + P_-(o) = \varepsilon(\omega) \tag{16}$$

giving

$$s(\omega) = \frac{P_+(o)+P_-(o)}{P_o}$$

$$= \frac{y_{12}}{y_{11}} - \frac{\varepsilon(\omega)}{P_o y_{11}} \tag{17}$$

$$s(\omega) \cong y_{12}/y_{11} \tag{18}$$

Equation (18) is the desired result. It is a first order perturbation of the ideal porous surface sensor, the perturbation consisting of the introduction of y_{11} and y_{12} of the porous surface instead of the ideal value r^{-1}.

III. APPLICATION TO AN IDEAL POROUS SURFACE OF FINITE THICKNESS

The admittances y_{11} and y_{12} of a purely resistive (the ideal porous material) porous material have been developed in Appendix 2:

$$y_{11}\, r = \frac{\gamma d}{\tanh \gamma d} \tag{19a}$$

$$y_{12}\, r = [\sinh(\gamma d)]^{-1} \tag{19b}$$

where d is the thickness of the porous material. With (19) in (18) we get

$$s(\omega) = [\cosh(\gamma d)]^{-1} \tag{20}$$

Finally, using the notation of Appendix 3

$$\gamma d = (1+i)\beta \tag{21}$$

$$\beta^2 = \frac{k_o d}{2} \quad \frac{r}{\rho_o c_o} \quad \Omega\alpha \tag{22}$$

we get

$$s(\omega) = [\cos\beta\cosh\beta + i \sin\beta\sinh\beta]^{-1} \tag{23}$$

The value of $s(\omega)$ is calculated in Fig. 2 and plotted as a function of β^2; since β^2 is proportional to frequency, the curve of Fig. 2 becomes a normalized frequency response of a porous surface sensor when the porous material is purely resistive.

The results of Appendix 5 indicate that for the values of $r/\rho_o c_o$ required by porous surface sensors, the real porous materials investigated behave very nearly like a purely resistive porous material. Hence, we could use Fig. 2 to predict the frequency response of a real porous surface sensor.

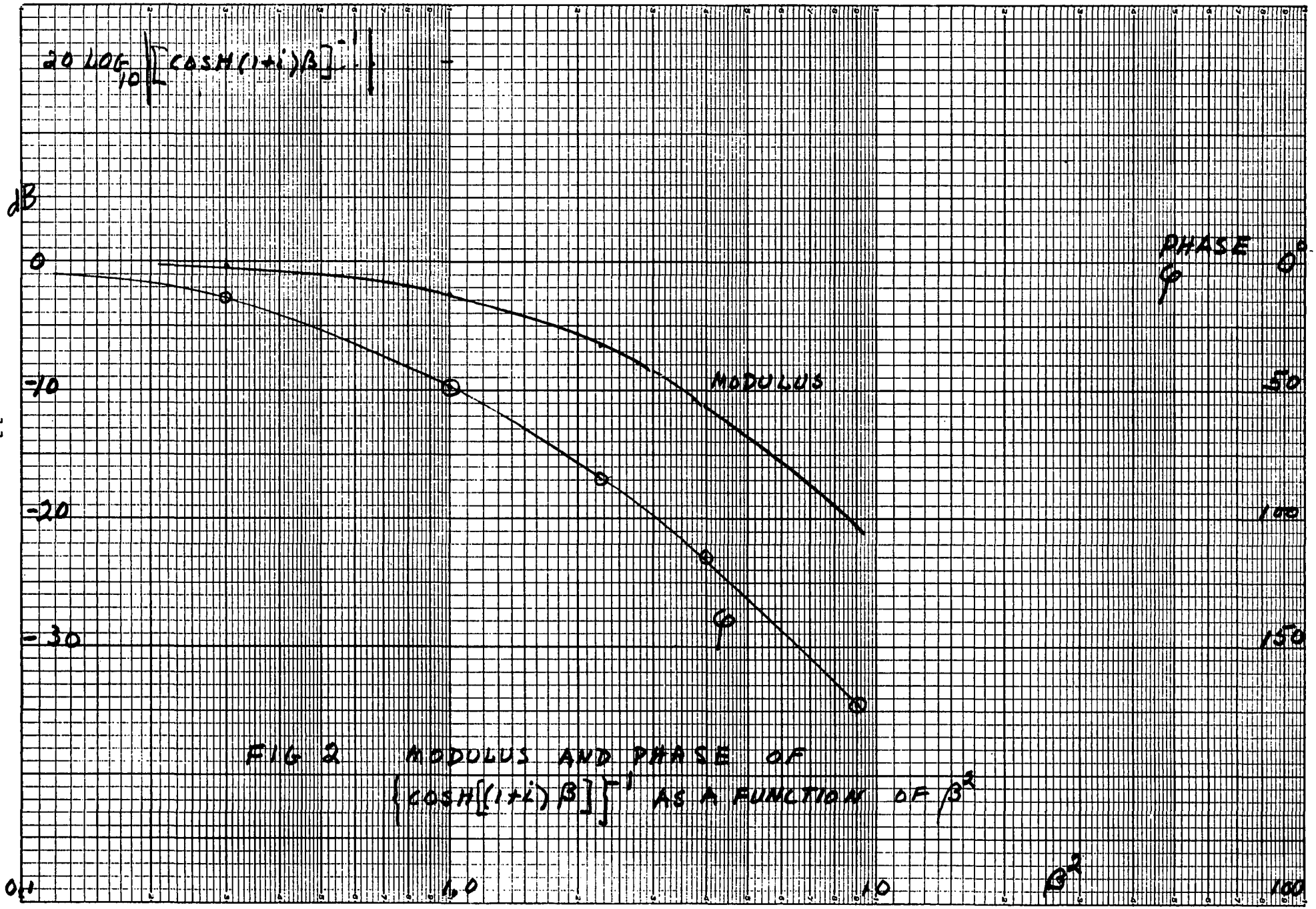

FIG 2 MODULUS AND PHASE OF $\{\cosh[(1+i)\beta]\}^{-1}$ AS A FUNCTION OF β^2

IV. EXAMPLES

Consider the materials listed as Samples #1 and #6 of Appendix 5. These materials were used in the Porous Strip Sensor and in the Porous Pipe sensor; however, the specific materials used in each sensor were selected for the correct value of the specific resistance r, which is not exactly the value of the sample tested in Appendix 5. Using the values of β^2 at 10 kHz reported in Table II of Appendix 5 and the value of $r/\rho_o c_o$ of each sample, then changing the value of β^2 for each semsor to correspond to the actual value of $r/\rho_o c_o$ selected for these sensors we get a correct value β'^2 at 10 kHz for each sensor. Then this value of β'^2 at 10 kHz is entered in Fig. 2 to obtain their calculated frequency responses. Finally, the measured frequency response of each sensor is compared in Fig. 3 with the calculated values.

The following table shows the calculation procedure

$$\beta'^2 = \beta^2 \times \frac{r'}{r} \quad \text{at 10 kHz}$$

Sample #	$r/\rho_o c_o$	β^2 at 10 kHz	Sensor	$r'/\rho_o c_o$	β'^2 at 10 kHz
1	73	5.4	Porous Strip	60	4.5
6	140	9	Porous Pipe	130	8.4

The agreement between the measured and calculated frequency responses of the two sensors is remarkably good; it is within approximately 2 dB. This agreement is by far the best one we have obtained so far in our attempts to explain the drop in frequency response of porous surface sensors.

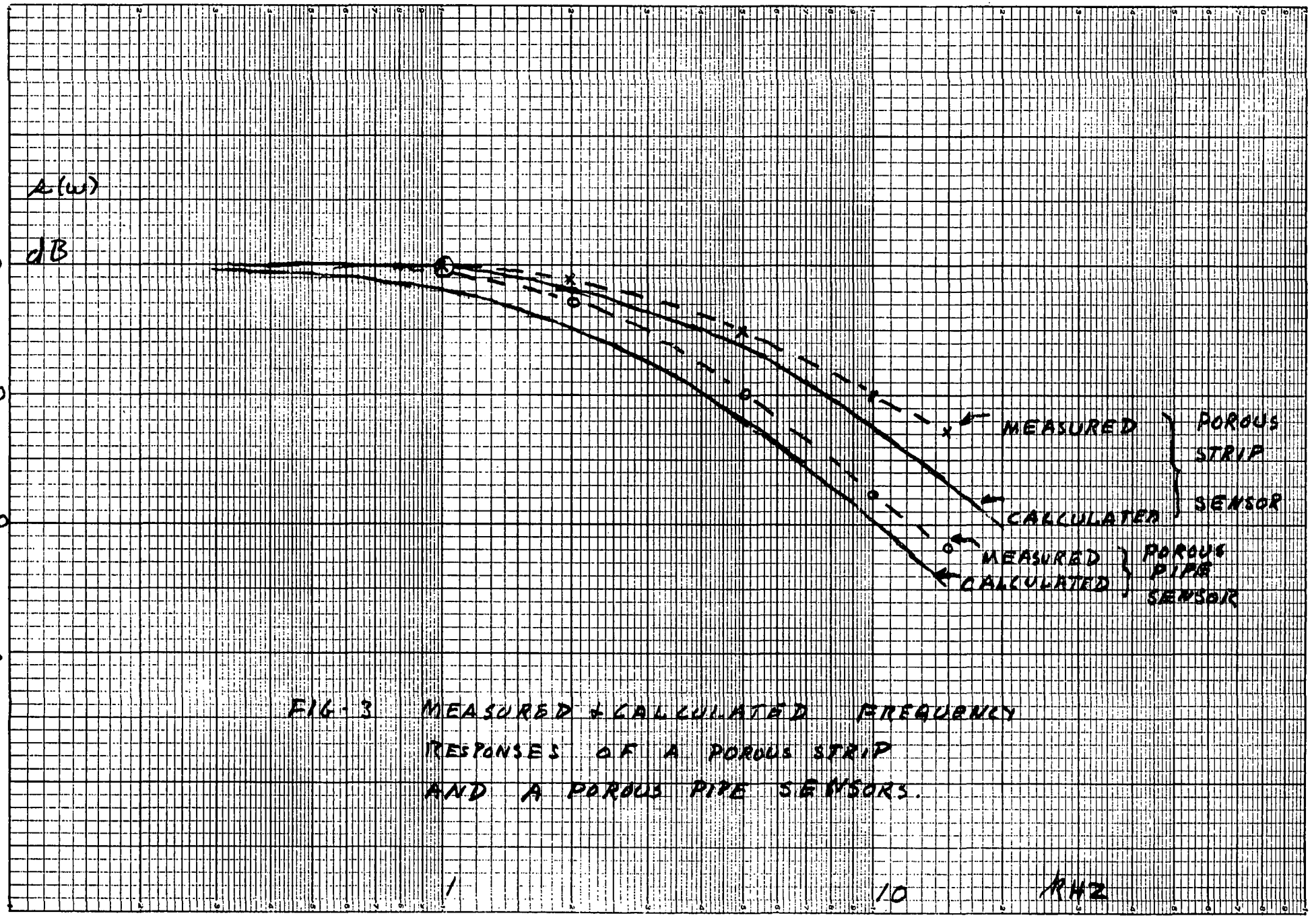

FIG-3 MEASURED & CALCULATED FREQUENCY RESPONSES OF A POROUS STRIP AND A POROUS PIPE SENSORS.

Although the analysis leading to Eq. (18) is not exact, (it neglects the shear viscous layer inside the sensors; it considers a one-dimensional wave propagation) it appears to be sufficient to predict the frequency response of the types of porous sensors which we have deisgned, within a reasonable accuracy. It follows that the parameter β^2 of porous surface materials could be used with some confidence in the design of porous surface sensors: the value of β^2 should not exceed unity at the highest frequency of interest.

APPENDIX VIII

TESTS OF TWO SPECIAL POROUS MATERIALS

This appendix describes the properties of two porous materials which have been ordered specially to meet the requests of the Airfoil Sensor. These materials, as specified, are not under current production.

These two materials and their characteristics are discussed in the following sections. Section I examines the uniformity of flow resistance. Section II shows the measured transfer admittance and the linearity.

The two special materials are identified by the companies which produced them under our specifications:

- Fiber Felt Metal from Michigan Dynamics Corporation, and
- Sintered Porous Steel from Mott Mettallurgical Corporation.

I. Uniformity of Acoustic Resistance

1. Fiber Felt Metal From Michigan Dynamics Corp.

Four sheets of porous felt metal, each 12 inches x 6 inches and 0.020" thick have been tested.

The uniformity of flow resistance has been examined acoustically. The technique consists of applying a known acoustic pressure at one face of the porous material and measuring the acoustic pressure generated at the other face where a known closed cavity is located. The pressure in the cavity is directly related to the acoustic velocity through the material, and hence, from the known blocked pressure, the acoustic resistance of the material is calculated. The measurements are done at a low frequency, 200 Hz, to avoid corrections which would otherwise be necessary.

Each measurement of acoustic resistance is made over an area of one half inch in diameter; the measurements are separated at half inch intervals along strips marked on the material. Figure 1 shows the results of the measurements on one sample: it is the best sample for uniformity. The sheet was divided into 12 columns, 5/8 inch wide, and measurements in each column made at 1/2 inch intervals.

The average flow resistance had been specified to be 25 $\rho_0 c_0$ (28 dB re $\rho_0 c_0$). The average flow resistance was controlled by calendering: this process is unfortunately likely to degrade the uniformity.

The results of Fig. 1, which represent the best sample, show that the average flow resistance is almost satisfied in the central

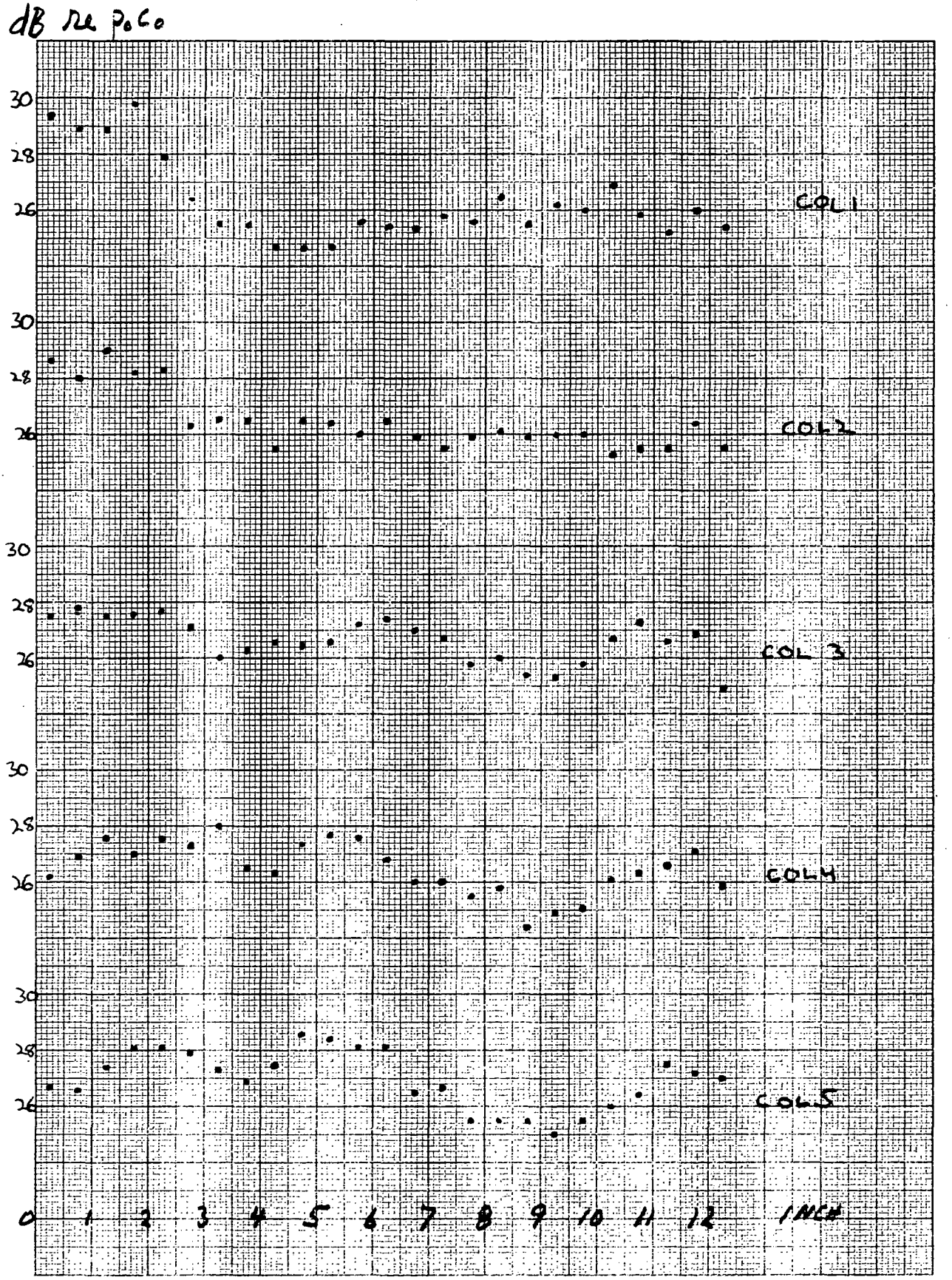

FIG. 1 ACOUSTIC RESISTANCE OF SAMPLE #2 OF FIBER FELT METAL FROM MICHIGAN DYNAMICS.

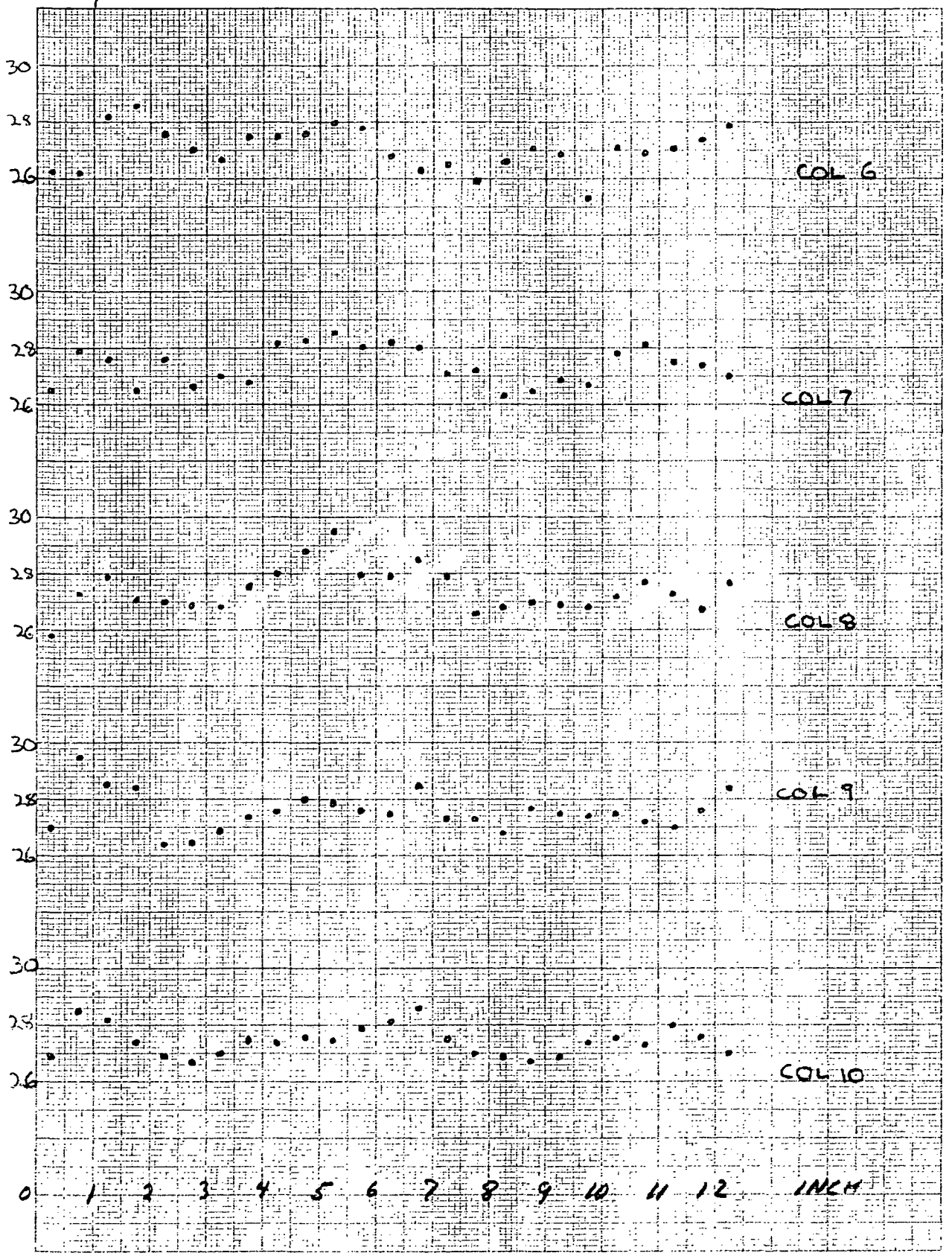

FIG 1. (CONTINUED)

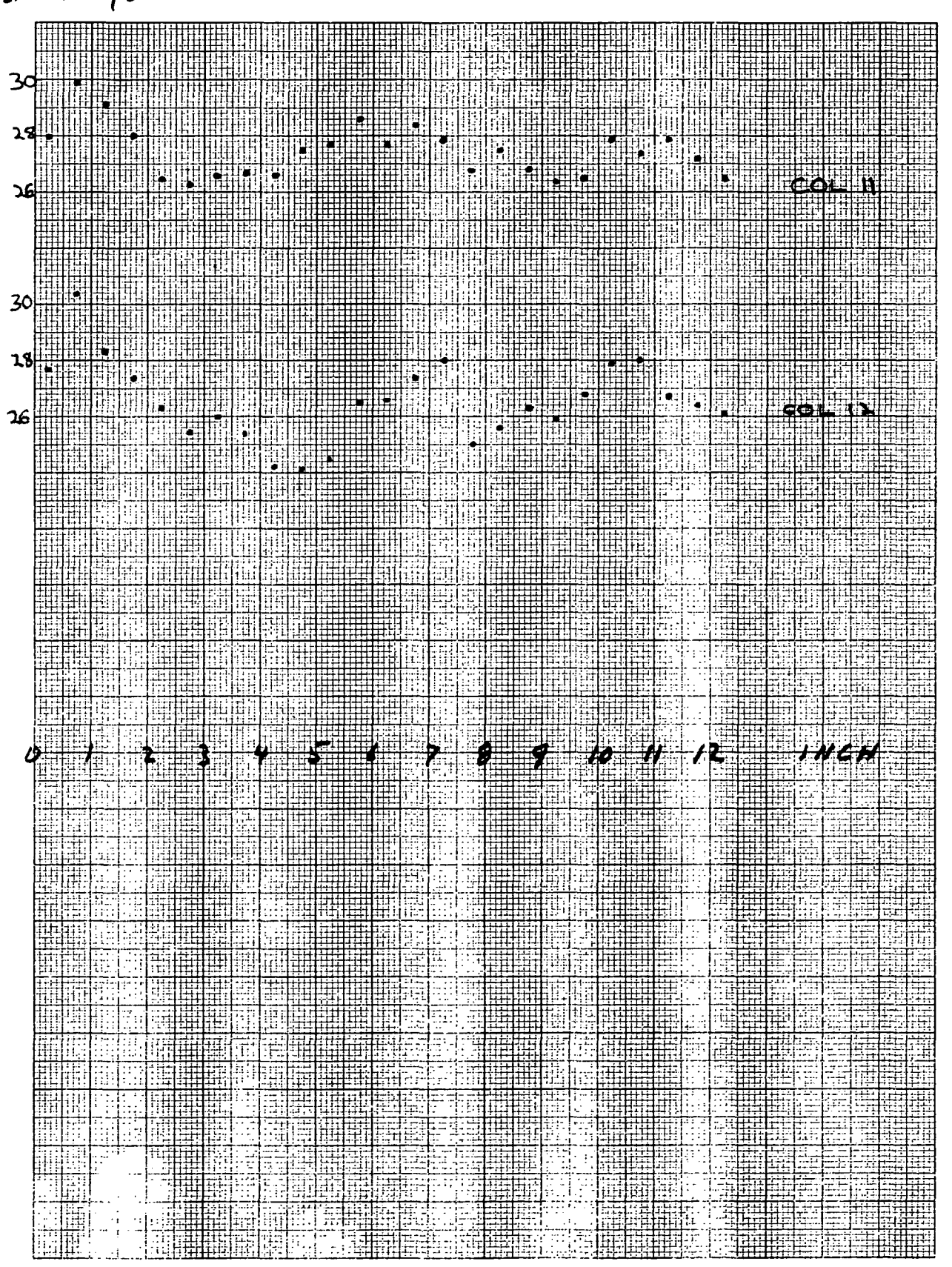

FIG. 1. (CONTINUED)

region of the sample. The variation of resistance is approximately ±1 dB in the more uniform region and degrades rapidly to ±2 dB and more in the other regions. The other samples, also satisfied the requirement of average resistance in the central region, but had greater variations about the mean values of each column.

The uniformity of resistance of Fig. 1 is not as good as we were led to believe. It is, however, better than any other material previously tested.

2. Sintered Porous Steel from Mott Metallurgical Corporation

The material has been ordered in strips of 12 inches by 2 inches wide, 0.025 inch thick. The average resistance was required to be 50 $\rho_0 c_0$ (34 dB re $\rho_0 c_0$).

The strips were molded and sintered individually instead of being molded and sintered in larger sheets and cut from the large sheets. By fabricating smaller strips, it was hoped that the uniformity of flow resistance would be better controlled. Each sample could produce at least three strips. Figure 2 shows the flow resistance at the center line of 7 samples.

From these samples we find the average resistance varies from 30 to 36 dB re $\rho_0 c_0$. The variation about the mean of each sample could be as low as ±1 dB over most of the length of a sample, to ±2 dB.

For the 30 samples which have been purchased we expect to be able to select portions of strips having the same average value and a deviation not exceeding ±1 dB, and of sufficient total length to use in at least three complete sensors.

In addition to the results shown, it appears possible to modify the average flow resistance, by burnishing lines which can

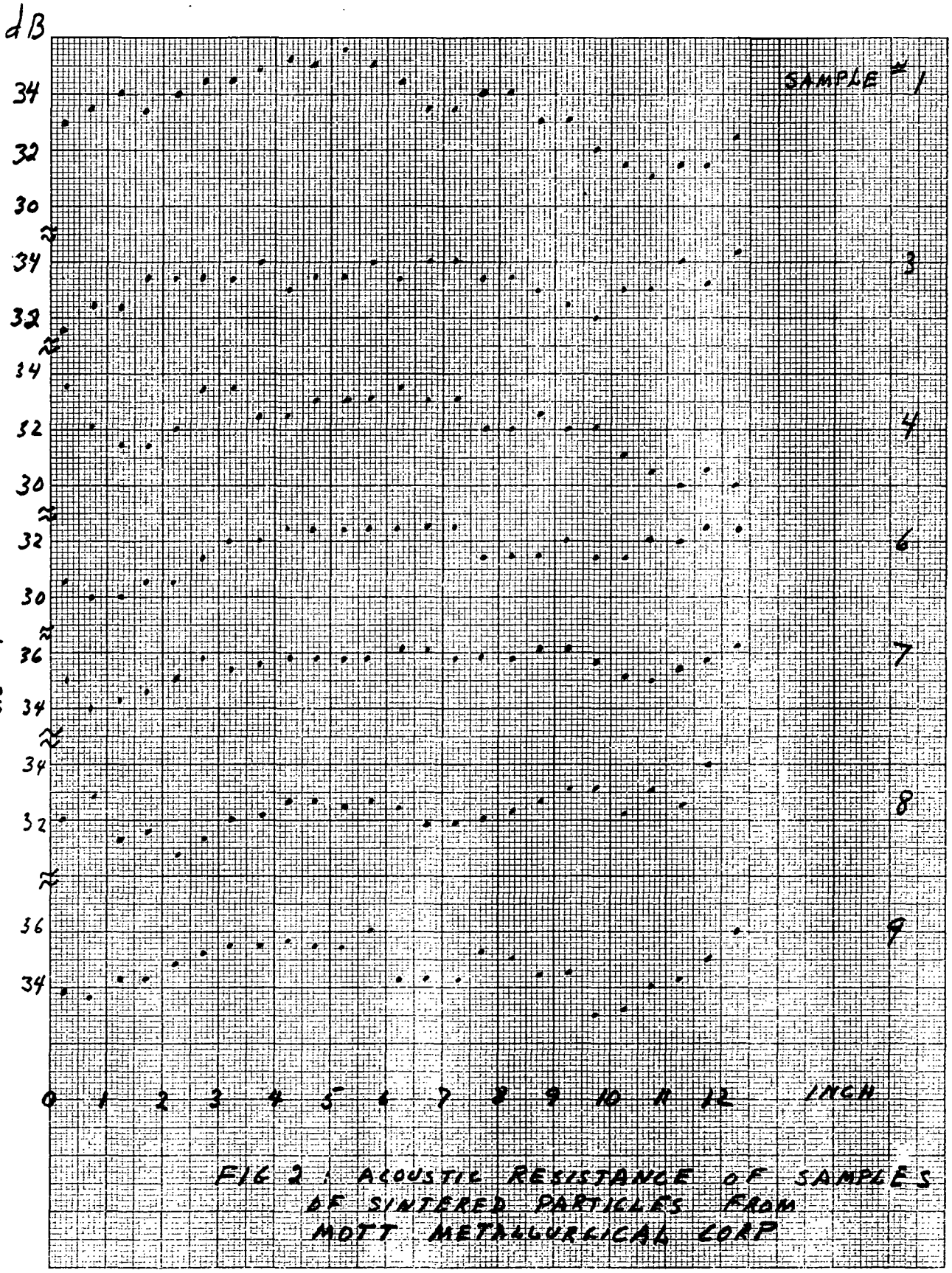

FIG 2 : ACOUSTIC RESISTANCE OF SAMPLES OF SINTERED PARTICLES FROM MOTT METALLURGICAL CORP

increase the resistance by about 1 dB. Hence, the net yield of adequate strips of the correct final average resistance and having a deviation of ±1 dB is likely to possibly be twice as large as can be obtained from the initial state of the material.

3. Conclusions

It is clear that neither one of the two processes, sintered felt or sintered particles, can be controlled to the desired accuracy in average resistance and in local deviation from the average. The calendering done by Michigan Dynamics tends to bring the average resistance closer to its desired value but at the cost, we feel, of larger local deviations.

The high cost of the sintered felt produced by Michigan Dynamics, (this cost is approximately three times that of the sintered particles) is a serious disadvantage for the sintered felt.

The porous material from Mott Mettallurgical Corp. has been finally selected for the porous sensors because of its lower cost and its higher elastic modulus.

II. Transfer Admittance and Linearity

The two samples had different specifications,

Mott: 0.025 inch thick; 50 $\rho_0 c_0$

Michigan D: 0.020 inch thick; 25 $\rho_0 c_0$

because the second sample could be fabricated in thinner sheets than the first one and was claimed to achieve a very good uniformity; hence, the second sample could be used in narrower strips than the first sample, and yield a more uniform frequency response than the first sample. It turned out that the uniformity of the acoustic resistance of either sample is not very good and that the strips will have to be selected anyway; the narrower strip envisioned with the second sample became impractical. In addition, the second sample has a much lower Young's modulus than the first sample, leading to undesirable bending resonances of the strip within the frequency range of interest. In fact, the second sample, in the sample holder of the test, exhibited a first bending resonance at 9 kHz, which prevented the measurement of the phase of its transfer admittance in this important frequency region. (A smaller test sample could have been made, but it was already decided not to use this sample in the final design of the sensor.) The modulus of the transfer admittance was calculated in the normal way except that the resonance near 9 kHz was ignored.

A comparison of the test results of the special Mott material with those of the Mott material used in the first porous surface microphone (see Sample No. 1, Mott 5 micron, reported in 5) shows that the phase of y_{12} of this special material is very nearly that of sample No. 1 but shifted upwards in frequency by more than a factor of 3. In fact, when the phase of y_{12} of the special Mott

material is matched with the phase of the ideal porous material (as shown in Fig. 1a, Appendix 3) we arrive at a value of $\beta^2 = 1.2$ at 10 kHz. With this value, we get from Fig. 2 of Appendix 7 a predicted frequency response of the sensor which is down -3.5 dB at 10 kHz.

The linearity of the two new samples is very good, as shown by the third harmonic distortion as a function of acoustic pressure level, the Mott sample being slightly superior.

TABLE 1

CHARACTERISTICS OF SPECIAL POROUS SAMPLES

Sample No.	7,	8,
Process	A	B
Supplier	Mott	Michican Dynamics
Grade	2μ	--
Material	Stainless 316L	Stainless 304 L
thickness	0.617 mm	0.485 mm
ρ_s: sample density	5.23 g/cc	4.74 g/cc
ρ_m: material density	7.9 g/cc	8.0 g/cc
Ω: porosity	.338	.407
$r/\rho_0 c_0$: specific resistance	49.5	28.5
Frequency Characteristic	Fig. 3	Fig. 4
Distortion Characteristic	Fig. 5	Fig. 6

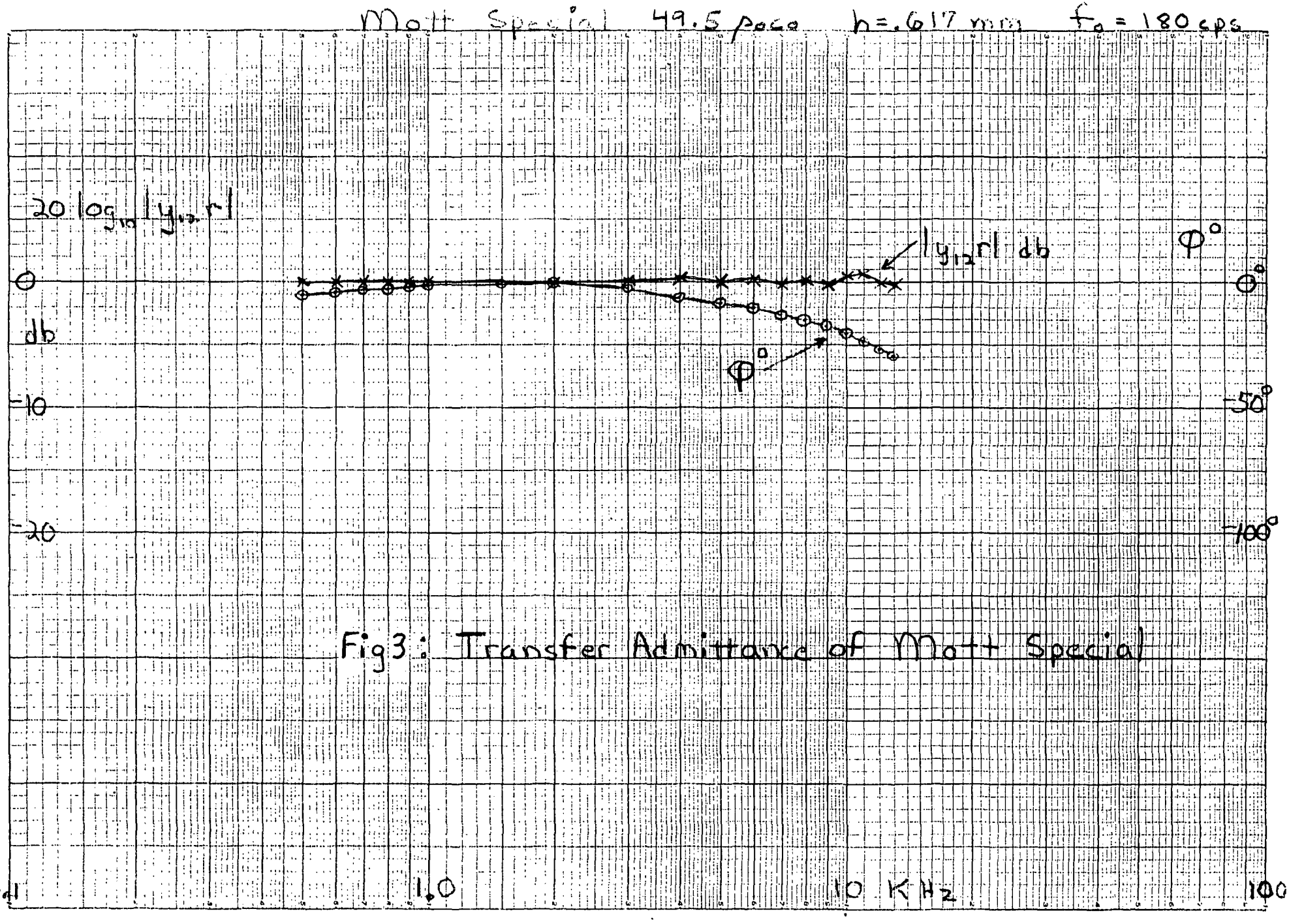

Fig 3: Transfer Admittance of Mott Special

Michigan Dynamics Special 28.5 pcs $h = .485$ mm $f_o = 305$ cps

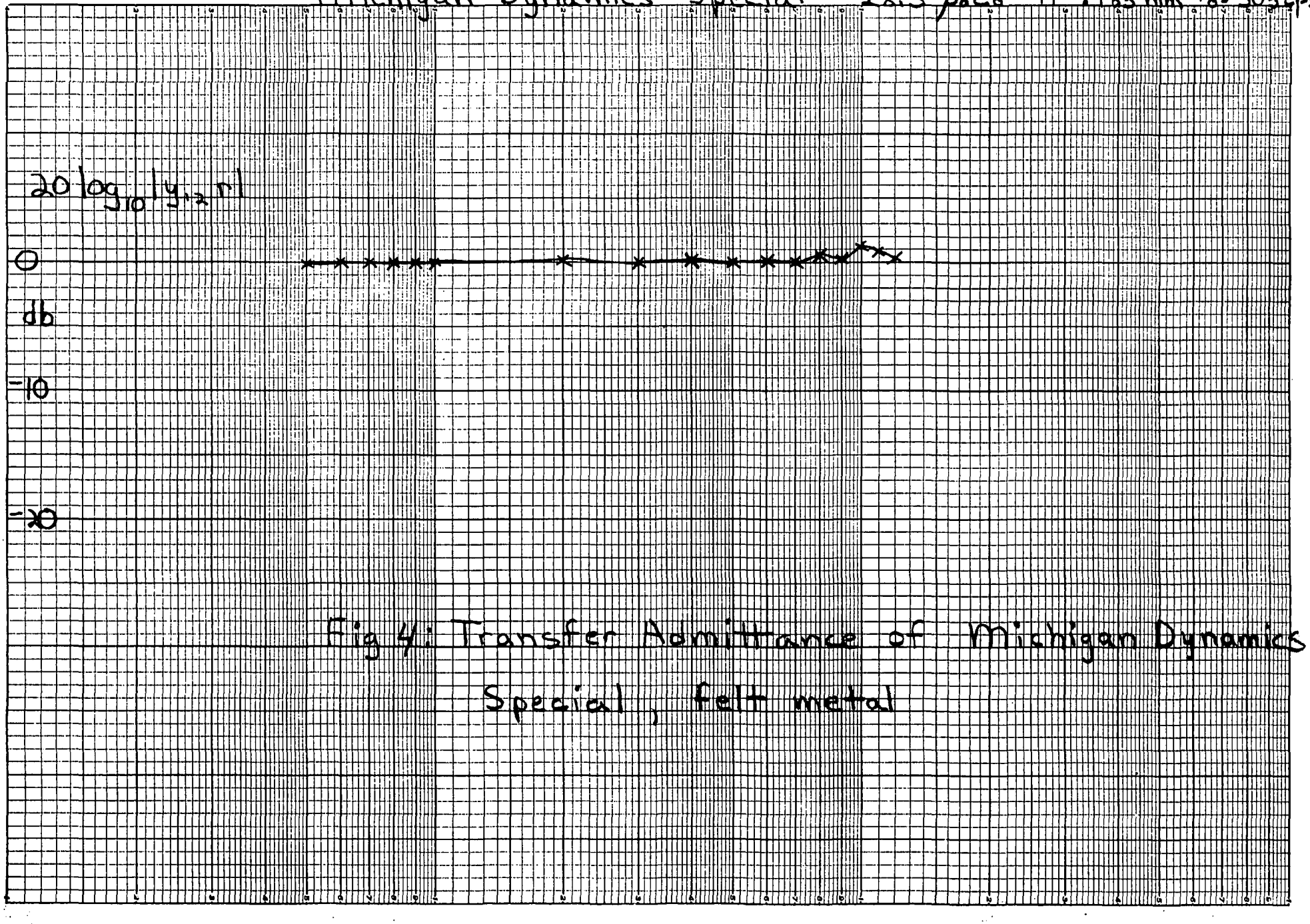

Fig 4: Transfer Admittance of Michigan Dynamics Special, felt metal

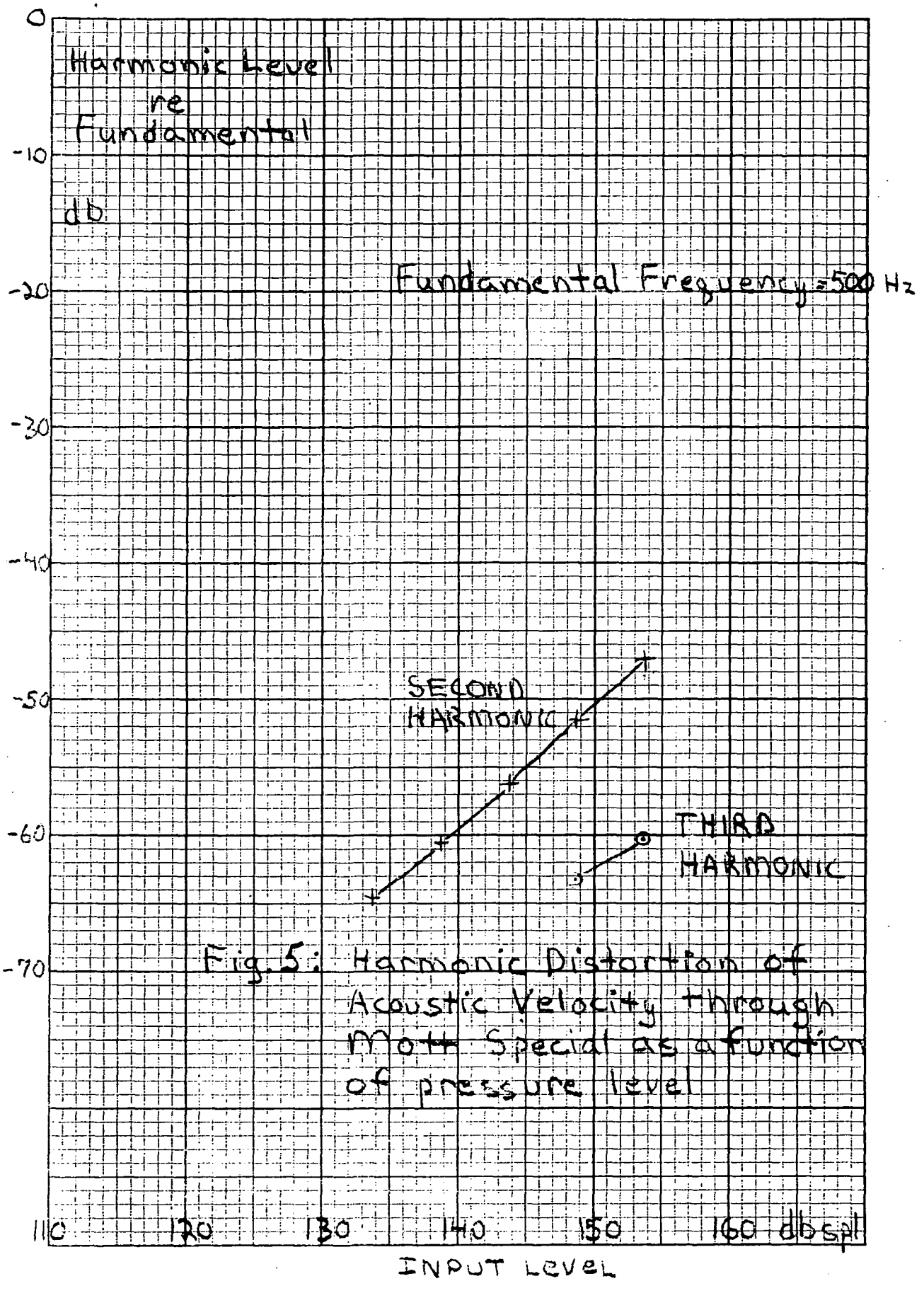

Fig. 5: Harmonic Distortion of Acoustic Velocity through Moth Special as a function of pressure level

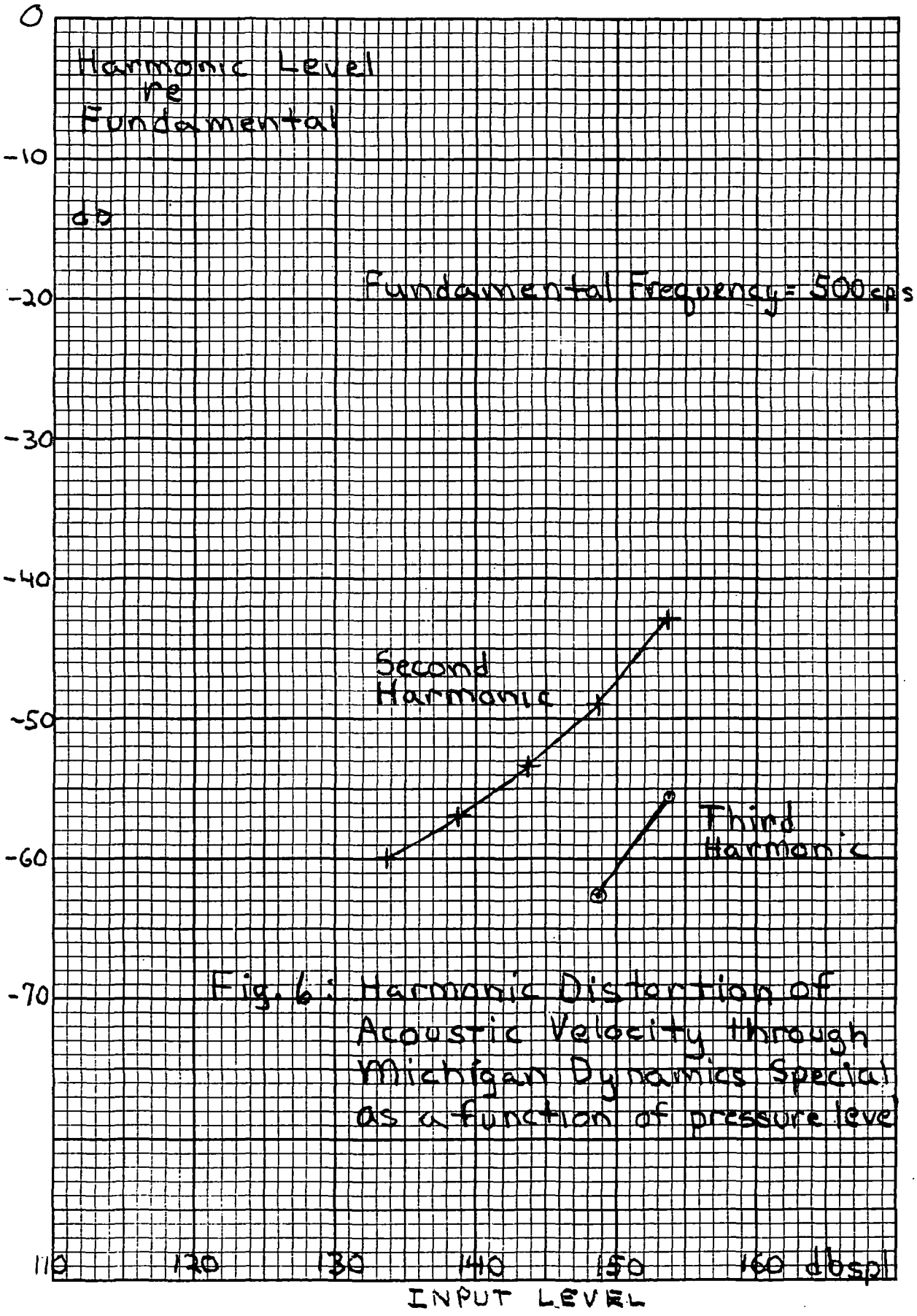

Fig. 6: Harmonic Distortion of Acoustic Velocity through Michigan Dynamics Special as a function of pressure level

APPENDIX IX

ACOUSTIC TESTS OF THE NEW POROUS SURFACE MICROPHONE IN AN AIRFOIL, MODEL 342

This appendix presents the acoustic calibration of the new Porous Surface microphone in an airfoil.

1. POROUS SURFACE MICROPHONE IN AN AIRFOIL

The new design of the Porous Surface Microphone in an airfoil has been assigned the model number 342. This is the first unit.

The airfoil is a NACA-64-012 section of thickness slightly less than 1.58 cm (5/8 inch); it is an epoxy cast which includes the required internal acoustic cavities. Two threaded rods, cast in the airfoil, provide the mechanical connections to a microphone base which is a continuation of the airfoil; this base attaches to a stand. The base was designed to carry the microphone preamplifier and to provide an internal path for the electrical leads. Figure 1 is a photograph showing the Porous Surface Microphone and its base; the base is in two parts.

Two porous strips, each 35.5 cm (14 inches) long and 1.27 cm (0.5 inch) wide, are cemented symmetrically on opposite sides of, and flush with, the airfoil surface. The porous material is a special sintered stainless steel (see Sample No. 7, Appendix 7) supplied by Mott Metallurgical Corporation; its thickness is 0.63 mm (0.025 inch) and its nominal specific acoustic resistance is 50 $\rho_0 c_0$, where $\rho_0 c_0$ is the characteristic impedance of air.

The porous strips consist each of two shorter strips selected for the average value and uniformity of acoustic resistance. The local variation of the specific acoustic resistance along the length of the two strips is shown in Fig. 2; the top and bottom strips are identified by the sketch in the same figure. The local variations are within ±1 dB of the average value. (The strip

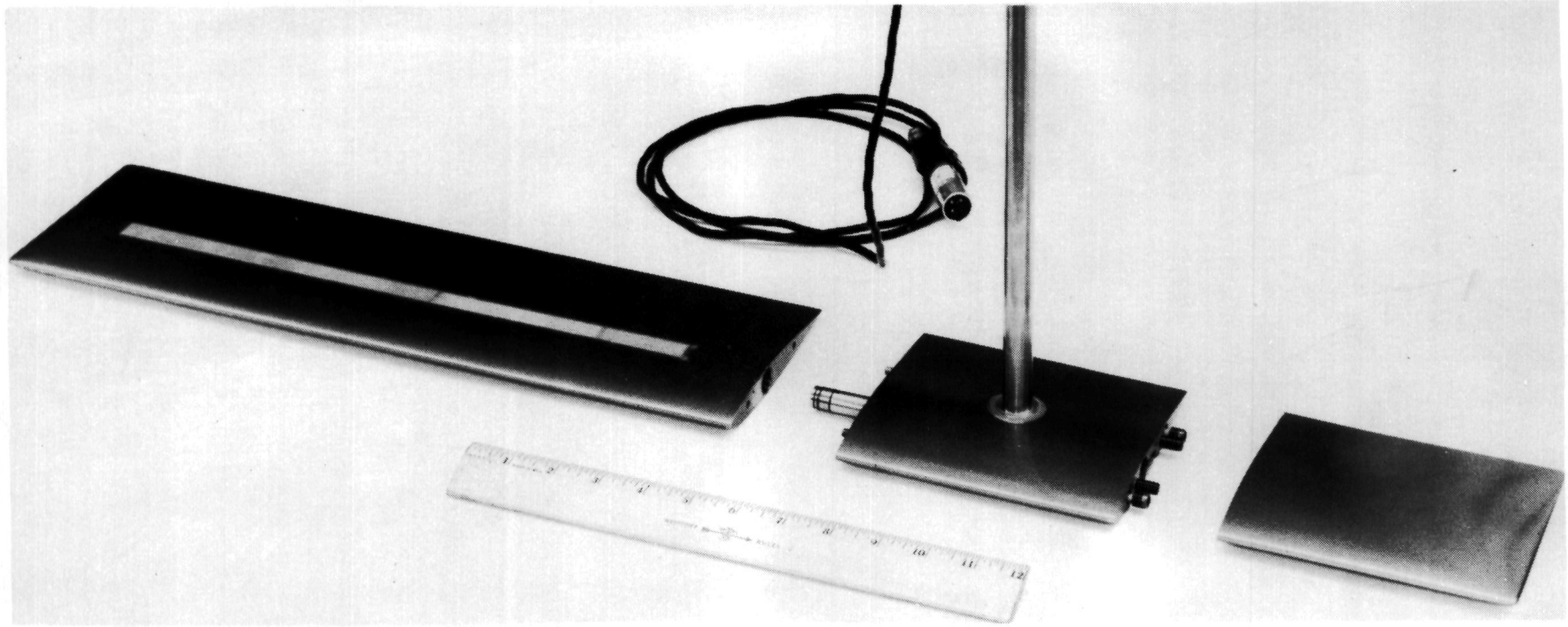

FIG. 1 POROUS SURFACE MICROPHONE IN AIRFOIL MODEL 342, AND ITS BASE

numbers are shown in parenthesis and the selected sections of each strip are identified in Fig. 2 for future reference.)

A Bruel and Kjaer half-inch condenser microphone and pre-amplifier is inserted in the Porous Surface Microphone. The grid cap of the microphone cartridge is removed and the microphone and preamplifier are screwed in the threaded hole of the Porous Surface Microphone. The cartridge type should be a B&K model 4134, which has a *pressure* response (in contrast to free field response) which is essentially flat up to 20 kHz. This selection of cartridge type is dictated by the analysis of the response of the Porous Surface Microphone which gives the pressure *at the surface* of the microphone in terms of the outside pressure of a plane wave.

The base of the Porous Surface Microphone, shown in Fig. 1, uses the General Radio preamplifier type 1560-P42, because its cable is more flexible than the cable of the B&K preamplifier and could be bent more easily into the Base and its pipe. (The pipe will fit into an airfoil stand for the wind tunnel tests.)

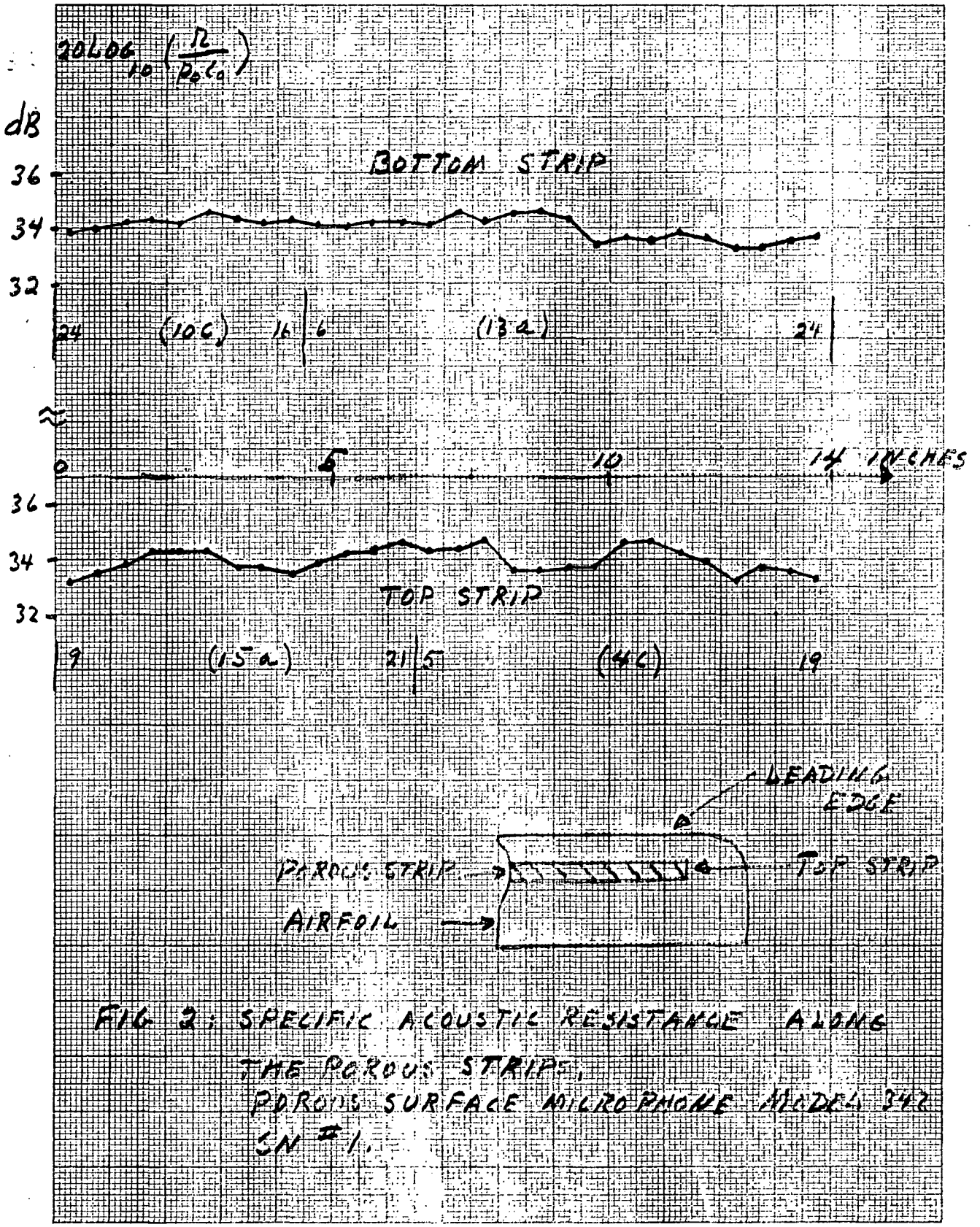

FIG. 2: SPECIFIC ACOUSTIC RESISTANCE ALONG THE POROUS STRIPS, POROUS SURFACE MICROPHONE MODEL 342 SN # 1.

2. ACOUSTIC TESTS

2.1 Acoustic Resistance

The acoustic resistance seen by the surface of the microphone cartridge should be the characteristic impedance of air, $\rho_0 c_0$, because the Porous Surface Microphone is designed to be anechoic in the direction away from the surface of the microphone cartridge. The D.C. value of this resistance was measured with a steady air flow. Its value is $1.07\ \rho_0 c_0$, which is within the tolerances of the specific resistance of the porous strips.

2.2 Frequency Response

The frequency response of the Porous Surface Microphone is shown in Fig. 3, giving the ratio of the pressure P_M at the surface of the microphone cartridge to the pressure P_o of a plane acoustic wave incident along the axis of the Porous Surface Microphone. The frequency response of Fig. 3 combines the results of two tests: a test at low frequencies, 30 to 400 Hz, in a plane wave tube; at test in the anechoic room, from 500 to 20,000 Hz.

The low frequency test shows a small drop of the response with increasing frequency. This result is not quite understood. We suspected at first that the microphone cartridge was not perfectly sealed to the end of the acoustic cavity: the threaded metal sleeve was removed and another sleeve reset in its place. We also suspected that the presence of the porous surfaces of the microphone in the plane wave tube did cause some acoustic absorption of the plane acoustic wave. This possibility was also examined and shown to be not significant. Some of the drop in the frequency response should result from the shear boundary layer inside the acoustic cavity. This effect is well

known for tubes of uniform cross section, and with hard walls. In air the attenuation α in nepers per unit length, of a plane acoustic wave in a circular tube of radius a is

$$\alpha = \frac{3.18 \times 10^{-5}}{a} \quad (f)^{1/2} \qquad \text{nepers/cm}$$

where a is in cm and the frequency f is in Hertz. If we apply this attenuation to the acoustic cavity of the Porous Surface Microphone, using a radius equal to the radius of the microphone cartridge, we find that the attenuation would be 1.7 dB at 10 kHz and 0.17 dB at 100 Hz. This rough calculation does not appear to explain the drop in response at low frequencies. An earlier attempt at including in the analysis of porous surface sensors the effect of the internal shear boundary layer had had considerable difficulties; this attempt had not been pursued further.

The high frequency part of the test is shown separately in Fig. 4. The small variations in the response are caused by the feedback system of the reference microphone. Two regions of this response are discussed: the gradual drop at high frequencies below 14 kHz, and the resonances in the region of 20 kHz.

The gradual drop in the frequency response is explained by the properties of the porous surface. In fact, that response can be calculated from the measured values of the transfer admittance y_{12}, modulus and phase, of the porous strips. For this calculation, the phase ϕ of y_{12} is especially useful. We use the calculation procedure discussed in Appendix 3 and 7 and the experimental values of y_{12} shown in Appendix 8 for the particular porous material used in the Porous Surface Microphone. When the phase ϕ measured is matched with the phase of an ideal porous material (given in Fig. 1a of Appendix 3) we get a value $\beta^2=1.2$ at 10 kHz. With this value of β^2, the modulus of the frequency

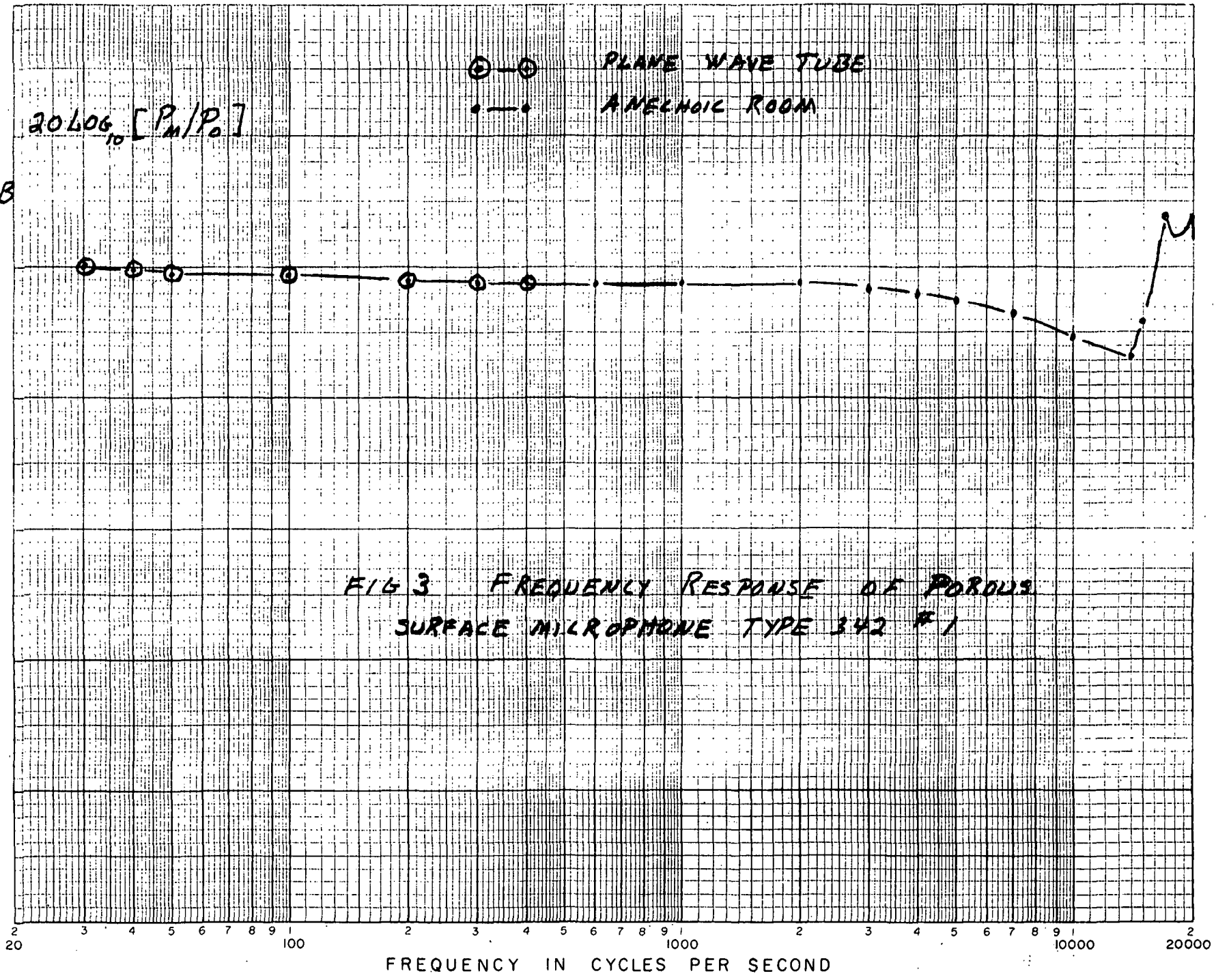

FIG 3 FREQUENCY RESPONSE OF POROUS SURFACE MICROPHONE TYPE 342 #1

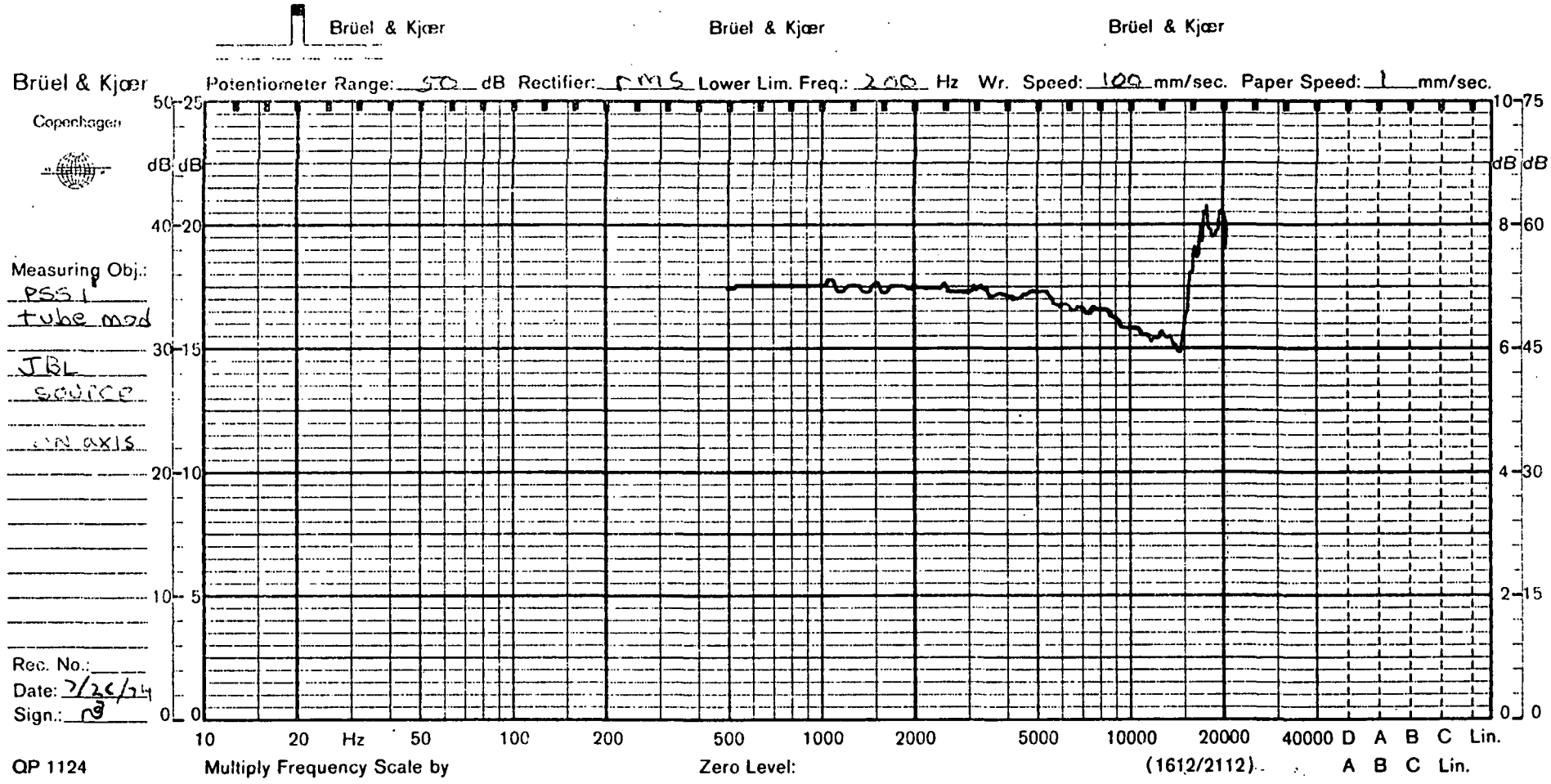

Fig. 4 Frequency response of the porous surface microphone in an airfoil, Model 342 S/N #1, in the anechoic chamber

response of an ideal Porous Surface Sensor is obtained from Fig. 2 of Appendix 7. This ideal response is compared in Fig. 5 with the measured frequency response (after the low frequency drop in the measured response is removed by normalizing the measured response to its mid-frequency value). The measured values are shown only up to 14 kHz because the resonances in the 20 kHz region do not belong to this calculation.

At frequencies near 20 kHz we identify in Fig. 4 two resonances. The lower frequency resonance at approximately 17 kHz is associated with the first bending mode of the porous strips. Using the Young's modulus of the porous material, which is 7.8 x 10^6 psi as quoted by Mott, and its density and assuming that strips are clamped-at their edges, we calculate a first resonance frequency of 17.5 kHz. (In fact, this calculation had been used to determine what is the lower limit of the thickness of the strip for the chosen design width such that the first bending resonance would be beyond the frequency range of interest. The width of the strip has been chosen to be consistent with the diameter of the test area in the measurements of the local variation of acoustic resistance: 0.5 inch diameter.) This bending resonance could be shifted to higher frequencies by using either a narrower strip of the same thickness or a thicker strip of the same width as the present strip. The first solution indirectly demands that the local variation of the specific resistance of the porous strip be known in finer details than what has been measured, see Fig. 2. The second solution would increase the drop in high frequency response shown in Fig. 5.

The second resonance at 20 kHz is believed to represent the effect of a cross mode in the rectangular cavity leading to the microphone cartridge. This cavity has a constant width of 0.437 inch. The first cross mode, corresponding to a half wavelength

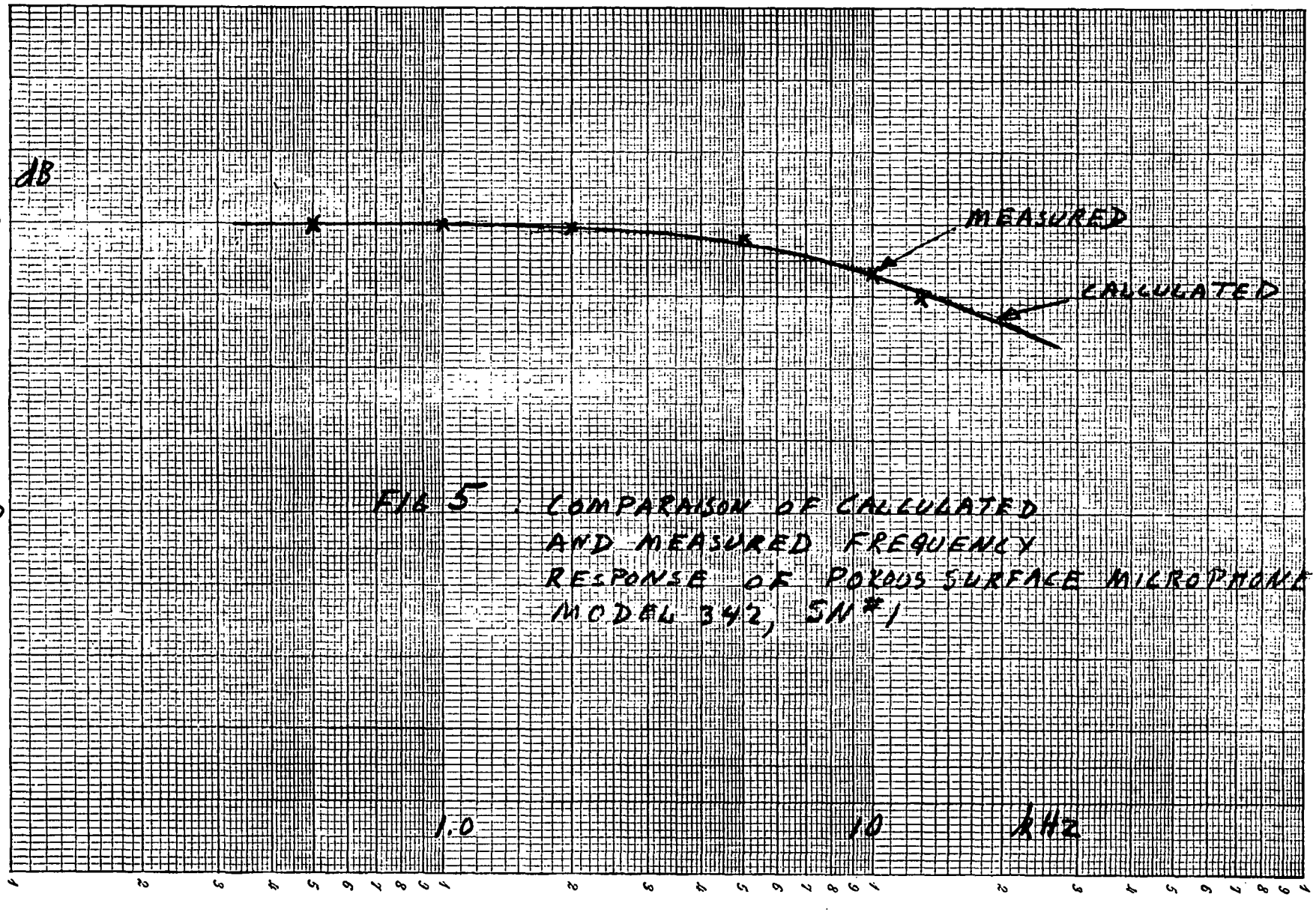

FIG 5 : COMPARAISON OF CALCULATED AND MEASURED FREQUENCY RESPONSE OF POROUS SURFACE MICROPHONE MODAL 342, SN #1

across the width of the cavity would occur at 10 kHz; but its pressure distribution is an odd function with respect to the center of the microphone cartridge, hence, the microphone surface would average out the pressure associated with this mode. However, the second mode across the width of the rectangular cavity, which occurs at 20 kHz, is an even function and its pressure would be sensed by the surface of the microphone cartridge: we believe it is this mode that has been excited by the nonuniformity of the porous strip that is being sensed by the microphone cartridge. This acoustic mode could be "removed" by adding a longitudinal porous partition inside the acoustic cavity. The plane wave mode, which is the main transmission mode used in the design, would not be attenuated; only the cross modes would be attenuated by the losses through the acoustic resistance of the porous partition.

2.3 Directivity

The directivity patterns of the Porous Surface are measured for two axes of rotation. Axis of rotation parallel to the main chord of the airfoil, shown in Fig. 6, and axis of rotation perpendicular to the main chord, shown in Fig. 7.

The envelope of the directivity pattern, at 10 kHz, of an ideal line sensor of the same length as the porous strips, is also shown in Figs. 6 and 7.

The measured directivity patterns of the major lobe and of the first minor lobe are close to the directivity of an ideal line sensor of the same length as the porous strips. However, for the higher order lobes, the envelope of the measured directivity tends to level off at approximately -27 dB, whereby the directivity of the ideal line sensor continues decreasing towards -36.5, at 10 kHz. This leveling of the measured directivity is attributed

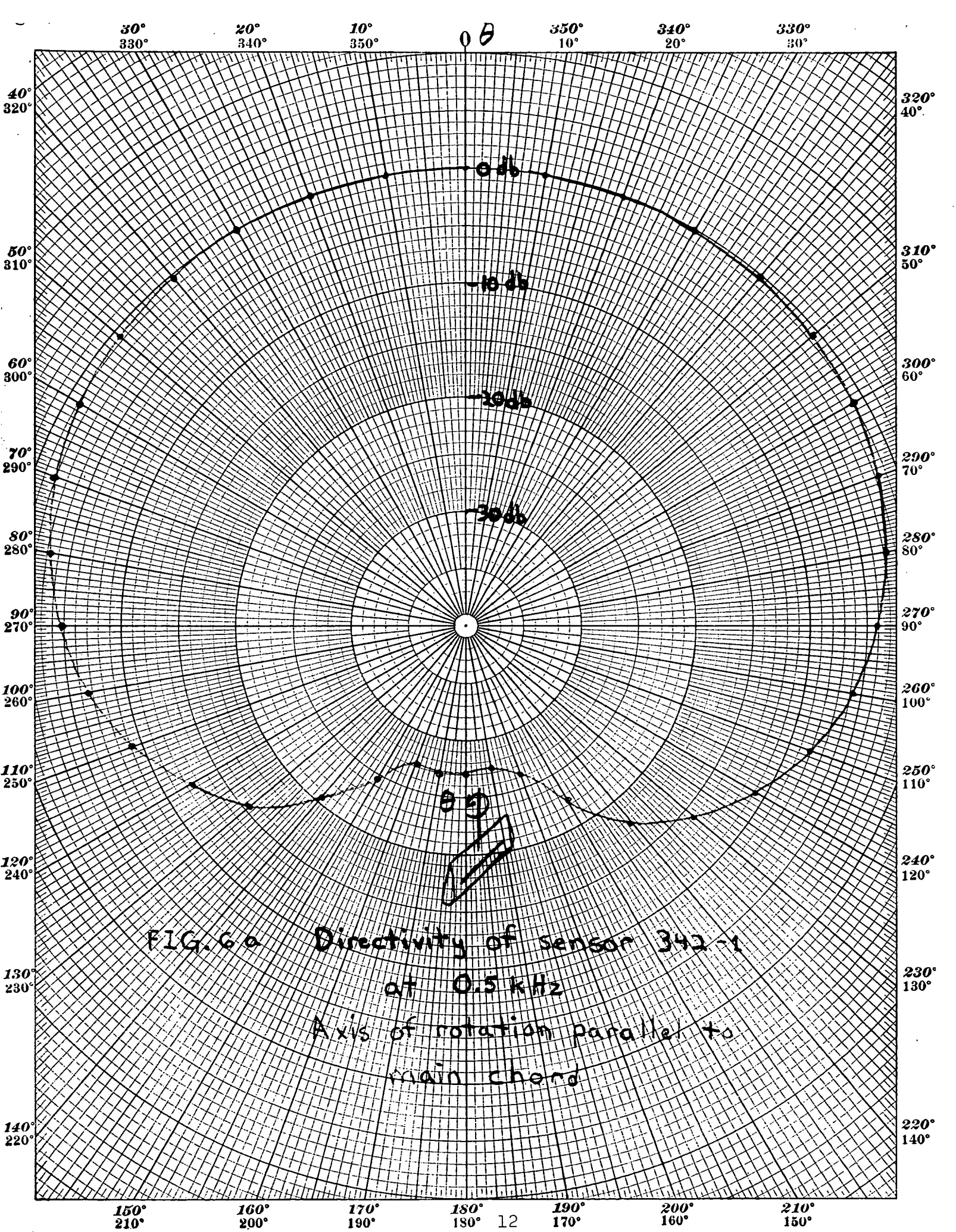

FIG. 6a Directivity of sensor 342-1 at 0.5 kHz Axis of rotation parallel to main chord

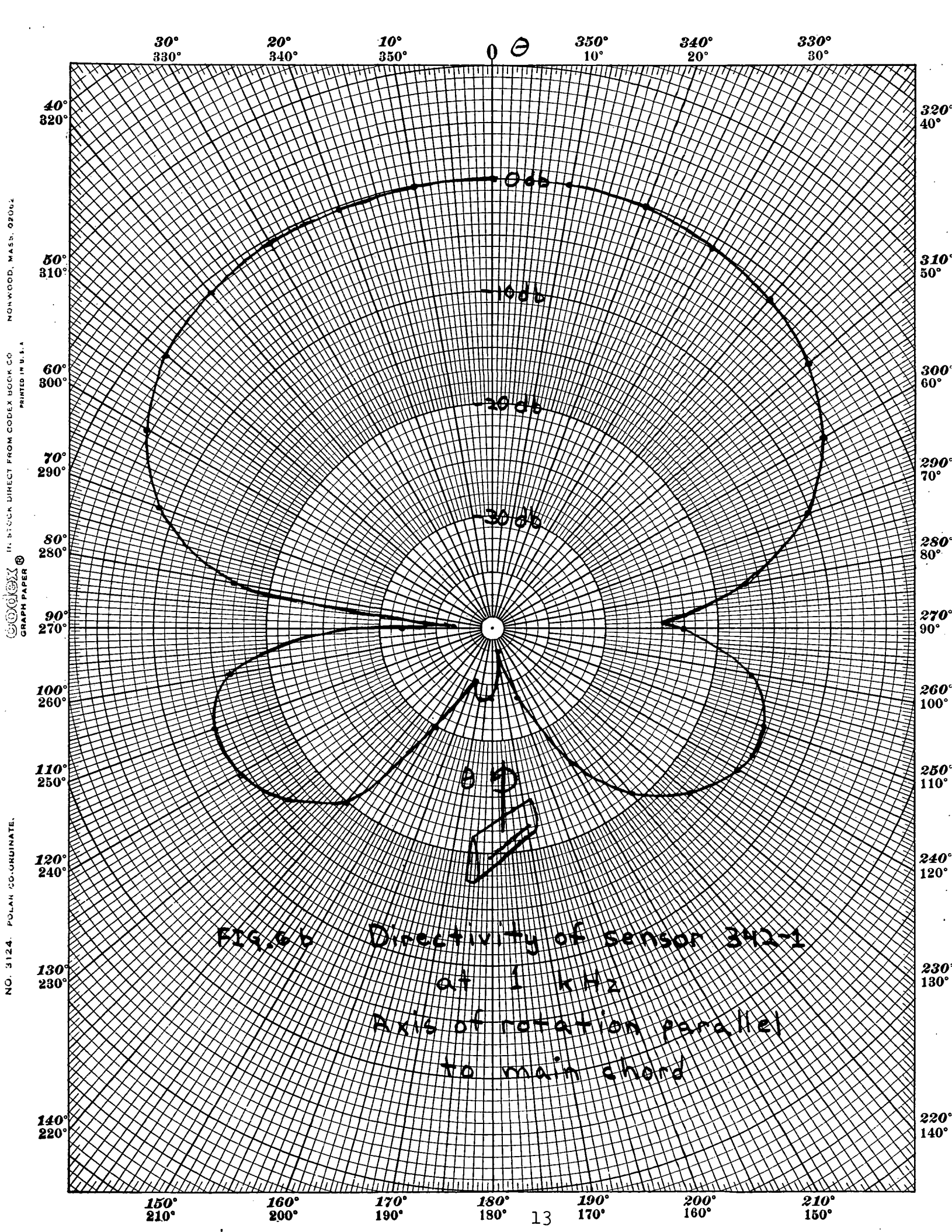

Fig. 6 b Directivity of sensor 342-1
at 1 kHz
Axis of rotation parallel
to main chord

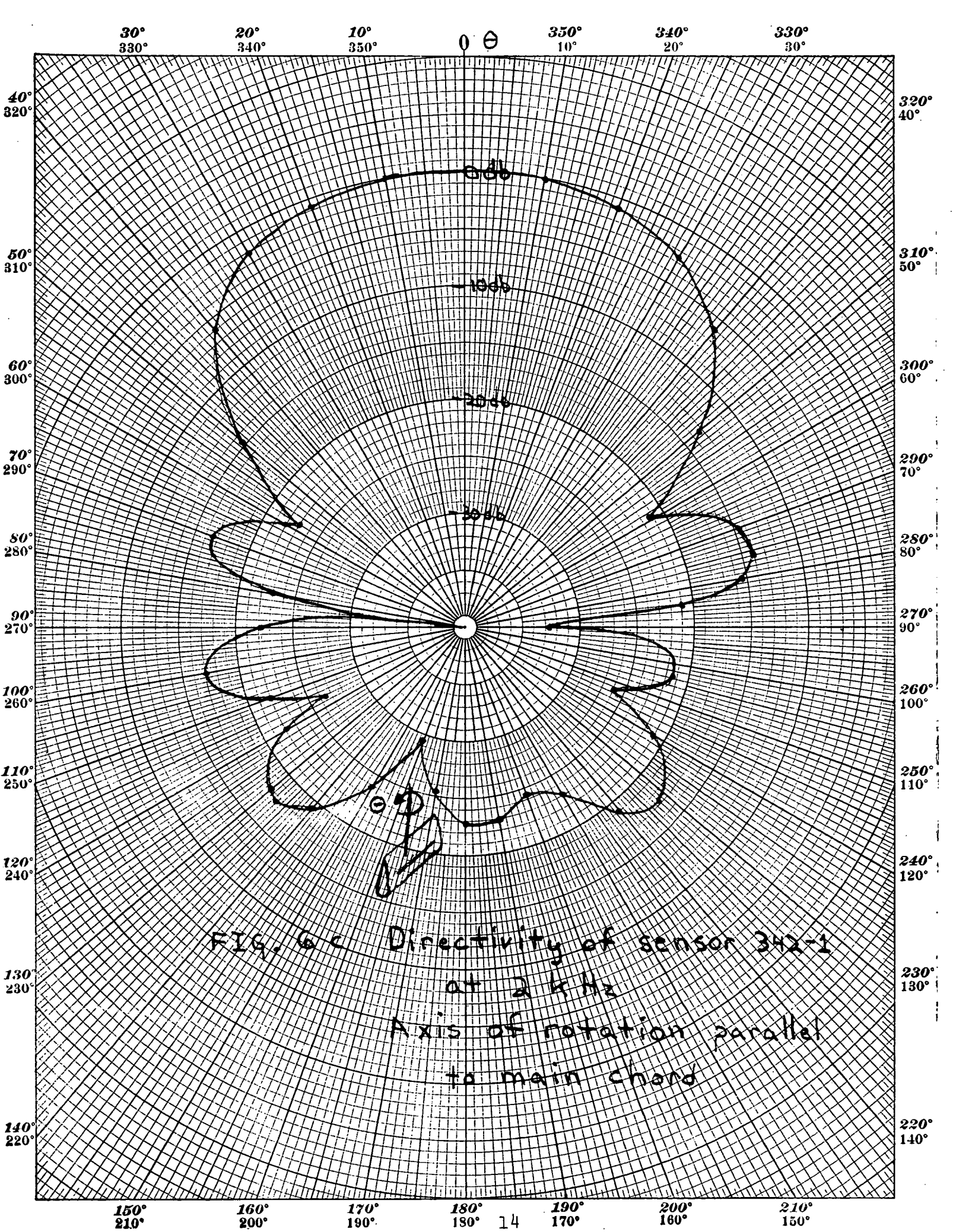

FIG. 6c Directivity of sensor 342-1
at 2 kHz
Axis of rotation parallel
to main chord

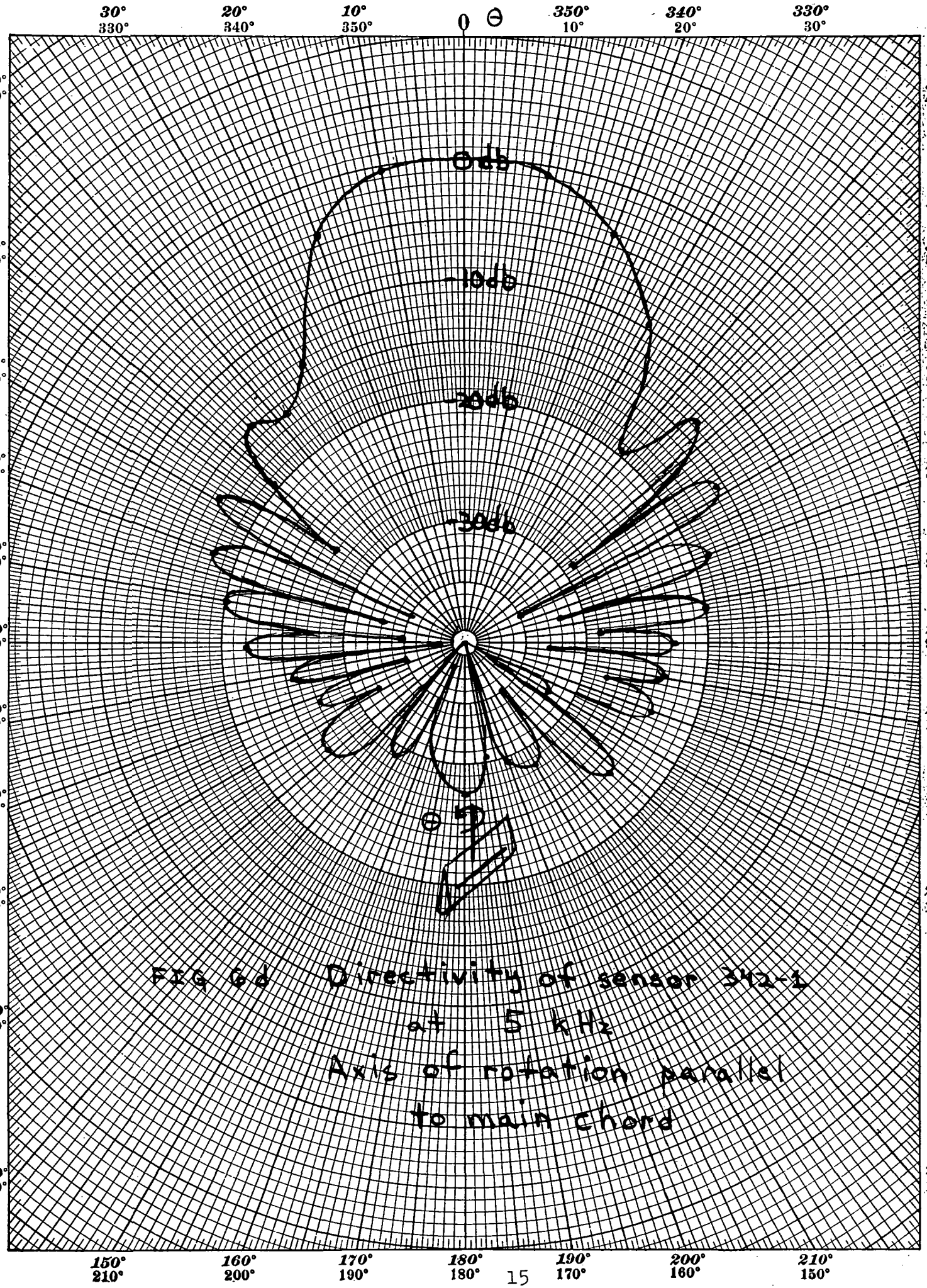

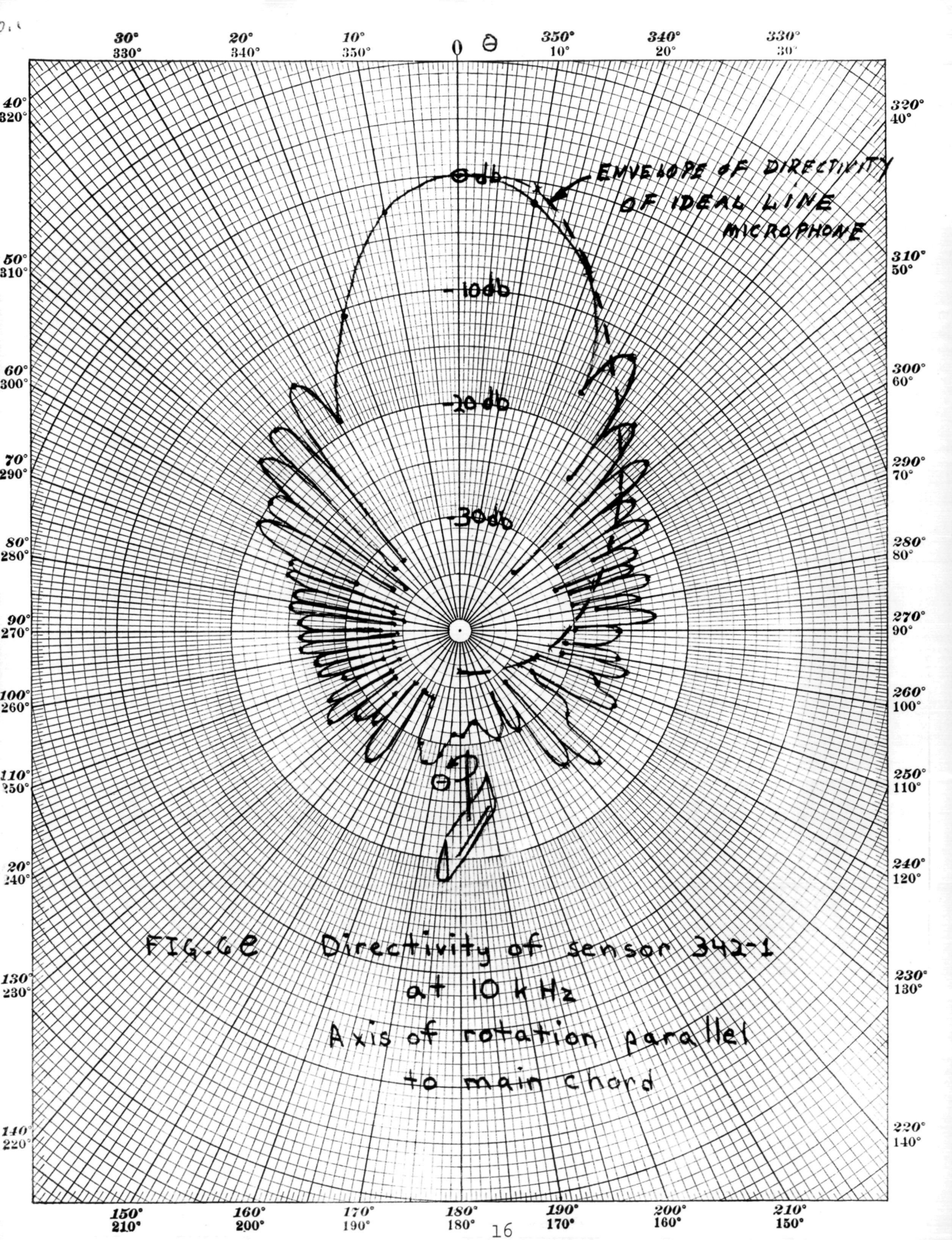

FIG. 6e Directivity of sensor 342-1
at 10 k Hz
Axis of rotation parallel
to main chord

to the nonuniformity of the specific resistance of the porous surface. This effect has been analyzed previously* and the analytical results are roughly consistent with the experimental ones.

This leveling off of the envelope of the minor lobes is detrimental to the flow noise rejection of the sensor. Hence, the importance of using a very uniform porous surface. We have not been as successful as we hoped in finding this material. Nevertheless, the flow noise rejection should at least be as good as obtained with the earlier design; the net flow noise should in fact, be better because the noise generation by the new airfoil will be less than with the older airfoil.

The directivity patterns for an axis of rotation perpendicular to the main chord of the airfoil follow more closely the ideal directivity patterns than for the other axis of rotation. This is due to the smaller scattering of the pressure field by the sensor in the first case than in the second case. In fact, it is because of this scattering that two symmetrical strips have been set in the airfoil; the symmetrical strips tend to cancel out, at the microphone element, the scattered part of the pressure field.

---

*NASA-CR-114593

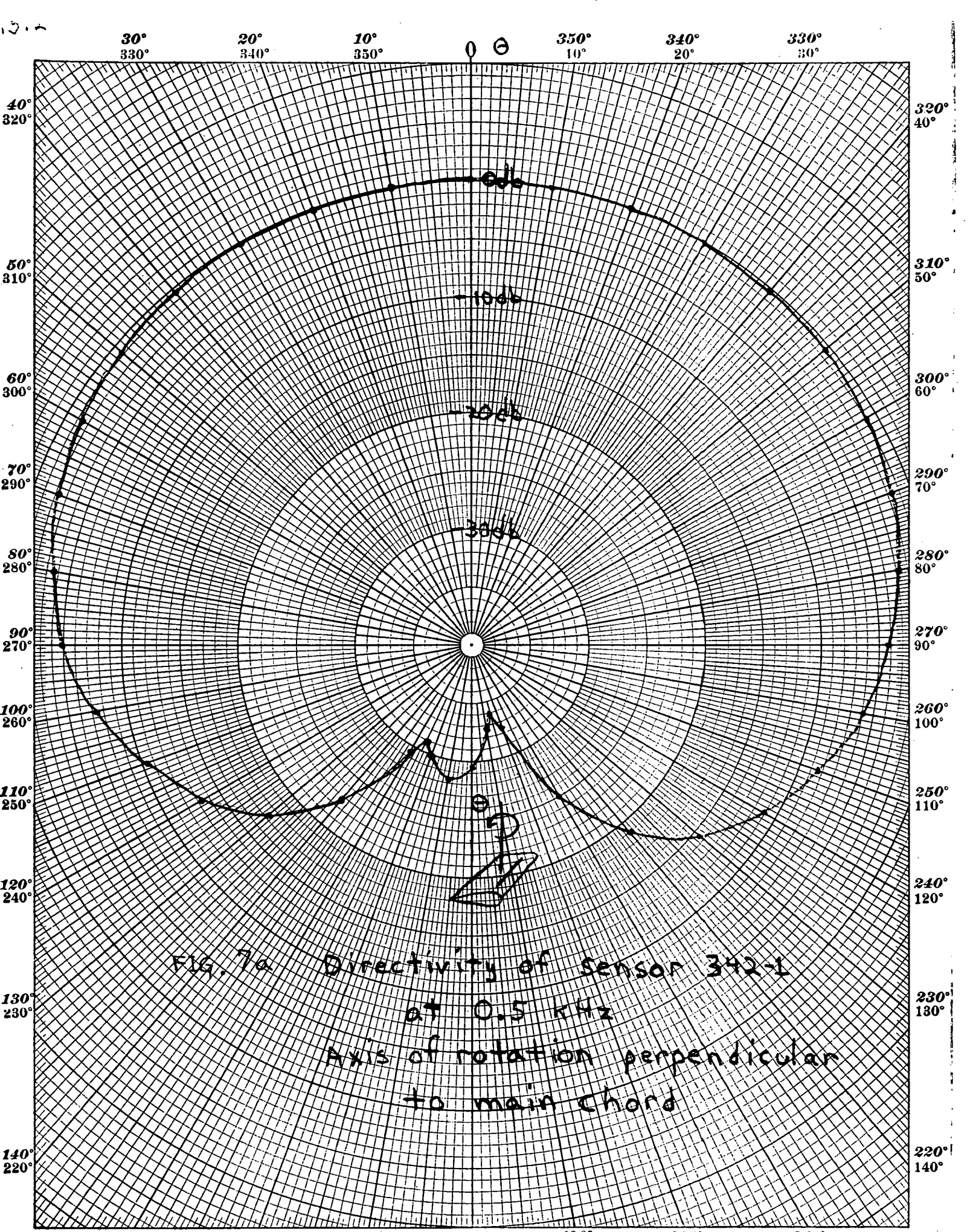

Fig. 7a. Directivity of sensor 342-1 at 0.5 kHz Axis of rotation perpendicular to main chord

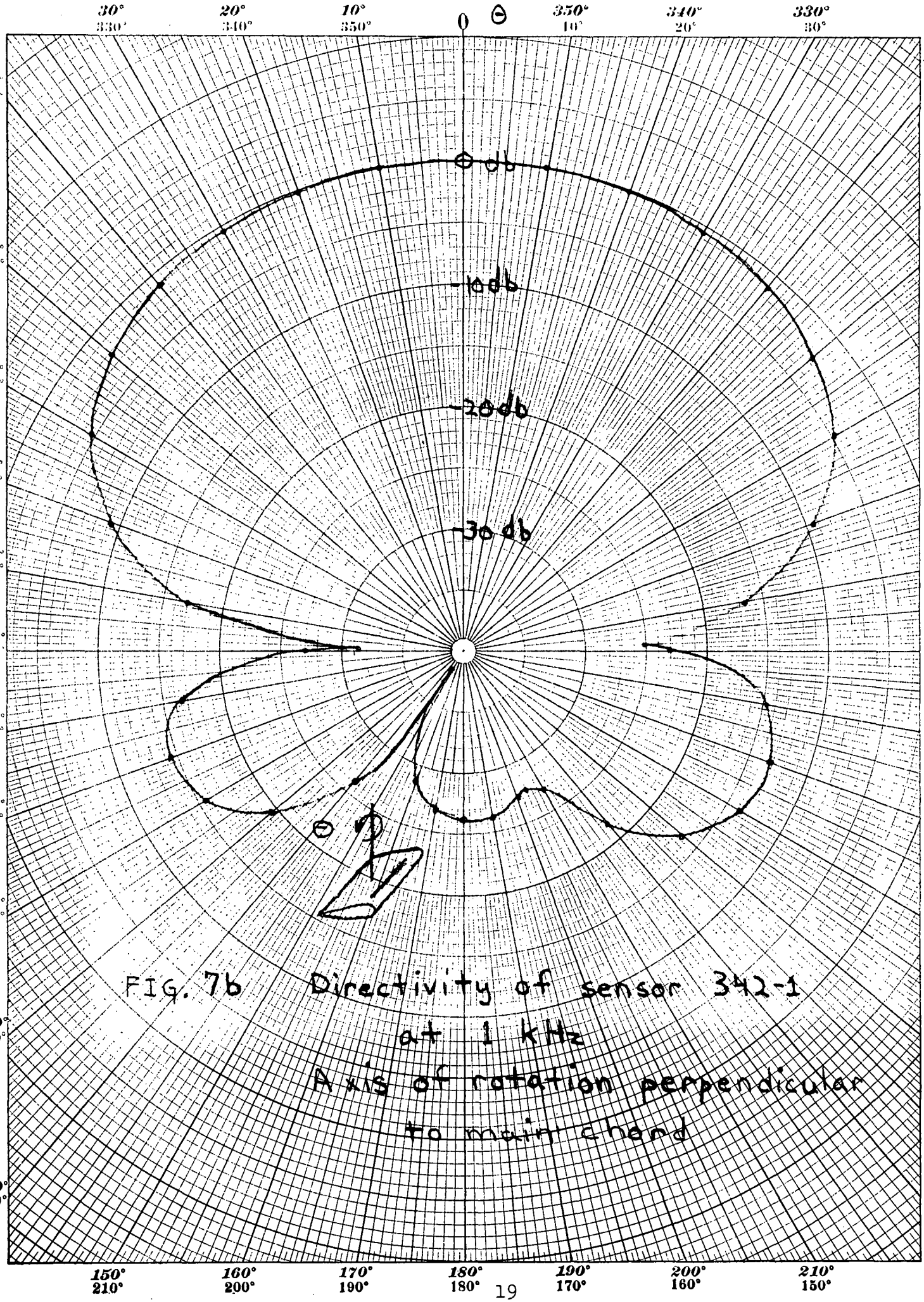

FIG. 7b Directivity of sensor 342-1 at 1 kHz
Axis of rotation perpendicular to main beard

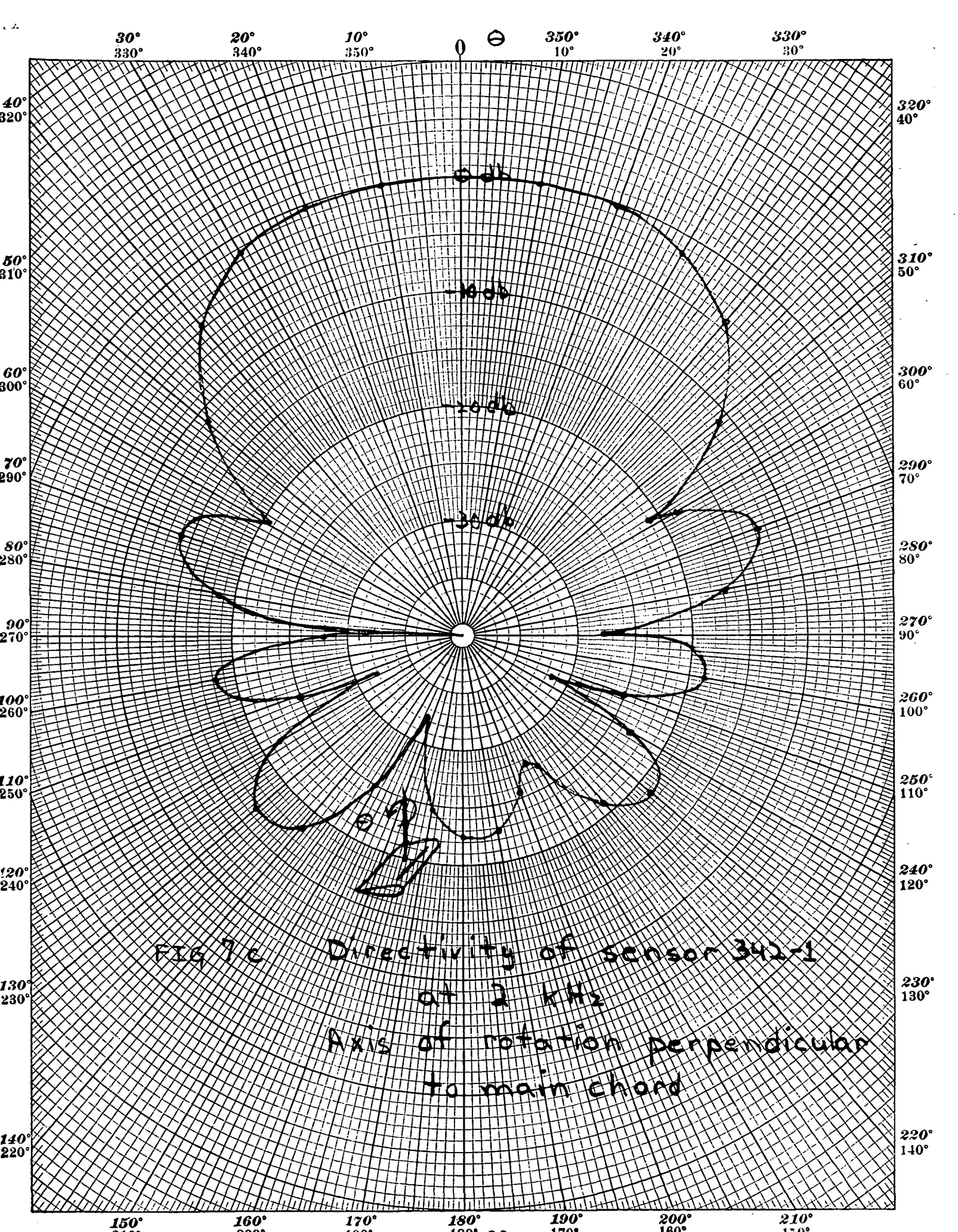
30° 330°
20° 340°
10° 350°
0 θ
350° 10°
340° 20°
330° 30°
40° 320°
50° 310°
60° 300°
70° 290°
80° 280°
90° 270°
100° 260°
110° 250°
120° 240°
130° 230°
140° 220°
320° 40°
310° 50°
300° 60°
290° 70°
280° 80°
270° 90°
260° 100°
250° 110°
240° 120°
230° 130°
220° 140°
150° 210°
160° 200°
170° 190°
180° 180°
190° 170°
200° 160°
210° 150°
0 db
-10 db
-20 db
-30 db
e
FIG 7c Directivity of sensor 342-1
at 2 KH2
Axis of rotation perpendicular
to main chord

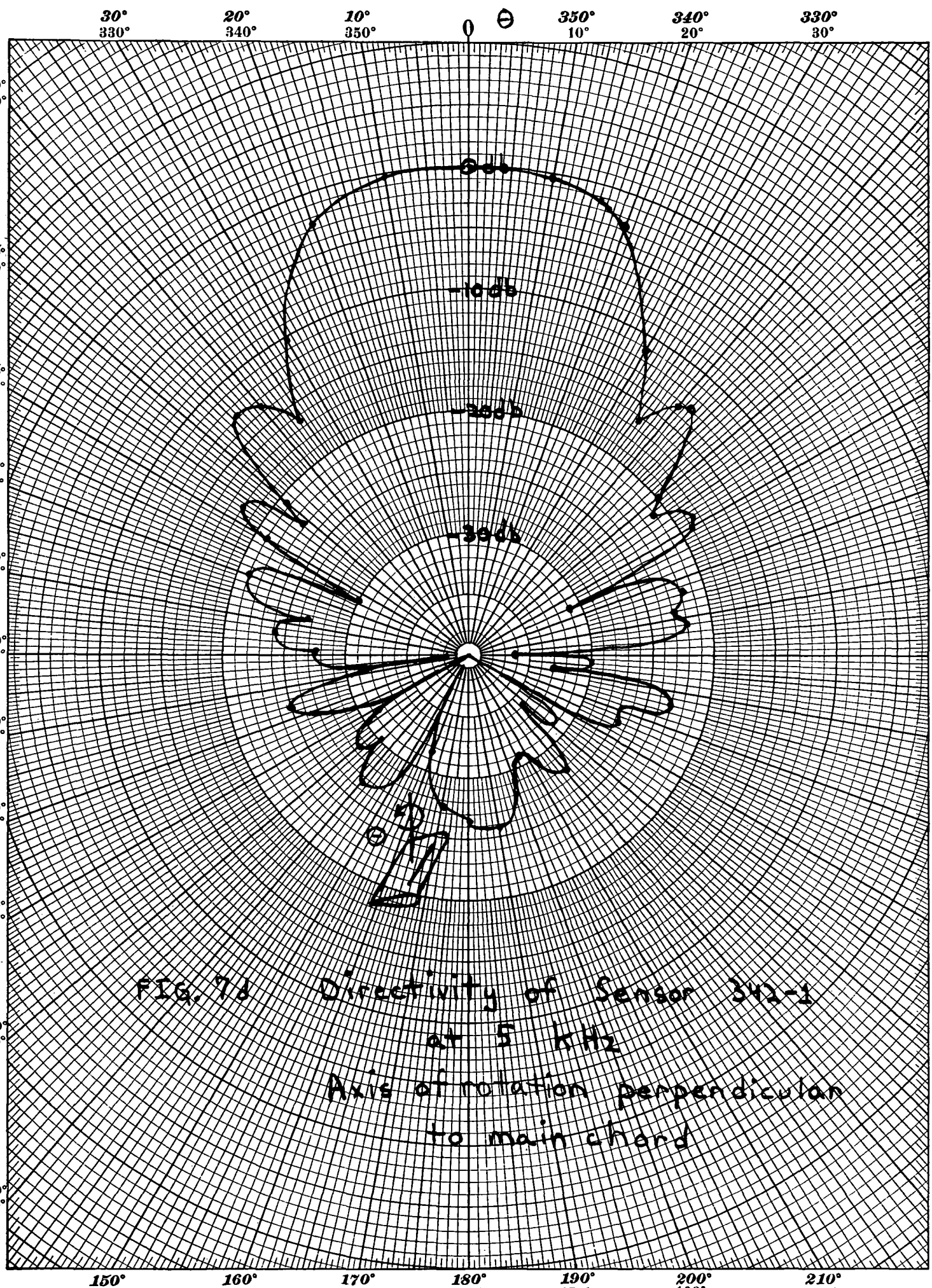

FIG. 7d Directivity of Sensor 342-1
at 5 KHz
Axis of rotation perpendicular
to main chord

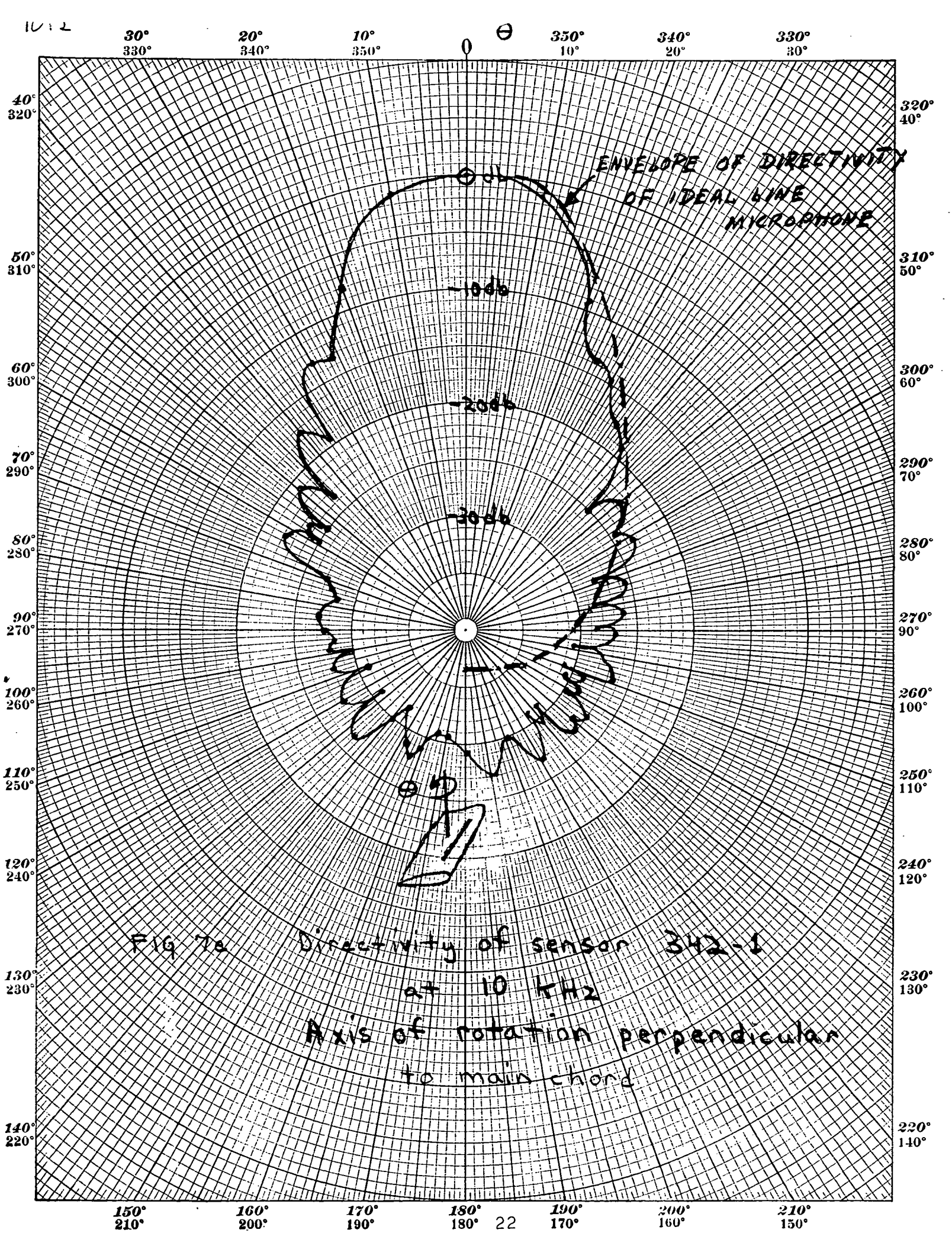

FIG 7a Directivity of sensor 342-1 at 10 kHz Axis of rotation perpendicular to main chord

3. CONCLUSIONS

The acoustic tests have shown that one of the main objectives of the new design of the Porous Surface Microphone in an Airfoil has been achieved. Its high frequency response has been considerably improved, for example, at 10 kHz the response is down only 3 dB from its mid-frequency response; this drop should be compared with 10 to 13 dB in the earlier design.

The low frequency drop, in the frequency region of 30 to 400 Hz had not been anticipated. In fact, we suspect that measurements made on earlier models of porous sensors which show a flat response in this frequency region may have been in error.

The directivity patterns of the new sensor have not been significantly affected by the larger size of the airfoil, because of the symmetrical design of porous surfaces.

The uniformity of the resistance of the porous strips is not as good as we would have liked. This nonuniformity increases the levels of the minor lobes of the directivity patterns and hence, the flow noise rejection would not be as good as the ideal directivity would predict.

APPENDIX X

FLOW NOISE TESTS OF THE AIRFOIL POROUS SURFACE SENSOR MODEL 342 AND OF THE B&K HALF INCH CONDENSER MICROPHONE WITH NOSE CONE

1. INTRODUCTION

The Airfoil Porous Surface Sensor, Model 342, and the Bruel and Kjaer half-inch condenser microphone with nose cone have been tested in a quiet wind tunnel at flow velocities from 25 m/sec. (84 ft/sec) to 70 m/sec (235 ft/sec). Their flow noises are compared.

The B&K sensor is used as a reference to show the flow noise reduction achieved by the Airfoil Sensor. The B&K sensor is always pointed directly into the flow. The Airfoil Sensor is pointed at different yaw angles in the flow, in the range of 0° to 90°. Since the B&K sensor is essentially omnidirectional over its effective frequency range, up to 15 kHz, there is no reason to orient it differently than directly towards the flow; in fact, if it is pointed towards otherwise, its flow noise increases rapidly with the angle between its axis and the flow direction.

The relevant properties of the wind tunnel are given in Section 2, including its spectrum of turbulence. Section 3 describes the test setup. Section 4 presents the data of flow noise with discussion of the results. Section 5 offers some conclusions.

2. WIND TUNNEL

The flow noise tests were made in the new BBN quiet wind tunnel. Figure 1a and 1b show the elevation and plan views of the facility: it is a free jet in a semi-anechoic room.

A new nozzle was added to increase the flow velocities: it is a rectangular nozzle with dimensions of 28 inch high by 40 inch wide at the exit. The larger width is convenient for testing models, like the Airfoil Porous Surface Sensor which are long and thin in the horizontal plane. The maximum flow velocity attained 70 m/sec, (235 ft/sec). The minimum flow velocity, 24 m/sec, corresponds to the idling speed of the diesel.

The velocity profile at the exit face of the nozzle is very uniform over the full range of flow velocities with a rapid but smooth decrease of velocity at the sides of the nozzle: there is no flow separation on the sides of the nozzle.

The level of turbulence at the exit of the nozzle is very low. At the location of the microphone, one meter away from the exit plane, the turbulence spectrum on the axis of the nozzle is shown in Fig. 2, in third octave bands, for three different flow velocities: 100, 150 and 200 ft/sec. The low frequency part of the spectrum, below 100 Hz is attributed to the fan. The central part of the spectrum, from 100 Hz to 4 kHz at 100 ft/sec, to 8 kHz at 150 ft/sec and to 12.5 kHz at 200 ft/sec is the normal turbulence of the wind tunnel. The high frequency part above 12.5 kHz has a rising spectrum, with a slope of +9 dB per octave for third octave bands (or 6 dB/octave on a linear frequency scale): this part is not considered to represent free flow turbulence, but is believed to be caused by the hot wire probe. Nevertheless, the turbulence is very low over the whole frequency range of interest: 100 Hz to 10 kHz.

The wind tunnel is operated with open cycle air intake and exhaust.

BBN HIGH SPEED FREE JET ACOUSTIC WIND TUNNEL
– ELEVATION –

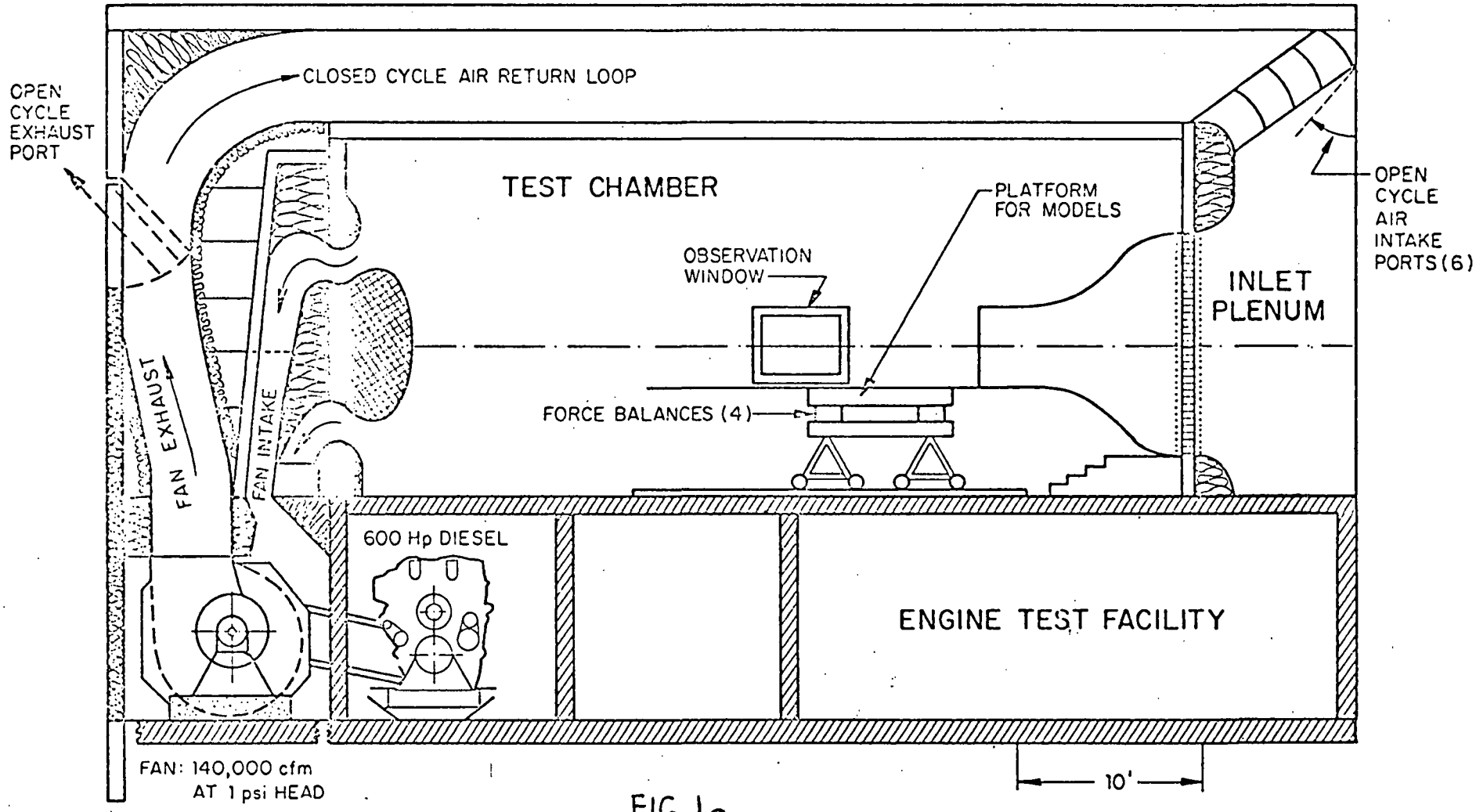

FIG. 1a

BBN HIGH SPEED FREE JET ACOUSTIC WIND TUNNEL
- PLAN VIEW -

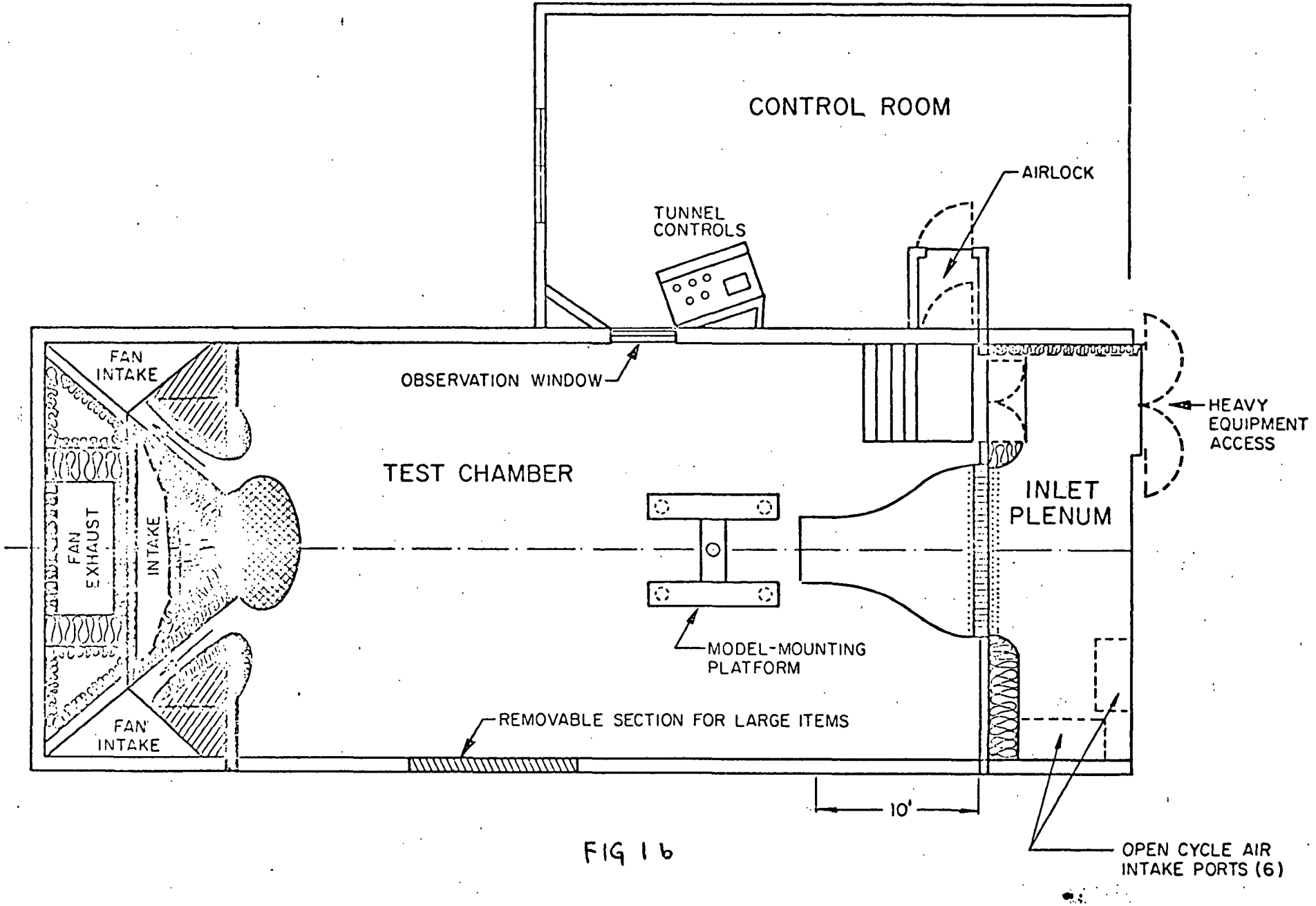

FIG 1 b

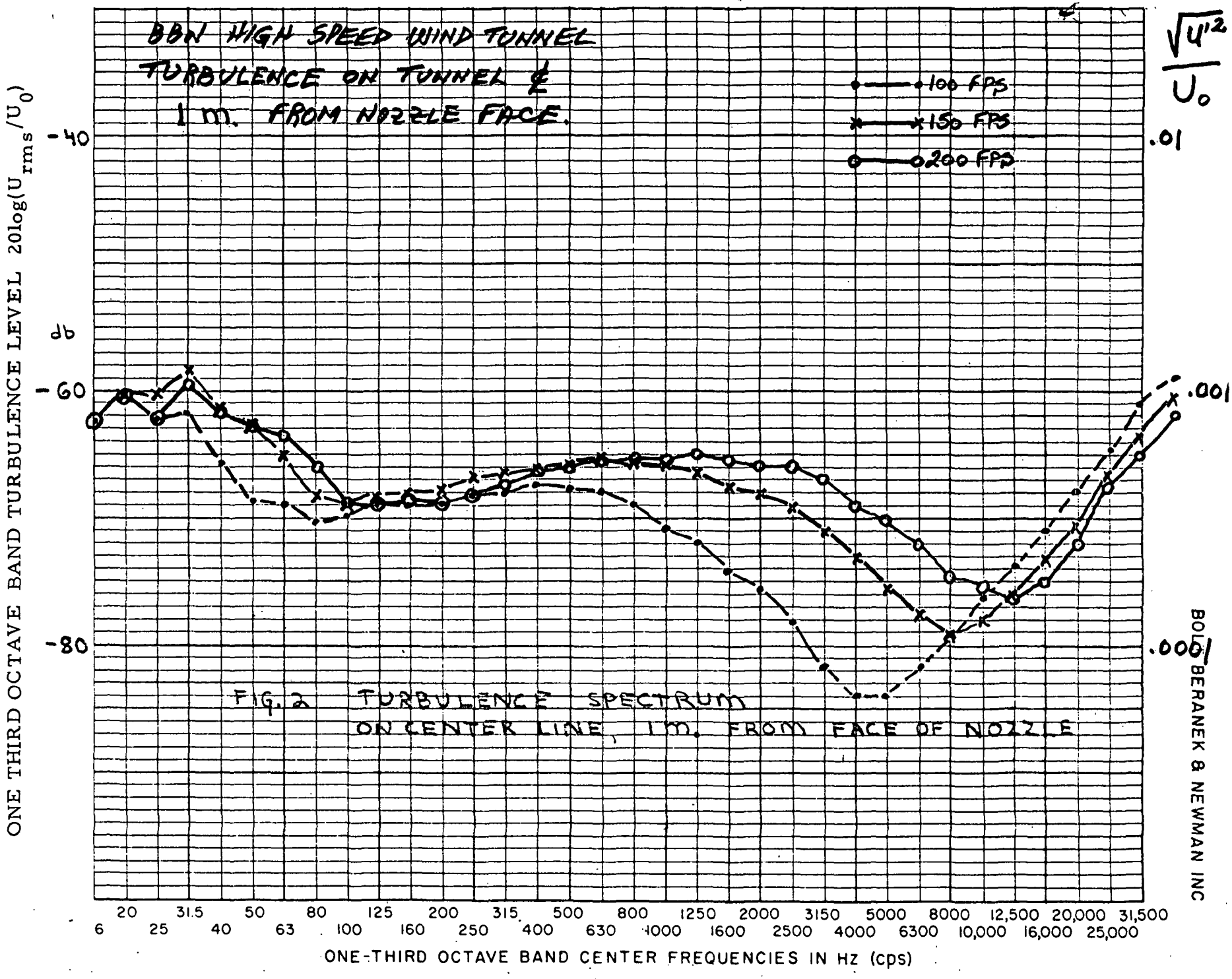

FIG. 2 TURBULENCE SPECTRUM ON CENTER LINE, 1 M. FROM FACE OF NOZZLE

3. TEST STAND

The Airfoil Sensor, its preamplifier base and tail end form an aerodynamic shape. The pipe cemented to the preamplifier base carries the electrical leads of the preamplifier; the pipe fits vertically inside the aerodynamic stand. The Airfoil sensor can be rotated horizontally with respect to the stand. The stand is bolted to a horizontal plate which is attached to the test platform. A protractor on the underside of the plate measures the yaw angle α, which is the rotation of the pipe and Airfoil Sensor with respect to the aerodynamic stand. Figure 3 shows the Airfoil sensor on the stand for zero yaw angle.

The Bruel and Kjaer half-inch condenser microphone uses the same stand as the Airfoil Sensor. An aerodynamic top is added to the stand as shown in Fig. 4. The preamplifier, which is a standard B&K preamplifier type 2615, is set inside an aerodynamic housing to which is soldered a vertical pipe which carries the electrical leads. The microphone and its preamplifier can be rotated in a horizontal plane, with respect to the stationary test stand. In all the tests, the nose cone used is the newer B&K type UA 0386, instead of the older type shown in the photograph.

FIG. 3 PHOTOGRAPH OF THE AIRFOIL SENSOR ON THE TEST STAND. YAW ANGLE $\alpha = 0$

FIG. 4 PHOTOGRAPH OF THE B&K ½ INCH CONDENSER MICROPHONE WITH NOSE CONE, AND THE AERODYNAMIC HOUSING OF THE PREAMPLIFIER, ATTACHED TO THE TEST STAND.

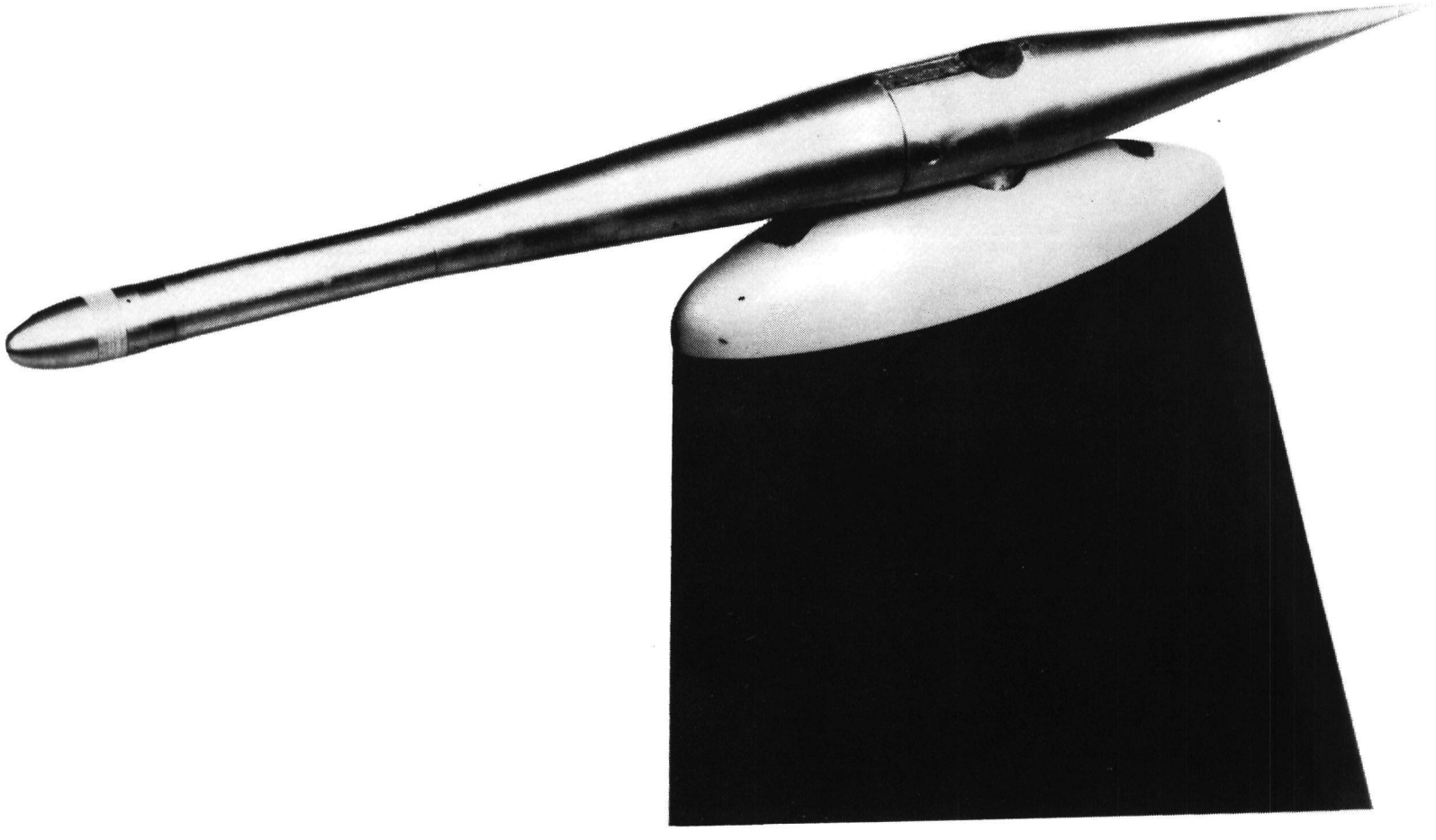

4. FLOW NOISE TESTS

4.1 Test Conditions

All the results of flow noise are reduced to equivalent acoustic pressures of a plane wave incident along the axis of the sensors; i.e., the flow noise data are corrected for the frequency response of each sensor.

The frequency response of the Airfoil Sensor is shown in Fig. 5. The frequency response of the B&K half-inch microphone with nose cone is shown in Fig. 6: the microphone cartridge type 4133 and the nose cone type UA-0386 are used. The small scale variations in the frequency response of Fig. 6 are caused by the test setup in the anechoic room.

The centers of each sensor during the tests are located at approximately one meter from the face of the nozzle.

When the fan is off the background acoustic and electronic noise of the sensors are shown in Fig. 7. The low frequency part of the noise is mostly acoustic noise and 60 cycle hum pickup.

The aerodynamic stand on which sits the airfoil sensor or the B&K sensor generates a certain amount of noise which will contribute to the net flow noise measured by the sensors. The turbulent mixing region between the free jet and the free air strikes the stand in an area below the sensors; the fluctuating pressures generated in this area radiate as dipoles oriented perpendicular to the surface and the frequency spectrum of the noise radiated has a broad maximum at a low frequency given approximately by

$$f = \frac{0.2\ U_\infty}{h} \quad , \text{Hz}$$

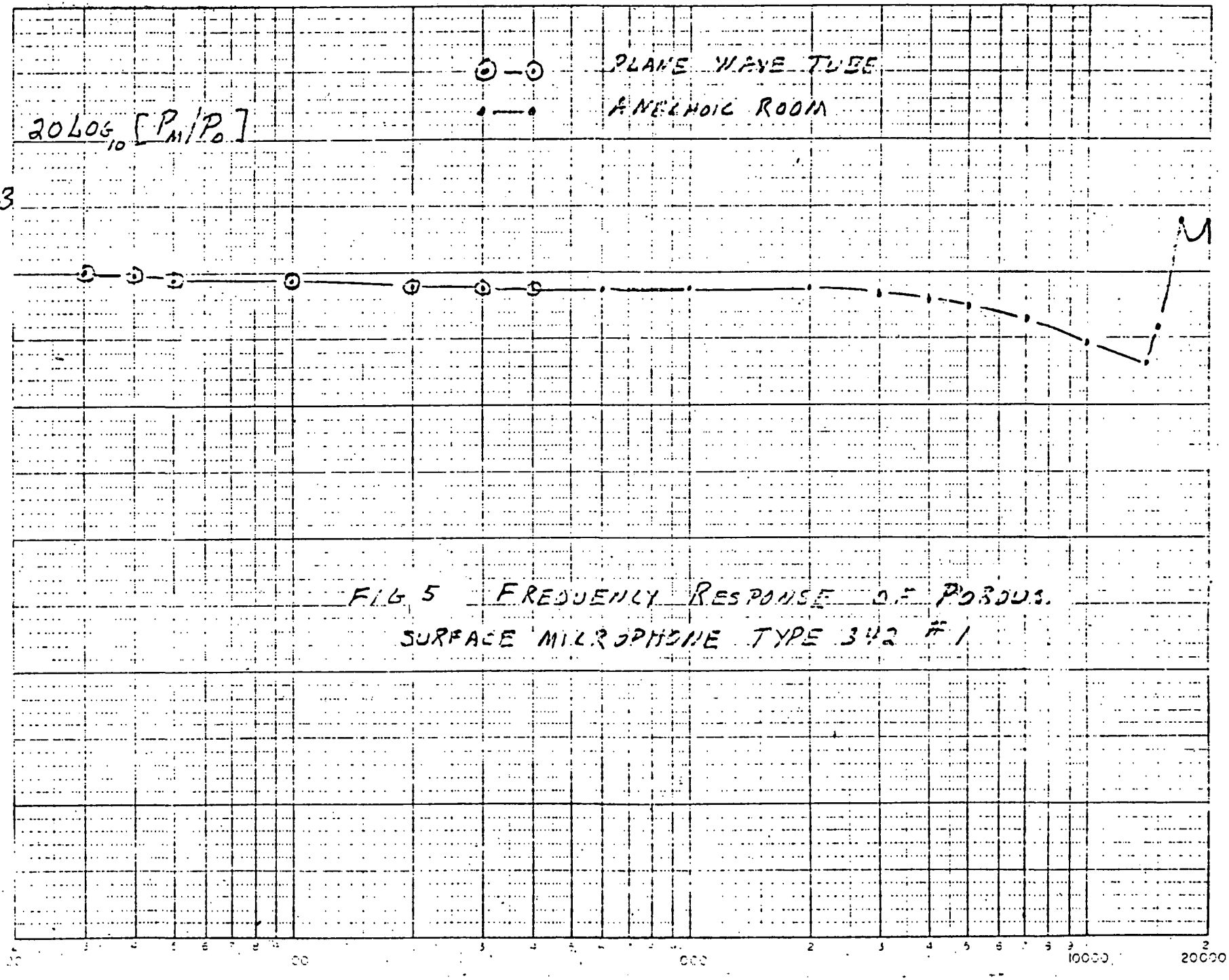

FIG 5 FREQUENCY RESPONSE OF PORous SURFACE MICROPHONE TYPE 342 #1

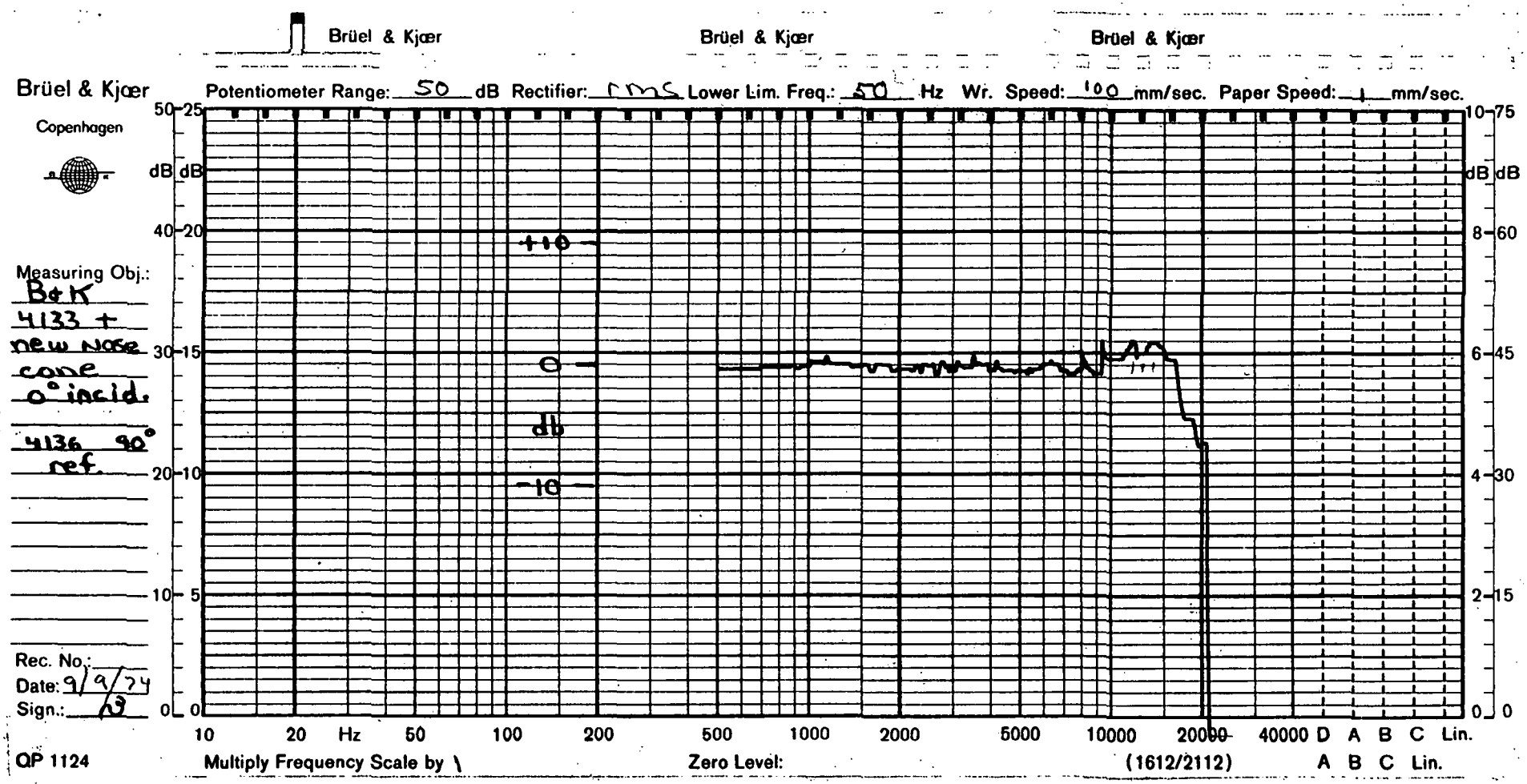

FIG 6 FREQUENCY RESPONSE OF B&K

½ INCH CONDENSER MICROPHONE

4133 WITH NOSE CONE UA-0386

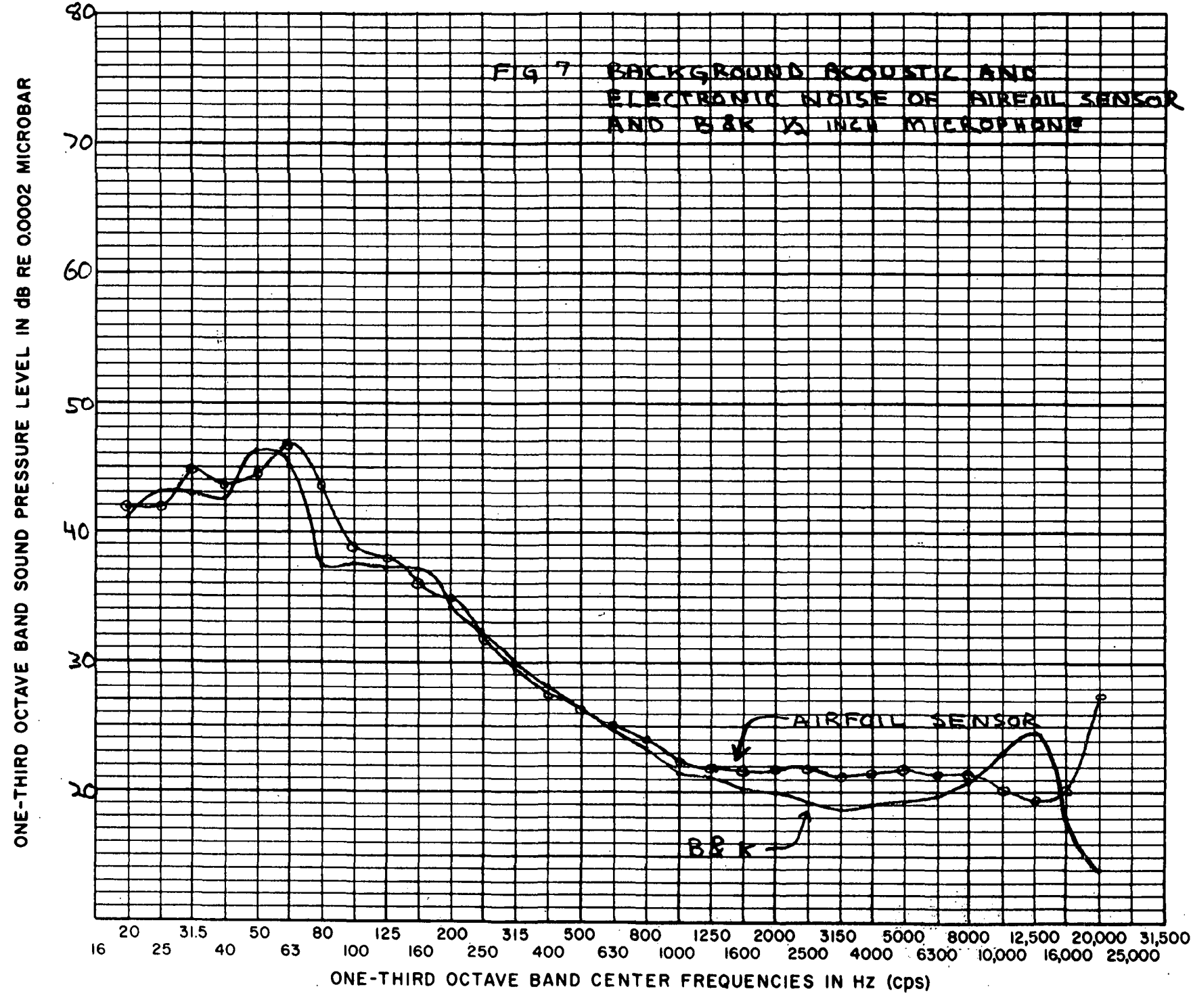
FIG 7 BACKGROUND ACOUSTIC AND ELECTRONIC NOISE OF AIRFOIL SENSOR AND B&K ¼ INCH MICROPHONE
ONE-THIRD OCTAVE BAND SOUND PRESSURE LEVEL IN dB RE 0.0002 MICROBAR
80
70
60
50
40
30
20
AIRFOIL SENSOR
B&K
16 20 25 31.5 40 50 63 80 100 125 160 200 250 315 400 500 630 800 1000 1250 1600 2000 2500 3150 4000 5000 6300 8000 10,000 12,500 16,000 20,000 25,000 31,500
ONE-THIRD OCTAVE BAND CENTER FREQUENCIES IN Hz (cps)

where h is the thickness of the mixing region and U is the mean flow velocity; this frequency is roughly 100 to 200 Hz. It follows that the directivity pattern of this radiated noise has a minimum in the direction of flow (corresponding to yaw angle of 0° for the Airfoil Sensor) and increases gradually for directions perpenticular to the flow. The Airfoil Sensor at yaw angle near 0°, and the B&K sensor (which is always pointed into the flow) will be near a minimum of this radiated noise.

This low frequency noise generated by the stand could have been almost eliminated by extending the lower lip of the nozzle beyond the stand. But this extended surface would also create other noises, like radiation from its boundary layer and from the vibration of the surface, and would cause undesirable acoustic reflections. Hence, it was decided to accept the low frequency, low level, of the noise generated on the stand by the mixing region of the flow.

The trailing edge of the stand will create a similar but high frequency noise associated with the thickness of the boundary layer.

The noise radiated by the stand and the Airfoil Sensor were measured outside the free jet and mixing region at two locations which are specified in Fig. 8. At location 1, which is at the same elevation and axial distance from the nozzle as the sensor but immediately outside the mixing region, the pressure spectrum, measured with the B&K sensor, is shown in Fig. 9. At location 2, which is under the axis of the jet in front of the stand but outside of the jet and its mixing region we get the pressure spectrum of Fig. 10. The low frequency spectrum of the out-of-flow noise at location 2 is roughly 30 dB lower than at location 1: location 2 is in a null of the directivity of the noise

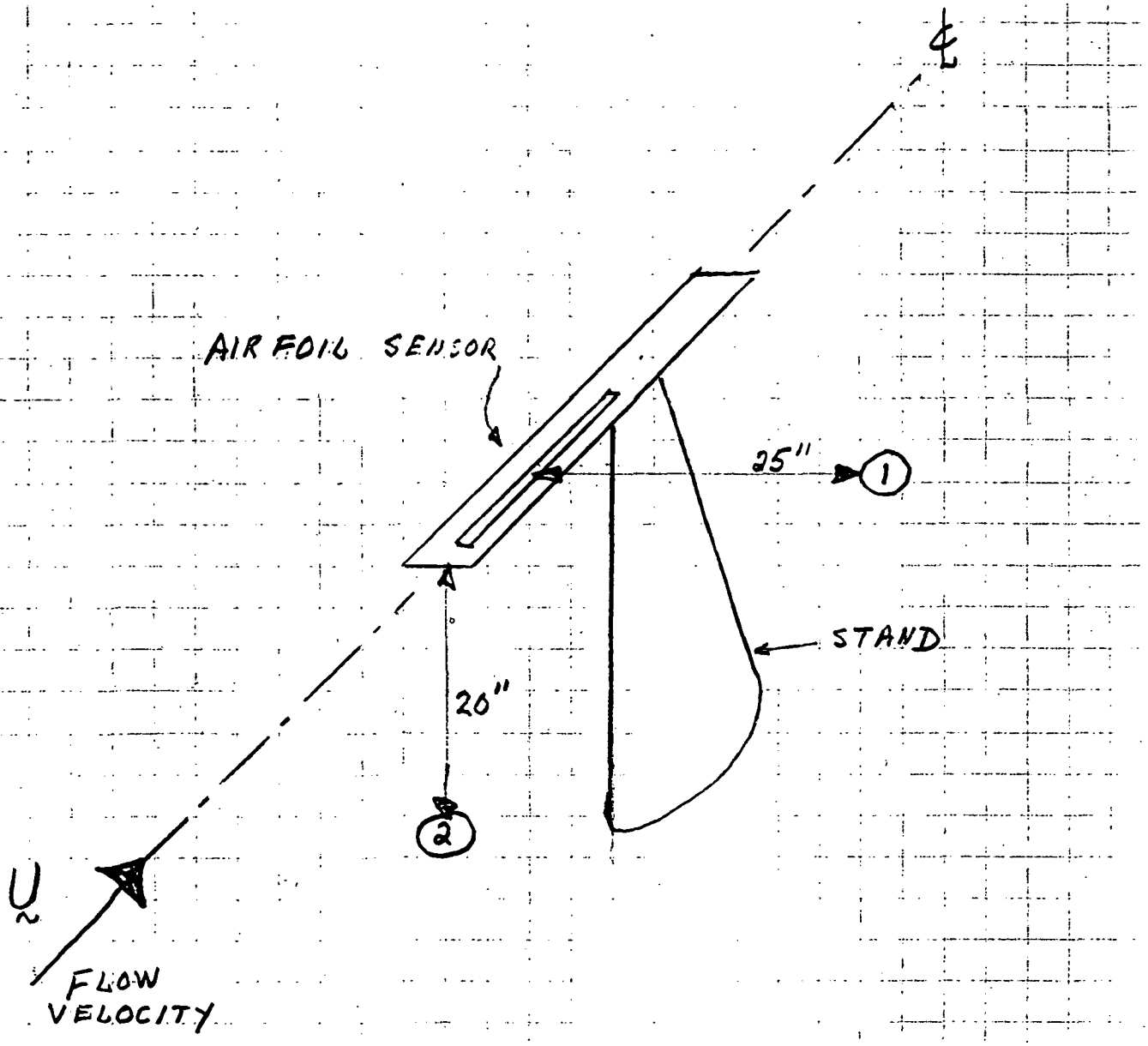

FIG. 8 : LOCATIONS 1 AND 2 OF MICROPHONES FOR THE MEASUREMENTS OF OUT-OF-FLOW NOISE

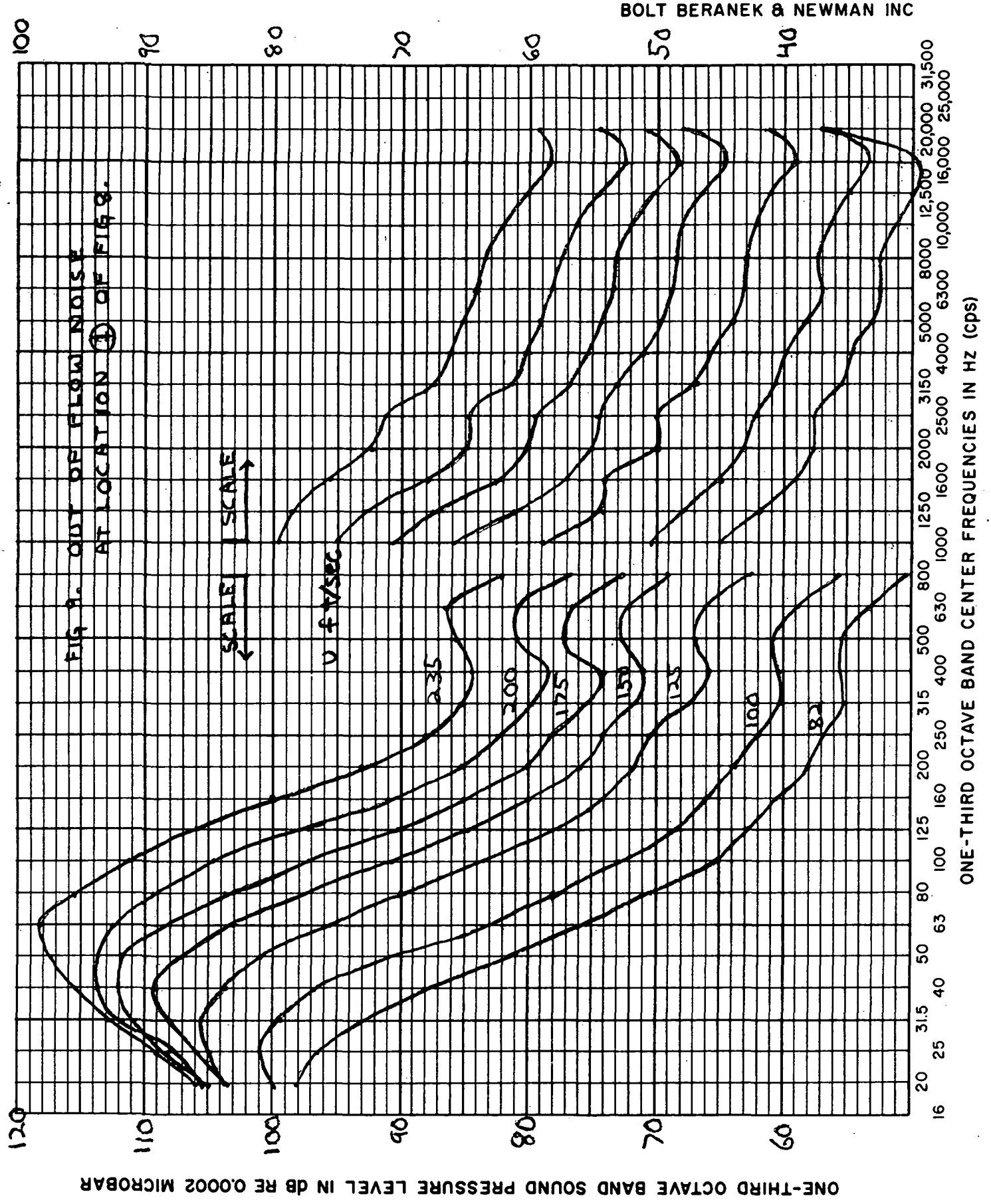

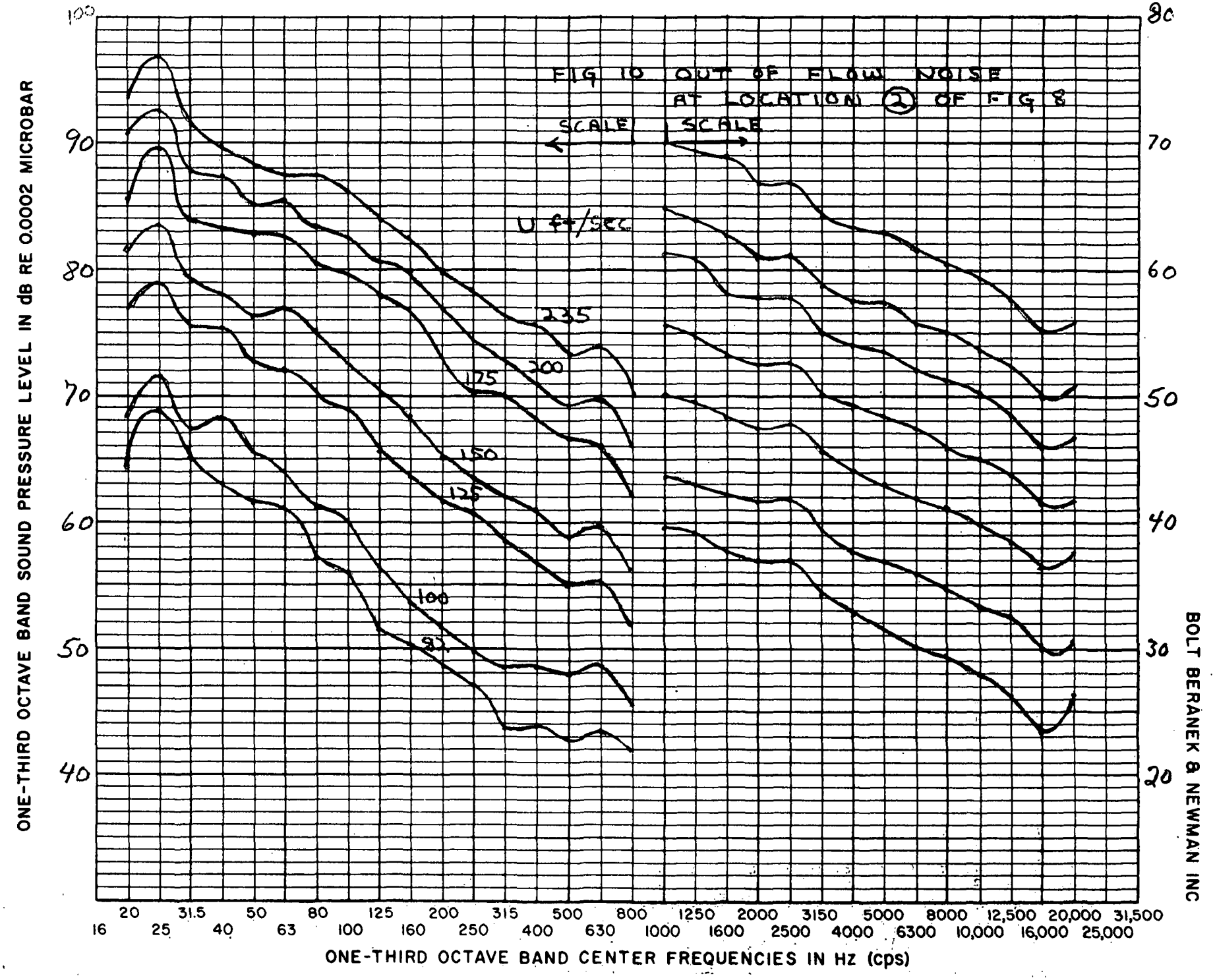
FIG 10 OUT OF FLOW NOISE
AT LOCATION (2) OF FIG 8
SCALE
SCALE
U ft/sec
235
200
175
150
125
100
93
100
90
80
70
60
50
40
90
70
60
50
40
30
20
20 31.5 50 80 125 200 315 500 800 1250 2000 3150 5000 8000 12,500 20,000 31,500
16 25 40 63 100 160 250 400 630 1000 1600 2500 4000 6300 10,000 16,000 25,000
ONE-THIRD OCTAVE BAND CENTER FREQUENCIES IN Hz (cps)
ONE-THIRD OCTAVE BAND SOUND PRESSURE LEVEL IN dB RE 0.0002 MICROBAR
BOLT BERANEK & NEWMAN INC

generated by the mixing region hitting the stand; also the acoustic noise radiated through the nozzle is baffled by the nozzle itself. At high frequencies the noise at station 2 is also lower than at station 1 because station 2 is in a null of the pressure radiated by the trailing edge of the stand.

4.2 Flow Noise of the B&K Half-Inch Condenser Microphone With Nose Cone

The spectrum of the flow noise measured by a B&K half-inch condenser microphone with nose cone, pointing directly into the flow, is shown in Fig. 11, in third octave bands and for different flow velocities from 24 to 70 m/sec.

The levels of flow noise of Fig. 11 is lower than the out-of-flow noise measured at location 1 of Fig. 8, except towards high frequencies where they become roughly equal. The lower levels of Fig. 11 were anticipated because the B&K sensor is in a null of the directivity of the noise generated by the stand. When the levels of flow noise of Fig. 11 are compared with the out-of-flow noise measured at location 2 of Fig. 8, they are found to be higher; hence, the flow noise of the B&K sensor is dominated by the turbulence of the free jet reacting on the surface of the B&K sensor and its preamplifier base.

The flow noise of Fig. 11 will be the reference to which the flow noise of the Airfoil Sensor will be compared.

4.3 Flow Noise of the Airfoil Sensor

The frequency spectra, in third octave bands, of the flow noise of the Airfoil Porous Surface Sensor, are shown in Figs. 12 through 18, for yaw angles α from 0° to 90° in increments of 15° and for flow velocities of 25 to 70 m/sec in increments of 8 m/sec (25 ft/sec).

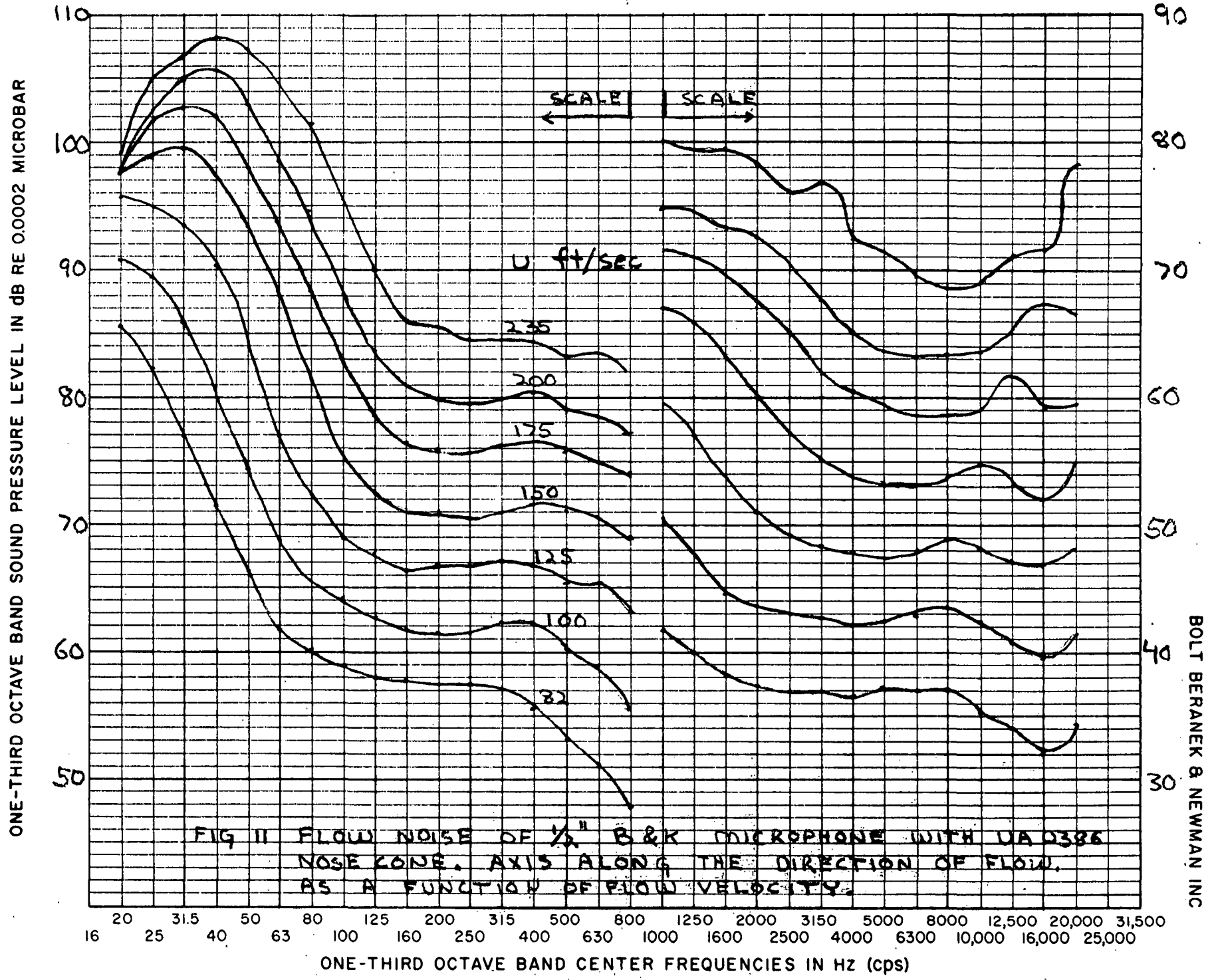

FIG 11 FLOW NOISE OF ½" B&K MICROPHONE WITH UA 0386 NOSE CONE. AXIS ALONG THE DIRECTION OF FLOW. AS A FUNCTION OF FLOW VELOCITY.

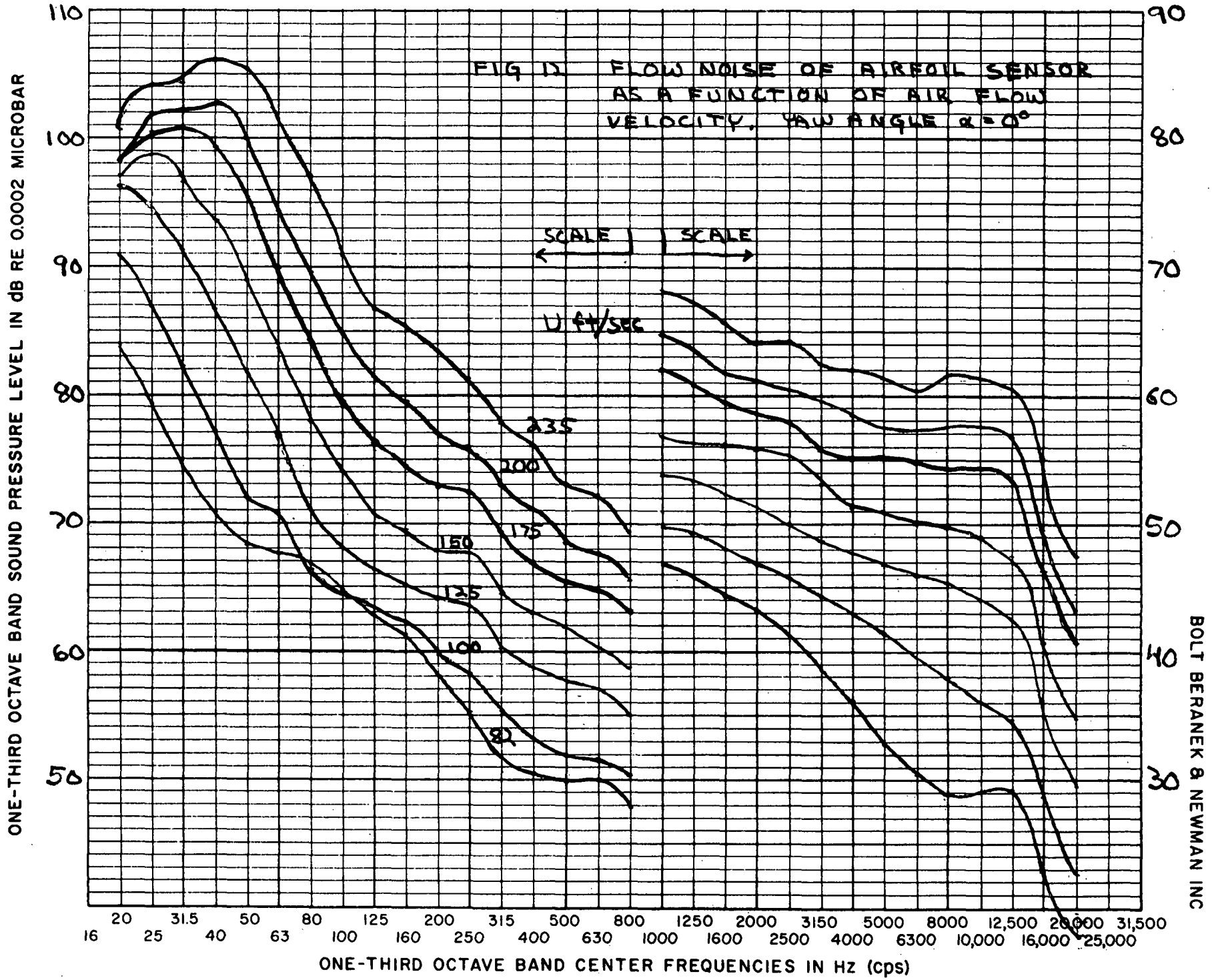
FIG 11 FLOW NOISE OF AIRFOIL SENSOR AS A FUNCTION OF AIR FLOW VELOCITY, YAW ANGLE α = 0°
SCALE
SCALE
U ft/sec
235
200
175
150
125
100
80
ONE-THIRD OCTAVE BAND SOUND PRESSURE LEVEL IN dB RE 0.0002 MICROBAR
110
100
90
80
70
60
50
90
80
70
60
50
40
30
16 20 25 31.5 40 50 63 80 100 125 160 200 250 315 400 500 630 800 1000 1250 1600 2000 2500 3150 4000 5000 6300 8000 10,000 12,500 16,000 20,000 25,000 31,500
ONE-THIRD OCTAVE BAND CENTER FREQUENCIES IN Hz (cps)
BOLT BERANEK & NEWMAN INC

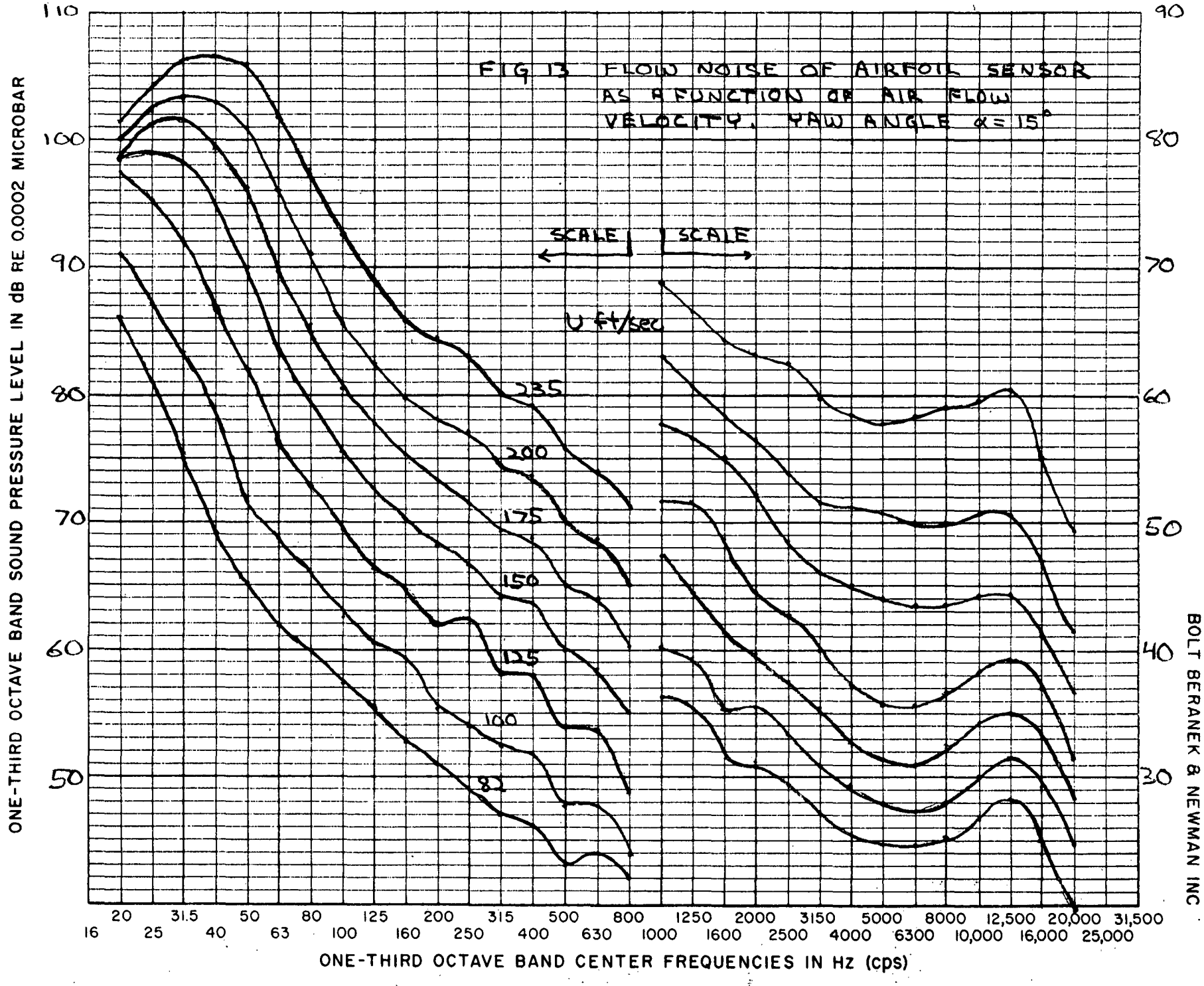
FIG 13 FLOW NOISE OF AIRFOIL SENSOR AS A FUNCTION OF AIR FLOW VELOCITY, YAW ANGLE α = 15°
SCALE
SCALE
U ft/sec
235
200
175
150
125
100
82
ONE-THIRD OCTAVE BAND SOUND PRESSURE LEVEL IN dB RE 0.0002 MICROBAR
110
100
90
80
70
60
50
90
80
70
60
50
40
30
16 20 25 31.5 40 50 63 80 100 125 160 200 250 315 400 500 630 800 1000 1250 1600 2000 2500 3150 4000 5000 6300 8000 10,000 12,500 16,000 20,000 25,000 31,500
ONE-THIRD OCTAVE BAND CENTER FREQUENCIES IN Hz (cps)
BOLT BERANEK & NEWMAN INC

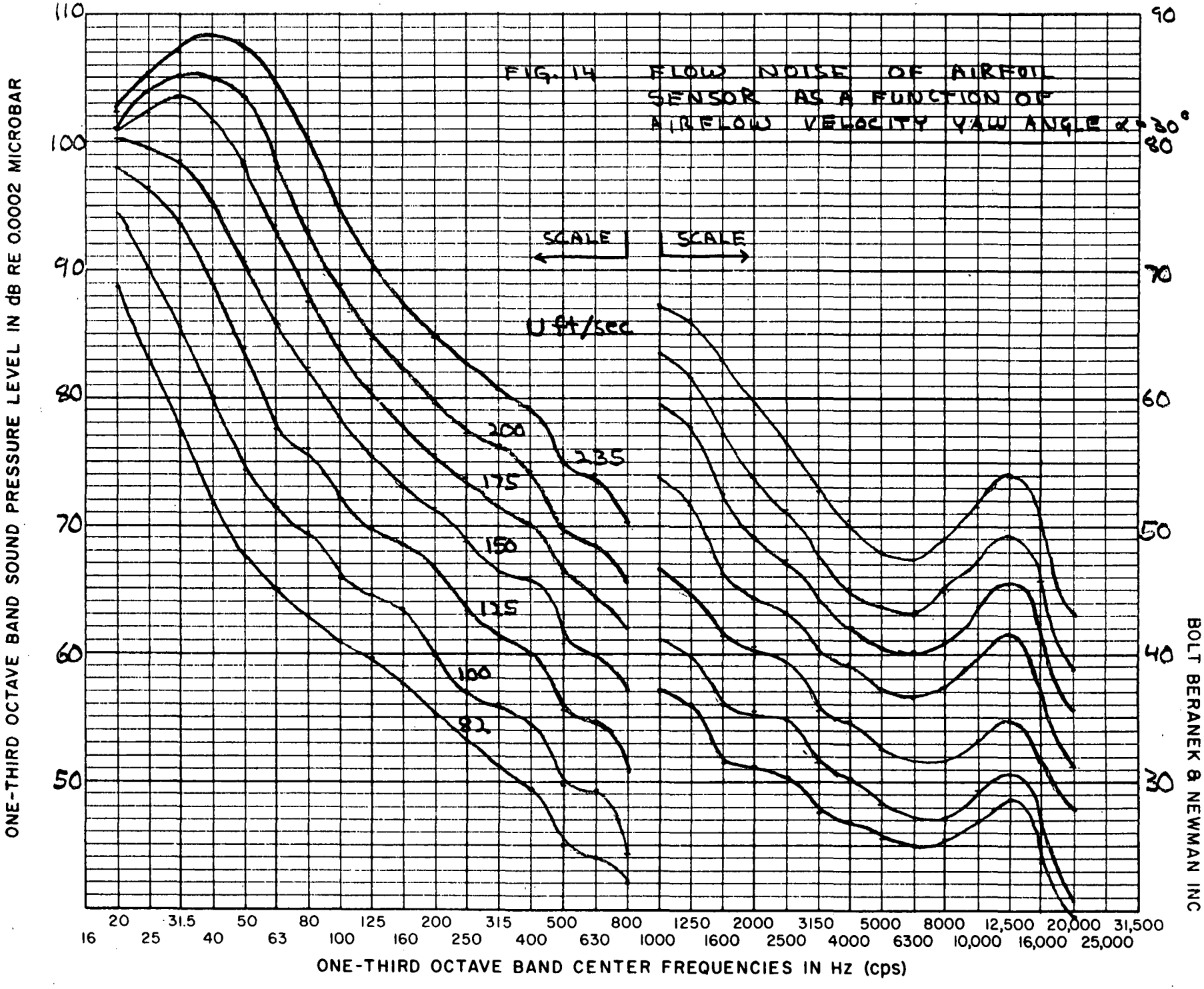
FIG. 14 FLOW NOISE OF AIRFOIL SENSOR AS A FUNCTION OF AIRFLOW VELOCITY YAW ANGLE α = 30°
SCALE
SCALE
U ft/sec
200
175
150
125
100
92
235
110
100
90
80
70
60
50
90
80
70
60
50
40
30
ONE-THIRD OCTAVE BAND SOUND PRESSURE LEVEL IN dB RE 0.0002 MICROBAR
16 20 25 31.5 40 50 63 80 100 125 160 200 250 315 400 500 630 800 1000 1250 1600 2000 2500 3150 4000 5000 6300 8000 10,000 12,500 16,000 20,000 25,000 31,500
ONE-THIRD OCTAVE BAND CENTER FREQUENCIES IN Hz (cps)
BOLT BERANEK & NEWMAN INC

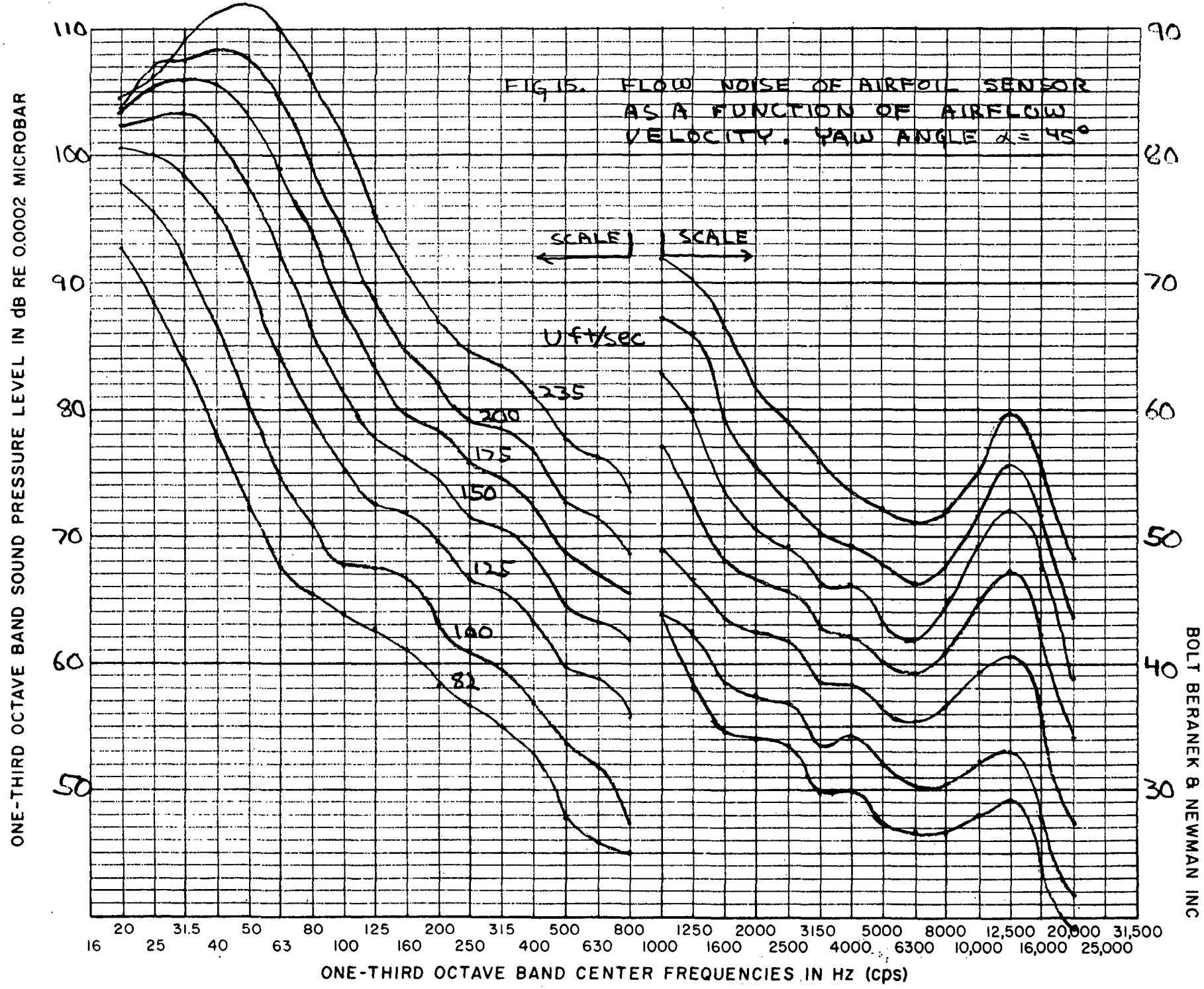
FIG 15. FLOW NOISE OF AIRFOIL SENSOR AS A FUNCTION OF AIRFLOW VELOCITY. YAW ANGLE α = 45°
SCALE
SCALE
U ft/sec
235
200
175
150
125
100
82
ONE-THIRD OCTAVE BAND SOUND PRESSURE LEVEL IN dB RE 0.0002 MICROBAR
110
100
90
80
70
60
50
90
80
70
60
50
40
30
20 31.5 50 80 125 200 315 500 800 1250 2000 3150 5000 8000 12,500 20,000 31,500
16 25 40 63 100 160 250 400 630 1000 1600 2500 4000 6300 10,000 16,000 25,000
ONE-THIRD OCTAVE BAND CENTER FREQUENCIES IN Hz (cps)
BOLT BERANEK & NEWMAN INC

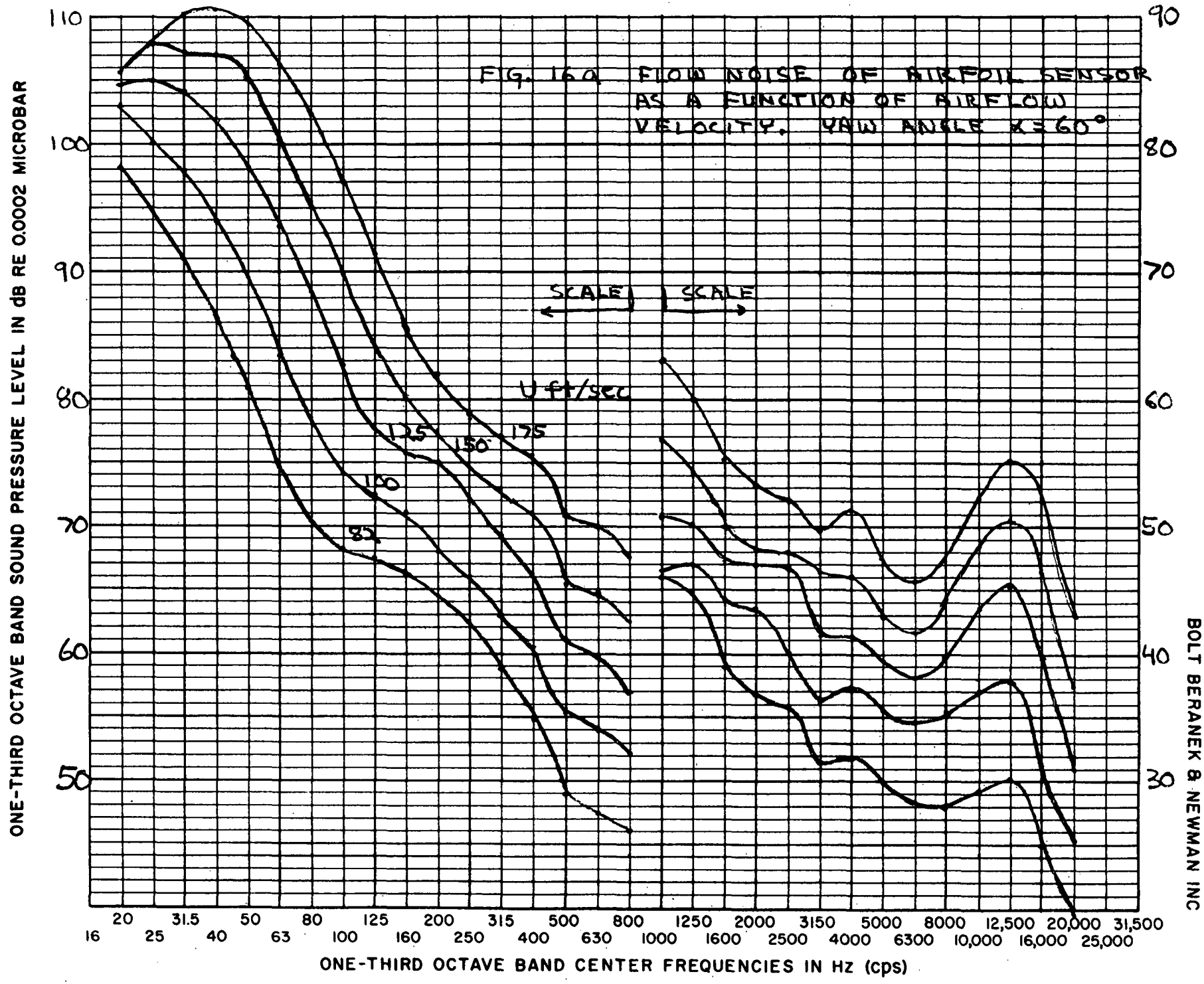
FIG. 16a FLOW NOISE OF AIRFOIL SENSOR AS A FUNCTION OF AIRFLOW VELOCITY. YAW ANGLE χ = 60°
SCALE
SCALE
U ft/sec
175
150
125
100
85
ONE-THIRD OCTAVE BAND SOUND PRESSURE LEVEL IN dB RE 0.0002 MICROBAR
110
100
90
80
70
60
50
90
80
70
60
50
40
30
16 20 25 31.5 40 50 63 80 100 125 160 200 250 315 400 500 630 800 1000 1250 1600 2000 2500 3150 4000 5000 6300 8000 10,000 12,500 16,000 20,000 25,000 31,500
ONE-THIRD OCTAVE BAND CENTER FREQUENCIES IN Hz (cps)
BOLT BERANEK & NEWMAN INC

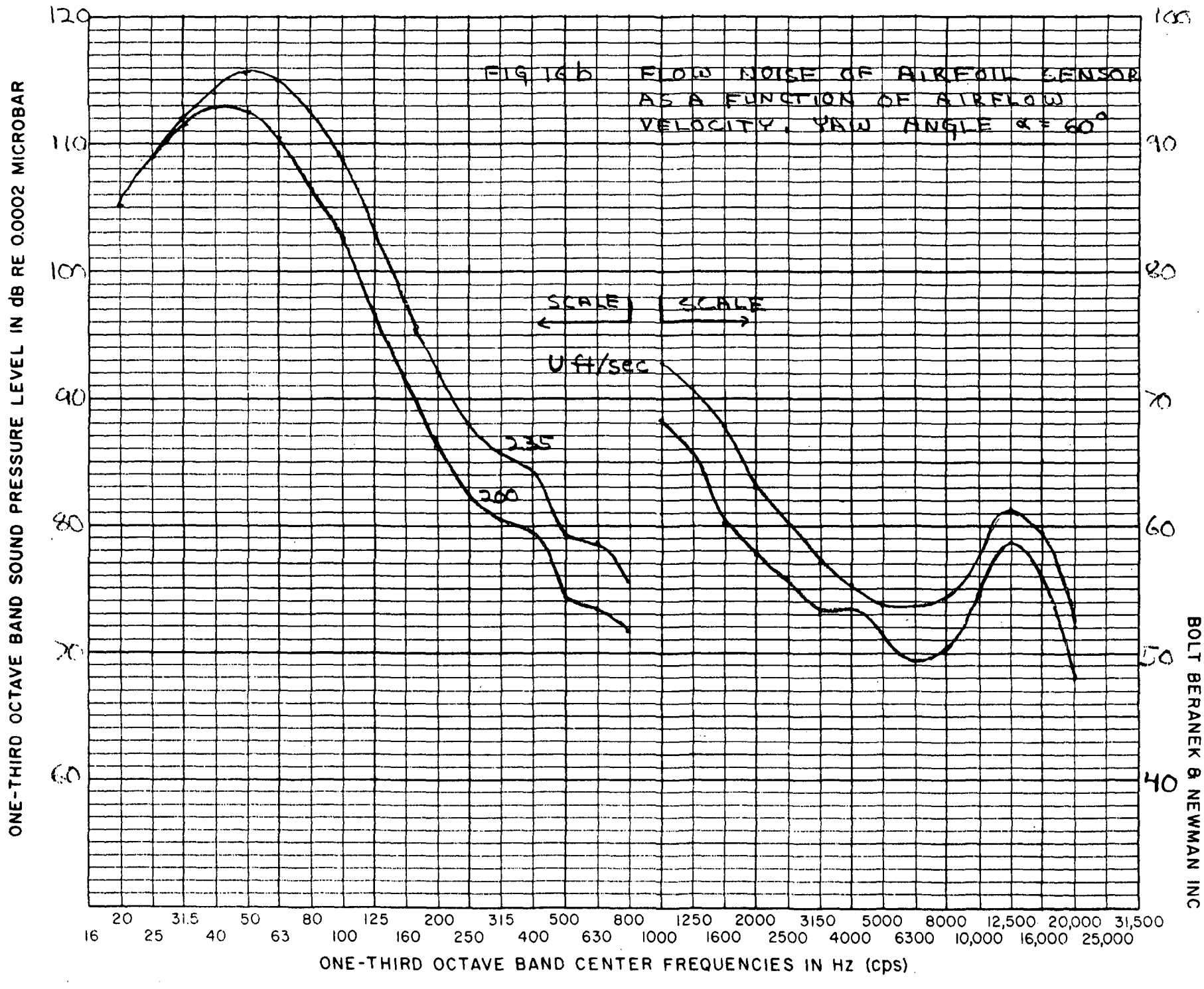
FIG 16b FLOW NOISE OF AIRFOIL SENSOR AS A FUNCTION OF AIRFLOW VELOCITY, YAW ANGLE α = 60°
SCALE
SCALE
U ft/sec
235
200
ONE-THIRD OCTAVE BAND SOUND PRESSURE LEVEL IN dB RE 0.0002 MICROBAR
120
110
100
90
80
70
60
105
90
80
70
60
50
40
20 31.5 50 80 125 200 315 500 800 1250 2000 3150 5000 8000 12,500 20,000 31,500
16 25 40 63 100 160 250 400 630 1000 1600 2500 4000 6300 10,000 16,000 25,000
ONE-THIRD OCTAVE BAND CENTER FREQUENCIES IN Hz (cps)
BOLT BERANEK & NEWMAN INC

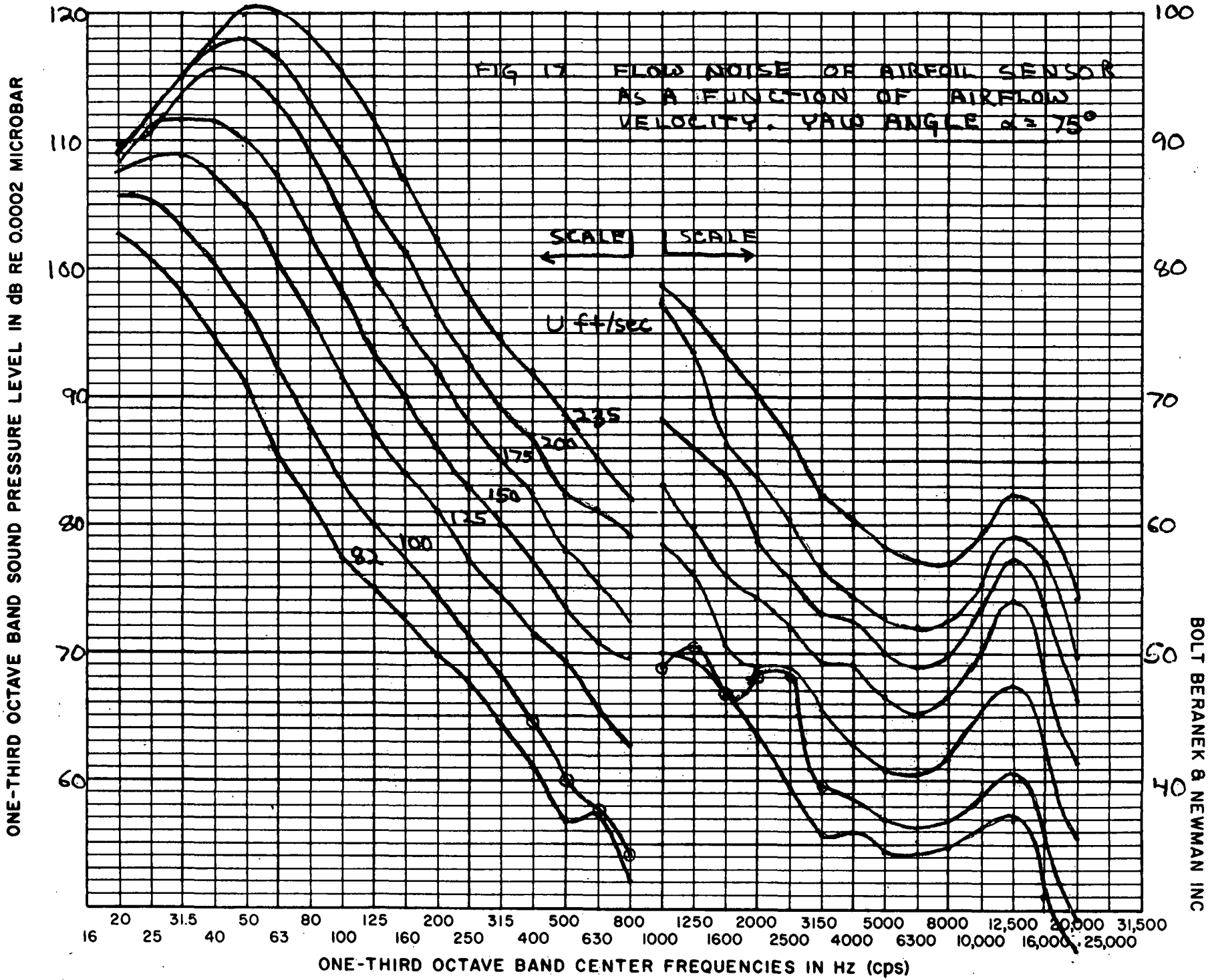
FIG 17 FLOW NOISE OF AIRFOIL SENSOR AS A FUNCTION OF AIRFLOW VELOCITY. YAW ANGLE α = 75°
SCALE
SCALE
U ft/sec
235
200
175
150
125
100
80
120
110
100
90
80
70
60
100
90
80
70
60
50
40
ONE-THIRD OCTAVE BAND SOUND PRESSURE LEVEL IN dB RE 0.0002 MICROBAR
16 20 25 31.5 40 50 63 80 100 125 160 200 250 315 400 500 630 800 1000 1250 1600 2000 2500 3150 4000 5000 6300 8000 10,000 12,500 16,000 20,000 25,000 31,500
ONE-THIRD OCTAVE BAND CENTER FREQUENCIES IN Hz (cps)
BOLT BERANEK & NEWMAN INC

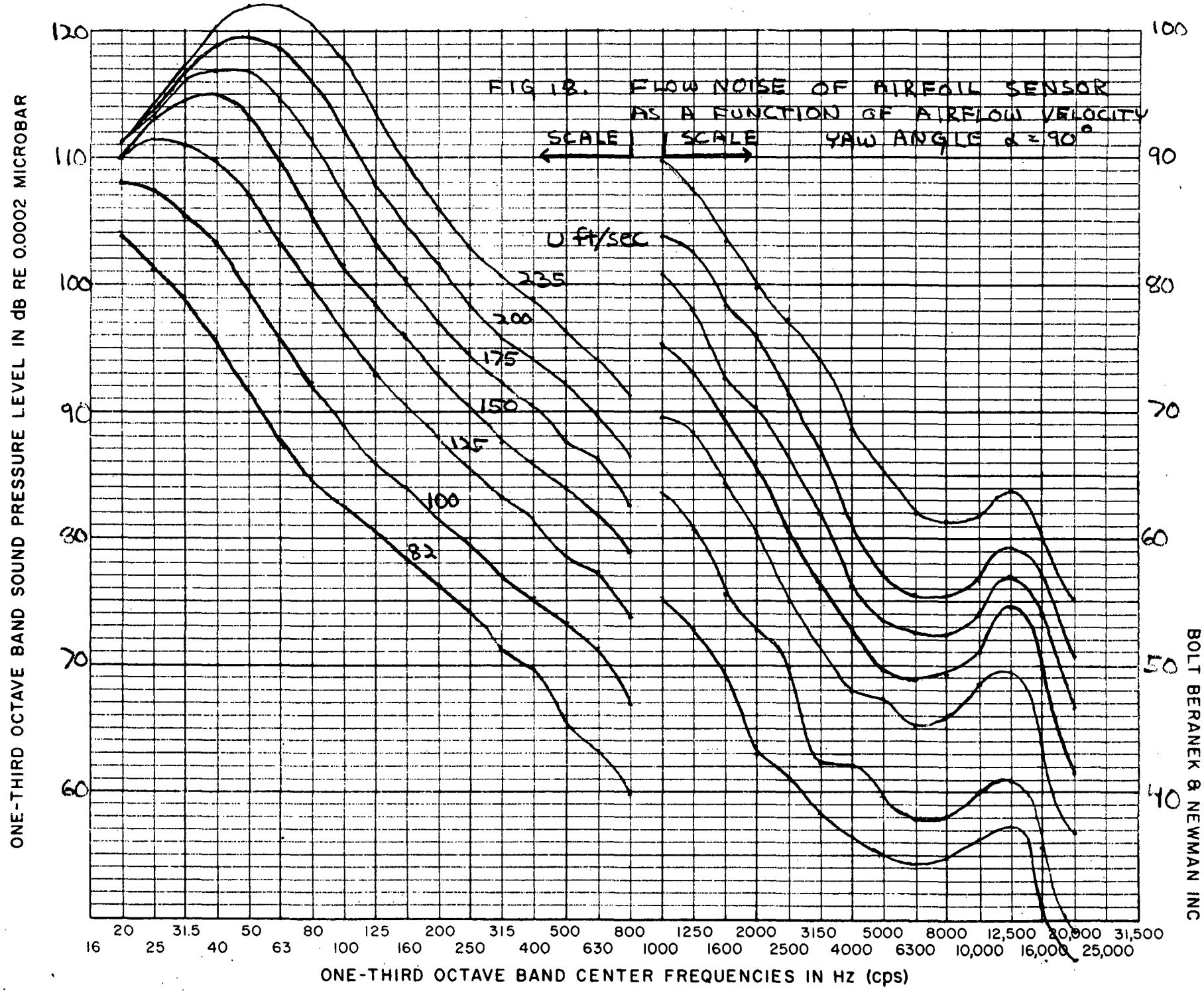
FIG 18. FLOW NOISE OF AIRFOIL SENSOR AS A FUNCTION OF AIRFLOW VELOCITY
YAW ANGLE α = 90°
SCALE
SCALE
U ft/sec
235
200
175
150
125
100
82
ONE-THIRD OCTAVE BAND SOUND PRESSURE LEVEL IN dB RE 0.0002 MICROBAR
120
110
100
90
80
70
60
100
90
80
70
60
50
40
16 20 25 31.5 40 50 63 80 100 125 160 200 250 315 400 500 630 800 1000 1250 1600 2000 2500 3150 4000 5000 6300 8000 10,000 12,500 16,000 20,000 25,000 31,500
ONE-THIRD OCTAVE BAND CENTER FREQUENCIES IN Hz (cps)
BOLT BERANEK & NEWMAN INC

(1) In general, the spectrum of the flow noise at any flow velocity and yaw angle does not exhibit any conspicous local rise which could be associated with a coherent noise mechanism like a coherent vortex shedding. The accurate airfoil shape of the new design did not allow the generation of any significant noise of this type. However, there are indications that low levels of coherent noise are generated, which can be inferred from the small fluctuations in the noise spectra. These small fluctuations in the flow noise spectra could be separated and identified by using a narrow band analysis.

During the flow tests at different yaw angles and flow velocities, an observer near the airfoil but outside of the flow could, at times, detect the presence of some weak tones (≈400 Hz) emanating from the sensor (or the stand?); those weak tones, when they occur, would not be amplified nor shifted in frequency by an increase in flow velocity; they are like tones from cavity resonances rather than from vortex shedding. Their origin was not found.

(2) The general comment above about the low level of coherent noise of the new airfoil is further corroborated by comparing the flow noise of the older design and of the new design. Both can be compared only at low flow velocities because the older design was tested in a small wind tunnel only at 23 m/sec (74 ft/sec).

Comparing the flow noise of the new Airfoil Sensor at flow velocity of 25 m/sec (84 ft/sec) with the flow noise of the old design* at 22 m/sec (74 ft/sec), we find the following: at a yaw angle of 0°, the new design is quieter by about 5 dB. At a yaw

*NASA CR-114593, Appendix VI, Fig. 6.

angle of 30° the new design is quieter by roughly 10 dB. At a yaw angle of 60° the new design is quieter by roughly 15 dB; the rise in noise spectrum at 4 kHz, in the old design, and which was attributed to coherent flow noise of a turbulent boundary layer at the trailing edge, is not found in the new design.

The lower flow noise of the new design compared with the older design, is associated with the more accurate and the thinner airfoil (smaller thickness to chord ratio) of the new design and possibly to the more accurate directivity function of the new design at the small wavelengths of turbulence.

The turbulence spectrum of the new wind tunnel in which the new Airfoil Sensor is tested is in fact slightly higher, by a few dB, than the turbulence spectrum of the old wind tunnel in which the old design was tested. Although the scale of turbulence in the two wind tunnels have not been measured and compared, it is almost certain that in the *new* wind tunnel the old design would sense a higher flow noise than in the old wind tunnel.

(3) At 12.5 kHz the noise spectrum of the new Airfoil Sensor has a distinct "hump" which is not shifted in frequency by changes in flow velocity. The presence of this "hump" has not been explained. It would appear that this "hump" belongs to the frequency response of the Sensor. Perhaps it could be associated with a subsonic flexural wave of the porous strip; however, this possibility would contradict our earlier conclusion* that the first bending resonance of the porous strip occurs at 17 kHz and was identified in the frequency response of the sensor.

---

*See Appendix 9.

This "hump" of flow noise at 12.5 kHz, although not a very large one, merits further investigation.

(4) The flow noise at yaw angles of 15° and 30° is generally, lower than the flow noise at 0°.

As the yaw angle is increased towards 30° there are two competing effects: first, the wavenumber component of the flow noise projected along the axis of the porous strips decreases and therefore the filtering action of Airfoil Sensor decreases and the net flow noise should increase. In contrast, the path length on the porous strip, over which a pressure disturbance propagates is shortened as the yaw angle is increased. If the strength of this pressure disturbance is increasing with the path length over the surface of the airfoil, or is experiencing instability as in a transition from a laminar to a turbulent boundary layer, then the shorter path length with increasing yaw angle would produce a lower flow noise. In this competition a minimum flow is reached at yaw angle α of 30°; for larger yaw angles the noise filtering of the directivity function decreases rapidly.

A further source of noise, at large yaw angles is the noise radiated by the stand. This noise was discussed in Part 2 of Section 4.

(5) We cannot determine with the present test setup whether the boundary layer over the porous strips become turbulent.

Taking a Reynolds number R_x for the length x from the tip of the Airfoil Sensor to the far end of the porous strip and using the results obtained with a smooth flat plate with sharp leading edge, we would evoke a critical Reynolds number of 2×10^6 at which transition to turbulent flow can take place.

The numerical value of this critical Re is consistent with the relatively low intensity of turbulence of the free jet. For a yaw angle of 0° the path length x is 16.5 inches. Hence, the transition may start at flow velocities of 230 ft/sec.

Even if transition to a turbulent boundary layer would start to occur at the far end of one porous strip, the net increase in flow noise could not be large because only a small fraction of the strip is exposed to this transition.

4.4 Comparison Between the Flow Noises of the Airfoil Sensor and the B&K Half-Inch Condenser Microphone with Nose Cone

We recall that the B&K sensor is always pointed towards the airflow and that the Airfoil Sensor is oriented with different yaw angles α, 0° to 90° with respect to the flow. Also, the tests are made in very low turbulence.

(1) Low Frequency Noise Below 100 Hz

The low frequency noise below 100 Hz is primarily noise caused by the fan; since neither one of the two sensors has any directivity at low frequencies, they should sense equally well this noise. This is the case for yaw α of the Airfoil Sensor up to $\alpha = 45°$. At larger yaw angles, the Airfoil Sensor becomes somewhat noisier. This increase in noise is probably the low frequency noise generated by the stand; the directivity of this noise has a null at $\alpha = 0°$ such that the B&K sensor is not exposed to it. As the yaw angle of the Airfoil Sensor is increased, this sensor becomes progressively more exposed to the noise of the stand.

(2) Noise Spectrum Above 100 Hz and Low Flow Velocity

At low flow velocities and for zero yaw angle of the Airfoil Sensor, the flow noises are about the same. At larger yaw angles of 15° to 45° the Airfoil Sensor is quieter than the B&K sensor; at $\alpha = 60°$ they are about the same. At larger yaw angles of 75° and 90° the Airfoil Sensor is noisier by approximately 10 dB except above 3.1 kHz where they are about the same.

(3) Noise Spectrum Above 100 Hz; High Flow Velocities

For the different yaw angles α of the Airfoil Sensor we find the following:

$\alpha = 90°$: the Airfoil Sensor is quieter than the B&K sensor only above 3.1 kHz.

$\alpha = 60°$: the Airfoil Sensor is quieter than the B&K sensor above 400 Hz; the difference can be as much as 15 dB at 6.3 kHz.

$\alpha = 45°$: the Airfoil Sensor is quieter than the B&K sensor above 250 Hz; the difference can be as much as 20 dB at 5 kHz.

$\alpha = 30°$: this yaw angle yields the minimum flow noise of the Airfoil Sensor, especially at high frequencies; the airfoil sensor is quieter than the B&K sensor for frequencies above 200 Hz; the difference can be as much as 25 dB at 5 kHz.

$\alpha = 0°, 15°$: the flow noise of the Airfoil Sensor is everywhere lower than the flow noise of the B&K sensor; the difference is about 12 dB at 1 kHz and remains approximately 10 dB above 1 kHz.

5. CONCLUSIONS

The new Airfoil Porous Surface Sensor has shown significantly lower flow noise than the older design. This is due to the accurate airfoil section and to its small thickness to chord ratio.

Over the full range of flow velocities of the wind tunnel, 25 to 70 m/sec, and at any yaw angle of the Airfoil, the new design did not create in its flow noise any significant "tones".

The flow noise of the Airfoil Sensor is generally lower than the flow noise of the B&K half inch microphone with nose cone, for a wide range of yaw angles, 0° to 45°. At larger yaw angles, 60° to 90° the Airfoil Sensor is noisier, probably because it senses the noise generated by the stand on which it is mounted.

All these results of flow noise apply to very quiet flow. At higher turbulence than the turbulence of the present tests, the Airfoil Sensor is expected to be much quieter than the B&K sensor.

APPENDIX XI

SPECIFICATIONS OF THE POROUS SURFACE AIRFOIL MICROPHONE MODEL 342

In this appendix, we gather the specifications of the Porous Surface Airfoil Microphone Model 342. These specifications give the airfoil cross-section, the porous strips, the microphone, and finally detailed drawings of the Airfoil Sensor and its base.

1. Airfoil

The airfoil for the original Porous Strip Sensor, tested under a previous NASA contract[1], followed roughly the NACA-0015 basic thickness form (in fact, the thickness-to-chord ratio was 16.5%). The flow noise sensed by the sensor at yaw angles greater than 45° (and an angle of attack of 0°), showed an increase of level in the frequency region around 4 kHz, at flow velocities of 20 m/sec. This increase is approximately 15 dB over the spectrum extrapolated from the low frequency region.

By choosing a more favorable airfoil, the excess flow noise level noted in our previous experiments should be reduced. A thickness-to-chord ratio equal to or less than 12% has been recommended by the technical statement of the present contract. This recommendation certainly falls in line with our previous experiments where decreasing the thickness-to-chord ratio has decreased the level of excess noise and shifted its spectrum to higher frequencies. With a smaller thickness-to-chord ratio the adverse pressure gradient is decreased and consequently the thickness of the boundary layer is decreased. Hence, the level of flow noise is decreased and the peak frequency of flow noise is moved to higher frequencies according

---

[1]D. Noiseux, "Study of Porous Surface Microphones for Acoustic Measurements in Wind Tunnels," NASA CR-114593, April 1973.

to a Strouhal number for the boundary layer thickness; furthermore, the edge noise will be further away from the porous strip, giving an additional attenuation.

For higher flow velocities, like 70 m/sec, it is even more important that any adverse pressure gradient in the region of the porous strip be maintained very low in order to insure that the airflow will remain laminar over the porous surface. For this reason a modern cross-section like NACA-64-012 has some advantage over the older type of section like NACA-0012. These advantages are:

1. The boundary layer is thinner at the trailing edge than found in a low number section because an adverse pressure gradient exists only beyond the point of maximum thickness where the porous strip will be located.

2. The flow will remain laminar over more than 50% of the chord.

3. The laminar flow will be rather insensitive to small angles of attack: the marked drop in the drag coefficient for angles of attack of less than $\pm 2^\circ$ is indicative of this insensitivity.

We have calculated a section which will have a thickness of slightly less than 12% (approximately 11.5%) following the specification of the NACA section 64-012, with a proportional decrease in thickness.

2. Porous Material

The porous material finally selected is a thin plate of sintered stainless steel particles. This material was supplied under special specifications by:

Mott Metallurgical Corporation
Farmington, Connecticut 06032

The specifications are as follows:

- Product type: MWO-12-0865-01
- Strips: 0.025" ± 0.003" thick × 12-3/4" × 2"
- Flow: 20 scfm/ft^2 at 10" H_2O (approximately 2 micron material, 316 stainless)
- Smooth and flat finish

It is almost necessary to purchase a fairly large number of strips because the process used by Mott is not very well controlled. Out of 30 strips we have purchased, we could obtain only two sets of narrow strips for two sensors, satisfying the design specifications at every half inch along the narrow strips: specific flow resistance + 34 dB re $\rho_0 c_0$ ±1 dB, where $\rho_0 c_0$ is the characteristic impedance of air. The flow specified in the specifications correspond to the mean value of specific flow resistance.

Each strip as received from the manufacturer is tested for its flow resistance in narrow bands of 1/2-inch wide and at every 1/2-inch of the bands. The bands satisfying the design specifications are selected, cut and assembled end-to-end by soldering. It requires two to three shorter bands to give the final length of 14 inches. Appendices 8 and 9 describe the testing technique and the results of the final strips selected.

The final strips are set in the airfoil, with an epoxy like Epoxi-Patch distributed by:

Hysol Division
The Dexter Corporation
Olean, New York 14780

This epoxy is widely distributed as a convenient two part kit. It hardens into a very hard solid with excellent bonding. The porous strips become effectively clamped to the airfoil so that the first resonance frequency of the strips in the airfoil is approximately 20 kHz. Other epoxy meeting these same characteristics can obviously be used.

In setting the porous strips on the airfoil, the epoxy is applied to the airfoil and not to the porous strips; only enough epoxy is applied to insure a continuous and strong bond of the edges of the porous strips to the airfoil.

3. Microphone and Preamplifier

The Airfoil Sensor is designed to accept only the Bruel & Kjaer half-inch condenser microphone cartridge. The type 4134 must be used because it has the required flat *pressure* response up to almost 20 kHz.

The preamplifier could be either the B&K preamplifier type 2615 or 2619, or the General Radio preamplifier type 1560-P42.

When the base of the Airfoil Sensor, described in Sec. 4 is used, the G.R. preamplifier is preferred because it has electrical leads of smaller diameter than the B&K preamplifier; these leads can be bent more readily into the base and fed into the central pipe.

4. Drawings of the Assembly

Two drawings are attached to this appendix. They show the dimensions of the Airfoil Sensor and of the base and tail end which were used during our tests. Other types of base and tail end would be designed to fit the Airfoil Sensor and the particular stand supporting the assembly. Photographs of

the complete assembly of the sensor and of its stand are shown in Appendices 9 and 10.

The airfoil is cast as a single piece, including the microphone ring, made of Devcon F-3 epoxy. This epoxy has a relatively large internal damping which is useful in controlling the amplitude of bending waves excited by turbulent flow. However, the acoustic response of the sensor is very insensitive to bending vibrations because of its symmetrical design.

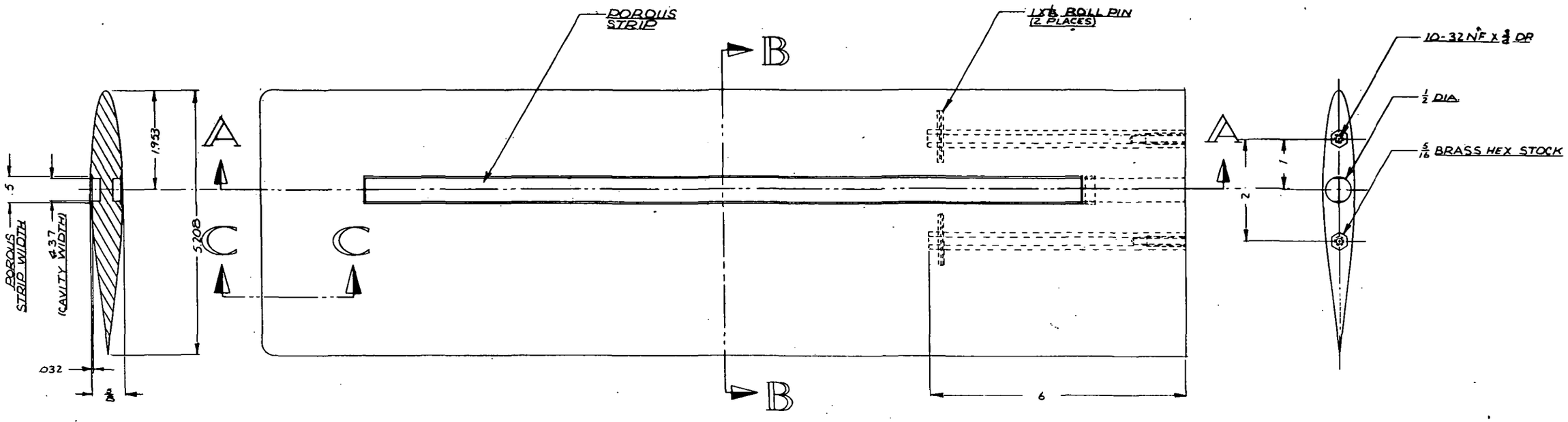

SECTION BB

SECTION AA

SECTION CC

SHAPE THICKNESS PROPORTIONAL TO LEADING EDGE OF AIRFOIL

NOTES:
1 AIRFOIL NACA-64-012
2 CASTING MATERIAL DEVCON E3

POROUS STRIP SENSOR